AN ABSTRACT OF THE DISSERTATION OF

Matthew P Ryder for the degree of Doctor of Philosophy in Chemical Engineering presented on February 7, 2014.

Title: Binding of Bacterial Lipopolysaccharide by the Cationic Amphiphilic Peptide WLBU2 at Interfaces.

Abstract approved:

_____

Joseph McGuire Karl F. Schilke

Passage of blood through a sorbent device for removal of bacteria and endotoxin by specific binding with immobilized, membrane-active, bactericidal peptides holds promise for treating severe blood infections. Peptide insertion in the target membrane and stable binding is desirable, while membrane disruption and release of degradation products to the circulating blood is not desirable. Here we describe interactions between bacterial endotoxin (lipopolysaccharide, LPS) and the membrane-active, bactericidal peptides WLBU2 and polymyxin B (PmB). Analysis of the interfacial behavior of mixtures of LPS and peptide using air-water interfacial tensiometry and optical waveguide lightmode spectroscopy strongly suggested insertion and stabilization of intact LPS vesicles by WLBU2, while no such peptide-LPS interactions were evident with PmB. Analysis with dynamic light scattering showed in fact that LPS vesicles appear to undergo peptide-induced destabilization in the presence of PmB. Circular dichroism spectra confirmed that WLBU2, which shows disordered structure in aqueous solution and substantially helical structure in membrane-mimetic environments, is stably located within the LPS membrane in peptide-vesicle mixtures. Interactions between LPS and WLBU2 were also evaluated following immobilization of the peptide at uncoated and polyethylene oxide (PEO)-coated hydrophobic surfaces. PEO layers were prepared by radiolytic grafting of selected PEO-polypropylene oxide (PPO)-PEO triblock surfactants to silanized, hydrophobic surfaces. Immobilization of WLBU2 at the PEO layers was achieved by its noncovalent entrapment among the pendant PEO chains and in separate experiments, its covalent coupling to PEO chains that had been end-activated with pyridyl disulfide groups. Analysis of peptide-LPS interactions using

a quartz crystal microbalance with dissipation monitoring showed that upon introduction of LPS suspension to a flow cell housing a surface presenting tethered WLBU2, LPS located at the interface in a fashion irreversible to elution. Circular dichroism spectra recorded for suspensions of LPS and (silanized) hydrophobic silica nanoparticles to which WLBU2-triblock constructs had been adsorbed, confirmed that binding of LPS by tethered WLBU2 is mediated through peptide insertion and conformational change within the LPS membrane. LPS capture by tethered WLBU2 was detected in the presence of fibrinogen as well. However, that outcome is best considered tentative, as it was associated with potentially complex interactions between fibrinogen, LPS, and WLBU2, that remain uncharacterized. In summary, the results of this study strongly suggest that presentation of tethered WLBU2 within a sorbent device will enable the capture of endotoxin from suspension without reintroduction of degradation products to the circulating stream. Thus, they provide a rationale for hypotheses to drive further development of perfusion for the treatment of severe blood infections.

Binding of Bacterial Lipopolysaccharide by the Cationic Amphiphilic Peptide WLBU2 at Interfaces

by
Matthew P Ryder

A DISSERTATION

submitted to

Oregon State University

in partial fulfillment of
the requirements for the
degree of

Doctor of Philosophy

Presented February 7, 2014
Commencement June 2014

Doctor of Philosophy dissertation of Matthew P Ryder presented on February 7, 2014.

APPROVED:

Co-Major Professor, representing Chemical Engineering

Co-Major Professor, representing Chemical Engineering

Head of the School of Chemical, Biological, and Environmental Engineering

Dean of the Graduate School

I understand that my dissertation will become part of the permanent collection of Oregon State University libraries. My signature below authorizes release of my dissertation to any reader upon request.

Matthew P Ryder, Author

ACKNOWLEDGEMENTS

Nature abhors a vacuum. As it turns out, so do research efforts. At Oregon State University I truly feel that I have been able to stand on the shoulders of giants, and like many before me, utter that one, all-encompassing word: “huh?” What has always brought me out of this stupor has been my many talented friends and colleagues both at OSU and UW, whether through lively conversation about science or philosophy, or simply enjoying the distraction of one another’s company.

I owe particularly large debt of gratitude to my mentors of almost 10 years now, Dr. Joseph McGuire and Dr. Michelle Bothwell. The former for his advocacy, kindness, and understanding, as well as his perseverance in getting ideas and love through my anatomically implausibly thick skull. To the latter for helping me on a path of deep understanding of ethics and engineering morality, and for always believing me to be more than I thought I could be.

I also thank Dr. Karl “Rat” Schilke, my first and only mentor in the laboratory. Not many people get the opportunity to see a dear friend move on in his career, and then get to work with him. His fastidiousness with regard to laboratory procedure and science in general is an inspiration, and an insurmountable goal always to be sought, rarely to be achieved.

I would be remiss if I did not acknowledge my esteemed and venerable committee members, Dr. Adam Higgins, Dr. Jeff Nason, and Dr. Deborah Pence. I had the great fortune of taking one of Dr. Higgins’ first classes, which I will never forget. Dr. Nason has always been a source of great support and kindness, and is more committed to our department than most. Dr. Pence, my graduate council representative, has believed in me from the beginning of my graduate education, and has a way of being able to always make me smile.

I extend my greatest gratitude to the multitude of students I have had the privilege to work with in the McGuire and Schilke laboratories. In no particular order: Xiangming “Kain” Wu, Greg McKelvey, Will Denton, Gershon Starr, Fallon Fumasi, Dan Cheung, Anthony Amsberry, Miranda Raper, and Ashaen Patel, to name a few. These folks helped me to grow as a mentor and a colleague, and helped pull me from the bubble of my research world to show me how much more complicated lab management can be.

I have the rare ability to say that my major advisors, mentors and committee members are not just educators, but my dear friends as well.

My person hardly stops at my research and education, and I cannot truly express how deeply and truly grateful I am for my now and future partner Elizabeth Beaudry. It is unfathomable to me that one woman can have so much patience and love for me as I traversed the landscape of graduate education, being forced to move apart for two long years. While I am extremely proud of what I have accomplished, it is her pride in me, and my fool luck to be with her that makes me smile every day.

Finally, to my loving family, my mother, who’s pride exceeds reality, my father, who’s words still resound in my head, “If you have what it takes to get a PhD, you should get a PhD.” And to my grandmother, the sun in the solar system of the Ryder family.

CONTRIBUTION OF AUTHORS

Portions of the text and figures were developed by Xiangming “Kain” Wu, whom I collaborated with extensively during my tenure here at Oregon State University, and who’s contributions appear in chapters 5 and 6 primarily through his work and analysis of Circular Dichroism (CD). Julie Auxier performed ELISA studies with fibrinogen, described in chapter 3. Greg McKelvey worked on DLS, described in chapter 5, and NMR, described in chapter 6. Miranda Raper’s contributions are shown in chapter 5 and chapter 6, where she collected interfacial tensiometry data, and CD spectra, respectively. Dr. Karl F Schilke, my co-advisor, worked on analysis, writing and submission of our work for publication, as did Dr. Joseph McGuire, my other co-advisor.

TABLE OF CONTENTS

Page

TABLE OF CONTENTS (Continued)

Page

TABLE OF CONTENTS (Continued)

Page

TABLE OF CONTENTS (Continued)

Page

LIST OF FIGURES

LIST OF FIGURES (Continued)

LIST OF FIGURES (Continued)

LIST OF FIGURES (Continued)

LIST OF FIGURES (Continued)

LIST OF TABLES

LIST OF APPENDIX FIGURES

LIST OF APPENDIX FIGURES (Continued)

LIST OF APPENDIX FIGURES (Continued)

DEDICATION

This work is dedicated to my grandmother,

Peggy Joy Ryder, who is the light at the end of every tunnel.

INTRODUCTION

Significance

Severe sepsis is a blood infection that in the US alone affects about 750,000 people each year, killing 28-50% of them.[1-3] The number of sepsis-related deaths continues to increase, and is already far greater than the annual number of deaths in the US from prostate cancer, breast cancer and AIDS combined. During bacterial growth or as a result of the action of antibacterial host factors, lipopolysaccharide (LPS, endotoxin) is released from the cell wall of Gram-negative bacteria. The high immunostimulatory potency of endotoxin causes dysregulation of the inflammatory response with elevated production and release of proinflammatory cytokines,[4] leading to blood vessel damage and organ failure.[5-7] Hemoperfusion, involving passage of blood through a sorbent device for the removal of selected targets, holds promise for treating sepsis.

A hemoperfusion device for removal of endotoxin by specific binding with the antimicrobial peptide polymyxin B (PmB) has been used clinically in Japan since 1994.[8,9] However, such devices have not been adopted elsewhere, as clinical trials have shown no significant change in either endotoxin or cytokine concentrations, or in incidence of mortality.[4,8,10] Several studies indicated that hemoperfusion results in significant depletion of both white blood cells and platelets.[11,12] PmB is covalently attached to a polystyrene fiber matrix within such devices, and it is fair to expect that immobilization in that way would strongly inhibit peptide mobility, accessibility, and activity. In addition, nonspecific loss of blood protein, platelets and cells through interaction with the otherwise unprotected polystyrene surface is a fair expectation. The clinical utility of PmB itself has been limited due to nephrotoxicity and neurotoxicity, monocyte stimulation (IL-1 release), and substantial blood protein losses during operation of devices with immobilized polymyxin.[13-15] In addition, PmB resistance among common pathogens is not rare.[16]

Cationic amphiphilic peptides (CAPs) constitute a major class of antimicrobials that provide neutrophils and epithelial surfaces with a means to rapidly inactivate invading pathogens. A number of CAPs have been shown to bind LPS with affinities comparable to PmB.[17,18] The CAP human cathelicidin peptide LL-37 has been shown to neutralize the biological activity of LPS and to protect rats from lethal endotoxin shock, revealing no statistically significant differences

between it and PmB in relation to antimicrobial and anti-endotoxin activities.[19] Despite the broad activity of LL-37 and other natural CAPs, their potency can be inhibited in the presence of physiological concentrations of NaCl and divalent cations. However the 24-residue, *de novo* engineered peptide WLBU2, a synthetic analogue of LL-37, shows highly selective, potent activity against a broad spectrum of Gram-positive and Gram-negative bacteria at physiologic NaCl and serum concentrations of Mg^{2+} and Ca^{2+}.[20-23] Moreover, WLBU2 shows greater antimicrobial activity than either LL-37 or polymyxin B, and works against a much broader spectrum of bacteria.[24,25]

The signature attribute of CAPs is their capacity to adopt an amphiphilic secondary structure in bacterial membranes, typically involving segregation of their positively-charged and hydrophobic groups onto opposing faces of (usually) an α-helix. The propensity for α-helix formation in cell membranes correlates positively with CAP activity as well as selectivity of bacterial over human cells, and WLBU2 has been optimized specifically for formation of an amphipathic α-helix conformation in cell membranes.[20-22,25] Finally, in addition to high, broad-spectrum potency in blood, WLBU2 retains potency while bound to solid surfaces[23,24,26,27] and importantly, shows high affinity for adhesion of susceptible bacteria.[24] For more information on sepsis, endotoxin and the peptides used in this work, see the Appendix.

HYPOTHESIS AND OBJECTIVES

Successful hemoperfusion for sepsis treatment requires surface modification that will ensure highly selective capture of bacteria and endotoxin that enter the interface, without evoking a host cell response, without nonspecific adsorption of protein, and without platelet activation and blood cell damage owing to surface interaction. *Our central hypothesis is that stable location of the antibacterial peptide WLBU2 at an otherwise nonfouling polyethylene oxide (PEO) brush-coated interface, in a fashion allowing peptide mobility and solvent accessibility to be largely preserved, will enable these requirements to be met.* Such a coating will show better safety and efficacy than immobilized polymyxin B in relation to endotoxin removal, and provide direction for the optimal development of hemoperfusion in the prevention and treatment of sepsis. We will test this hypothesis by meeting four experimental objectives.

Objective 1. Quantify the adsorption behavior of WLBU2, polymyxin B, and LPS on model surfaces.

To satisfy this objective, we first must ensure the quality of the surfaces used for analysis. The major method by which we will quantify these characteristics is by optical waveguide lightmode spectroscopy (OWLS) and Atomic Force Microscopy (AFM). To prepare surfaces for adsorption we first investigate appropriate cleaning methods for *ex situ* and *in situ* cleaning of the waveguiding surface. Furthermore, we describe methods for modifying surface characteristics to more closely mimic those that might be observed in a commercial application, i.e. making the surfaces positively or negatively charged, or making them hydrophobic. The second aspect of this objective is to assess the adsorption behavior of the various constituents used in this research. In particular, we assess the interaction between endotoxin and our CAPs by sequential adsorption and elution of both components, as well as by competitive adsorption. This will also be done in the presence (or absence) of common blood proteins.

Achieved through published work described in chapters 3, 4, and 5.

Objective 2. Quantify the adsorption behavior of WLBU2 and LPS at covalently stabilized PEO brush layers.

For this objective, we first investigate the stability and nature of covalently attached PEO brush layers, and quantify adsorption behavior of proteins using two model proteins: the CAP, nisin, and fibrinogen, a common procoagulant blood protein. Upon completion of the first task, we investigate the adsorption behavior of WLBU2 and LPS, sequentially and competitively. In this objective the secondary structure of WLBU2 is also assessed in order to understand the correlation between structure and adsorption behavior.

Achieved through published work described in chapter 3, and work to be submitted for publication in chapter 6.

Objective 3. Compare the interaction between LPS and covalently stabilized WLBU2, with that between LPS and covalently stabilized polymyxin B.

In this objective we begin to move toward a system more similar to what would be expected for a commercially viable hemoperfusion device. Specifically, we will covalently attach WLBU2 and PmB to waveguiding surfaces and compare their interaction with LPS in suspension.

Achieved through published work described in chapter 5, and work in chapter 6 to be published.

Objective 4. Describe the feasibility of LPS capture by WLBU2 tethered to PEO chain ends within a brush layer.

The most significant aspect of this objective is to use end group activated PEO (EGAP) to tether WLBU2 in a manner that will preserve adequate WLBU2 mobility. In this way it should be able to capture LPS without loss of WLBU2, PEO, or captured LPS. This will be accomplished through the association between WLBU2 modified to contain an –SH group and conjugated with EGAP containing a pyridyl disulfide (PDS) group. The modified peptide will be purchased, while the EGAP-PDS has been received as a gift from Allvivo Vascular Inc. These constructs will be evaluated primarily using circular dichroism (CD) and quartz crystal microbalance, with dissipation (QCM-D). Further evaluation will need to be done on the effect of γ-irradiation on peptide activity and structure.

Achieved through work in chapter 6, to be published.

The objectives described above can be summed up visually as shown in Figure 1 below.

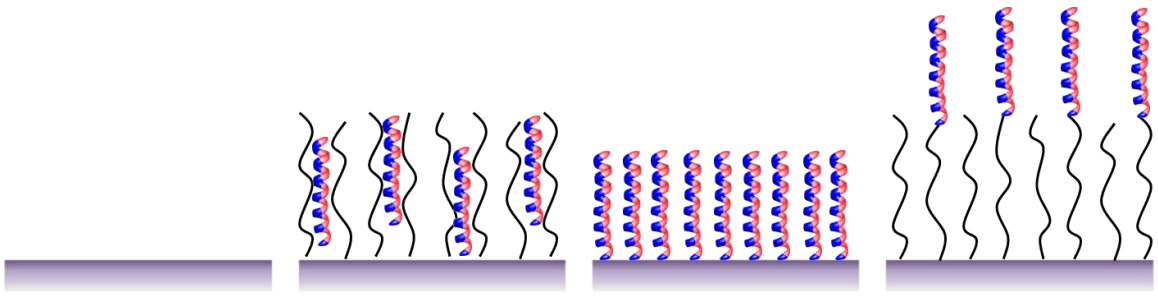

Figure 1: Visual representation of the objectives of the work presented in this document. Objectives appear in order from left to right. In each case, the primary objective is to evaluate the surface shown, and its interaction with lipopolysaccharide (LPS)

LITERATURE REVIEW

Sepsis

Sepsis is a complicated and complex clinical syndrome characterized by multiple features of systemic inflammation that results from damaging host response to infection.[5,7,28] Often described as "blood poisoning," sepsis can be caused by any type of infection,[29] resulting in 215,000 deaths every year (more than breast cancer, prostate cancer, and HIV/AIDS combined)[1] and has an associated mortality rate of 28-50%.[2,3] In 2010, experts from around the world convened at the "Merinoff Symposium," and constructed some official definitions of sepsis. The first is intended for the public and states,

> *Sepsis is a life threatening condition that arises when the body's response to an infection injures its own tissues and organs. Sepsis leads to shock, multiple organ failure and death especially if not recognized early and treated promptly. Sepsis remains the primary cause of death from infection despite advances in modern medicine, including vaccines, antibiotics and acute care. Millions of people die of sepsis every year worldwide.* [1]

Sepsis is clearly a worldwide problem, and a global call to action asks that medical and research professionals recognize this issue. One report claims that only 33% of people in the United States have ever heard the word "sepsis,"[29] yet costs of sepsis reaches almost $17 billion annually for surviving patients, costing over $22,000 per patient with an average hospital stay of nearly 20 days.[3] This problem is ubiquitous around the world, with researchers in Brazil reporting a mortality rate of 47.3% for patients with severe sepsis.[30] The costs associated with the treatment of sepsis are primarily associated with costs of intensive care units (ICUs)[31] and give an indication of how problematic sepsis really is.

As previously stated, sepsis is a complex clinical syndrome that arises from the host's response to bacterial infection, and so is not related to any one specific infective agent, but may result from ANY infection. Currently, it is estimated that roughly 60% of sepsis cases are caused by Gram-negative bacteria, while Gram-positive account for the rest.[5-7] The Merinoff Symposium provided a molecular definition of sepsis:

> *Host-derived molecules and foreign products of infection converge on molecular mechanisms that cause unbalanced activation of innate immunity. Foreign and endogenous molecules interact with pathogen recognition receptors expressed on or in cells of the immune system. Activation of pathogen recognition receptors culminates in the release of immune mediators that produce the clinical signs and symptoms of sepsis.* [1]

Generally, what this means is that sepsis typically results in a severe inflammation event that results from a dysregulation of the body's typical immune response. Upon diagnosis of sepsis, medical protocol requires three treatment methodologies: antimicrobial therapy (drugs), source control (eradication), and supportive therapy (fluids).[32] Current research in alternative therapies of sepsis focus on source control, and many of those, including the research proposed here, focus on interactions with lipopolysaccharides (LPS, endotoxin). Source control is the best option for treatment of sepsis because it, like antimicrobial therapy, it is an active response to the infection, but unlike those therapies, the technology described in this work is unlikely to lead to resistant pathogens. This is because our aim is not to kill bacteria within the human body, but merely to capture the bacteria and their fragments from solution. Further, this capture occurs at a highly conserved portion of the bacterial system, namely the Lipid A region, reducing the possibility of resistance even more. LPS comprises much of the outer membrane of Gram-negative bacteria, and is the leading cause of the disregulated immune response leading to sepsis. LPS is comprised of three main components (Figure 14).[33] The lipid A portion, which anchors the LPS molecule to the cell membrane, is the most conserved section among Gram-negative bacteria. The core oligosaccharide resides just outside the cell membrane. The O-antigen is the most diverse section of LPS and is the farthest component from the cell wall. Many therapies targeted at LPS target the Lipid A portion of LPS, as it is the most conserved, and therefore give their target therapeutic the greatest spectrum of activity. In solution, LPS tends toward the formation of vesicles (Figure 2), which in complex fluids may resemble the original bacterium. This leads us to hypothesize that the ability to capture LPS strongly suggests the same ability for whole bacterial cells.

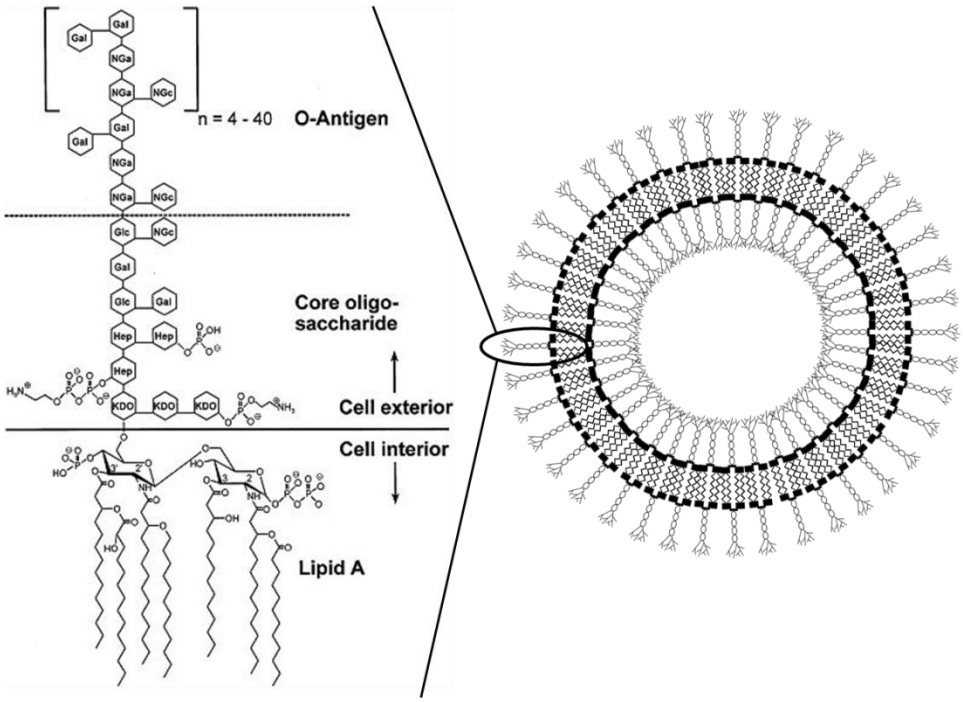

Figure 2: (Left) Schematic of LPS from *E. coli* O111:B_4. Genetic conservation increases as the molecule approaches the cell interior, with the Lipid A portion the most conserved. The image presented is for illustrative purposes only, and not to be taken as the only possible structure of LPS. Image from Petsch and Anspach (2000). (Right) Cartoon representation (not to scale) of LPS vesicle.

LPS is particularly potent because it is recognized by multiple receptors on host cells.[7] While not all diagnoses of sepsis are attributed to Gram-negative bacteria, it has been suggested that Gram-positive bacteria release "superantigenic toxins" that induce hypersensitivity to LPS, so it is still advantageous to target LPS even for infections caused by Gram-positive bacteria, or infections involving both.[7]

Nisin

Nisin is an antimicrobial peptide comprised of 34 amino acids, of which 13 undergo post-translational modification.[34] Nisin very effectively kills Gram-positive bacteria without adverse effects to mammalian cells.[35-37] Because of its broad range of activity against Gram-positive bacteria and its low toxicity in humans, nisin has been used extensively as a food preservative and is considered GRAS (generally regarded as safe) by the FDA.[35-38]

Nisin was first described in the literature in 1944 by Mattick and Hirsch,[39] but was discovered in 1933 from cultures of milk that would not grow a starter culture of bacteria to develop enough acidity for cheese-making.[40] By the early 1950s methods for growth and production of nisin using the bacterial strain *Streptococcus lactis* were described,[41] and in 1952, the substance produced was purified into a number of sub-structures, and the nisin we use today, called nisin A, was found;[42] currently nisin is purified from strains of *Lactococus lactis*.[36,37,43] The structure of nisin was finally described in 1971 by Gross and Morell (Figure 3),[34] and the rigid structure caused by lanthionine rings was revealed. Because of the lanthionine ring structures, nisin and similarly heavily modified antimicrobial peptides are classified as lantibiotics.[44,45] This name comes from "lanthionine-containing antibiotics," coined by Schnell *et al.* in 1988.[46]

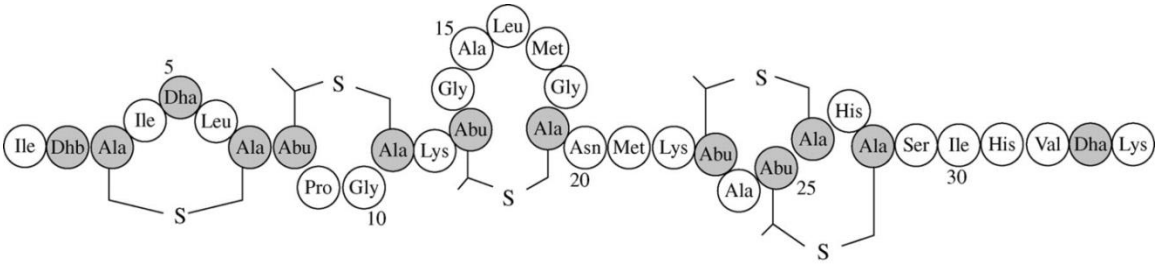

Figure 3: Structure of nisin, reprinted from Piper *et al.*[47] Nisin is comprised of 34 amino acids, 13 of which (grayed units) have undergone posttranslational modification. Typically this is a dehydration of the base amino acid, and an intramolecular addition of Cys thiols to those amino acids,[45] resulting in 5 lanthionine rings. Abu = aminobutyric acid; Dha = dehydroalanine; Dhb = dehydrobutyrine (*β*-methyldehydroalanine).[34]

The direct mechanism of action first began to be understood in 1999 by Breukink *et al*. who discovered that nisin forms pores in Gram-positive bacteria through interaction with Lipid II.[48] Later, more precise determination of exactly how nisin interacts with lipid II and then forms pores in the cell wall was discerned, and is shown in Figure 4a.[36,37,43] In 2004, the interaction between lipid II and nisin was further refined, revealing a tight interaction between nisin, indicating that the first two rings of nisin form a cage around the pyrophosphate in lipid II, shown in Figure 4b.[49]

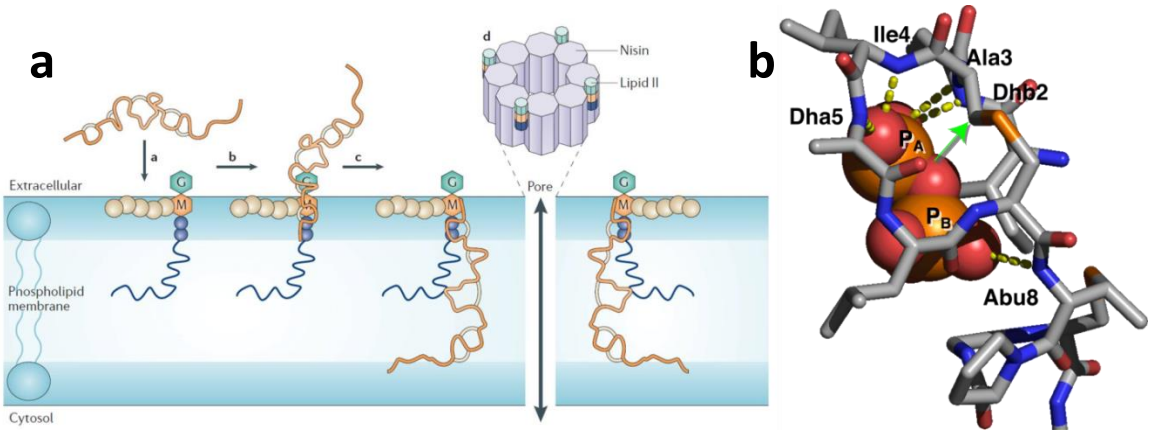

Figure 4: (a) nisin interaction with lipid II and eventual pore formation on Gram-positive bacteria. Note that it takes 8 nisin and 4 lipid II molecules to create a single pore. (b) Pyrophosphate cage: nisin (stick model) wraps around the pyrophosphate of lipid II (space-fill), like a baseball glove, using its first two lanthionine rings. Images from Breukink and de Kruijff.[50]

In 2009, researchers posited an alternative mechanism pathway for lantibiotic peptides targeting lipid II. They found that nisin and nisin mutants that could not form pores in certain bacteria remained potently bactericidal. They propose that while the lantibiotic does not form pores in that situation, they do still result in displacement of lipid II from its functional location in Gram-positive bacteria.[51]

Although nisin seems like an ideal peptide for functionalization of biomaterials, particularly for protection against common Gram-positive bacteria such as *Staphylococcus aureous* and *S. epidermidis*, nisin is not highly soluble or active in aqueous solutions at physiological pH. Furthermore, it has shown to be inactivated by common tethering techniques such as PEGylation.[52] In that study, the authors attached PEG chains to each end of the nisin molecule and found that activity was reduced effectively to zero.

Polymyxin B

Originally called "Aerosporin," Polymyxin B (PmB) is a cationic amphiphilic peptide (CAP) that disrupts the outer cell membrane of Gram-negative bacteria.[53,54] It has a molecular weight of 1301.56 Da. Generally, PmB contains ten amino acids, with seven comprising a heptapeptide ring, and most of which are 2,4-diaminobutyric acid (Dab) residues, with one D-phenylalanine in the ring structure (Figure 5).[55]

PmB was discovered in 1946 and isolated from a Gram-positive, rod shaped bacterium described as *Bacillus aerosporus*, later confirmed to be synonymous with *B. polymyxa*.[53] PmB is active against Gram-negative organisms, and was originally proposed for use as an intramuscular drug as it was shown to be effective against many genera implicated in human illness,[56] and was originally thought to be equal in chemotherapeutic activity against Gram-negative organisms as penicillin is against Gram-positive.[53] In 1971, further investigation into the fate of PmB in animal models it was discovered in rabbits that PmB accumulates in kidney and brain tissues, and is persistent for days after drug administration has ceased.[57] This accumulation of drug leads to significant neuro- and nephrotoxicity[58,59] in animal models. It is suggested that PmB binds to negatively charged phospholipids in mammalian tissues via its free amino acid groups, however the direct cause of PmB toxicity is not clear (some suggest it is due to slow degradation *in vivo* because of the D-amino acids[60]). The incidence of renal toxicity has been shown to occur in 20-25% of patients with recommended dosing, whole neurotoxicity occurs in 7.3%.[55] For this reason, PmB is rarely used for internal medicine, but because of its high affinity for Gram-negative organisms, it is still a potent antibiotic for use topically, and is in fact one of the three active ingredients in Neosporin®.[61]

The activity of PmB on Gram-negative bacteria began to be understood in the early 1970s, when researchers discovered that PmB targets lipopolysaccharides (LPS), otherwise known as endotoxin.[62,63] More specifically, PmB interacts with the Lipid A portion of LPS,[63] and a more exact mechanism of interaction was proposed by Thomas, et al in 1998.[64] In that model the LPS-PmB interaction is a two-step process, starting with a complex of the large ring (see Figure 5, left) of PmB with the outer portion of the lipid bilayer, followed by insertion of the acyl chain of PmB into the lamellar phase of the bilayer. This is illustrated in Figure 5, right.

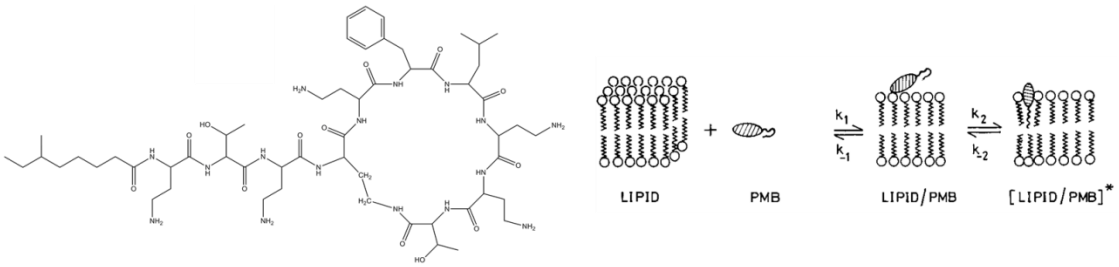

Figure 5: (left) Schematic of PmB, there are 10 total amino acids in the structure, and 7 in the ring. Most of the peptides are Dab, one is D-Phe. (right) Proposed mechanism of action of PmB. First, the heptapeptide ring approaches the hydrophilic outer membrane, then the hydrophilic tail dissolves into the bilayer structure, weakening and ultimately disrupting the cell membrane, causing cell death. Image reprinted from Thomas *et. al.*[12]

Polymyxin B for use as an antimicrobial therapeutic is further undesirable because of the rise of drug resistant strains of bacteria. Hogardt, et al. showed that 6.7%, 17.0% and 29.9 % of strains of *P. aeruginosa, S. maltophilia*, and, *A. xylosoxidans* (respectively) collected between 2000 and 2002 were resistant to PmB.[16] In the more recent literature, PmB and the closely related colistin (formerly known as Polymyxin E, differing from PmB by only one amino acid[15,55,65]) have seen a resurgence as therapeutic anti-infective agents because of the rise of multidrug-resistant Gram-negative bacteria.[15,66] Colistin and PmB have rarely been used (and so there are fewer resistant strains) because of the side effects associated. PmB has also found use as an inhibitor for LPS contamination for recombinant proteins.[67] The most relevant current use of PmB to the work presented here is Toraymyxin™ column, developed in Japan. In brief, Polymyxin is covalently attached to chloromethyl-activated polystyrene fibers in a column through one of the amino groups of the α,γ-diaminobutyric acid (Dab) residues[8,9] (seen in Figure 5 as the $-NH_2$ groups far from the ring). Despite the adoption of this technique as a treatment method for sepsis in Japan, these devices have not been adopted elsewhere due to the lack of convincing evidence of benefit.[8]

Cationic Amphiphilic Peptides and WLBU2

Cationic amphiphilic peptides (CAPs) represent an enormous opportunity for understanding and engineering antibiotic function and activity. These peptides are cationic at physiological pH, and are generally comprised of 12 to 45 amino acid residues.[68-70] These peptides can generally be categorized into a number of classes, generally organized by structure, or derivation.[69] Regardless of secondary structure, and the enormous variety of sequences and structure, these

peptides generally contain an excess of basic lysine and arginine residues (these make up the positive charge distribution) and around 50% hydrophobic amino acids.[70] This class of peptides is also considered to be ubiquitous in nature, and are considered the first line of cellular defense against potentially infectious agents.[18,71] The specific folding configuration of these peptides typically leads to well separated charged and hydrophobic domains[70] making CAPs well suited to interacting with membranes.[18,68-75] Because of their specificity toward negatively charged membranes, these peptides can have a wide spectrum of antibacterial and anti-infective activity, and provide an opportunity to engineer therapies to combat Gram-negative bacterial infection, which, prior to 1994 had not been widely studied.[75] One of the most promising therapeutic uses of CAPs is for antiendotoxin activity. CAPs are proposed to interact with LPS membranes by one of two major mechanisms that ultimately have the same result, cell death (Figure 6). In this model, proposed by Hancock and Chapple,[72] CAPs either engage the LPS vesicle directly, neutralizing the charge over a patch of the membrane and creating cracks (Figure 6 –left) or by binding to divalent cation binding sites and disrupting the membrane (Figure 6 –right).

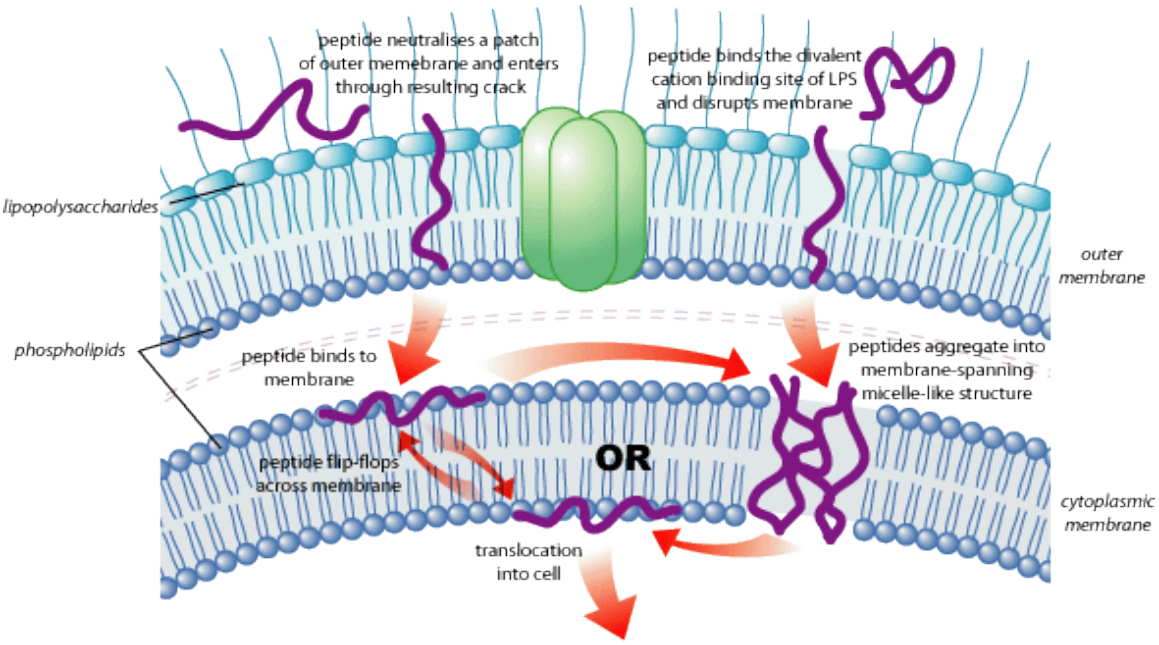

Figure 6: Proposed mechanism of CAP activity against LPS membrane and subsequent activity for cell death. CAPs either interact directly with the outer membrane, creating and entering through a resultant crack in the membrane (left), or by interaction with a cation binding site (right). Figure taken from Wilcox.[76]

In humans, there are two structurally distinct types of CAPs, β-sheet defensins and the α-helical LL-37.[77] LL-37 is of more interest of these because it shows greater spectrum and activity than the defensins. In humans, the typical concentration of LL-37 in saliva is between 2-5 μg/mL, but during infection that number increases almost 5-fold.[78,79] While the exact mechanism of activity for LL-37 has not been found, LL-37 was shown to adopt similar structural attributes to a more studied CAP, CAP-18, derived from rabbits. Both of these peptides adopt a random coil configuration in aqueous solutions, but form a straight, stable amphipathic α-helix in the presence of lipid A.[77,80] LL-37 has also been shown to protect rats against sepsis-induced mortality, but in that study they also found that LL-37 was not statistically better at protecting rats than was PmB, which is known to have toxic effects of its own *in vivo*.[19] Nevertheless, LL-37 proved to be an effective option for protecting against sepsis, and opens a window into a new breed of antibacterial therapies. Because of the broad spectrum activities of peptides like LL-37 and CAP-18, there has been a concerted effort to both discover the mechanism of interaction between CAPs and LPS, as well as to find more potent and broad spectrum CAPs for therapeutic use.

Another class of CAPs has been discussed by Mietzner and coworkers. These peptides were derived from the viral envelope of HIV-1, and are designated as lentivirus lytic peptides (LLPs).[81] These peptides were found to be structurally similar, if not in sequence, to other known CAPs and were shown to be bactericidal to both Gram-positive and Gram-negative organisms.[81] It was discovered that one of the key differences between LLPs and other CAPs was a high percentage of arginine residues but a lack of lysine residues. Furthermore, unlike other arginine rich CAPs, which often are proline rich or folded into β-sheets, these form α-helices.[81] These LLPs inspired a host of *de novo* engineered peptides that are arginine rich, are amphipathic, and form α-helices. In 2005, Deslouches *et. al.* reported on the effect of length and tryptophan substitution on engineered peptides comprised solely of arginine and valine residues called lytic base units (LBUs).[21] In that work, they found the most effective of their engineered peptides to be WLBU2 (tryptophan substituted lytic base unit 2) comprised of 24 amino acids. The structure of WLBU2 is shown in Figure 7.[82] WLBU2 shows the greatest antimicrobial potency and spectrum of the *de novo* engineered peptides tested in that work, and so has become the subject of further research.[21]

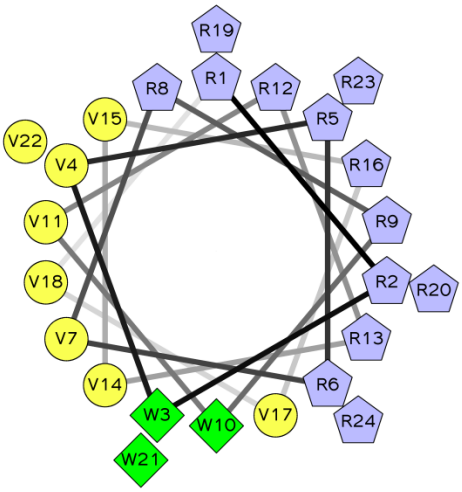

Figure 7: Helix wheel structure of WLBU2. This peptide has 24 residues, 13 Arg, 3 Trp, and 8 Val. The sequence of WLBU2 is RRWVRRVRRWVRRVVRVVRRWVRR and has a molecular weight of 3400.1 Da.

Further testing using WLBU2 in human serum and whole blood showed that WLBU2 has little cytotoxicity to mammalian cells,[20,21] and showed the ability to specifically eliminate a model Gram-negative bacteria (*E. coli*) from whole blood. These early results established the potential for WLBU2 to be used in the treatment of bacterial sepsis.[20] Further, WLBU2 showed activity in physiological salinity as compared to LL37, described previously, which had suppressed activity in the presence of human serum, and typical cations.[20] WLBU2 was then tested *in vivo* in a murine model to show its potential to prevent the progression of a *P. aeruginosa* infection to bacterial sepsis, and was shown to be effective in doses as low as 3 mg/kg.[22] PmB, on the other hand has been administered at 2.5 mg/kg (or in a 50 mg single dose), but the compound accumulates in serum, reaching concentrations upwards of 15 µg/mL.[55] Since this discovery, WLBU2 has been used investigated for its bactericidal activity against various organisms, including oral bacteria such as *S. gordonii, F. nucleatum,* or *P. gingivalus,*[83] and sexually transmitted organisms like *C. trachomatis.*[25] Most recently, WLBU2 has been shown to be able to be locally delivered using a cellulose acetate phthalate/Pluronic® blend, with retained bactericidal activity against *E. coli* and *S. gordonii*.[84] Due to its broad spectrum activity for both Gram-negative and Gram-positive bacteria, it is expected that WLBU2 interacts directly with LPS molecules (left, Figure 6), rather than through a cation binding site.

Optical Waveguide Lightmode Spectroscopy

Optical Waveguide Lightmode Spectroscopy (OWLS) is a technique used for the label free investigation of adsorption and desorption to an optical waveguiding surface. Like a similar technique, Surface Plasmon Resonance (SPR), OWLS measures the change in the refractive index of an adsorbed layer, which can be related to the adsorbed mass in that layer. Unlike SPR, OWLS does not require a so-called "noble metal," that is, a surface with mobile electrons that absorb light at a particular wavelength and angle depending on the adsorbed mass and material type on the adlayer. OWLS senses this same change in the adlayer, but relies instead on the incoupling of linearly polarized light that couples with a waveguide layer. Incoupling of laser light into thin films using similar diffraction gratings has been used since 1970,[85] while their usefulness in sensing applications was not discovered until 1984,[86] but the use of this phenomenon in a user-friendly instrument was not introduced until 1990.[87] This incoupling is a resonance phenomenon that exists at two discrete angles, one for the transverse electric (TE) mode of light, and one for the transverse magnetic (TM) mode.[87-90] A schematic for the sensor chip and principle is described in Figure 8.

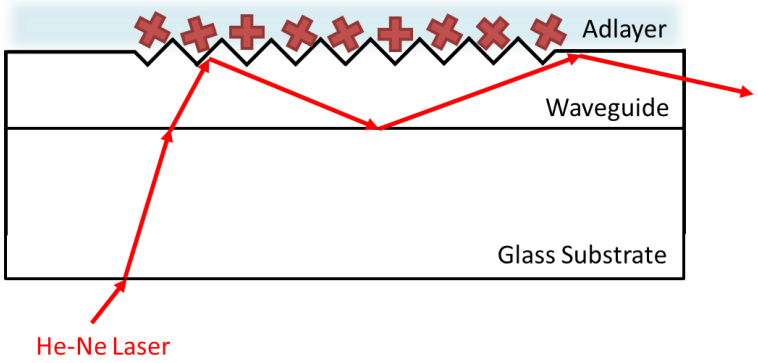

Figure 8: Sensor surface and sensing principles. Laser light (633 nm) is incoupled and sensed exiting the waveguide layer. The incoupling angle depends on the refractive layer of the adlayer, all other parameters being constant.

The incoupled light is detected by sensors at either side of the waveguide and housing, thus, light can be detected that has been incoupled at both positive and negative angles with regard to the normal surface of the waveguide. The resultant lightmode spectrum contains four peaks that are monitored in real time, and used to calculate adsorbed mass. A typical peak spectrum is shown in Figure 9. The peaks from collected by the system are very nearly identically Gaussian, as shown by Horváth *et al.*[89]

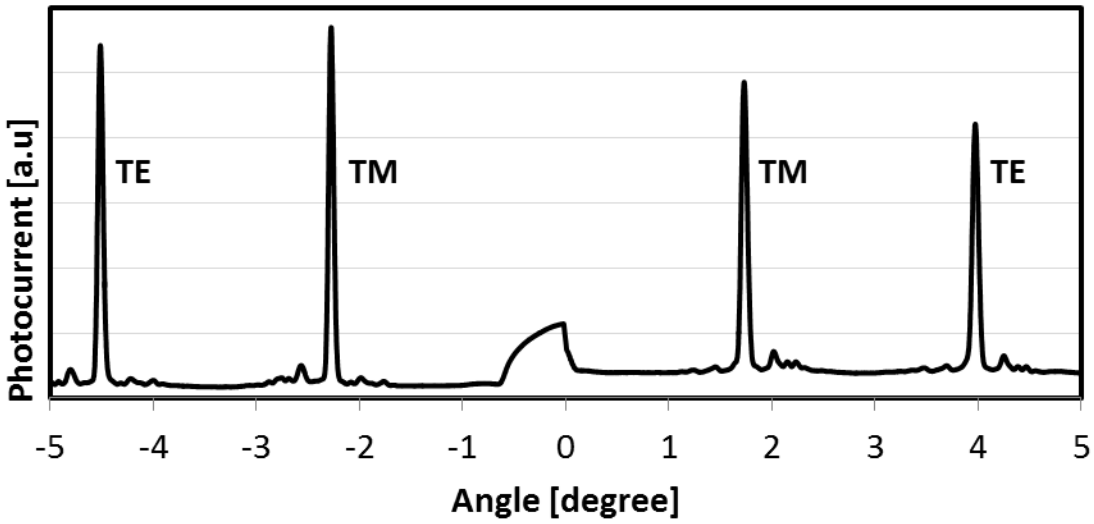

Figure 9: Typical lightmode spectra from which changes in adsorbed mass are calculated. For He-Ne laser light, the inner peaks are from the transverse magnetic (TM) mode of light, and the outer from the transverse electric (TE).

The OWLS system used in the Biomaterials and Biointerfaces lab is an OWLS 210 from MicroVaccuum, (Budapest, Hungary), and contains temperature control and the proprietary OWLS 210 optical system, reprinted from Székács *et al.*[91] in Figure 10.

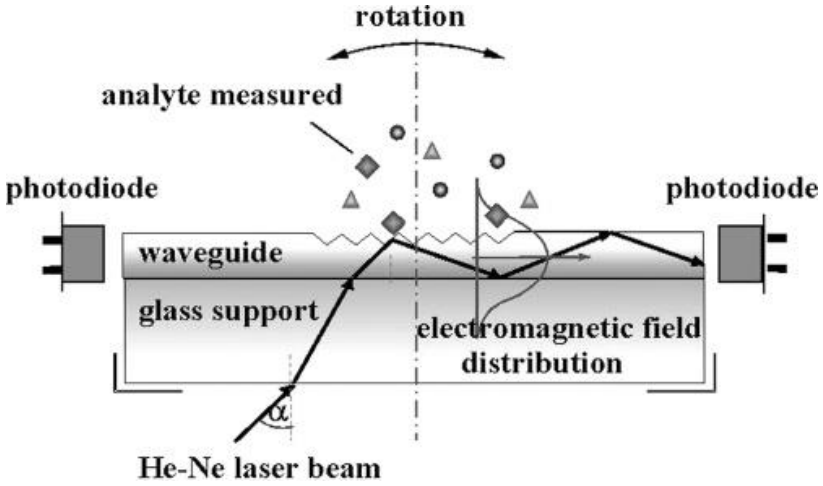

Figure 10: A profile view of the OWLS waveguide system is shown. The He-Ne source is at a fixed vertical position and the entire flow cell is rotated to vary the incident angle (α). Any analyte interacting with the waveguide surface will cause changes in the optical refractive index of that layer and be detected by changes in the incident angle required for incoupling.

By flowing solutions containing various analytes of interest through the OWLS flow chamber (~4 µL volume), we are able to deduce interactivity between analytes and surface chemistries, analytes and surface bound proteins, and any mass adsorption or desorption that happens within the sensing field of the instrument.

In brief, knowing the incoupling angles for the TE and TM modes of the incoming light from the He-Ne laser, which allows the software to calculate the effect refractive indices of those modes, and knowing constant parameters of the system, including the optical parameters of the waveguiding layer and substrate, and the refractive index of the covering medium, the thickness of the added layer can be calculated. Assuming a linear relationship between areal mass and thickness, the mass can be calculated according to the following equation.[92]

$$M = d_A \frac{n_A - n_c}{dn/dc}$$

Where M is mass (ng/cm^2), d_A is the adlayer thickness, n_A is the refractive index of the adlayer, n_c is the refractive index of the cover medium, and dn/dc is a parameter dependent on the analyte in question. Note that for proteins, dn/dc is almost universally 0.182 cm^3/g.[93,94]

Because all of these changes can be monitored in real-time, kinetic adsorption rates can be modeled for a given system if the user has an appropriate model of adsorption (or desorption), and uses a flow rate that maintains the system in the kinetically-limited regime. From this, we can gain a better understanding of the factors that contribute to increase and decreases in kinetic adsorption, as well as some sense of the affinity for analytes for a given system or surface.

Quartz Crystal Microbalance with Dissipation

Quartz Crystal Microbalance with Dissipation (QCM-D) is a technique for the label-free investigation of adsorption and desorption of molecules and analytes to a conductive material (typically Au) coated quartz crystal. Unlike OWLS and SPR, QCM-D does not rely on optics or optical properties of an adlayer, but rather works by measuring the change in the resonance frequency of the quartz crystal caused by the addition or removal of small amounts of mass to the surface. For rigid materials, such as metal oxide layers, and even small peptides, the change

in frequency can be directly related to the change in adsorbed mass by the Sauerbrey equation, developed in 1959.[95]

$$\Delta m = -C\frac{1}{n}\Delta f$$

Where *Δm* is the change in adsorbed mass, *Δf* is the change in frequency, *n* is the frequency overtone, and *C* is a constant parameter characteristic to the quartz crystal, very commonly 17.7 ng/cm^2·s.

For rigid analytes, adsorption should not change the native dissipation of the sensing surface. This can be thought of similarly to a tuning fork. When the tuning fork is struck, it resonates, creating sound waves; if layers of metal are added to the fork, the frequency may change, but the length of time the fork resonates, the dissipation of the energy, will likely remain relatively constant. Conversely, if soft material is added to the tuning fork, both the frequency and the dissipation will change. The situation is much the same for QCM-D, rigid materials do not alter the dissipation (*ΔD*), but soft, viscoelastic materials, like large proteins, etc. will increase the dissipation. By measuring both *Δf* and *ΔD*, one can get a sense of the adsorbed mass and the viscoelastic properties of the adlayer. This concept is illustrated in Figure 11 (left), reprinted from Martins *et al*.[96], along with a more technical analogue of the QCM-D analysis method is the dashpot (Figure 11, right), an electrical version of the physical methods at work in QCM-D.[97,98]

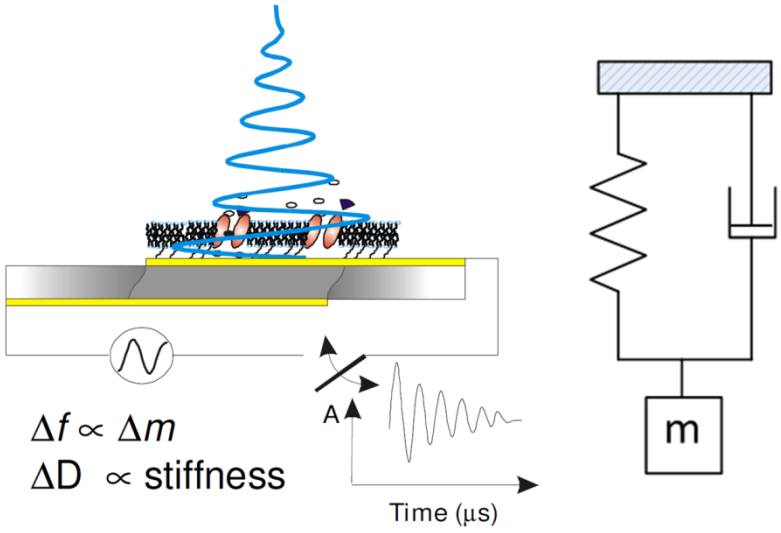

Figure 11: Graphical representation of ΔF and ΔD, image taken from Q-Sense[99] (left). Schematic of a spring-dashpot, and electrical analogue to the QCM-D sensing method (right).

Shifts in frequency and dissipation can be collected along fundamental resonance modes of the QCM-D crystal, called overtones. The fundamental frequency of the system is directly related to the properties of the QCM crystal, which will experience strong responses to frequency stimulus at every odd overtone (i.e. 1, 3, 5, etc.). Changes in frequency and dissipation along each of these overtones can also give important information about the interface during, or after adsorption. For example, if each of the shifts in frequency, when normalized to the overtone overlap identically, or nearly, this likely means the system is rigid, and can be modeled using the Sauerbrey equation. If however, a user sees substantial spreading of the frequency shifts, along with dissipation shifts, the system must likely be modeled using the Voigt viscoelastic model, represented by the schematic in Figure 11 (right). Data of each type is represented in Figure 12.

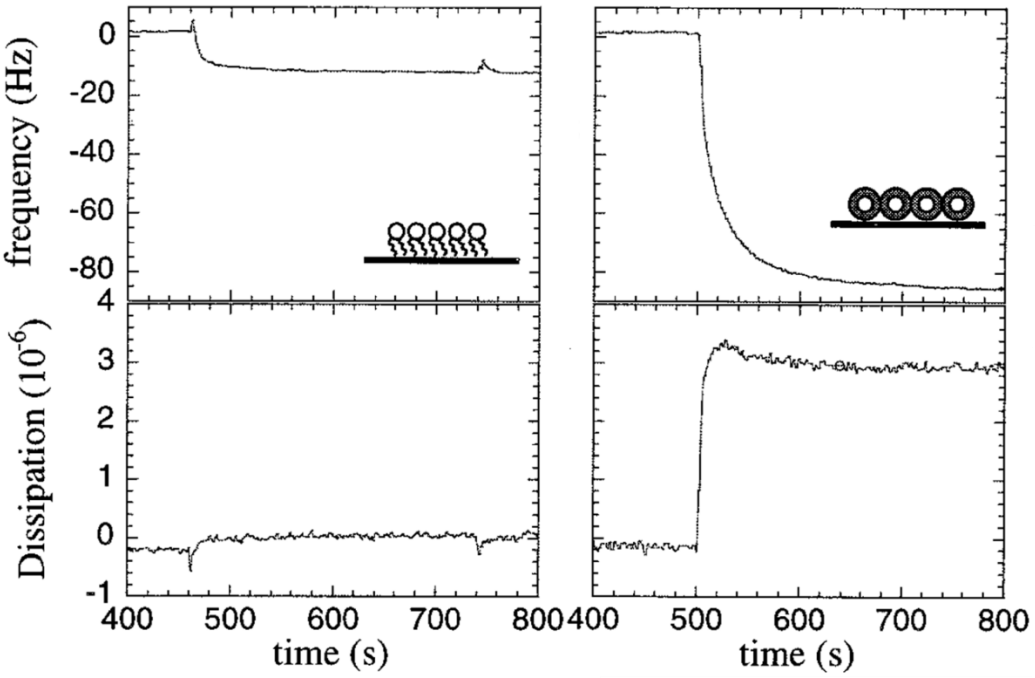

Figure 12: Representative data that can be modeled using the Sauerbrey model (left) and data requiring the Voigt model (right). Note that the dissipation does not vary much for rigid (Sauerbrey) layers. Image adapted from Keller and Kasemo.[100]

Typically, the fundamental overtone is ignored when collecting and analyzing QCM-D data. This is because the fundamental frequency collects signal from the largest radius (Figure 13, adapted from Q-Sense[99]), meaning it is the most susceptible to distortion of the crystal caused by the

flow cell, as well as changes in flow regimes. Anecdotally, the 3rd and the 5th overtones are most commonly presented in the literature.

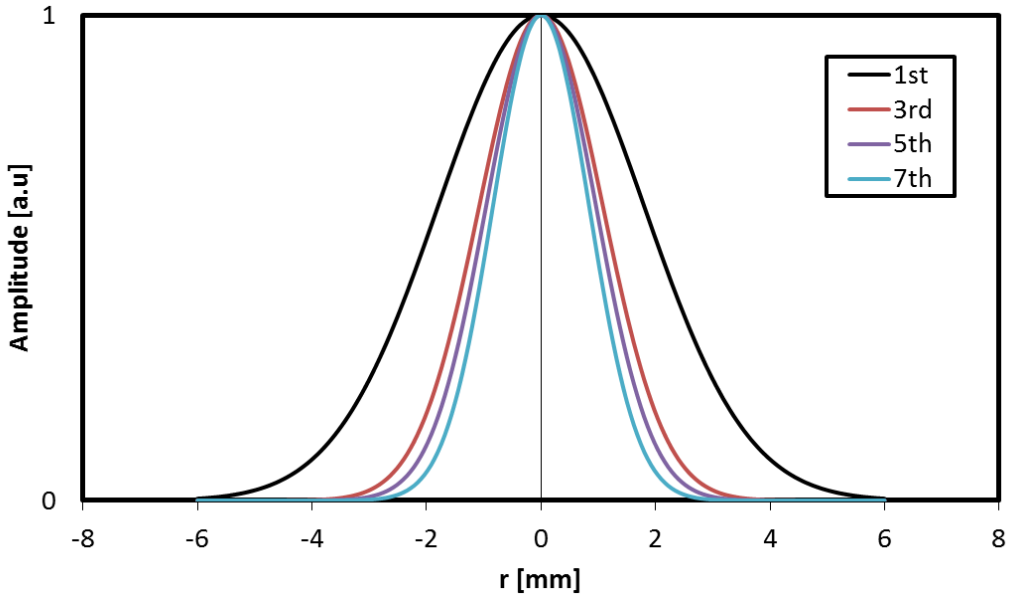

Figure 13: Normalized radial amplitude distribution for sensitivities of data collected from the various overtones. Note that the 1st overtone has the widest distribution, making it the most sensitive to edge effects and flow parameters.

Like OWLS and SPR, the data collected in QCM-D is in realtime, meaning kinetic adsorption rates can be modeled for a given system if the user has an appropriate model of adsorption (or desorption), and uses a flow rate that maintains the system in the kinetically-limited regime. From this, we can gain a better understanding of the factors that contribute to increase and decreases in kinetic adsorption, as well as some sense of the affinity for analytes for a given system or surface. Furthermore, in QCM-D, we can also begin to describe the nature of the overlayer and make claims regarding changes in physical structure upon adsorption.

The system used in the Biomaterials and Biointerfaces laboratory is a Q-Sense E4 system (Biolin Scientific, Stockholm, Sweden). This system allows for the simultaneous collection of data along four separate flow chambers (i.e. four separate sensors). These chambers can be set up in parallel or in series for analysis.

NISIN ADSORPTION TO POLYETHYLENE OXIDE LAYERS AND ITS RESISTANCE TO ELUTION IN THE PRESENCE OF FIBRINOGEN

Matthew P Ryder, Karl F. Schilke, Julie A. Auxier, Joseph McGuire, and Jennifer A. Neff

Journal of Colloid and Interface Science

www.elsevier.com/locate/jcis

Issue 350, Pages 194-199

Abstract

The adsorption and elution of the antimicrobial peptide nisin at silanized silica surfaces coated to present pendant polyethylene oxide chains was detected *in situ* by zeta potential measurements. Silica microspheres were treated with trichlorovinylsilane to introduce hydrophobic vinyl groups, followed by self-assembly of the polyethylene oxide-polypropylene oxide-polyethylene oxide (PEO-PPO-PEO) triblock surfactant Pluronic® F108, or an F108 derivative with nitrilotriacetic acid endgroups. Triblock-coated microspheres were γ-irradiated to covalently stabilize the PPO-surface association. PEO layer stability was evaluated by triblock resistance to elution by SDS, and layer uniformity was evaluated by fibrinogen repulsion. Introduction of nisin to uncoated or triblock-coated microspheres produced a significant positive change in surface charge (zeta potential) as a result of adsorption of the cationic peptide. In sequential adsorption experiments, the introduction of fibrinogen to nisin-loaded triblock layers caused a decrease in zeta potential that was consistent with partial elution of nisin and/or preferential location of fibrinogen at the interface. This change was substantially more pronounced for uncoated than triblock-coated silica, indicating that the PEO layer offers enhanced resistance to nisin elution.

Keywords: nisin adsorption; zeta potential; Pluronic® F108; PEO-PPO-PEO triblock surfactant; EGAP-NTA

Introduction

Nisin is a small (3.4 kDa) amphiphilic peptide with five lanthionine rings. It is cationic at neutral pH, due to an isoelectric point above 8.5. Nisin is an effective inhibitor of Gram-positive bacteria, including the two most frequently encountered biomaterial-associated pathogens *Staphylococcus aureus* and *Staphylococcus epidermidis*,[101-103] and holds potential for use as an anti-infective agent in medical device coatings.[104,105]

Tai et al.[106] reported results of an ellipsometric analysis of nisin adsorption and elution at surfaces coated with the PEO-PPO-PEO surfactant Pluronic® F108. Those results suggested that nisin adsorption occurred via penetration of and entrapment within the PEO layer, as opposed to adsorption onto the mobile PEO chains. It is generally understood that PEO resists protein interactions, and the protein repellent properties of the F108 layer, if retained after nisin adsorption or integration, would inhibit displacement of the antimicrobial peptide by blood proteins. In this way, nisin loading could impart an active protective function, and increase the effectiveness of such a coating. In this regard Tai et al.[107] evaluated the antimicrobial activity of nisin-loaded, F108-coated polystyrene microspheres and polyurethane catheter segments after incubation with blood proteins for up to one week. F108-coated surfaces were observed to retain more antimicrobial activity than uncoated surfaces, suggesting that the pendant PEO chains inhibited displacement or elution of nisin by contact with blood proteins.

The F108 triblocks used by Tai et al. were bound to the base substrates only by hydrophobic association of the polymer and PPO centerblock. It is thus possible that adsorbing nisin dislocated the adsorbed Pluronic at the surface, rather than being integrated into the brush layer itself. Important conclusions relating to nisin entrapment among PEO chains, as well as the enhanced resistance to elution of nisin bound in this way, have thus remained somewhat tentative. In this paper we describe the individual and sequential adsorption of nisin and fibrinogen at silanized silica surfaces coated with covalently-bound PEO-PPO-PEO triblocks. Zeta potential was recorded after protein adsorption to microsphere suspensions coated with F108, or with F108 that had been end-activated with nitrilotriacetic acid groups (EGAP-NTA).

While an abundant literature describes the protein repelling mechanisms of material surfaces presenting pendant PEO, there are very few reports describing the adsorption of small proteins to PEO layers. It has been argued that once a sufficiently high chain density is achieved, the rejection capacity of the pendant polymer phase is determined by protein size, relative to the average distance between polymer chains.[108,109] Archambault and Brash[110] suggested that grafting densities consistent with the brush configuration would be required before protein discrimination based on size would become evident. Halperin[111] formulated a model for protein adsorption in a PEO brush based on kinetic and thermodynamic considerations, and predicted two possible modes of protein adsorption: primary adsorption (at the surface itself) and secondary adsorption (at the periphery of the grafted PEO chains). Multilayer formation or integration of protein within the PEO chains is not predicted by this simplified model. However, based on surface force experiments involving compression of PEO brushes by protein-coated surfaces, Sheth and Leckband[112] suggested that polymer chains in a PEO brush may exhibit coexistence between an inner, dense, hydrophobic phase and a dilute hydrophilic phase at the outer edge of the brush. Such coexistence would give rise to an inner region "attractive" for protein adsorption. Nisin adsorption within PEO layers may thus be attributable to its high amphiphilicity, in addition to its small size.

Fang et al.[113] formulated a model for protein interaction with PEO brushes based on a generalized diffusion approach. Their model showed that adsorption and desorption kinetics depend on protein size and brush layer thickness. In particular, when the pendant chain layer thickness is greater than the size of the protein, adsorption and desorption kinetics both decrease with increasing chain length. In fact, their model indicated that the adsorption time is so large that, for any practical purpose, protein adsorption is negligible. A particularly interesting outcome of their approach was that proteins may become "trapped" between the surface and the barrier presented by the pendant chains. Increasing the chain length increases the steric barrier to elution, and the rate of protein desorption is thus decreased. Based on that result, they suggested that such a trapping mechanism could be used in the design of strategies for the controlled release of proteins from surfaces.

Some studies have shown that protein adsorption is insensitive to PEO end group chemistry while others have reported significant effects. Mathematical models of PEO in the brush configuration indicate that it is highly unlikely that end group chemistry would affect interaction with proteins. For example, Halperin[111] showed that chain ends are statistically distributed throughout the brush, with a maximum occurring at a distance about 70% of the chain length from the surface. Unsworth et al.[114] showed experimentally that protein repulsion at PEO brushes was uniquely determined by chain density, independent of chain length and end group chemistry. However, beyond a critical chain density, it was observed that brushes with –OH end groups were observed to remain nonfouling, while brushes with $–OCH_3$ end groups promoted protein adsorption. The authors suggested that the high densities of terminal methoxy groups may have resulted in increased inter-chain association and/or adsorption-induced protein denaturation. The formation of terminal $–OCH_3$ "islands" and defects in the brush layer are also predicted theoretically in a random-sequential-adsorption model advanced by Katira et al.[115]

Materials and Methods

Proteins and Surfactants

A commercial purified nisin preparation was obtained from Prime Pharma (Gordons Bay, South Africa), and was dissolved as needed in filtered (0.2 μm), 10 mM monobasic sodium phosphate solution with 150 mM NaCl. To this was added filtered, 10 mM dibasic sodium phosphate with 150 mM NaCl to bring the pH to 7.4. Fibrinogen (MW 340 kDa, Sigma-Aldrich, St. Louis, MO) was dissolved in filtered, 10 mM phosphate-buffered saline (150 mM NaCl, pH 7.4, PBS), incubated at 37 °C for 4 h with gentle mixing, and then passed through a 0.45 μm syringe filter to remove aggregates. All protein solutions were prepared immediately prior to use. BASF Pluronic® triblock surfactant F108 (PEO141–PPO44– PEO141), and an end-group activated form of Pluronic® F108, with the terminal hydroxyl groups of the PEO chains converted to nitrilotriacetic acid groups (EGAP-NTA), were obtained from Allvivo Vascular, Inc. Polyclonal anti-human fibrinogen antibodies modified with horseradish peroxidase (HRP) were purchased from U.S. Biological (Swampscott, MA). All other reagents and solvents were purchased from commercial sources, and were of the highest practical purity. All solutions and buffers were made with HPLC-grade H2O to minimize contamination.

Silica Surface Modification

Monodisperse, 1 μm silica microspheres (Fiber Optic Center, New Bedford, MA) were used as the base substrate for all zeta potential measurements. The microspheres were washed with H_2O:30% NH_4OH:30% H_2O_2 (5:1:1 v/v) at 80 °C for 10 min, followed by H_2O:37% HCl:30% H_2O_2 (5:1:1 v/v) at 80 °C for 10 min to remove organic contaminants.[106] The washed (bare) microspheres were then rinsed with H_2O three times, dried at 110 °C, and stored desiccated. The washed microspheres were modified to render the silica surfaces sufficiently hydrophobic for triblock coating with two different, vinyl-containing silanes: trichlorovinylsilane (TCVS, Aldrich, St. Louis, MO), and allyldimethylchlorosilane (ADCS, Alfa Aesar, Ward Hill, MA). In each case, bare silica microspheres were suspended in a freshly-prepared 5% (v/v) solution of either TCVS or ADCS in dry chloroform at room temperature for 3 h. The microspheres were then washed three times each with dry chloroform, dry ethanol and HPLC-grade H_2O (the residual ethanol facilitates H_2O wetting of the now-hydrophobic surface).[116] The silanized microspheres were dried overnight at 110 °C, and stored desiccated under inert gas in the dark to prevent oxidation of the vinyl groups.

Silicon wafer disks (1.0 cm^2, WaferNet, San Jose, CA) were used as the substrate for enzyme-linked immunosorbent assay (ELISA) experiments. Wafers were washed as described above, and then modified with TCVS by a vapor deposition procedure.[117] Clean, dry wafers were placed in a vapor-phase reactor to which flowing dry nitrogen was introduced for 1 h. The nitrogen stream was then passed through a reservoir containing liquid TCVS at 25 °C to entrain the silane vapor. After about two hours, the TCVS had completely evaporated (leaving a small amount of non-volatile residue), and the nitrogen was allowed to flow for another hour to purge the reactor. The TCVS-modified wafers were stored desiccated in the dark under inert gas.

Surface Coating with F108 and EGAP-NTA Triblocks

Triblocks were covalently attached to the silanized microsphere surfaces according to methods described by McPherson et al.[116] and Park et al.,[118] in which PEO-PPO-PEO triblocks were adsorbed on the hydrophobic surfaces produced by reaction of metal oxides with a vinyl silane, then subjected to γ-irradiation. Absorption of radiation or interaction with water-derived

radicals forms surface-bound free radicals, which attack the neighboring adsorbed PPO block, forming covalent bonds between the surface and polymer.[116]

TCVS-treated microspheres were coated by overnight incubation with a 0.50% solution of either F108 or EGAP-NTA triblock in PBS (the ADCS-treated samples were coated with F108 only). After incubation, some of the samples were washed three times with PBS prior to γ-irradiation; the remaining samples were kept in the 0.50% triblock coating solution. The surfactant-coated microspheres were irradiated to a dose of 0.3 Mrad by a ^{60}Co source, then washed twice with PBS. Un-irradiated triblock layers (i.e. F108/EGAP-NTA bound to the vinyl-rich microsphere surface by hydrophobic association only) served as controls for layer stability tests. The stability of the triblock/surface association was evaluated by incubation of coated microspheres with 5% SDS in PBS for 1 h to dislocate non-covalently bound surfactant. Zeta potential measurement was used to evaluate the stability of the triblock coating.

Individual and Sequential Protein Adsorption

Silanized, triblock-coated or uncoated microspheres (10% w/v) were incubated for 4 h with PBS or with PBS containing 10 mg/mL nisin or 10 mg/mL fibrinogen, then rinsed with 2 volumes of PBS. The rinsed microsphere suspensions were further incubated with PBS or with fibrinogen in PBS for 4 h. All microsphere samples were then rinsed twice with PBS to remove loosely-bound protein.

Zeta Potential Analysis

A 10 µL aliquot of a 10% microsphere suspension was diluted into 2 mL of 1 mM KCl (pH 7.55) in a disposable polystyrene cuvette. The diluted sample was then analyzed for 5 cycles of 30 recordings/cycle, using the phase analysis-light scattering (PALS) mode of a ZetaPALS system (Brookhaven Instruments Corp., Holtsville, NY).

Enzyme-linked Immunosorbent Assay (ELISA)

Flat, TCVS-modified silicon wafers were incubated with F108 (10 mg/mL in PBS) for 4 h, and irradiated in the presence of the F108 coating solution as described above. Wafers with and without F108 coatings were incubated with PBS or a 0.05 mg/mL solution of commercial nisin

(Sigma-Aldrich N5764) in PBS for 4 h. F108-coated and uncoated wafers, with and without adsorbed nisin, were then transferred to the bottoms of BSA-blocked wells in a polystyrene micro-test plate. Each sample was covered with fibrinogen (0.01 mg/mL in PBS) for 1 h, and then rinsed three times with PBS. Samples were incubated for 1 h with the HRP-labeled anti-fibrinogen antibody and rinsed again according to manufacturer's instructions (with the exception that HEPES-buffered saline with BSA was prepared in the absence of Tween 20 to reduce the possibility of elution of loosely-held fibrinogen). Bound HRP was quantified by reaction with *o*-phenylenediamine and H_2O_2 for 20 min. The reaction was quenched with sulfuric acid, and the absorbance of each sample (490 nm) used to calculate the adsorbed amount of fibrinogen.

Results and Discussion

Silanization with TCVS vs. ADCS

McPherson et al.[116] and Park et al.[118] described the covalent binding of PEO-PPO-PEO triblocks to TCVS-modified glass, metal and pyrolytic carbon surfaces by γ-irradiation. In the present study, triblock immobilization on layers formed by the monofunctional silane ADCS was also evaluated; this reagent cannot polymerize, and thus was expected to produce a smoother, more uniform layer for triblock coating than TCVS.[119] Representative zeta potential measurements of uncoated and F108-coated TCVS/ADCS-treated microsphere suspensions which were not γ-irradiated are shown in Figure 14. Surfaces treated with TCVS consistently showed less negative zeta potentials than their ADCS counterparts. We ascribe this effect to the thicker layers typically produced by polymerization of the trifunctional silane TCVS. Although coating with F108 could be expected to mask variations in surface charge (zeta potential) caused by differences in silane layer thickness, this effect was not observed (Figure 14). It is possible that the TCVS treatment leaves a relatively rough surface, which better accommodates a dense packing of the triblocks. But whether silanized by TCVS or ADCS, all un-irradiated surfaces coated with F108 exhibited a significantly more negative zeta potential upon SDS challenge, to an extent consistent with near-complete removal of the F108. The zeta potential of uncoated, silanized microspheres remained largely unchanged following treatment with SDS; this is an expected result for reversible binding of SDS on a stable surface layer.

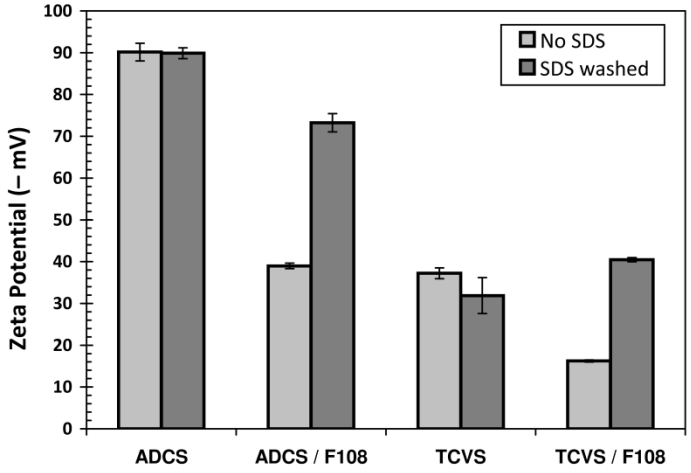

Figure 14: Effect of SDS washing on measured zeta potential of uncoated and F108-coated microsphers silanized with TCVS or ADCS. These samples were not subjected to γ-irradiation.

Representative zeta potentials for uncoated and F108-coated microsphere suspensions that were subjected to γ-irradiation are shown in Figure 15. The F108-coated microsphere suspensions were γ-irradiated either in PBS after washing three times with the same buffer ("washed"), or in the presence of the 0.50% F108 solution used for coating ("unwashed"). The washed samples (i.e. those irradiated in PBS) had a consistently more negative zeta potential than their unwashed counterparts, regardless of the silane used for pretreatment. This suggests that irradiation of silanized surfaces in the presence of F108 produced a denser, more uniform triblock coating. Moreover, the TCVS-silica samples irradiated in F108 showed essentially no significant change in zeta potential upon challenge with SDS, while those pretreated with ADCS showed a substantial negative shift upon challenge with SDS. As with the unirradiated samples (Figure 14), the zeta potential of the uncoated samples remained largely unchanged upon treatment with SDS, consistent with reversible SDS binding.

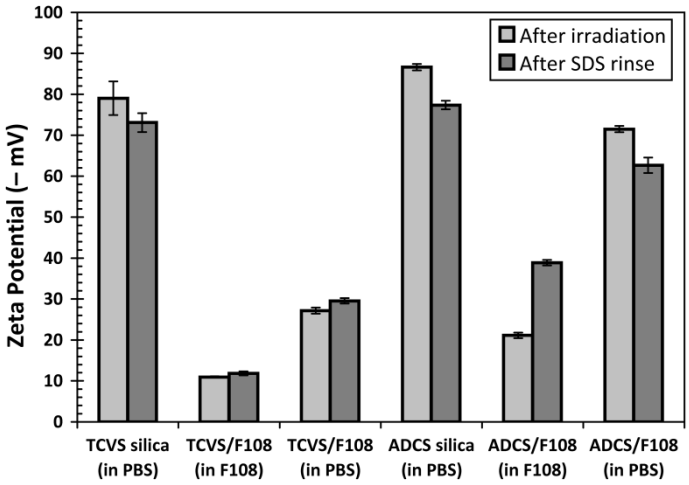

Figure 15: Effect of SDS washing on measured zeta potential of uncoated and F108-coated microspheres silanized with TCVS or ADCS, and subjected to γ-irradiation. Microspheres were irradiated either in PBS ("washed") or in the F108 coating solution ("unwashed").

The zeta potential for uncoated TCVS-treated microspheres (about -37 mV; Figure 14) became significantly more negative (about -79 mV) after γ-irradiation. McPherson et al. attribute this increase in negative surface charge density to radiation-induced loss of the vinyl-rich surface layer itself, exposing the silica substrate. However, the zeta potential of the irradiated uncoated TCVS samples was more negative than that of unmodified silica itself (-70 mV, data not shown), yet stable coatings were also formed in the presence of F108. We speculate that dissolved O_2 contributes to the radiation-induced oxidation of the vinyl C=C bonds to form ionizable, hydrophilic species.

The results of Figure 14 and Figure 15 indicate that γ-irradiation of TCVS-treated, F108-coated surfaces in the presence of the F108 coating solution produced denser, more stable F108 layers than washed or ADCS-treated surfaces. Based on these results, all triblock coatings for further individual protein and sequential adsorption experiments were produced by TCVS treatment and γ -irradiation in the triblock coating solution.

Triblock Layer Stability

Figure 16 shows the zeta potentials of TCVS-treated microspheres coated with EGAP-NTA, with and without stabilization by γ -irradiation in the presence of 0.50% EGAP-NTA in PBS. For comparison, the analogous data for F108-coated microspheres (Figure 14 and Figure 15) have

been redrawn in Figure 16. The more negative zeta potential recorded for microspheres coated with EGAP-NTA relative to F108 is attributed to the highly anionic NTA end group. But while γ - stabilization of the EGAP-NTA layer was accompanied by a change in zeta potential to a less negative value, these layers appeared to remain somewhat elutable by SDS. Experimentally, the microsphere suspensions coated with EGAP-NTA tended to resist pellet formation upon centrifugation. Following SDS challenge, the efficient washing with PBS was hindered by attempts to minimize bead loss, and so the observed high negative surface charge may be due in part to residual negatively-charged SDS near the interface.

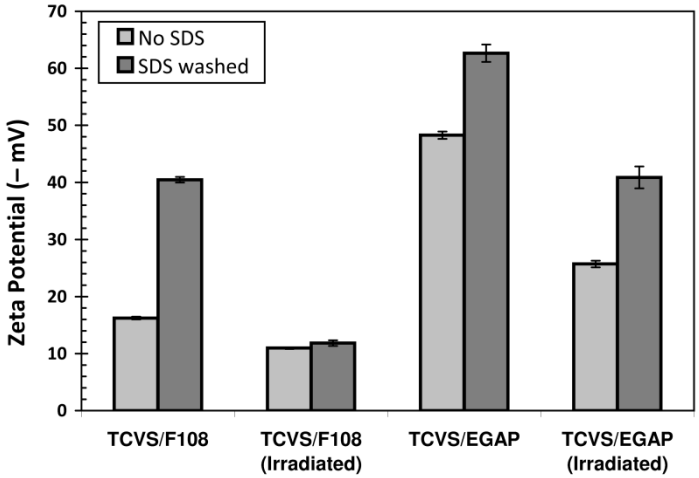

Figure 16: Effect of γ-irradiation on the resistance of F108 and EGAP-NTA layers to elution by SDS, as determined by zeta potential of TCVS-treated, triblock-coated microspheres. Microspheres were γ-irradiated in the triblock coating solution in each case.

Individual Protein and Sequential Adsorption of Nisin and Fibrinogen

Uncoated, F108-coated and EGAP-NTA-coated microspheres were incubated with nisin or with fibrinogen in independent experiments. Microsphere samples were also incubated with nisin, rinsed and then incubated with fibrinogen (sequential adsorption). Figure 17 shows zeta potential changes due to protein adsorption on uncoated surfaces. The surface charge of uncoated microspheres became positive (+30 mV) after nisin contact, consistent with adsorption of the cationic polypeptide at the surface. The high negative charge density of the uncoated microspheres remained negative, but was masked appreciably after incubation with fibrinogen, consistent with fibrinogen adsorption at the silanized microsphere surface. Fibrinogen has an isolectric point between 5.1 and 6.3, and therefore has a net negative charge at neutral pH.

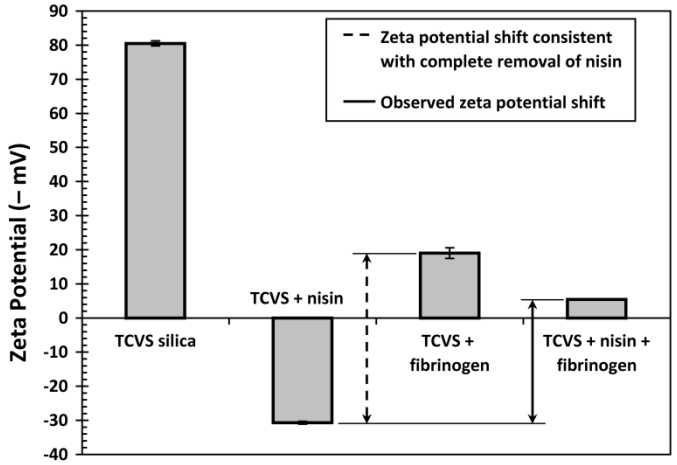

Figure 17: Zeta potential detection of protein adsorption to uncoated, TCVS-modified and irradiated microspheres incubated with nisin alone, with fibrinogen alone, and incubated sequentially with nisin followed by fibrinogen. Microspheres were γ-irradiated in PBS (i.e. no triblocks adsorbed) prior to protein contact.

The difference between the second and third bars in Figure 17 (i.e. zeta potential of nisin- and fibrinogen-contacted surfaces) quantifies a shift in potential that would be consistent with the complete replacement of nisin on a TCVS-modified surface by fibrinogen. The difference between the second and fourth bars in Figure 17 (adsorption of nisin vs. sequential adsorption of nisin and fibrinogen) is the actual (observed) shift in zeta potential. It is instructive to compare the observed shift to the maximum possible value. The positive charge density produced by incubation with nisin alone became substantially negative after subsequent incubation with fibrinogen, indicating significant removal of adsorbed nisin. In particular, contact with fibrinogen produced a shift in zeta potential equivalent to 73% of that associated with the complete removal of nisin.

Figure 18 and Figure 19 show zeta potential changes due to protein adsorption on F108- and EGAP-NTA-coated surfaces. Similar to the results just discussed, these results show that the observed surface charge density became positive after nisin contact, indicative of nisin adsorption at these PEO layers. Zeta potentials recorded after incubation with fibrinogen are in each case consistent with good fibrinogen repulsion by each type of PEO layer. The very small shift in zeta potential to a more negative value after fibrinogen contact observed with the F108 layer (Figure 18) can probably be attributed to non-uniformities in the triblock layer,[115] giving

rise to regions of unprotected hydrophobic silica that allow unhindered adsorption of fibrinogen.

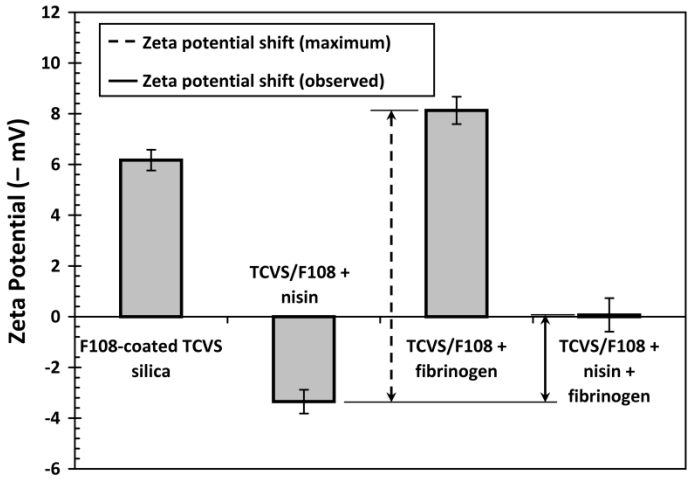

Figure 18: Zeta potential detection of protein adsorption to F108-coated, TCVS-modified microspheres incubated with nisin alone, with fibrinogen alone, and incubated sequentially with nisin followed by fibrinogen. Microspheres were γ-irradiated in F108 coating solution prior to protein contact.

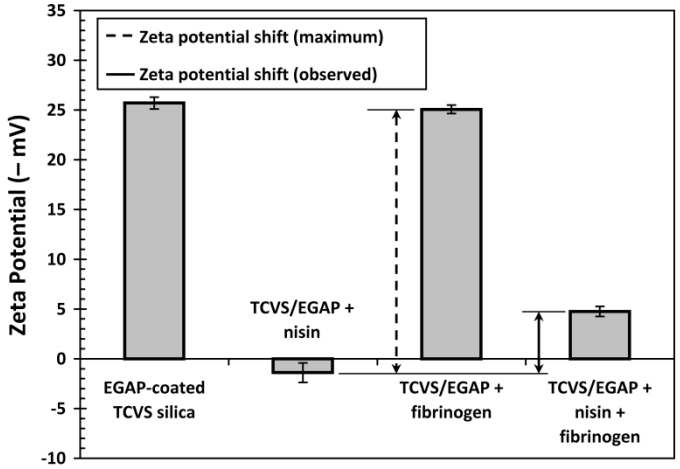

Figure 19: Zeta potential detection of protein adsorption to EGAP-NTA-coated, TCVS-modified microspheres incubated with nisin alone, with fibrinogen alone, and incubated sequentially with nisin followed by fibrinogen. Microspheres were γ-irradiated in EGAP-NTA coating solution prior to protein contact

The presence of nisin entrapped within immobilized PEO was validated in related experiments, using X-ray photoelectron spectroscopy (XPS). In those experiments, silicon wafers were made hydrophobic by treatment with octadecyltrimethoxysilane in ethanol to form a C_{18} surface coating. Triblocks with a polybutadiene centerblock (PEO-PBD-PEO) were adsorbed on these C_{18}

surfaces and immobilized by γ -irradiation as described above. In this system, the triblocks themselves contain the activated double-bonds that covalently bond with the otherwise inert C_{18}-modified surface.[116] After washing the irradiated surfaces to remove loosely-bound triblocks, the PEO brush layers were challenged with nisin in PBS, as described above, with reference to microsphere samples. After extensive washing with buffer and water to remove excess nisin, the wafers were dried under vacuum and examined by XPS (Thermo-Fisher ESCALAB 250) equipped with a monochromatic Al Kα X-ray source (1486.6 eV). Survey and high-resolution C_{1s}, N_{1s}, O_{1s}, and $S_{2s/2p}$ spectra were recorded at a take-off angle of 0°. The high-resolution peaks were quantified using Shirley background removal and the manufacturer's sensitivity factors. The C_{1s} peak was deconvoluted using the supplied peak-fitting software. A distinct C_{1s} peak was observed at 286.3 eV on the triblock-coated, irradiated surface; this binding energy corresponds to polyether C-O bonds and is consistent with a stable PEO coating. Following incubation with nisin and several washes, the PEO-coated surfaces exhibited a strong N_{1s} peak and small $S_{2s/2p}$ peaks, indicating the presence of nisin protein at the surface PEO layer. The calculated atom% ratio of N_{1s}:S_{2p} was 5.6 (data not shown), consistent with a N/S ratio of 6.0 calculated from the known composition of nisin. Although taken from a different triblock coating, these XPS results indicate that nisin can be entrapped within immobilized PEO.

Both Figure 18 and Figure 19 show that the positive charge density evident after incubation with nisin alone became negative again following subsequent incubation with fibrinogen, indicating some removal of entrapped nisin in the presence of fibrinogen. But in contrast to uncoated silica, the sequential contact with fibrinogen in these cases produced a smaller shift in zeta potential, only 30% of that consistent with the complete removal of nisin at the F108 layer, and 23% of that consistent with the complete removal of nisin at the EGAP-NTA layer.

These data indicate that nisin integrates into covalently stabilized, fibrinogen-repellent PEO layers. Moreover, we observed nisin to be substantially more resistant to elution by fibrinogen when entrapped in PEO than when simply adsorbed at an uncoated surface. If present at the interface in multilayer quantities, we should expect nisin located nearer the chain ends to be less resistant to elution than nisin located deeper within the PEO.[113] Thus the sequential adsorption results can be taken as consistent with the outermost nisin molecules being eluted

while PEO segments extending beyond the level of entrapped nisin retain their steric repulsive character. On the other hand, the results shown in Figure 17, Figure 18, and Figure 19 do not preclude the possibility of fibrinogen adsorption, presumably at regions of the nisin-loaded PEO layer where electrostatic interactions could be important and the steric repulsive capability of the PEO could be compromised, due to the presence of the peptide.

Any preferential location of a procoagulant protein such as fibrinogen at a peptide-loaded PEO layer would significantly reduce the viability of a medical device coating based on this approach. Figure 7 shows results of ELISA experiments performed with uncoated and F108-coated silica samples, in the presence and absence of adsorbed nisin. These results suggest that the presence of nisin in the PEO layer evoked a fibrinogen loading that is not substantially greater than with PEO alone. However, the presence of fibrinogen was apparent on each of the F108-coated surfaces tested. The fibrinogen detected at these surfaces may be explained by the reasonable assumption of PEO layer non-uniformities that compromise fibrinogen repulsion, but may also be an outcome of the ELISA technique itself, including difficulties associated with ensuring the absence of nonspecific adsorption by HRP-labeled anti-fibrinogen. Questions surrounding fibrinogen adsorption in this context warrant further investigation with a more direct, surface analytical approach, and will contribute to the subject of a future report.

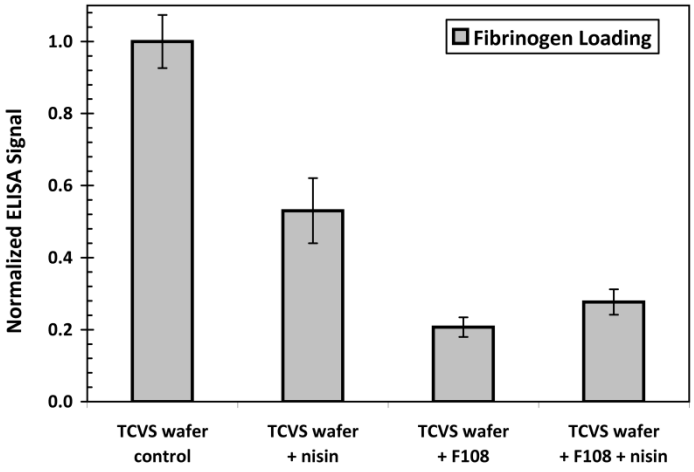

Figure 20: Relative fibrinogen adsorption on uncoated and F108-coated TCVS-modified surfaces in the presence and absence of adsorbed nisin. Uncoated surfaces were γ-irradiated in PBS prior to protein contact; the F108-coated surfaces were γ-irradiated in F108 coating solution. Values shown are normalized to the response of fibrinogen adsorbed to the uncoated, TCVS-treated silica.

Summary

Hydroxyl- and nitrilotriacetic acid-terminated PEO-PPO-PEO triblock coatings adsorbed on silica surfaces modified with TCVS and γ -irradiated in the presence of triblock solution were resistant to elution by SDS and showed good fibrinogen repulsion. Nisin adsorption to these PEO layers was detected by zeta potential measurements. Nisin appeared substantially more resistant to elution in the presence of fibrinogen when entrapped in PEO than when adsorbed at an uncoated surface. Tentatively, the sequential adsorption results reported here are consistent with the partial elution of nisin in the presence of fibrinogen, but retention of the steric repulsive quality of the layer.

Acknowledgments

This work was supported in part by the National Institute of Diabetes and Digestive and Kidney Diseases (grant no. 2 R44 DK 072560-02). The authors would like to thank the staff at Allvivo Vascular Inc. for synthesizing the EGAP-NTA used in this work, and Dr. Tom Shellhammer of OSU for use of his ZetaPALS instrument.

CLEANING REQUIREMENTS FOR SILICA-COATED SENSORS USED IN OPTICAL WAVEGUIDE LIGHTMODE SPECTROSCOPY

Matthew P Ryder, Joseph McGuire, and Karl F. Schilke

Surface and Interface Analysis

Wileyonlinelibrary.com

Volume 45, Issue 11-12, Pages 1805-1809

Abstract

Optical Waveguide Lightmode Spectroscopy (OWLS), based on the incoupling of laser light into a waveguide sensor by an optical grating, allows for the *in situ* measurement of protein adsorption. Few reports have described cleaning methods for the surfaces of such sensors, and in this investigation we compare common methods for cleaning of silica surfaces in relation to their effectiveness for cleaning silica-coated waveguide sensors used in OWLS. For this purpose AFM analysis of surface morphology and OWLS detection of protein adsorption kinetics were used to evaluate waveguide sensors before and after cleaning. While AFM line scans showed a substantial increase in average waveguide peak-to-valley height after RCA cleaning relative to all other methods tested, chemical etching owing to the alkaline component of the RCA method rendered the waveguide unusable for detection of protein adsorption with OWLS. A revised method, based on replacement of the alkaline step with immersion in SDS, was not only effective at cleaning OWLS waveguides off-the-shelf, but also showed excellent protein adsorption reproducibility after *ex situ* cleaning. Moreover, the revised method showed excellent reproducibility when applied *in situ*, between repeated adsorption-elution cycles.

Keywords: OWLS, adsorption kinetics, cleaning, RCA, AFM, waveguides

Short Title: Cleaning requirements for OWLS sensors

Introduction

Optical Waveguide Lightmode Spectroscopy (OWLS) is used to record changes in adsorbed mass during cyclic adsorption-elution experiments. OWLS relies on the use of a diffraction grating to propagate light through a waveguide film. This propagation is highly dependent on the angle of incident light, and is used to detect the effective refractive index of the guided mode, which is related to the refractive index of the covering medium.[120-123] These parameters are dependent on the properties of the chosen solvent, as well as the molecular adlayer at the interface.[120,123] Because optical sensing methods do not have chemical specificity, and they are by definition extremely sensitive to the composition of the adlayer, it is important that the waveguide surface be free of adsorbed contaminants prior to experimentation.[89]

The importance and effect of cleaning methods for optical sensing have been discussed in the literature,[124-129] but few reports describe cleaning methods on surfaces that require strict control of morphology and surface properties of a diffraction grating and there is no universally accepted cleaning protocol for use in this context.[125,129] Methods used for cleaning silica surfaces generally include solvent/acid mixtures,[125] hydrogen peroxide-based solutions,[128,129] surfactant washes,[124] and/or plasma[130-133] or UV/O_3.[134,135] Typically, for repeated use of biosensors the most important measure of cleaning success is provision of a surface enabling reproducible detection of solute adsorption.[129] As discussed by Calonder et al.,[136] in order to compare independent OWLS data sets in a quantitative way, it is important to use the same waveguiding surface each time. That is, in order to ensure good reproducibility a replicate experiment is best performed after *in situ* cleaning, as opposed to replacing with a new, repositioned waveguide after *ex situ* cleaning; it is also more economical to clean/reuse waveguides. The purpose of this investigation is to compare methods for *in situ* and *ex situ* cleaning of waveguide sensors used for detection of protein adsorption in OWLS.

Materials and methods

Solution Preparation

Bovine serum albumin (BSA) was obtained from Sigma (St Louis, MO) and dissolved in 10 mM HEPES (4-(2-hydroxyethyl)-1-piperazineethanesulfonic acid) with 150 mM NaCl, pH 7.4 (HBS buffer). The final concentration of BSA in HBS was 1 mg/mL. Buffer solutions were filtered (0.2 µm) and degassed under 700 torr vacuum for 30 min, and all other solutions were degassed for at least 30 min, immediately prior to use. Cleaning procedures tested are summarized in Table 1. All chemicals were reagent grade or better, purchased from commercial retailers, and used without further purification.

Surface Cleaning Methods

SiO_2-coated OW2400c waveguide sensors were purchased from MicroVacuum (Budapest, Hungary). Waveguides were used as provided by the manufacturer, or treated according to one of the *ex situ* cleaning methods identified in Table 1 prior to use in AFM analysis or in protein adsorption experiments in the OWLS system. Regardless of the method used, all sensor surfaces appeared completely wettable (i.e. spreading contact angle) immediately after cleaning. For this reason, contact angle was not a useful distinguishing factor in choosing a surface cleaning method.

Table 1: Summary of Cleaning Methods used in this study

Method	Steps
Chromic acid	Immerse waveguide in chromosulfuric acid at 20-25 °C for 10 min, rinse with HPLC H_2O, N_2 dry
RCA	Immerse waveguide in 1:1:5 NH_4OH:H_2O_2:H_2O at 80°C for 10 min (SC-1), H_2O rinse, 1:1:5 HCl:H_2O_2:H_2O at 80°C for 10 min (SC-2), H_2O rinse, N_2 dry
Weak RCA	Same as RCA, except with 10% (in H_2O) solutions of NH_4OH and HCl
Methanol:HCl	Immerse waveguide in 1:1 mixture of Methanol:HCl at 20-25 °C for 30 min, H_2O rinse, N_2 dry
SDS/SC-2	Immerse waveguide in 3% w/v solution of sodium dodecylsulfate (SDS) in HPLC H_2O at 20-25 °C for 30 min, H_2O rinse, 1:1:5 HCl:H_2O_2:H_2O at 80°C for 10 min, H_2O rinse, N_2 dry

Atomic Force Microscopy Measurements

AFM analysis was carried out using an Asylum Research MFP3D microscope (Santa Barbara, CA) and TAP300Al-G probes (BudgetSensors, Sophia, Bulgaria). Images (3×3 μm) were generated using intermittent contact mode; the location on the surface was chosen at random near the center of the waveguide, and scanning was performed perpendicular to the waveguide. Representative images were flattened by plane-fitting and rendered with ARgyle Light™ (Asylum Research). Line scans were used to determine an average peak-to-valley height and average roughness (RMS) was calculated from only the highest surfaces of the waveguide crests. Waveguide valleys and presumed contaminants[137] (greater than 8 nm) were masked for these calculations.

OWLS Measurements

Experiments were conducted in an OWLS 210 instrument with BioSense 2.6 software (MicroVacuum, Budapest, Hungary). A Rheodyne manual sample injector was used to inject sample solutions into a narrow-bore Tygon® flow loop (~2.0 mL) in line with the OWLS flow cell. Unless otherwise indicated, flow rates were maintained at 50 μL/min to allow for a 40 min adsorption step, and solution temperature was maintained at 20 °C by an internal temperature controller. OWLS waveguides were immersed overnight in HBS buffer prior to experimentation to equilibrate the surface with the buffer.[138] The waveguide was then removed, rinsed with H_2O, and dried with N_2 immediately before installation in the OWLS flow cell. Incident angle scans were performed from -6° to 6° at a step size of 0.1° from the surface normal. Peak angles (± TE/TM) were recorded about four times per minute. In all experiments, a stable baseline was achieved with HBS buffer prior to protein adsorption. A constant flow of BSA (1 mg/mL in HBS buffer) was introduced into the flow cell for 40 min, followed by 40 min of rinsing with HBS buffer.

For *in situ* cleaning, SDS (3% w/v in HPLC H_2O) was passed through the flow cell for 10 min at 200 μL/min, followed by 0.1 N HCl in HPLC H_2O for 10 min at the same flow rate. The flow rate was then returned to 50 μL/min, and the adsorption experiment was repeated. Adsorbed mass over time was calculated from changes in the refractive index of the adlayer, assuming a linear

relationship between refractive index and protein concentration.[93] The change in refractive index is nearly universal for proteins where dn/dc = 0.182 cm^3/g.[93,94]

Results and discussion

Choice of Cleaning Methods

Chromic acid cleaning has been the standard procedure in our lab for cleaning waveguides prior to use in the OWLS system. Chromic acid has several advantages in that it is simple, fast, and has been used extensively for cleaning of surfaces. Unfortunately, the reagent is highly corrosive, and contains toxic and carcinogenic Cr(VI) compounds. Chromic acid is thus expensive to dispose of properly, and use of the method can lead to surface contamination with chromium.[128]

The RCA method is a standard cleaning method for silicon substrates. It is more complicated than chromic acid, but it is less hazardous, chemical safety is easier to manage, and it is reliable. The RCA cleaning method[139] is comprised of two major steps, (i) removal of organic materials with hot NH_4OH, H_2O_2, and water (RCA standard clean 1, or SC-1), and (ii) removal of ionic and remaining contaminants with hot HCl, H_2O_2, and water (SC-2).[128] Initially our goal was to compare these two cleaning methods using AFM and OWLS. The methanol/HCl method[125] has been used for cleaning OWLS waveguides, and was also tested in this work. While AFM showed that MeOH/HCl cleaned an off-the-shelf waveguide with generally acceptable results (data not shown), there is no reason to expect it would be effective at removing adsorbed protein and other organic material from the waveguides after use, and it was not considered for further study. Other methods, not represented in Table 1, were also considered for comparison but ultimately not tested. These included Nocromix® and similar methods, which require strong sulfuric acid and include proprietary mixtures that are still hazardous and no data is available on their components. Piranha solutions (H_2O_2/H_2SO_4) were excluded because they are stronger, more hazardous versions of those used in the RCA method, and have been shown to present problems on common sensing surfaces such as gold.[131] Plasma treatment was also not tested because it has been shown to modify surface characteristics of polymer surfaces commonly used for optical sensing techniques.[140,141] Furthermore, plasma has been used to modify hydrophobic surfaces for improved cell adhesion,[142,143] and so was not deemed an appropriate

cleaning method. UV/O_3 was used in initial tests, but was ultimately excluded because surfaces did not appear to be improved by the process (data not shown), and UV radiation has been used to graft polymers to hydrophobic surfaces through UV-induced surface modification,[119] so as with plasma treatment, was deemed inappropriate for cleaning.

AFM analysis constitutes a fairly comprehensive means of assessing the general cleanliness of OWLS sensors, as (i) peak-to-valley height, (ii) roughness, and (iii) contamination of each waveguide can be assessed. AFM images were collected prior to and after cleaning of each waveguide and each cleaning method, and representative data are shown in Figure 21 for the RCA and chromic acid methods. Roughness was calculated by considering only the peaks of the waveguides (lighter portions seen in Figure 21). Chromic acid treatment caused a 0.19 nm decrease in roughness, while RCA caused an increase of 6.92 nm. This apparent shortcoming caused by the RCA method was overcome by a substantial increase recorded for peak to valley distance (22.9 nm), which was decreased as a result of chromic acid cleaning by 0.57 nm. Line scans across the waveguiding surface were averaged over the entire AFM image, and the average angle of the waveguide sides was calculated over all repeats in the line scan. For uncleaned waveguides, the average wall angle was 2.8° ± 0.6° from parallel. The CrO_3 cleaned waveguide had a similar angle of 1.8° ± 0.3°. However, after RCA cleaning, the average angle increased to 21.6° ± 1.5°, indicating etching of the waveguide surface. This change in the waveguide surface normal (and hence incoupling angle) is likely the cause of the substantial peak shift shown in Figure 22.

Protein Adsorption

We next compared the rate and extent of BSA adsorption on waveguides cleaned by each method. OWLS measures changes in the incoupling angle of light entering a waveguide upon adsorption of protein at the interface. These peak shifts, which are typically small, are correlated to total adsorbed mass. With the waveguide cleaned by the RCA method, we recorded an unanticipated, substantial peak shift from 4° to 0.5°, and a change in peak intensity of two orders of magnitude (Figure 22). These shifts result in an inability to correlate peak positions to adsorbed mass, rendering the RCA method entirely inappropriate for use on OWLS waveguides.

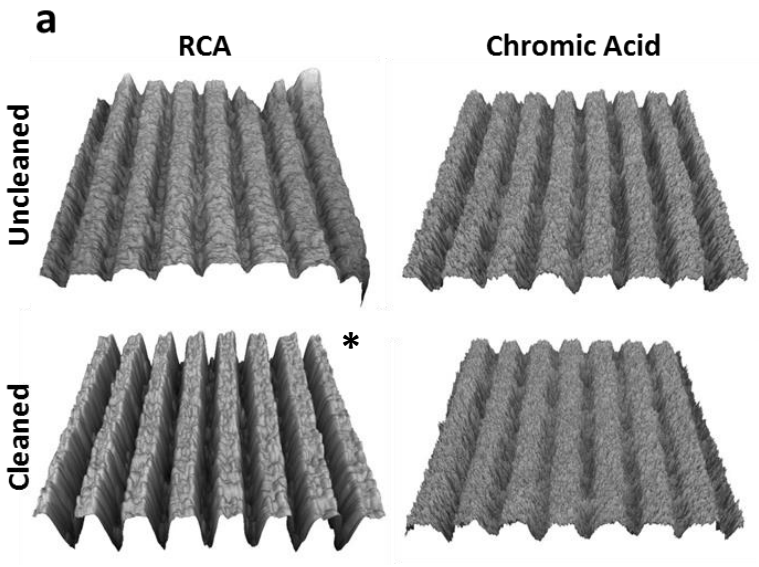

Figure 21: Morphology of uncleaned (top) and cleaned (bottom) waveguides. The RCA method (left) increased the peak-to-valley distance by 22.94 nm but increased roughness by 6.92 nm. The chromic acid method (right) decreased the peak-to-valley distance by 0.57 nm and decreased roughness by 0.19 nm. All images are of 3x3 µm square areas, with a height range of 15 nm (except * which has a height range of 60nm).

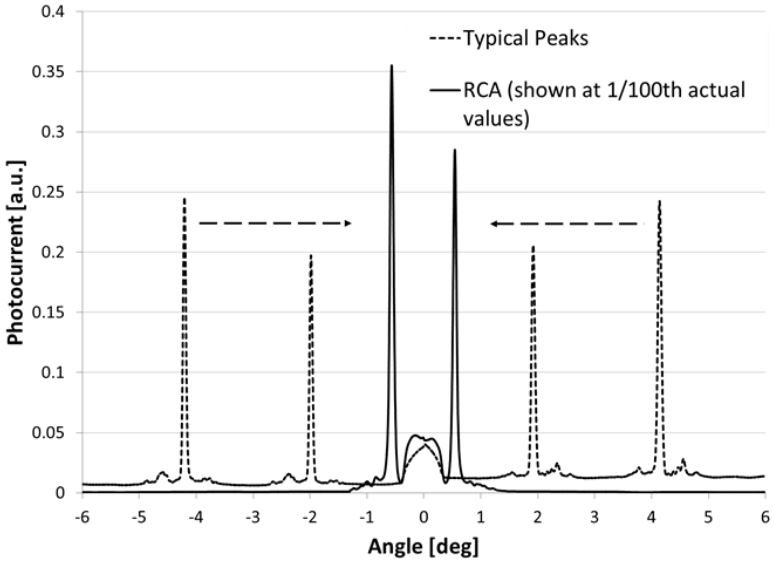

Figure 22: OWLS peak shift from 4° to 0.5° on RCA-treated waveguide. The shift in peak positions toward the center prevents correlation of mass adsorption to peak position. The RCA peaks are much more intense than peaks on untreated waveguides, and are shown at reduced scale to compare to typical peaks.

Chemical etching caused by base-acid methods similar to RCA has been attributed to the SC-1 cleaning step.[127] In an attempt to avoid the unacceptable peak shifts associated with base-acid methods, we modified the method to use substantially lower acid and base concentrations in a "weak RCA" method (1.4% acid/base vs. 14% in original SC-1/SC-2 method).

However, this weak RCA method showed characteristic peak behavior similar to that recorded with RCA and the method was not pursued further. Because the alkaline cleaning step is most often regarded as the cause of etching,[127] it was replaced with SDS. This replacement (SDS/SC-2) resulted in a decrease in roughness of 0.43 nm and a slight increase in the peak-to-valley distance from 5.24 to 5.46 nm (data not shown). Considering all cleaning methods tested, the average off-the-shelf roughness and peak-to-valley distance was 1.02 ± 0.36 nm and 3.85 ± 2.32 nm, respectively. Importantly, we recorded no evidence of large peak shifts that would lead to loss of signal in OWLS. Thus, we compared BSA adsorption on waveguides cleaned with chromic acid or SDS/SC-2, as detected by OWLS.

After the initial adsorption and elution of BSA, the waveguides were removed for *ex situ* cleaning by the same method initially used to clean the waveguide, and re-evaluated with AFM. Both cleaning methods resulted in a comparable decrease in surface roughness (0.25 nm), however the chromic acid method showed a decrease in the peak-to-valley distance of 0.18 nm while the SDS/SC-2 method showed an increase of 1.70 nm. After this *ex situ* cleaning the waveguides were used for a second BSA adsorption-elution cycle. Figure 23 shows the adsorption kinetics recorded for each of these cycles. The adsorption plateau recorded after cleaning with the SDS/SC-2 method is substantially greater than that recorded after cleaning with chromic acid. This is consistent with the presence of unremoved contaminants on the chromic acid treated waveguides. In addition, the initial slope of the protein adsorption kinetics is not only greater, but also more consistent between trials for the SDS/SC-2 cleaned waveguide in relation to the chromic acid cleaned waveguide (Figure 23). This reproducibility between adsorption and elution cycles with *ex situ* cleaning, and the absence of any chemical etching apparent in the SDS/SC-2 method suggests it would also be effective for cleaning sensors *in situ*. Colander et al. highlight the importance of *in situ* cleaning,[136] finding the reproducibility of adsorption characterized by standard deviations of the absolute rate curves to be less than 2%.

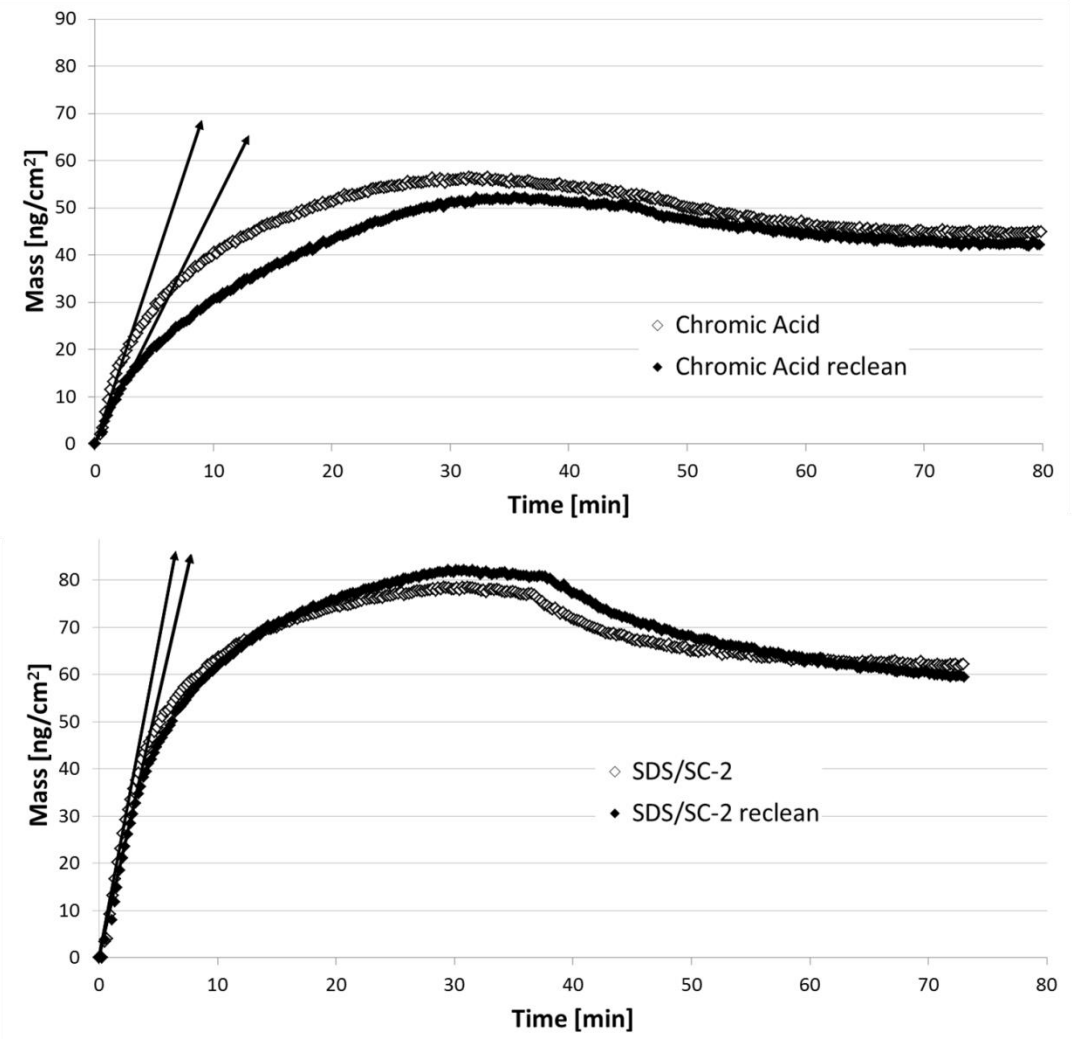

Figure 23: (Top) Adsorption and elution profile of BSA in 10 mM HBS buffer on a waveguide cleaned with chromic acid (◇), and then cleaned again with the same method after the first experiment (◆). (Bottom) Adsorption and elution profiles of BSA on waveguides cleaned with SDS/SC-2. The difference in the initial rates of adsorption on the chromic acid cleaned waveguides (arrows, top) suggests incomplete removal of protein from the waveguide surface. In contrast, BSA adsorbs to a greater extent and with better reproducibility on the SDS/SC-2 cleaned waveguide (top) than the chromic acid-cleaned waveguide (bottom).

As passing H_2O_2 at high temperature through the OWLS flow cell is not desirable for safety reasons, the SDS/SC-2 cleaning procedure was further modified for *in situ* application to eliminate hot H_2O_2. In this case, we introduced 3% SDS to the system at 200 µl/min for 10 min, then 0.1 N HCl at the same rate for the same period of time at 20 °C. BSA adsorption-elution

curves before and after *in situ* cleaning are quite similar (Figure 24), indicating that the waveguide was effectively cleaned by our *in situ* SDS/SC-2 method.

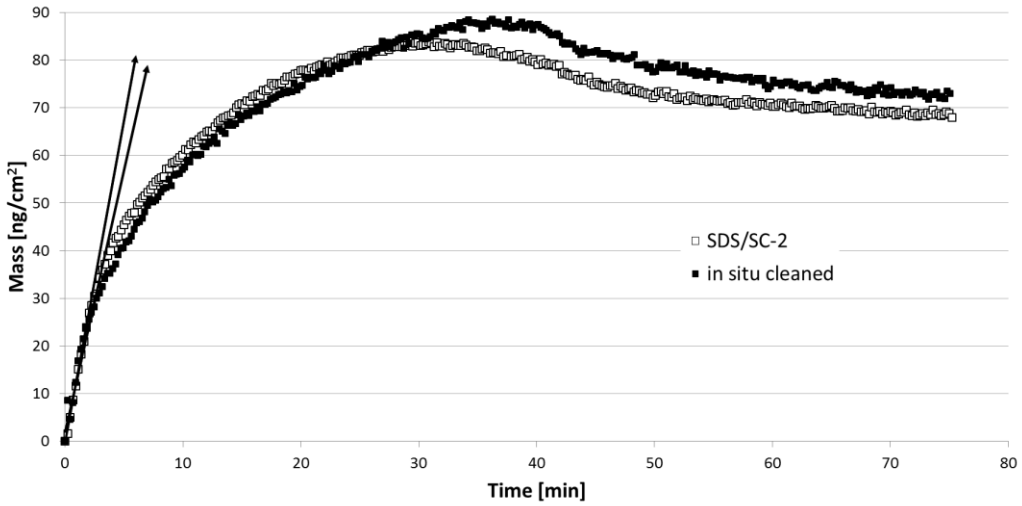

Figure 24: Adsorption of BSA on a SDS/SC-2 cleaned waveguide (□), followed by an *in situ* cleaning using SDS and HCl, and a final adsorption and elution of BSA on the same waveguide (■). The overall adsorption profile on the *in situ* cleaned waveguide is consistent with the original adsorption profile, indicating effective regeneration of the original waveguide surface.

Conclusions

AFM analysis of surface morphology and OWLS detection of protein adsorption kinetics were used to compare a chromic acid cleaning procedure for silica-coated OWLS waveguides with the RCA method commonly used for silicon substrates. Chemical etching caused by the alkaline cleaning step of the RCA method rendered the waveguide inappropriate for use in OWLS, leading to replacement of that step with immersion in SDS. The revised method (SDS/SC-2) was determined effective at cleaning OWLS waveguides off-the-shelf, and showed excellent protein adsorption reproducibility after *ex situ* and *in situ* cleaning of the waveguide. This cleaning method is safer than the other methods tested and might also be effective for cleaning surfaces used in other optical techniques. The SDS/SC-2 method was also tested on quartz QCM-D sensors carrying thin, patterned gold electrode overlayers (Q-Sense, Sweden). The gold electrodes were almost completely removed by the SC2 portion of the cleaning procedure, rendering the sensors useless. The SDS/SC-2 method presented herein is therefore not recommended for use on sensors which rely on thin coatings of noble or other metals (e.g.

QCM, SPR). Although substitution of other acids (e.g. nitric) in the SC-2 step may prevent damage to metal coatings, it is highly recommended that the method be carefully tested with model surfaces before using it to clean actual sensors.

Acknowledgements

The authors thank Dr. Ethan Minot of the OSU College of Physics for use of his AFM instrument. This work was supported in part by the National Institute of Biomedical Imaging and Bioengineering (NIBIB, grant no. R01EB011567). The content is solely the responsibility of the authors and does not necessarily represent the official views of NIBIB or the National Institutes of Health.

BINDING INTERACTIONS OF BACTERIAL LIPOPOLYSACCHARIDE AND THE CATIONIC AMPHIPHILIC PEPTIDES POLYMYXIN B AND WLBU2

Matthew P Ryder, Xiangming Wu, Greg R. McKelvey, Joseph McGuire, Karl F. Schilke

Submitted to Colloids and Surfaces B: Biointerfaces

www.elsevier.com/locate/colsurfb

Abstract

Passage of blood through a sorbent device for removal of bacteria and endotoxin by specific binding with immobilized, membrane-active, bactericidal peptides holds promise for treating severe blood infections. Peptide insertion in the target membrane and rapid/strong binding is desirable, while membrane disruption and release of degradation products to the circulating blood is not. Here we describe interactions between bacterial endotoxin (lipopolysaccharide, LPS) and the membrane-active, bactericidal peptides WLBU2 and polymyxin B (PmB). Analysis of the interfacial behavior of mixtures of LPS and peptide using air-water interfacial tensiometry and optical waveguide lightmode spectroscopy strongly suggests insertion and stabilization of intact LPS vesicles by the peptide WLBU2. In contrast, dynamic light scattering (DLS) studies show that LPS vesicles appear to undergo peptide-induced destabilization in the presence of PmB. Circular dichroism spectra further confirm that WLBU2, which shows disordered structure in aqueous solution and substantially helical structure in membrane-mimetic environments, is stably located within the LPS membrane in peptide-vesicle mixtures. We therefore expect that presentation of WLBU2 at an interface, if tethered in a fashion which preserves its mobility and solvent accessibility, will enable the capture of bacteria and endotoxin without promoting reintroduction of endotoxin to the circulating blood, thus minimizing adverse clinical outcomes. On the other hand, our results suggest no such favorable outcome of LPS interactions with polymyxin B.

Introduction

Severe sepsis is a blood infection that in the US alone affects about 750,000 people each year, killing 28-50% of them.[5,7,144] The number of sepsis-related deaths continues to increase, and is already greater than the annual number of deaths in the US from prostate cancer, breast cancer and AIDS combined. During bacterial growth or as a result of the action of antibacterial host factors, lipopolysaccharide (LPS, endotoxin) is released from the cell wall of Gram-negative bacteria. The high immunostimulatory potency of endotoxin causes dysregulation of the inflammatory response with elevated production and release of proinflammatory cytokines,[145] leading to blood vessel damage and organ failure.[5,7]

Hemoperfusion, involving passage of blood through a sorbent device for the removal of selected targets, holds promise for treating sepsis.[8,14,146] Toraymyxin™, a commercial hemoperfusion device, has been used clinically in Japan since 1994 for removal of endotoxin by specific binding with the immobilized antimicrobial peptide polymyxin B (PmB), and was introduced to the European market in 2002.[147] However, such devices have not been widely adopted elsewhere, as clinical trials have shown little significant change in either endotoxin or cytokine concentrations, or in incidence of mortality [8,148]. Several studies further indicated that hemoperfusion results in significant depletion of both white blood cells and platelets.[12,149] PmB is covalently attached to a polystyrene fiber matrix within such devices, and it is fair to expect that immobilization in that way would strongly inhibit peptide mobility, accessibility, and activity.[27,150,151] In addition, nonspecific loss of blood protein, platelets and cells through interaction with the otherwise unprotected polystyrene surface is likely. The clinical utility of PmB itself has been limited due to nephrotoxicity and neurotoxicity, monocyte stimulation (IL-1 release), and substantial blood protein losses can occur during operation of devices with immobilized PmB.[13,14,146,152] In addition, PmB resistance among common pathogens is not rare.[16] Successful hemoperfusion for sepsis treatment will require surface modification that will ensure highly selective capture of bacteria and endotoxin that reach the interface. In addition, surface coatings must provide pathogen binding functionality without evoking a host cell response, without nonspecific adsorption of protein, and without platelet activation and blood cell damage caused by cell-surface interactions.

Cationic amphiphilic peptides (CAPs) constitute a major class of antimicrobials that allow neutrophils and epithelial surfaces to rapidly inactivate invading pathogens.[70,73] A number of CAPs have been shown to bind LPS with affinities comparable to PmB.[153,154] For example, the CAP human cathelicidin peptide LL-37 has been shown to neutralize the biological activity of LPS and to protect rats from lethal endotoxin shock, revealing no statistically significant differences in antimicrobial or anti-endotoxin activities between LL-37 and PmB.[155] Despite the broad activity of LL-37 and other natural CAPs, their potency is inhibited in the presence of physiological concentrations of NaCl and divalent cations. However the 24-residue, *de novo* engineered peptide WLBU2, a synthetic analogue of LL-37, shows highly selective, potent activity against a broad spectrum of Gram-positive and Gram-negative bacteria at physiologic NaCl and serum concentrations of Mg^{2+} and Ca^{2+}.[22,23,156,157] Moreover WLBU2 shows greater antimicrobial activity than either LL-37 or PmB, and is active against a much broader spectrum of bacteria.[158,159]

A major distinguishing feature of CAPs is their capacity to adopt an amphiphilic secondary structure in bacterial membranes, typically involving segregation of their positively-charged and hydrophobic groups onto opposing faces of an α-helix.[70] The propensity for α-helix formation in cell membranes correlates positively with CAP activity and selectivity of bacterial over human cells, and WLBU2 has been optimized specifically for formation of an amphipathic α-helix conformation in cell membranes.[22,156,157,159] Finally, in addition to its broad-spectrum antimicrobial activity in blood, WLBU2 retains potency while bound to solid surfaces[23,26,27,84,158] and importantly, shows high affinity for adhesion of susceptible bacteria.[158]

In this paper we describe the outcomes of a comparative study of molecular interactions of WLBU2 and PmB with LPS. Analysis of the competitive adsorption behavior of peptide and LPS recorded with optical waveguide lightmode spectroscopy (OWLS) and interfacial tensiometry, and analysis of peptide structure and particle size distribution in peptide-vesicle suspensions with circular dichroism (CD) and dynamic light scattering (DLS), were used to evaluate differences in the stability of peptide-vesicle association, and hence the associated potential of each peptide for use in hemoperfusion for endotoxin removal.

Materials and Methods

Peptides and Lipopolysaccharides

Unless otherwise specified, all reagents were purchased from commercial vendors and were of analytical reagent or higher grade. WLBU2 (RRWVRRVRRWVRRVVRVVRRWVRR, 3400.1 Da) was obtained from GenScript (Piscataway, NJ). Polymyxin B sulfate (PmB, 1385.6 Da) and purified *Pseudomonas aeruginosa* lipopolysaccharide (LPS) were purchased from Sigma-Aldrich (St Louis, MO). All solutions were prepared using HPLC-grade water, and all peptides and LPS were used as received, without further purification.

Stock solutions of WLBU2 were made in phosphate buffered saline (PBS, 10 mM sodium phosphate with 150 mM NaCl at pH 7.4), or in 0.5M $HClO_4$ for circular dichroism. Working solutions at 50 µM or 5 µM concentrations were prepared in degassed PBS, using the calculated molar extinction coefficient at 280 nm (16,500 $M^{-1}\,cm^{-1}$) of WLBU2.[160] Similarly, 10 mg/mL stock solutions of PmB in degassed PBS were diluted to 50 µM or 5 µM. LPS was dissolved in PBS to 10 mg/mL, and diluted to 0.1 mg/mL in degassed PBS. All dilute peptide/LPS solutions were prepared and degassed under vacuum with sonication immediately before use.

Surface Modification of OWLS Sensors

SiO_2-coated OW2400c OWLS waveguides (MicroVacuum, Budapest, Hungary) were cleaned by submersion in 5% w/v sodium dodecyl sulfate (SDS) for thirty minutes, followed by 10 min at 80 °C in 5:1:1 H_2O:27% HCl:30% H_2O_2, then rinsed with HPLC H_2O and dried under a stream of N_2.[161] Cleaned waveguide surfaces were modified with trichlorovinylsilane (TCVS, TCI America, Portland, OR) by a variation of the method of Popat.[162-164] Briefly, clean OWLS sensors were exposed to flowing dry N_2 in a sealed vessel for 1 hr to remove any residual surface moisture, after which 200 µL of TCVS was added and allowed to vaporize at 25 °C, while flowing N_2 transported the TCVS vapor across the waveguide surfaces. The N_2 flow was maintained for three hours, after which the sensors were cured at 120 °C for 30 min to stabilize the vinylsilane layer. Cleaned and modified sensors were stored in 1.5 mL centrifuge vials under N_2 in the dark to prevent oxidation of the vinyl moieties.

Optical Waveguide Lightmode Spectroscopy

Silanized waveguides were equilibrated prior to use by incubation overnight in PBS,[165] then rinsed with HPLC H_2O, dried with N_2, and immediately installed in the flow cell (4.8 uL total volume) of a MicroVacuum OWLS 210 instrument (Budapest, Hungary) equipped with a 4 mL narrow-bore Tygon® flow loop in line with the flow cell. Incoupling peak angles (±TE and TM) were recorded about four times per minute at 20 °C, and a stable baseline was achieved with PBS prior to the injection of peptide or LPS. Unless otherwise indicated, flow rates were maintained at 50 µL/min during adsorption and elution steps. Peptides or LPS were either introduced singly (sequential adsorption) for 40 min, with a PBS rinse for 40 min between analytes, or as mixtures (competitive adsorption) for 40 minutes followed by a 40 minute PBS rinse.

Interfacial tensiometry

A FTÅ model T10 (First Ten Ångstroms, Portsmouth, VA) equipped with a Du Nuöy ring (CSC Scientific Co, Fairfax, VA) was used to measure the baseline surface tension of 6.5 mL of PBS, after which 500 µL of peptide or LPS stock solution was injected to reach final concentrations of 5 or 50 µM WLBU2 or PmB in PBS, with or without 0.1 mg/mL LPS. Data was collected for at least 20 min to determine the steady state surface tension of the resulting peptide and/or LPS solutions. The platinum ring was flamed to remove contaminants between experiments.

Dynamic Light Scattering

Apparent particle sizes of peptide and LPS solutions and mixtures were measured by dynamic light scattering (DLS) at 635 nm, using a Brookhaven Instruments 90 Plus Particle Size Analyzer (Holtsville, NY). Each sample was scanned for 1 minute at 20°C, and data from 10 scans was averaged. The cumulative size distributions were then extracted from multimodal size distribution data.

Circular Dichroism

Peptide secondary structure in the presence or absence of LPS was evaluated in triplicate by circular dichroism (CD) using a Jasco J-815 spectropolarimeter (Easton, MD) at 25 °C. Spectra

were recorded in a cylindrical cuvette (0.1 cm pathlength) from 185 to 260 nm in 0.5 nm increments after calibration with 0.6 mg/mL *D*(+)-camphorsulfonic acid, and 10 scans/sample were averaged to increase the signal-to-noise ratio. All concentrations of peptides and LPS were the same as for tensiometry and OWLS. The spectra from each of the three replicates for each sample were practically identical, with only slight (~5%) differences in signal intensity; thus, representative spectra are shown throughout. Peptide helicity was estimated from representative CD spectra using Dichroweb.[166,167]

Results and Discussion

Competitive adsorption of peptides and LPS at the air-water interface

Surface tension depression was recorded for mixtures of LPS (0.1 mg/mL) and peptide at high (50 μM) or low (5 μM) peptide concentrations in buffer (Figure 25 and Figure 26). In the absence of peptide, LPS vesicles decreased surface tension to a steady value of about 40 mN/m. In contrast, while 50 μM PmB slightly reduced surface tension, PMB had almost no effect on surface tension at 5 μM (Figure 25, top). However, when PmB is mixed with LPS, a faster rate of surface tension decrease is observed at each concentration, and, in the case of 50 μM PmB, the surface tension is reduced to a greater extent than observed with LPS alone (Figure 25, bottom).

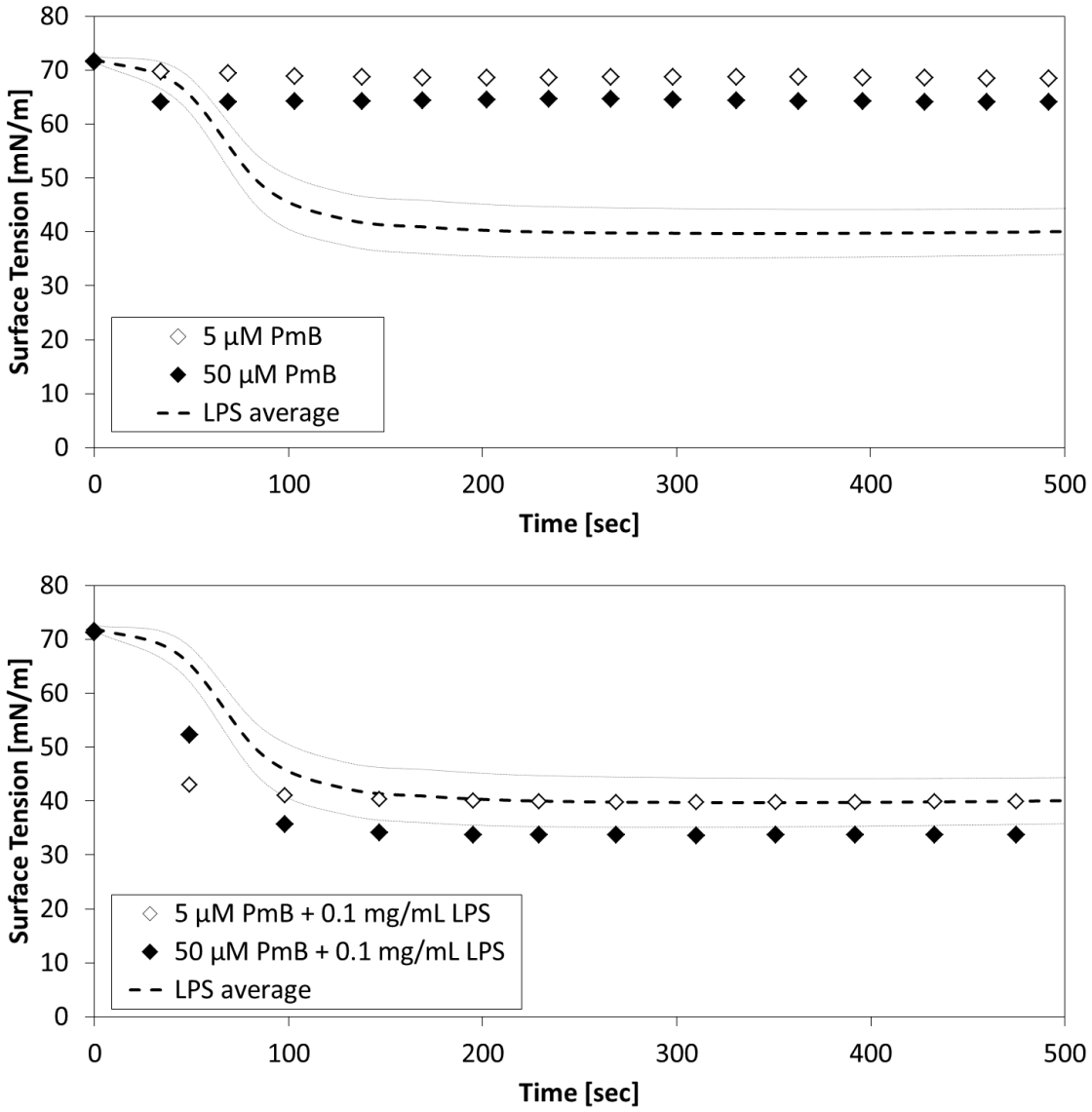

Figure 25. Air-water tensiometry of suspensions of 5 or 50 µM PmB and 1.0 mg/mL LPS in PBS, as individual species (top) and as mixtures of peptide and LPS (bottom). Average values (- - -) and standard deviation (*n* = 5, gray lines) are shown for LPS.

As with PmB, WLBU2 in the absence of LPS did not substantially decrease surface tension at either concentration (Figure 26, top). However, unlike PmB, the similarity in the rate and extent of surface tension depression at each WLBU2 concentration suggests that monolayer coverage of the interface is achieved in each case.

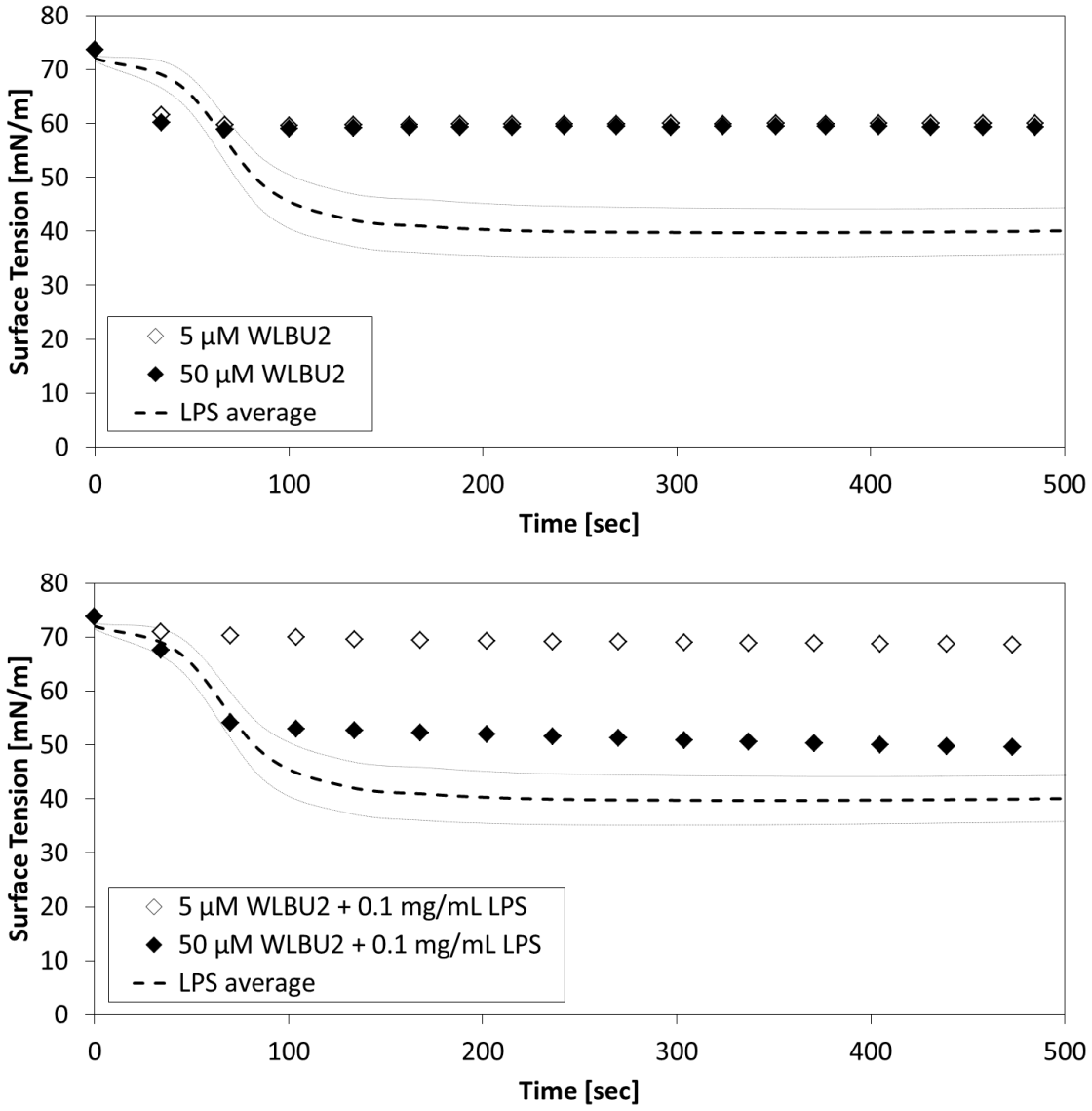

Figure 26. Air-water tensiometry of suspensions of 5 or 50 µM WLBU2 and 1.0 mg/mL LPS in PBS, as individual species (top) and as mixtures of peptide and LPS (bottom). Average values (- - -) and standard deviation (*n* = 5, gray lines) are shown for LPS.

The dimensions of the peptides were determined using the open-source viewer Jmol™ [168] from structures of PmB from the NCBI PubChem repository (CID 49800003), and a helical structure of WLBU2 predicted using PEP-Fold[169,170] (Figure 27). From those dimensions, the expected surface concentrations of PmB and WLBU2 peptides adsorbed in a monolayer in a "side-on" or "end-on" conformation were estimated, assuming a footprint of the solution dimensions and close-packed rectangular (side-on) or hex-packed circular (end-on) configurations (Table 2). The ratio of the surface tension depression for WLBU2 relative to PmB (Figure 25 and Figure 26, top

panels) is about 3.23 at 5 µM peptide, and about 1.55 at 50 µM peptide. These values fall within limits based on expectations for monolayer coverage.

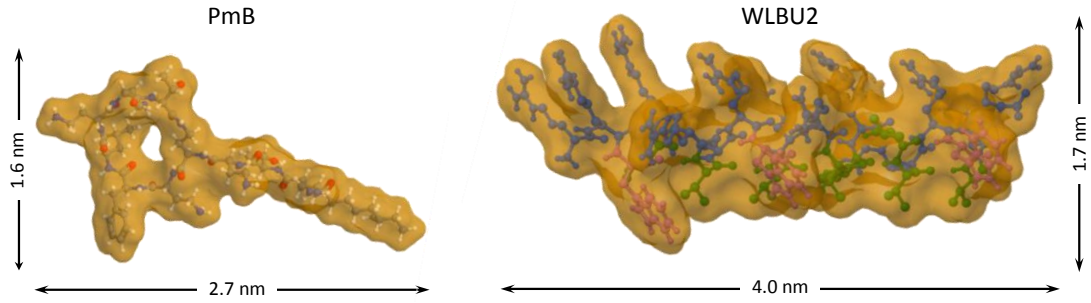

Figure 27. Molecular structure and approximate dimensions of PmB (left) and helical form of WLBU2 (right) peptide.

Mixtures of LPS and WLBU2 behave quite differently from the mixtures of PmB and LPS (Figure 25 and Figure 26, bottom panels). In particular, the presence of WLBU2 with LPS results in appreciably reduced surface tension depression when compared to LPS alone (Figure 26, bottom). At the low (5 µM) concentration of WLBU2, the surface tension depression is nearly negligible compared to that associated with either WLBU2 or LPS alone. At higher (50 µM) WLBU2 concentrations in an LPS-WLBU2 mixture, the surface tension was depressed substantially, but did not reach that of LPS alone.

These results strongly suggest that suspensions of LPS with WLBU2 are more stable than similar suspensions of LPS with PmB. In particular, suspensions of LPS with WLBU2 show substantially less surface activity (e.g., vesicle adsorption and spreading at the interface) than is exhibited by LPS alone (Figure 26, bottom). In contrast, suspensions of LPS with polymyxin B show greater surface activity than is observed for LPS alone (Figure 25, bottom).

These findings are potentially consistent with the notion that peptide insertion (into the vesicle membrane) and stabilization of intact LPS vesicles occurs in the case of WLBU2, while peptide-induced destabilization of LPS vesicles occurs in the case of PmB. We further tested this hypothesis by evaluating the adsorption behavior of peptide-LPS mixtures at a hydrophobic solid surface, and observation of peptide 2° structure and particle size distributions in such mixtures.

Table 2: Size and estimated packing density of PmB and WLBU2 adsorbed "side-on" and "end-on" at an interface. Dimensions were estimated from published (PmB) or predicted (WLBU2) molecular structures.

Peptide	MW (Da)	Length (nm)	Width (nm)	"Side-On" Monolayer (ng/cm^2)	"End-On" Monolayer (ng/cm^2)
PmB	1385.6	2.7	1.6	53	86
WLBU2	3400.1	4.0	1.7	83	180

Competitive adsorption of peptides and LPS at a hydrophobic solid surface

Figure 28 shows the adsorption and elution kinetics recorded with mixtures of LPS (0.1 mg/mL) and peptide at high (50 μM) or low (5 μM) peptide concentrations. The total mass remaining after elution was similar for both mixtures containing PmB, with final adsorbed masses of 74 or 55 ng/cm^2, respectively. The adsorption kinetics of LPS in the presence of PmB (Figure 28) are also consistent with the tensiometry results of Figure 25, and suggest that destabilized LPS vesicles adsorb and spread at the interface.

In contrast, the final adsorbed masses after elution for mixtures containing 0.1 mg/mL LPS and 5 or 50 μM WLBU2 were substantially different. The final adsorbed mass was nearly zero at the low peptide concentration, but reached 590 ng/cm^2 with 50 μM WLBU2. The observation of extremely low surface activity (i.e. adsorbed amounts) in WLBU2-LPS mixtures at low peptide concentration is consistent with the tensiometry results (Figure 26, bottom). It also suggests formation of LPS vesicles which are stabilized against spreading at the hydrophobic surface under these conditions, presumably due to their association with the membrane-active peptide WLBU2. The reason for the high value of adsorbed mass remaining after elution in the case of the 50 μM WLBU2-LPS mixture is not obvious. With reference to Figure 26 (bottom), however, the high adsorption would not be consistent with any enhancement of LPS vesicle spreading at the interface. Rather, it is possible that WLBU2-stabilized LPS vesicles locate at the interface under this condition.

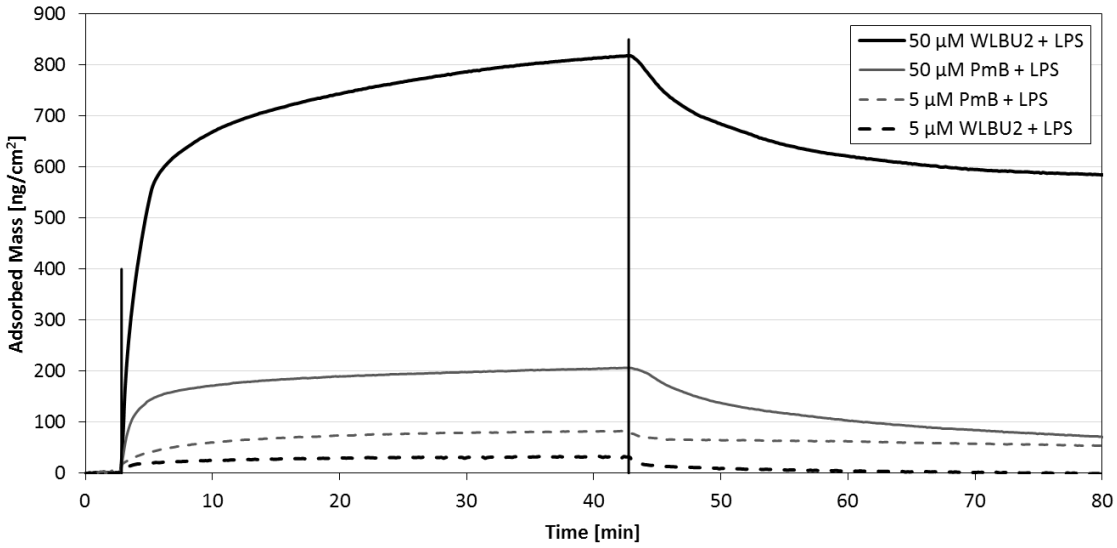

Figure 28. OWLS kinetic data for competitive adsorption from mixtures of LPS (0.1 mg/mL) and peptide at low (5 µM) and high (50 µM) peptide concentrations.

Peptide structure in peptide-LPS mixtures

WLBU2 structure is substantially disordered in aqueous solution, but becomes increasingly helical in the presence of certain anions (e.g. ClO4–),[171] membrane-mimetic solvents, or bacterial membranes. For example, Deslouches et al.[21] showed that WLBU2 has no appreciable stable structure in water, but reaches 81% α-helix content in an ideal membrane mimetic solvent (30% trifluoroethanol in phosphate buffer).[157] Circular dichroism shows that WLBU2 gains substantial helicity when mixed with LPS (Figure 29, left), reaching 78% α-helix content. This strongly suggests that the peptide is located almost exclusively within the membranes of the LPS vesicles. Due to its rigid, cyclic structure, PmB would not be expected to become substantially α-helical, and in fact shows no appreciable helical structure under any conditions (Figure 29, right). The CD spectrum from the PmB-LPS mixture appears to be primarily the sum of the CD signal from PmB and LPS alone.

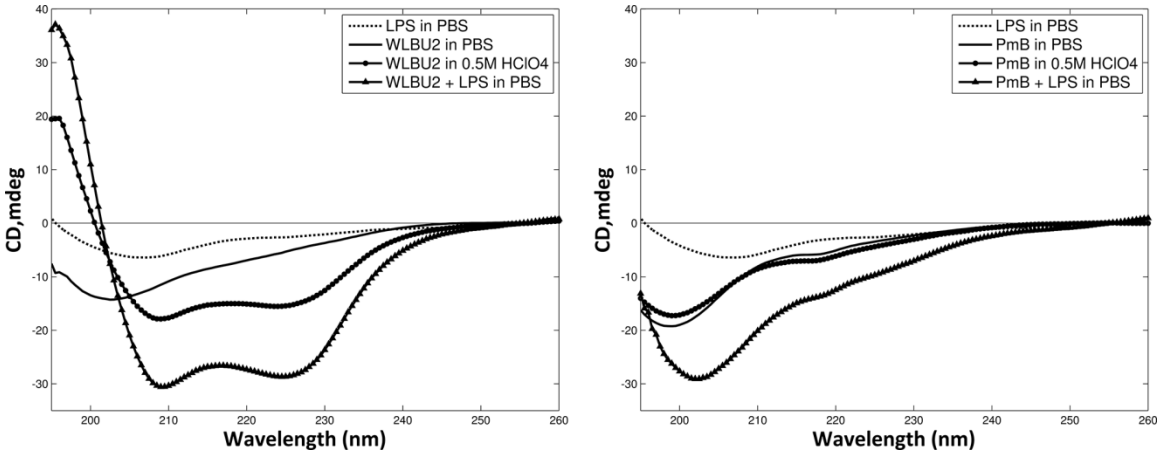

Figure 29. Circular dichroism (CD) spectra of WLBU2 (left) and PmB (right) in PBS, with helix-inducing perchlorate ions, or in the presence of LPS vesicles.

Vesicle size distribution in peptide-LPS mixtures

Dynamic light scattering analysis of peptide-LPS mixtures and peptide-free LPS suspensions are presented in Figure 30 as the intensity weighted cumulative oversize distribution of particle diameter. The particle size distribution was bimodal in all cases. At the lower mode, the presence of WLBU2 increased the apparent particle diameter of LPS, from 95±11 nm to 195±13 nm (mean ± standard deviation, *n* = 3), while addition of PmB had very little effect on particle size in the lower mode (89±19 nm). At the upper mode, however, the presence of PmB decreased the mean particle diameter from 408±56 nm to 262±26 nm, consistent with disruption of the LPS vesicles. In contrast, the presence of WLBU2 greatly increased both the mean and the range of particle sizes, with a mean diameter of 909±204 nm. This increase in particle size and polydispersity suggests that WLBU2 induces aggregation of LPS vesicles.

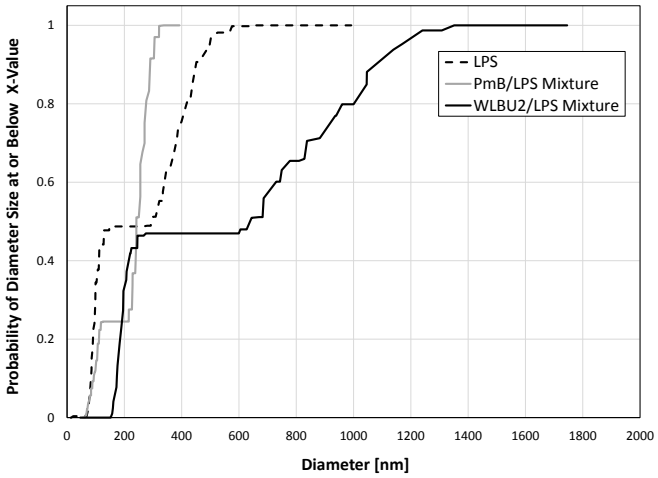

Figure 30. Cumulative oversize distribution of particle diameter in peptide-LPS suspensions from dynamic light scattering (DLS).

Anecdotal evidence recorded during preparation of peptide-LPS suspensions at high concentrations (700 µM peptide and 1.4 mg/mL LPS) suggest that the increase in LPS particle diameter in the presence of WLBU2 is not caused by an increase in the individual vesicle size, but rather is due to large-scale aggregation of vesicles (Figure 31). While there is a slight increase in turbidity of LPS suspensions when PmB is added, aggregation is not visible in either the PmB-LPS or peptide-free LPS suspensions.

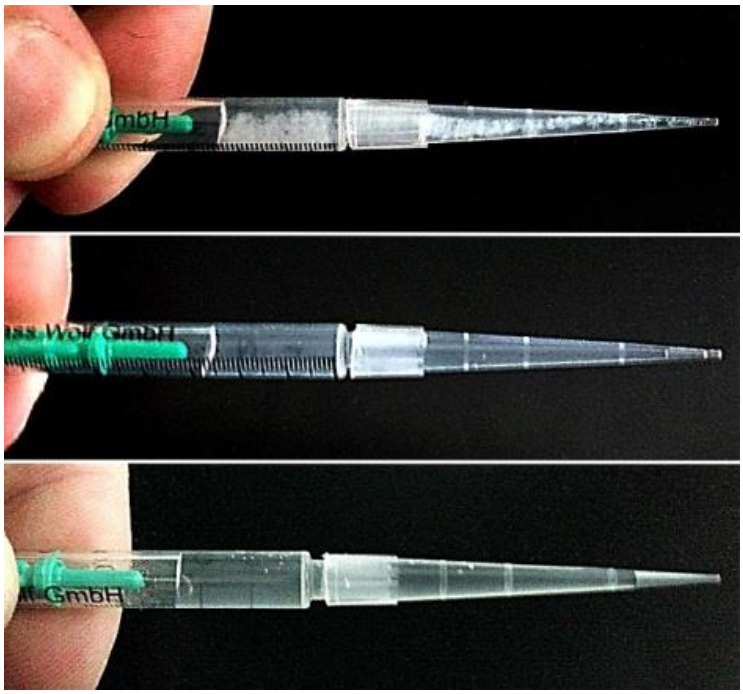

Figure 31. Visible aggregation rapidly occurs in concentrated mixtures of WLBU2 and LPS (top), but not in PmB-LPS (middle) or peptide-free LPS suspensions (bottom).

Taken together, the results described above strongly support the hypothesis that peptide insertion and stabilization of intact LPS vesicles occurs in the case of WLBU2, while PmB causes peptide-induced destabilization and disruption of LPS vesicles. Moreover, they suggest that the high value of adsorbed mass for WLBU2-LPS mixtures at high peptide concentration (Figure 28) can be attributed to location of intact WLBU2-LPS vesicles or vesicle aggregates at the interface. We are currently evaluating the feasibility of endotoxin capture using membrane-active peptides which have been covalently tethered to surfaces by short and long hydrophilic linkers, and results from that work will contribute to the subject of a future report.

Conclusions

Analysis of the interfacial behavior of mixtures of LPS and peptide using interfacial tensiometry as well as OWLS, evaluation of peptide structure in such mixtures using CD, and determination of the particle size distributions in such mixtures using DLS, all strongly suggest peptide insertion and stabilization of intact LPS vesicles in the case of WLBU2, while PmB appears to cause peptide-induced destabilization and disruption of LPS vesicles. In the context of blood purification with hemoperfusion, the most desired outcome is insertion and tight binding of the

peptide in the bacterial membrane or LPS vesicle, without destabilizing the membrane. Disruption and concomitant lysis of the membrane could cause the return of LPS or cellular degradation products to the circulating blood, and is not desirable. Thus, we expect that presentation of WLBU2 at an interface, tethered in a fashion preserving its solvent accessibility and mobility, may promote the capture of pathogens or endotoxin that reach the surface without destabilizing or disrupting the captured vesicle or pathogen. Based on the results provided here, there is no reason to expect a similar outcome with PmB.

Acknowledgments

The authors thank Dr. Kerry McPhail and Dr. Jeff Nason for the use of their CD and DLS instruments, respectively. This work was supported in part by the National Institute of Biomedical Imaging and Bioengineering (NIBIB, grant no. R01EB011567). The content is solely the responsibility of the authors and does not necessarily represent the official views of NIBIB or the National Institutes of Health.

BINDING OF BACTERIAL LIPOPOLYSACCHARIDE BY THE CATIONIC AMPHIPHILIC PEPTIDE WLBU2 AT INTERFACES

Matthew P Ryder, Xiangming Wu, Miranda Raper, Joseph McGuire, Karl F. Schilke

For submission to Biomaterials Literature

Abstract

Passage of blood through a sorbent device for removal of bacteria and endotoxin by specific binding with immobilized, membrane-active, bactericidal peptides holds promise for treating severe blood infections. Peptide insertion in the target membrane and rapid/strong binding is desirable, while competing interactions with blood proteins is not. Here we describe interactions between bacterial endotoxin (lipopolysaccharide, LPS) and the bactericidal peptide WLBU2 in surface bound, PEG entrapped, and PEG tethered motifs. Analysis of the interactions using QCM-D, and CD, as well as the effects of γ-irradiation on PEGylated WLBU2 using UV/Vis spectroscopy and NMR, all reveal that WLBU2 interacts with LPS whether irradiated, PEGylated, or tethered. Further, interactions between LPS and WLBU2 in these motifs in the presence of fibrinogen reveal a complicated interaction between fibrinogen and LPS, and between fibrinogen and WLBU2, but data analysis suggests that WLBU2 may still preferentially capture LPS over interactions with fibrinogen. We therefore expect that tethered WLBU2 in a hemoperfusive devise will enable the capture of bacteria and endotoxin without promoting reintroduction of endotoxin to the circulating blood.

Introduction

Severe sepsis is a blood infection that in the US alone affects about 750,000 people each year, killing 28-50% of them.[5,7,144] The number of sepsis-related deaths continues to increase, and is already greater than the annual number of deaths in the US from prostate cancer, breast cancer and AIDS combined. During bacterial growth or as a result of the action of antibacterial host factors, lipopolysaccharide (LPS, endotoxin) is released from the cell wall of Gram-negative bacteria. The high immunostimulatory potency of endotoxin causes dysregulation of the inflammatory response with elevated production and release of proinflammatory cytokines[145], leading to blood vessel damage and organ failure.[5,7]

Hemoperfusion, involving passage of blood through a sorbent device for the removal of selected targets, holds promise for treating sepsis.[8,14,146] Successful hemoperfusion for sepsis treatment will require surface modification that will ensure highly selective capture of bacteria and endotoxin that reach the interface. In addition, surface coatings must provide pathogen binding functionality without evoking a host cell response, without nonspecific adsorption of protein, and without platelet activation and blood cell damage caused by cell-surface interactions.

In a previous paper we demonstrated that WLBU2 inserts into, and stabilizes, the membrane of LPS. This was done in comparison to polymyxin B (PmB), a peptide used clinically for hemoperfusion in Japan.[8,9] PmB appeared to cause peptide-induced destabilization and disruption of LPS vesicles. That work was accomplished by analysis of the interfacial behavior of mixtures of LPS and peptide using interfacial tensiometry as well as OWLS, evaluation of peptide structure in such mixtures using CD, and determination of the particle size distributions in such mixtures using DLS. In the context of blood purification with hemoperfusion, peptide insertion in the susceptible membrane and tight binding is desired, while membrane disruption, concomitant lysis and return of degradation products to the circulating blood is not desired. In this work, we take the next step toward a prototype device, providing evidence that presentation of WLBU2 at an interface, tethered in a fashion preserving its solvent accessibility and mobility, can promote the capture of endotoxin that enters the interface. Tethered and entrapped peptide motifs (Figure 32) are compared.

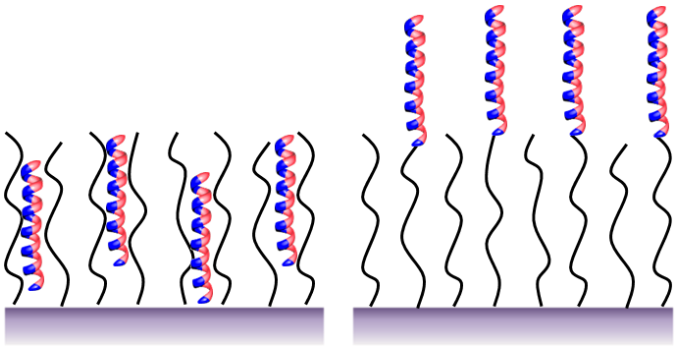

Figure 32: Cartoon illustration of WLBU2 at an interface in an entrapped (left) or tethered (right) motif. Image is not to scale.

Materials and Methods

Proteins, Surfactants, and Lipopolysaccharide

Unless otherwise specified, all reagents were purchased from commercial vendors and were of analytical reagent or higher grade. WLBU2 (RRWVRRVRRWVRRVVRVVRRWVRR, 3.4 kDa), CysWLBU2 ,and WLBU2Cys were obtained from GenScript (Piscataway, NJ). The latter peptides are structurally identical to the original WLBU2 except for an additional cysteine at the N-terminus and C-terminus, respectively. All peptides were used at 50 µM in phosphate buffered saline (10 mM PBS, 150 mM NaCl) unless otherwise noted. Fibrinogen from bovine plasma (Fib, 340 kDa), and purified *Pseudomonas aeruginosa* lipopolysaccharide (LPS) were purchased from Sigma-Aldrich (St Louis, MO). LPS was used at 0.1 mg/mL in PBS in all cases. All solutions were prepared using HPLC-grade water, and all peptides and LPS were used as received, without further purification. Fibrinogen was prepared in HPLC, incubated at 37 °C for 2 hr, and 0.45 µm filtered prior to use.[172] Fibrinogen was used at 2 mg/mL in all cases.

Self-assembled PEO brush layers were formed by suspension of hydrophobic silica nanoparticles (R816, Degussa, 190 m^2/g, 10-12 nm) in Pluronic® F127 (PEO_{101}-PPO_{56}-PEO_{101}, ≈12.6 kDa, BASF) in HPLC water (1 % wt/v) overnight on a rotator. F127 was also used in conjunction with QCM-D sensors, described later. End Group Activated F127 Pluronic, activated with pyridyl disulfide (EGAP-PDS) was obtained from Allvivo Vascular, Inc. EGAP-PDS was incubated with CysWLBU2 in equimolar concentrations for 8 hr at room temperature (EGAP-WLBU2) before use similar to F127. F127 was used instead of F108, as in previous chapters, because the EGAP from Allvivo is based on the F127 triblock.

Surface Modification of QCM-D sensors

QSX303 silicon dioxide QCM-D sensors were purchased from Biolin (Linthicum, MD) and were cleaned by 15 min UV/O_3 clean followed by 1 hr in 5 % w/v sodium dodecyl sulfate (SDS) and then another 15 min in UV/O_3. Cleaned sensor surfaces were modified with trichlorovinylsilane (TCVS, TCI America, Portland, OR) by a variation of the method of Popat.[162-164] Briefly, clean QCM-D sensors were exposed to flowing dry N_2 in a sealed vessel for 1 hr to remove any residual surface moisture, after which 200 µL of TCVS was added and allowed to vaporize at 25 °C, while flowing N_2 transported the TCVS vapor across the sensor surfaces. The N_2 flow was maintained for three hours, after which the sensors were cured at 120 °C for 30 min to stabilize the vinylsilane layer. Cleaned and modified senors were stored in 1.5 mL centrifuge vials under N_2 in the dark until further use. All silanized sensors were submerged in 1% w/v F127 or EGAP-WLBU2 and exposed to γ-radiation from a ^{60}Co source (Oregon State University Radiation Center) for a total dose of 0.3 Mrad to achieve polymer grafting.[116] Sensors were used immediately after surface preparation.

Au coated QCM-D sensors (Biolin, Linthicum, MD) were cleaned by 15 min UV/O_3 clean followed by 10 min in 5:1:1 H_2O:30% H_2O_2:27% NH_4OH solution at 80 °C, followed by another 15 min UV/O_3 clean. These sensors were used immediately after cleaning.

Quartz Crystal Microbalance with Dissipation

All modified sensors were submerged in HPLC water for 1 hr prior to instrument use to remove residual F127 or EGAP. The adsorption and elution of peptides, LPS, and Fibrinogen were measured with a Q-Sense E4 QCM-D (Q-Sense, Linthicum, MD). QCM-D allows simultaneous measurement of changes in resonance frequency (*Δf*) and energy dissipation (*ΔD*) caused by adsorbed mass on QCM-D sensors. For rigid layers, changes in mass can be directly calculated by the Sauerbrey equation[95]:

$$\Delta m = -C\frac{1}{n}\Delta f$$

Where *Δm* is the change in adsorbed mass, *Δf* is the change in frequency, *n* is the frequency overtone, and *C* is a constant parameter characteristic to the quartz crystal, very commonly 17.7 ng/cm^2·s.

A high precision peristaltic pump was used to flow sample solutions over QCM-D sensors. Flow rates were maintained at 50 µL/min, and solution temperature was maintained at 20 °C. QCM-D experiments began by collecting baseline data of a peptide free phosphate buffered saline solution (10 mM PBS, 150 mM NaCl) followed by introduction of WLBU2, or variant, followed by rinse with PBS, a subsequent challenge with LPS, Fibrinogen, or a mixture of both, and a final rinse with PBS. All adsorption and elution steps proceeded for 40 min. In all QCM-D data presented, the Δf is from the 5th overtone. All QCM-D data on surfaces containing pre-adsorbed triblock was baseline adjusted using MatLab prior to use. In brief, this was accomplished by modeling the baseline assuming a simple kinetic model for the removal of excess triblock, suggested by an initial increase in frequency. The model was fit to the baseline by minimizing the residual between the model and the data, and the model was subtracted from the whole subset of data.

Circular Dichroism

Peptide secondary structure in the presence or absence of LPS was evaluated by circular dichroism (CD) using a Jasco J-815 spectropolarimeter (Easton, MD) at 25 °C. Spectra were recorded in a cylindrical cuvette (0.1 cm pathlength) from 185 to 260 nm in 0.5 nm increments after calibration with 0.6 mg/mL *D*(+)-camphorsulfonic acid, and 10 scans/sample were averaged to increase the signal-to-noise ratio. All concentrations of solutions were the same as QCM-D. Representative spectra are shown throughout. Peptide helicity was estimated from representative CD spectra using DichroWeb.[166,167]

UV/Vis Spectroscopy

Peptide concentration, as well as the extent of WLBU2 attachment to EGAP-PDS was assessed using a Thermo-Electron Genesys 6 UV-Vis spectrophotometer (Madison, WI). Concentration of WLBU2 and variants was assessed using the calculated molar extinction coefficient at 280 nm (16,500 M^{-1} cm^{-1}) of WLBU2.[160] The extent of covalent attachment was assessed at 343 nm by the increase in pyridine-2-thione (P2T) concentration (8080 M^{-1} cm^{-1}).[173]

Nuclear Magnetic Resonance

Proton nuclear magnetic resonance (^{1}H-NMR) spectra were taken using a Brüker (Billerica, MA) Robinson 400 MHz NMR spectrometer with TopSpin 2.1 software at room temperature (25 °C) using ~1000 µM WLBU2 and γ-WLBU2 in D_2O. Each sample was measured using 128 scans. The spectra were post processed by setting the line broadening factor to 0.8 Hz.

Results and Discussion

Interaction between LPS and surface bound peptide.

The interaction between LPS (0.1 mg/mL) and surface bound WLBU2, and WLBU2 variants recorded by QCM-D are presented in Figure 33 and Figure 34. If a given system shows small or insignificant changes in dissipation, QCM-D data can be modeled using the Sauerbrey model,[95] which directly relates (negative) changes in frequency to changes in adsorbed mass. If the change in dissipation is large, modeling becomes more complex, requiring the Voigt model of viscoelasticity in fluids.[174,175] Adsorbed mass of WLBU2, CysWLBU2, and WLBU2Cys prior to LPS adsorption was ~300 ng/cm^2, ~425 ng/cm^2, and 400 ng/cm^2, respectively, calculated by the Sauerbrey equation[95]. Figure 33 shows that adsorption to a peptide coated surface is similar for all WLBU2 variants and is greater than adsorption of LPS to a bare gold surface. The enhanced adsorption of LPS vesicles at the peptide-coated surface is likely caused primarily by electrostatic interaction between the negatively charge LPS vesicle with WLBU2, which carries an out of balance charge of +13 at physiologic pH. WLBU2 with a cysteine added to either the amine- (CysWLBU2) or carboxy-terminated (WLBU2Cys) end is expected to adsorb "end-on" to the gold surface mediated by the high-avidity gold-thiol association. Chemical bonding energies can vary greatly, with hydrophobic association at ~0.8 kcal/mol,[176] common hydrogen bonds ranging from 2 to 7 kcal/mol,[177,178] C-C bonds at 83 kcal/mol,[179] and gold-thiol bonds at 45 kcal/mol.[180,181] As thiol-gold interactions approximate covalent attachment (45 v 83 kcal/mol, compared to 7 for H-bonding), it is expected that WLBU2 associated in this manner will not be replaced by LPS. On the other hand, WLBU2 randomly associated to a surface may be removable. As seen in the QCM-D data (Figure 33), adsorption of LPS to each of the three WLBU2-variant coated surfaces is similar. LPS association to end-on oriented WLBU2 molecules, presenting either the amine or carboxy end, behaves substantially the same as randomly adsorbed WLBU2, suggesting that LPS association to each of these layers is likely electrostatic,

and not indicative of higher order interaction. Since the orientation of WLBU2 does not seem to change the adsorption of LPS, and modifying peptides at the N-terminus is more straightforward than the C-terminus, only the CysWLBU2 variant was used for further experimentation.

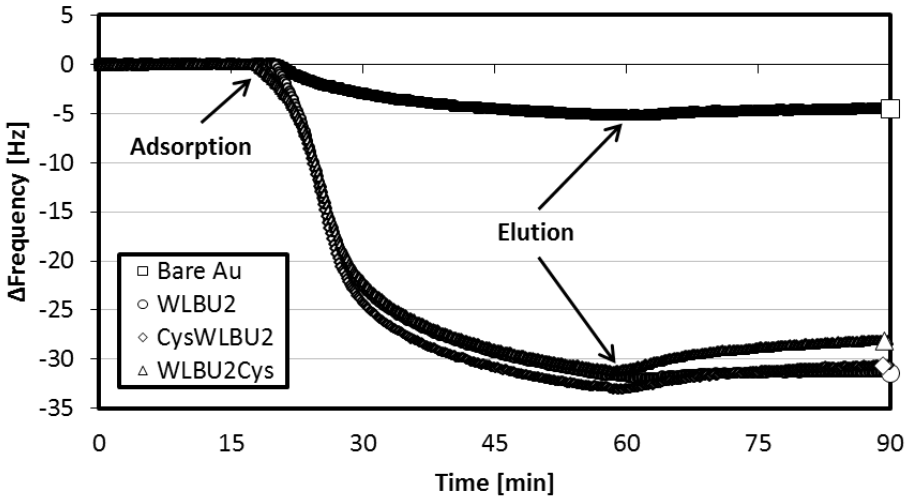

Figure 33: ΔFrequency for LPS on a bare Au surface (□), on a Au surface coated with WLBU2 (○), CysWLBU2 (◇), and WLBU2Cys (△).

Figure 34 shows dissipation vs frequency curves for each experiment. Data in this format allows visual inspection of the quality of the adsorbed layer. In particular, if the data shows hysteresis effects, adsorption is likely changing the structure of the adlayer. More generally, data displayed in this manner describes the comparable rigidity of a layer changing with adsorption and elution; as the slope decreases, the rigidity increases. The data shown in Figure 34 nearly overlap for each of the LPS on peptide experiments, with hysteresis ranging from 0.4 – 1.9%. This strongly suggests the structure of LPS does not change upon adsorption to a WLBU2 coated surface, whether adsorbed randomly or end on. For LPS adsorbed to Au, the slope of the dissipation versus frequency is greater than any of the LPS on peptide experiments, suggesting a much more rigid layer, and this curve shows hysteresis upon elution, with a change of nearly 18%. Taken together, this strongly suggests that LPS vesicles unfold at a gold surface, but remain largely intact and electrostatically adsorbed to a peptide coated surface.

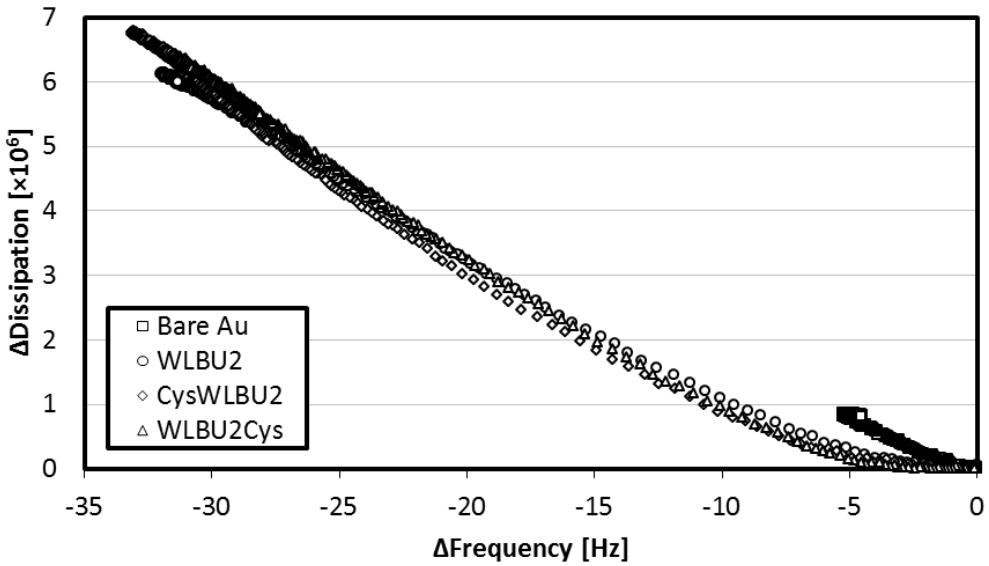

Figure 34: ΔDissipation vs ΔFrequency for LPS on a bare Au surface (□), on a WLBU2 coated Au surface (○), on a CysWLBU2 coated Au surface (◇), and on a WLBU2Cys coated Au surface (△).

Figure 35 shows CD spectra for WLBU2 in suspension with hydrophobic nanoparticles with and without LPS. The α-helicity changes from 10% on the bare particle without LPS to 23% with LPS included. This data supports the hypothesis drawn from the QCM-D data that surface bound WLBU2 does not substantially interact with LPS in a meaningful way.

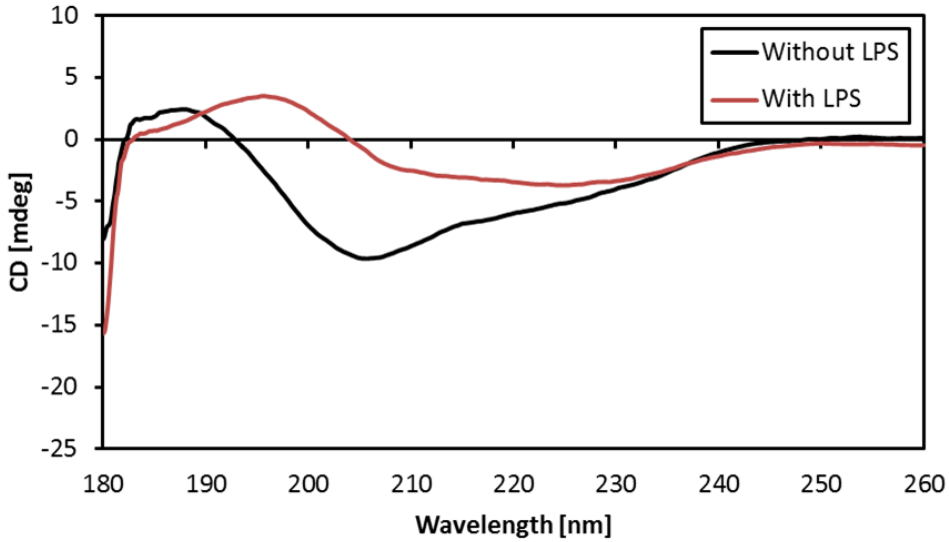

Figure 35: CD spectra of WLBU2 non-specifically bound to a hydrophobic surface before and after LPS interaction.

Interaction between LPS and PEO layers

PEO layers are commonly considered to be nonfouling. As such, we expect no irreversible location of LPS at pendent PEO layers. Figure 36 shows that this is indeed the case as change in both the frequency and dissipation returns to the original baseline upon elution.

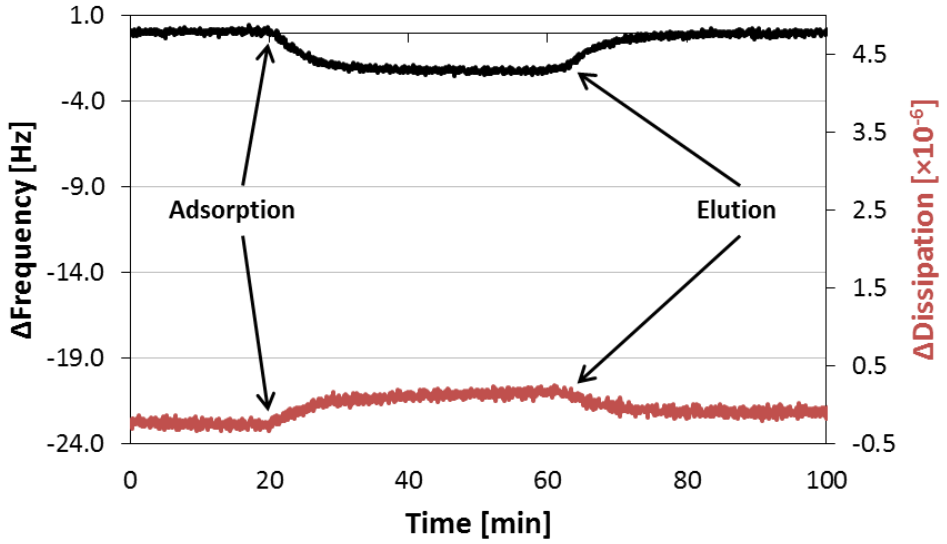

Figure 36: ΔFrequency (black line, primary y-axis) and ΔDissipation (red line, secondary y-axis) for LPS on a surface containing covalently attached F127 only.

Interaction between LPS and peptide at PEO layers

LPS at peptide entrapped layers

In previous work, we have demonstrated that WLBU2, among other peptides, is able to penetrate PEO brush layers. This tendency toward small peptide entrapment requires that, for the purposes of peptide tethering, EGAP-WLBU2 constructs must be prepared in advance of adsorption to a surface. If attachment were to be conducted *in situ*, location of WLBU2, either entrapped or tethered would not be discernable. Figure 37 shows QCM-D data for LPS association at peptide entrapped PEO layers. For the concentration used, we expect a maximum loading of WLBU2 to be around 0.2 molecules/nm^2 (~120 ng/cm^2) [Wu et al] for entrapped peptide in membrane mimetic solvents, which would encourage α-helicity. Because the manner in which WLBU2 entrapment was conducted, i.e. in PBS rather than perchloric acid, it is expected that the actual amount of WLBU2 will be substantially less than that seen in Wu *et al*. In fact, when calculating the concentration of WLBU2 in solution by UV/Vis spectroscopy for

entrapped WLBU2 on nanoparticles for CD analysis (Figure 41), the apparent concentration of WLBU2 was below the detectable limit. Figure 38 shows that for entrapped peptide, there is very little initial peptide present, but upon introduction of LPS, the α-helicity increases from 3% to 8%.

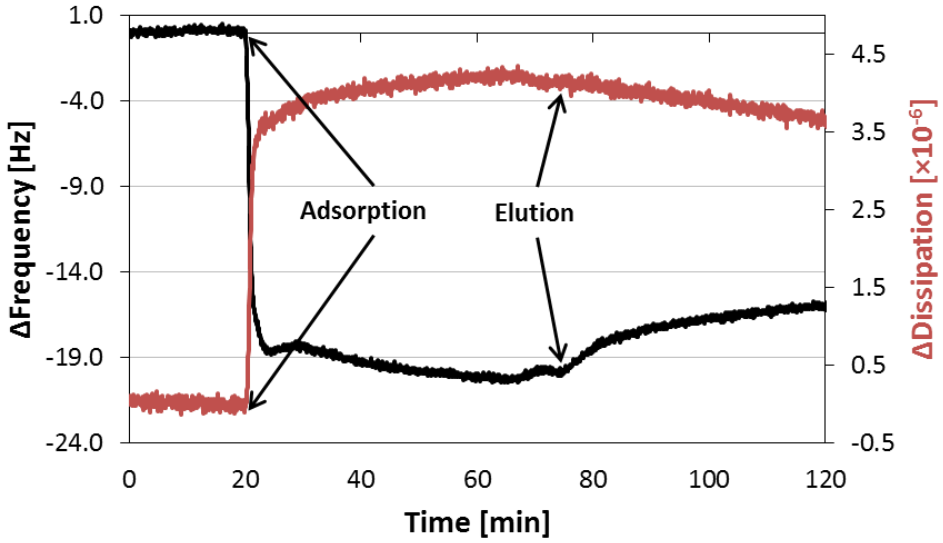

Figure 37: ΔFrequency (black line, primary y-axis) and ΔDissipation (red line, secondary y-axis) for LPS on a surface containing covalently attached F127 and entrapped WLBU2 peptide.

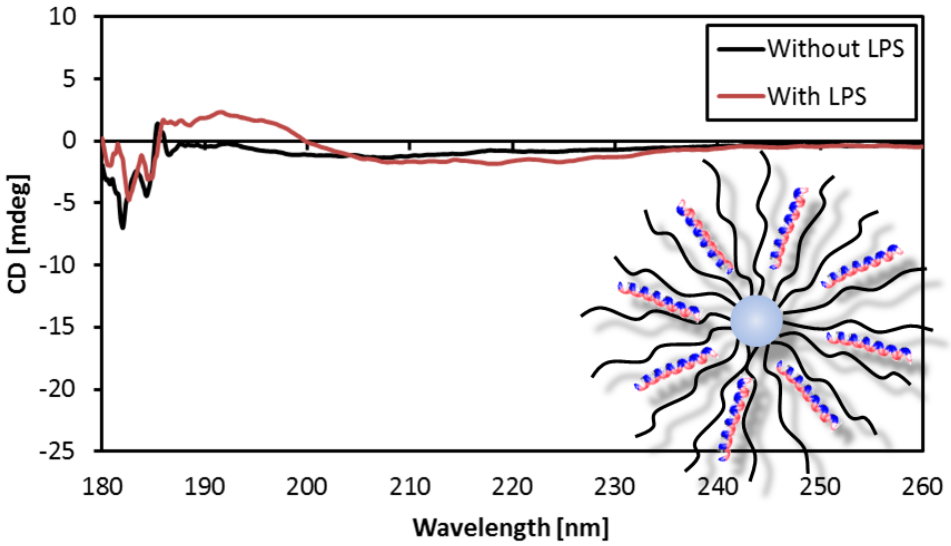

Figure 38: Evaluation of entrapped WLBU2 on hydrophobic nanoparticles mixed with 0.1 mg/mL LPS. α-helicity increases from 3% to 8% after introduction of LPS. Note-graphic is representative only, and not to scale.

LPS at peptide tethered PEO layers

In the context of LPS capture in a hemoperfusion device, it is paramount to retain the mobility and solvent accessibility of the active capture agent, in this case WLBU2. Further, management of peptide density and distance from the primary interface requires more control than peptide entrapment allows. Thus, the peptide must be tethered to the surface, and to avoid convolution with potential entrapment of the peptide, it is important to build the tethered-WLBU2 construct prior to surface immobilization. In our work, we have commonly used γ-irradiation to covalently attach triblocks to our surfaces. It is therefore important to first investigate the effect of both a tether and γ-irradiation on the structure and function of WLBU2. Covalent attachment of WLBU2 with EGAP-PDS occurs spontaneously at room temperature according to the reaction scheme presented in Figure 39. Constructs were prepared by mixing equimolar quantities of EGAP-PDS and CysWLBU2, average total conversion was greater than 50% as evaluated by the evolution of pyridine-2-thione (P2T) absorption at 343 nm (ε = 8080 M^{-1} cm^{-1}).

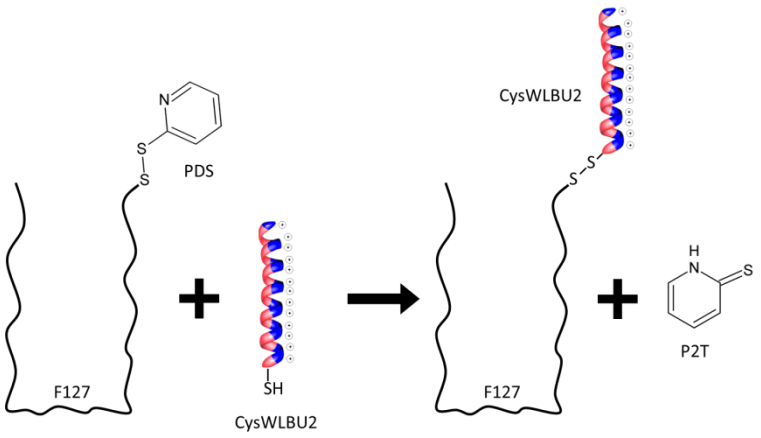

Figure 39: Covalent association of CysWLBU2 with EGAP-PDS to create EGAP-WLBU2. Release of P2T allows the direct calculation of total amount of construct produced. Note- schematic is not to scale.

Unmodified WLBU2 shows a substantial increase in α-helicity upon exposure to LPS, increasing in helicity from ~0 to 78%, illustrated in Figure 40.

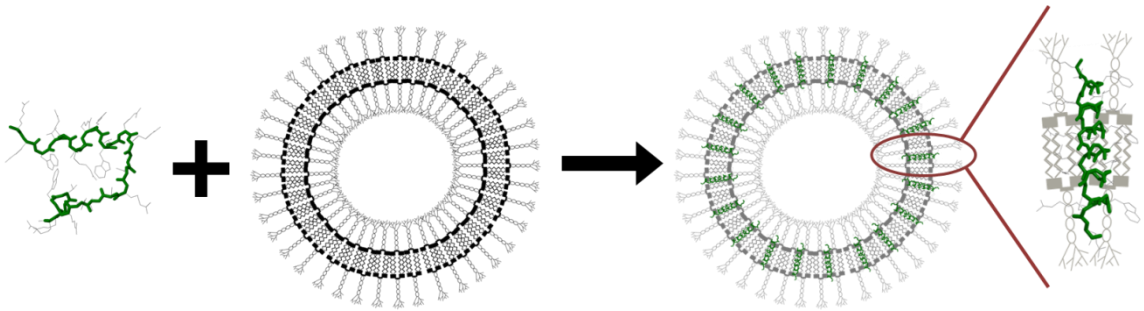

Figure 40: Cartoon schematic of WLBU2 interaction with LPS vesicles. Disordered WLBU2 adopts an α-helical conformation by penetrating the LPS vesicle and integrating into the Lipid A region of LPS. Images are not to scale.

This is owing to the WLBU2 infiltrating the lipid A region of the LPS vesicle, a prerequisite for vesicle capture. EGAP-WLBU2 was evaluated in a similar manner; results are shown in Figure 41. The data show an increase in helicity from 2% in HPLC H_2O to 16% upon addition of LPS to 0.1 mg/mL.

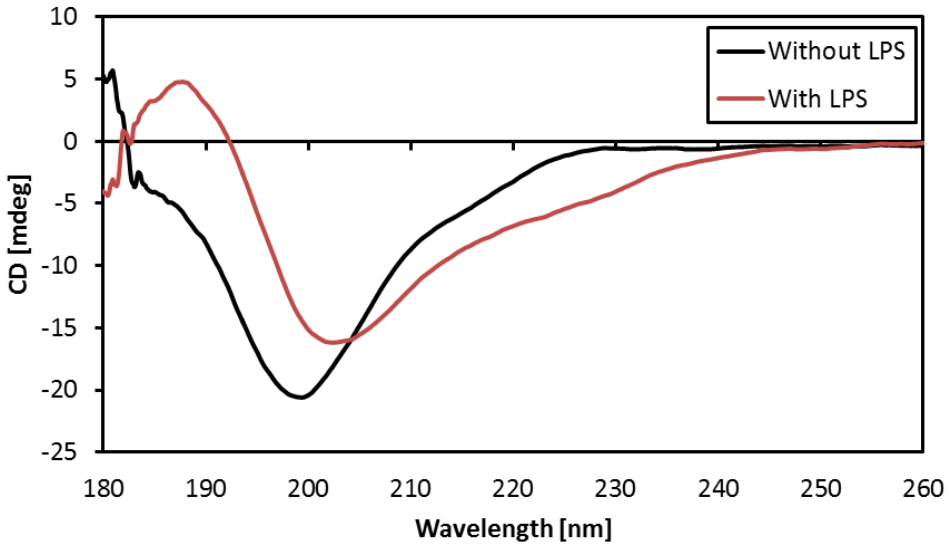

Figure 41: CD spectra of EGAP-WLBU2 mixed with 0.1 mg/mL LPS. α-helicity increases from 2% to 16% after introduction of LPS.

Figure 42 shows CD spectra of interaction of LPS with a tethered peptide associated with an interface. The data shows convincingly that WLBU2, when tethered to a surface retains its ability to adopt an α-helix upon introduction of LPS, changing from 2% helix without LPS to 17% including LPS.

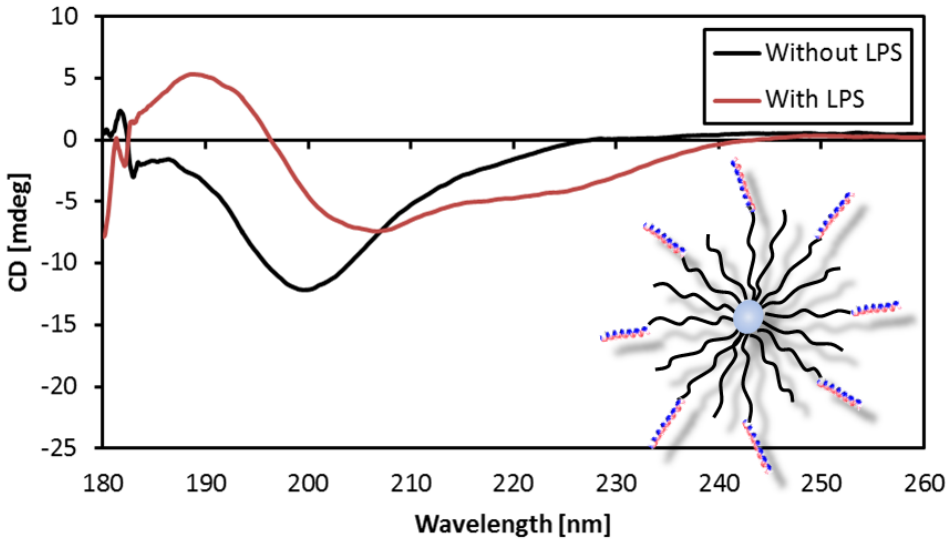

Figure 42: Evaluation of EGAP-WLBU2 on hydrophobic nanoparticles mixed with 0.1 mg/mL LPS. α-helicity increases from 2% to 17% after introduction of LPS. Note-graphic is representative only, and not to scale.

These data clearly indicate that the inclusion of a covalent tether, on the order of 12.5 kDa, does not prevent WLBU2 from interacting with LPS in a manner keeping with that of unmodified WLBU2, and further suggests that WLBU2 covalently tethered to a surface will retain the ability to interact with LPS, and therefore capture vesicles from solution.

While the data shown in Figure 41 and Figure 42 provide compelling evidence and support for the potential of tethered WLBU2 to capture LPS from solution, these systems had not been γ-irradiated. Figure 43 and Figure 44 show the effects of comparable doses of γ-irradiation as used for covalent attachment of triblocks as evaluated by NMR (Figure 43, ≈1000 µM WLBU2), and UV/Vis and CD (Figure 44, ≈35 µM WLBU2).

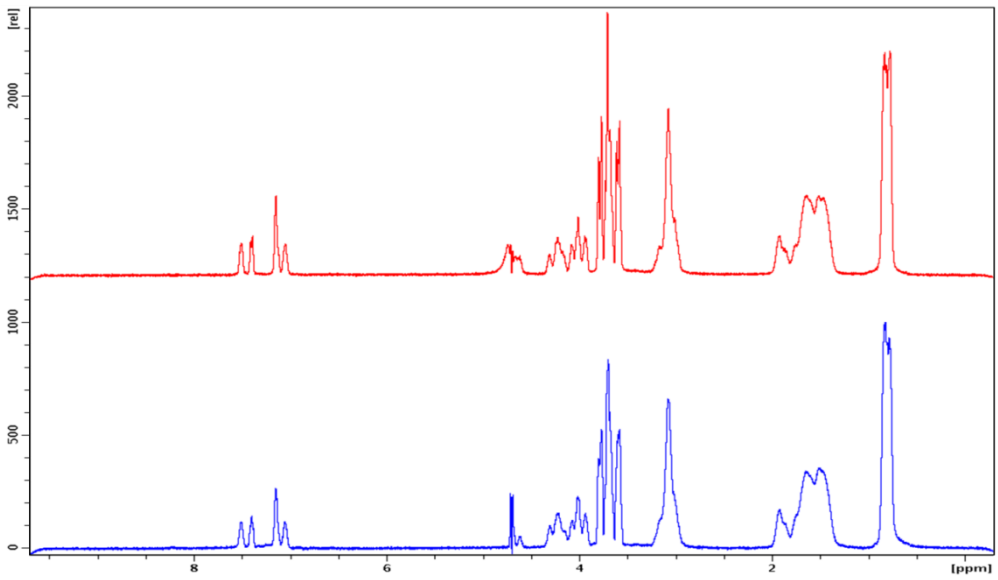

Figure 43: NMR spectra of non-irradiated WLBU2 (red) and 0.3 Mrad γ-irradiated WLBU2. Data shown is at the same scale.

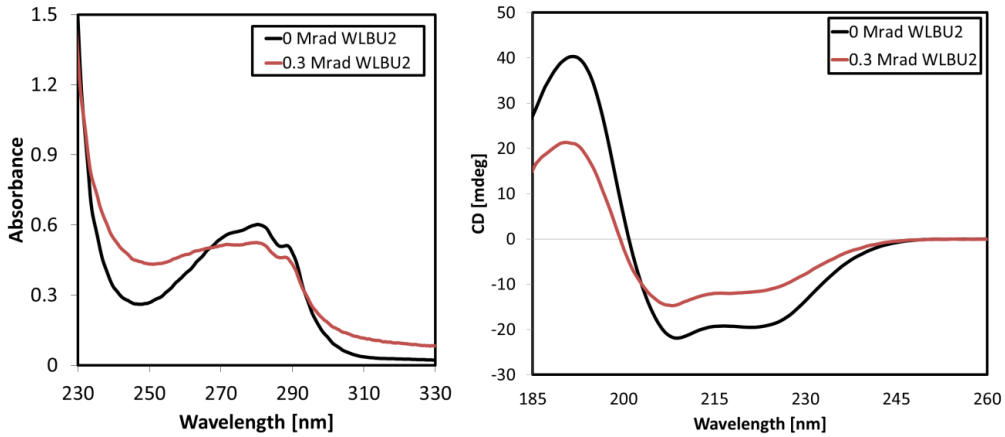

Figure 44: UV/Vis (left) and CD spectra (right), of non-irradiated (black) and 0.3 Mrad γ-irradiated WLBU2. UV/Vis was done with peptide in PBS while CD was collected on WLBU2 in perchloric acid.

The NMR spectra shown in Figure 43 show that the structure of WLBU2 remains intact upon irradiation, showing no significant difference in structure. Spectra recorded using UV/Vis spectroscopy (Figure 44, left) shows more substantial change in the characteristic curve, as the curve broadens, and its peak at 280 nm is reduced by 13%. Finally, in a helix inducing solvent (perchloric acid), WLBU2 is shown to decrease in α-helicity from 65% to 36% upon irradiation as indicated by the CD spectra shown in Figure 44 (right).

With the effects of tethering and γ-irradiation understood, we can more appropriately evaluate the capture of LPS by tethered WLBU2 as witnessed in QCM-D and shown in Figure 45. The QCM-D data presented shows clear evidence of LPS capture by tethered WLBU2 indicating that this system works.

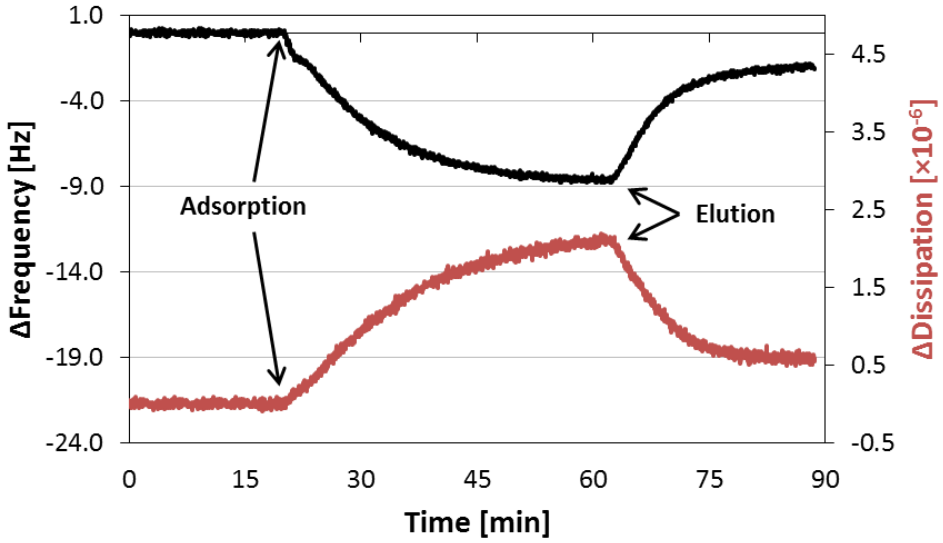

Figure 45: ΔFrequency (black line, primary y-axis) and ΔDissipation (red line, secondary y-axis) for LPS on a surface containing covalently attached EGAP-WLBU2.

When comparing the capture of LPS between entrapped peptide PEO layers (Figure 37) and tethered peptide PEO layers (Figure 45), it seems that the entrapped peptide captures a greater amount of LPS than does the tethered peptide, as $\Delta F_{entrapped}/\Delta F_{tethered} = 2.3$ at the end of the elution step, despite the lower surface concentration in the entrapped case. This result, however, is consistent with the removal of WLBU2 from an entrapped motif and the creation of peptide bridges and LPS aggregation as shown in previous work. In this case, the resultant LPS-WLBU2 association may not indicate capture, but merely that the aggregates resist the flow parameters and do not leave the interface, illustrated in Figure 46. This is further consistent with the very slow elution kinetics seen in Figure 37 and the low elutability of only 24%. Because WLBU2 cannot participate in LPS bridging in the tethered motif, what remains at the surface upon elution (76% elutability) is likely due only to capture, and not convoluting complexes.

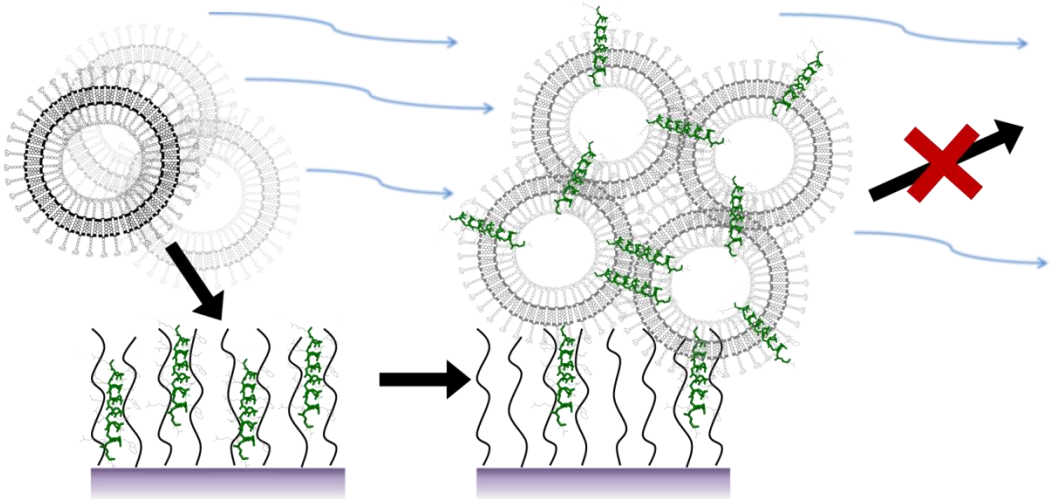

Figure 46: Cartoon illustration of hypothesis for why entrapped WLBU2 is able to "capture" LPS. The LPS-WLBU2 association may not indicate capture, but merely that aggregates resist the flow (blue arrows, 50 µL/min) and do not leave the interface.

Effect of fibrinogen on LPS capture

A clinically relevant device must be able to capture LPS from whole blood in a hemoperfusive device. To that end, we must be able to demonstrate LPS capture from a complex milieu containing blood proteins. Figure 47 shows QCM-D evidence that fibrinogen does not substantially adsorb or remain on a surface containing only F127. Thus, any interaction described upon the inclusion of LPS and/or WLBU2 would suggest that location of fibrinogen is modulated by those excipients, and not by the PEO brush layer itself.

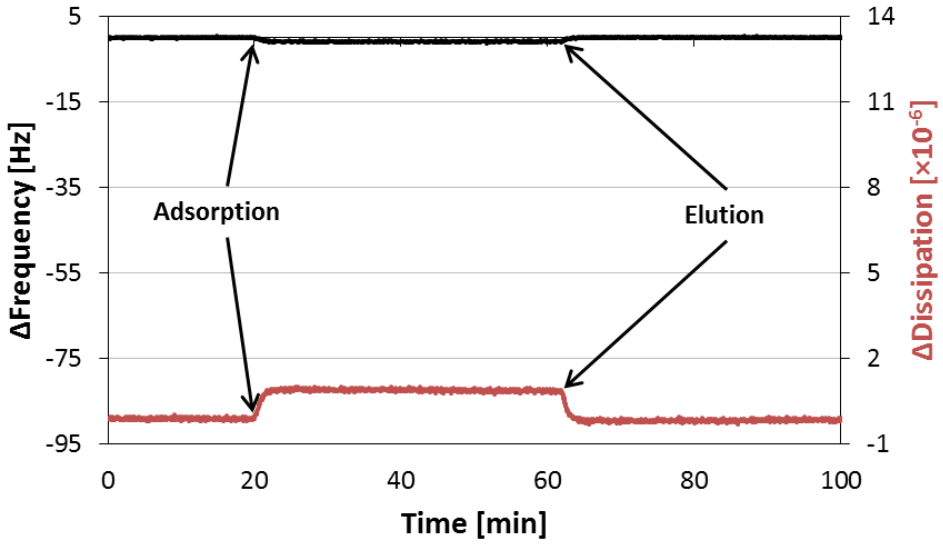

Figure 47: ΔFrequency (black line, primary y-axis) and ΔDissipation (red line, secondary y-axis) for fibrinogen on a surface containing covalently F127 only.

Figure 48 and Figure 49 show the adsorption and elution profiles, by *Δf* and *ΔD*, of a mixture of fibrinogen and LPS on a surface containing entrapped WLBU2 (Figure 48) and one with covalently attached EGAP-WLBU2 (Figure 49). The concentration of fibrinogen is physiologically relevant, at 2 mg/mL, and LPS is at the same concentration for all other experiments, 0.1 mg/mL.

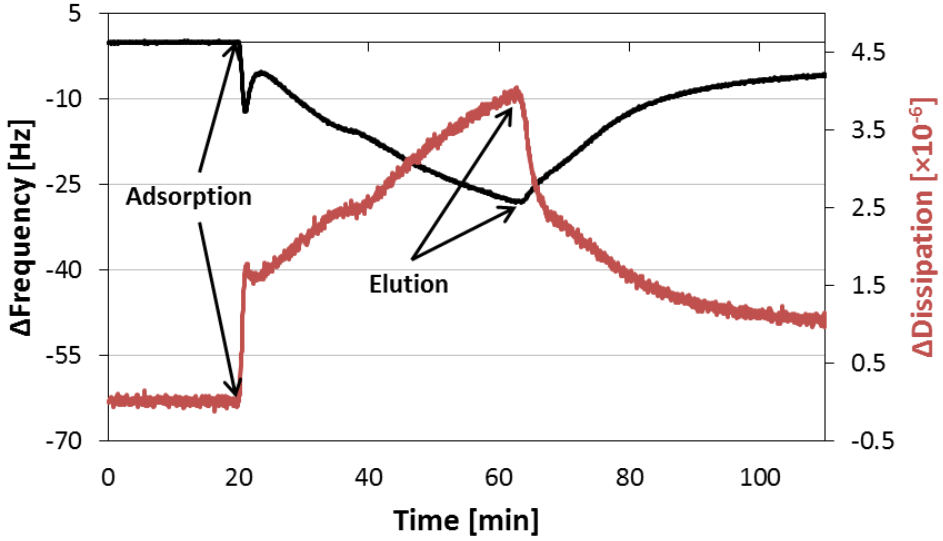

Figure 48: ΔFrequency (black line, primary y-axis) and ΔDissipation (red line, secondary y-axis) for a mixture of fibrinogen and LPS on a surface containing entrapped WLBU2.

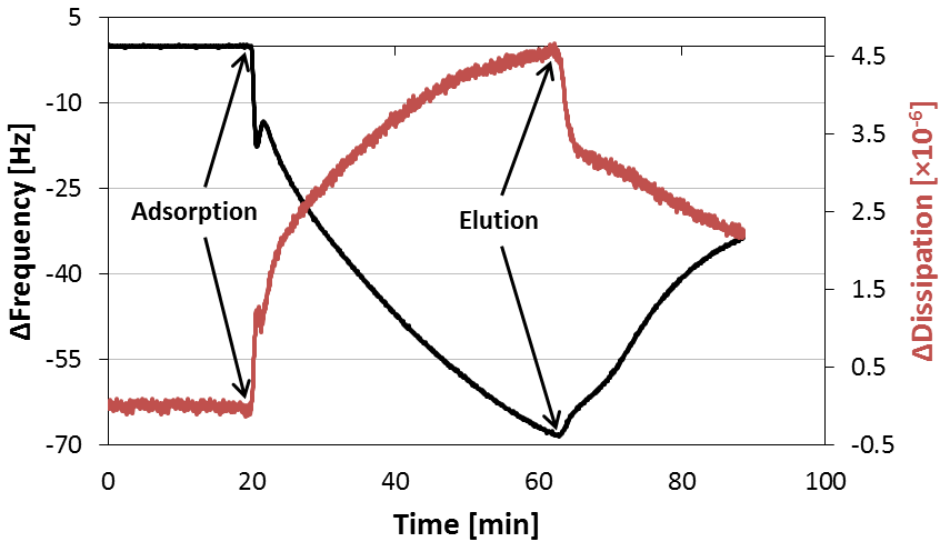

Figure 49: ΔFrequency (black line, primary y-axis) and ΔDissipation (red line, secondary y-axis) for a mixture of fibrinogen and LPS on a surface containing covalently attached EGAP-WLBU2.

It is clear from the shape of these curves that the adsorption and elution of fibrinogen/LPS mixtures is complex. For both sets of data, the total adsorbed amount is higher ($-\Delta f \propto \Delta m$) at the end of both the adsorption and elution steps in the experiment than for LPS adsorption on respective surfaces alone. In the case of entrapped peptide contacted by the mixture (Figure 48), 82% of the adsorbed mass is removed upon elution. For the EGAP-WLBU2 construct challenged by the mixture (Figure 49), 51% of the mass is removed upon elution. Because the total adsorbed mass of both fibrinogen/LPS mixtures was greater than that for LPS alone, it is clear that fibrinogen itself interacts with WLBU2, interacts with LPS in a manner further encouraging location or capture at the interface, or some combination of the two.

Figure 50 shows the comparison of Δf vs time for fibrinogen on an entrapped or tethered surface motif (Figure 50, top), and the Δdissipation vs Δf for these same surfaces (Figure 50, bottom).

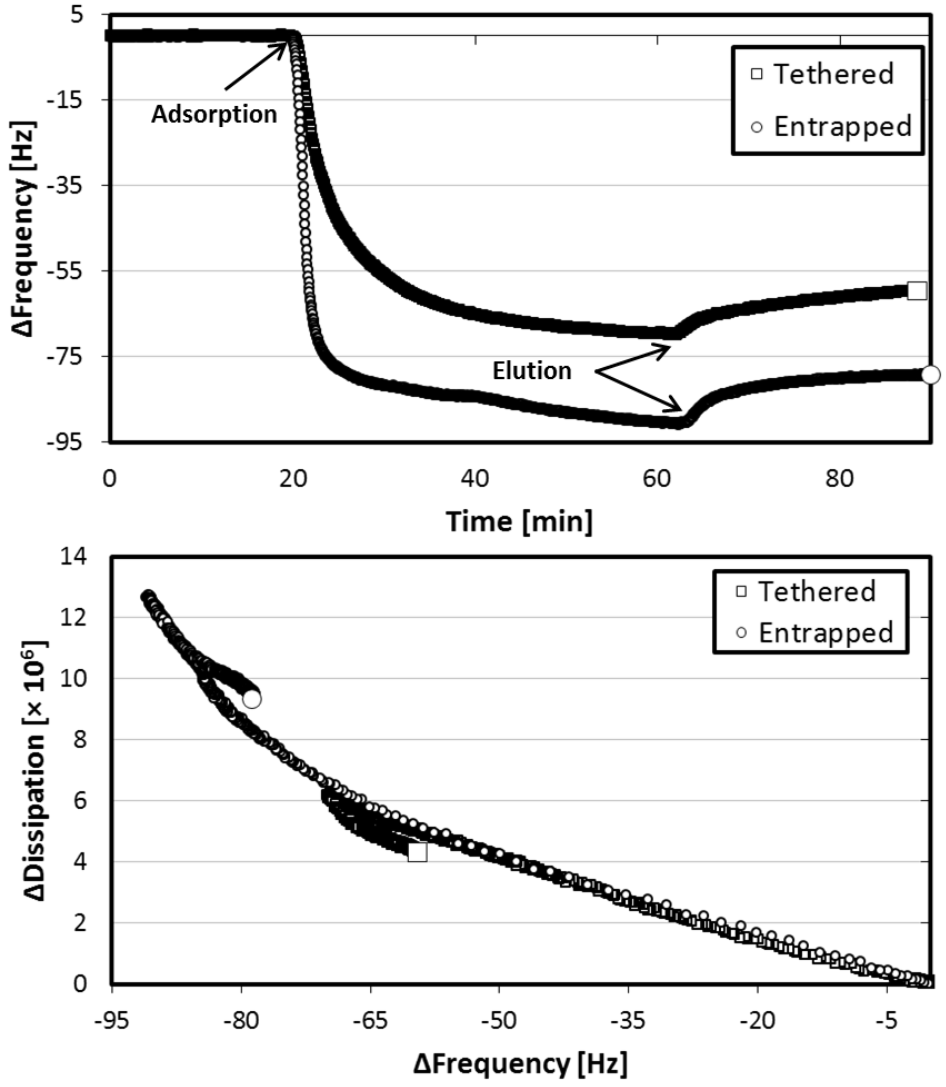

Figure 50: ΔFrequency vs time (top) of fibrinogen challenge of entrapped WLBU2 (○) and tethered WLBU2 (□). The data shows similar curves, albeit different mass loadings in each case. The ΔDissipation vs ΔFrequency (bottom) is shown to largely overlap for each case.

It is clear from the data shown in Figure 50 that fibrinogen does in fact interact with surfaces that contain WLBU2. The nature of this interaction appears not to depend on whether the surface contains entrapped or tethered WLBU2, as shown in Figure 50 (bottom), despite overall mass loading being dissimilar (Figure 50, top). Further evidence of this is that the percent mass eluted is 14% and 15% for fibrinogen on the entrapped or tethered peptide, respectively. This interaction is directly related to the inclusion of WLBU2, as fibrinogen does not substantially adsorb or remain on a surface containing only F127, shown in Figure 47.

The interaction between fibrinogen and WLBU2 associated surfaces is likely not due to a higher order interaction between the two proteins, but likely only suggestive of an electrostatic interaction between the two, as stated previously, WLBU2 contains an out of balance net positive charge of 13, while the outer regions of fibrinogen carry a net negative charge.[182] Interestingly, the adsorption and elution profile of fibrinogen as compared to fibrinogen/LPS mixtures adsorbs and retains more mass for both entrapped and tethered peptide. This strongly suggests that Fibrinogen/LPS mixtures exist as more than a binary mixture of discrete molecules, but rather as a fibrinogen-LPS complex. Further, although the experiments include a physiologically relevant concentration of fibrinogen, the concentration of LPS is well beyond what may be expected in a clinical setting; the 0.1 mg/mL used in this work corresponds to 500 g of LPS circulating in the human body. For this experimentation, using smaller concentrations of LPS may not be efficacious because the capture seen already by this non-optimized device analogue is rather low (Figure 45). More direct investigation of the interactions of fibrinogen and LPS may be required to elucidate nuances shown in the data presented in this work, but for the purposes of a clinical device, it may be more worthwhile to continue investigations in other avenues.

Despite clear evidence that fibrinogen interacts with surfaces containing WLBU2, and that LPS and fibrinogen may create a complex structure, Figure 51 and Figure 52 suggest that WLBU2, whether entrapped or tethered may in fact preferentially capture LPS over fibrinogen. The data shown is of the ratio of Δf to ΔD vs time. Data shown in this manner allows for more direct comparison of surface characteristics with respect to adsorption and elution of various species, and time. Further, viewing the data in this manner reveals intricacies not captured by other graphical methods. For instance, as the ratio $-\Delta f/\Delta D$ increases, the adsorbed mass is changing more rapidly than is the dissipation, suggestive of increasing rigidity. Conversely, as this ratio decreases, the dissipation is increasing more rapidly than the frequency (or is decreasing less rapidly), indicating the overlayer becomes less rigid.

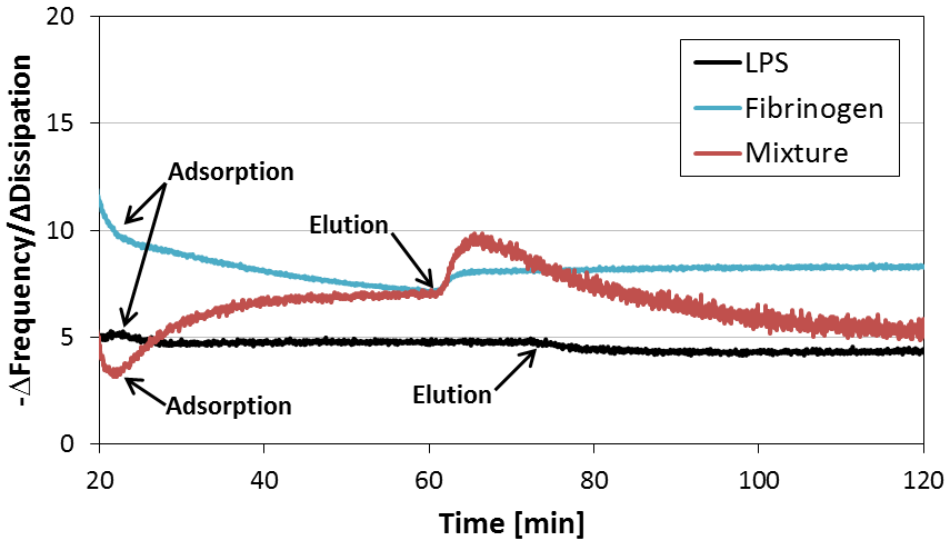

Figure 51: -ΔFrequency/ΔDissipation of LPS (black), Fibrinogen (blue), and a Fibrinogen/LPS mixture (red) on surfaces with entrapped WLBU2. Data shown contains only adsorption and elution ratios. Mass loading was seen to decrease upon elution in all cases.

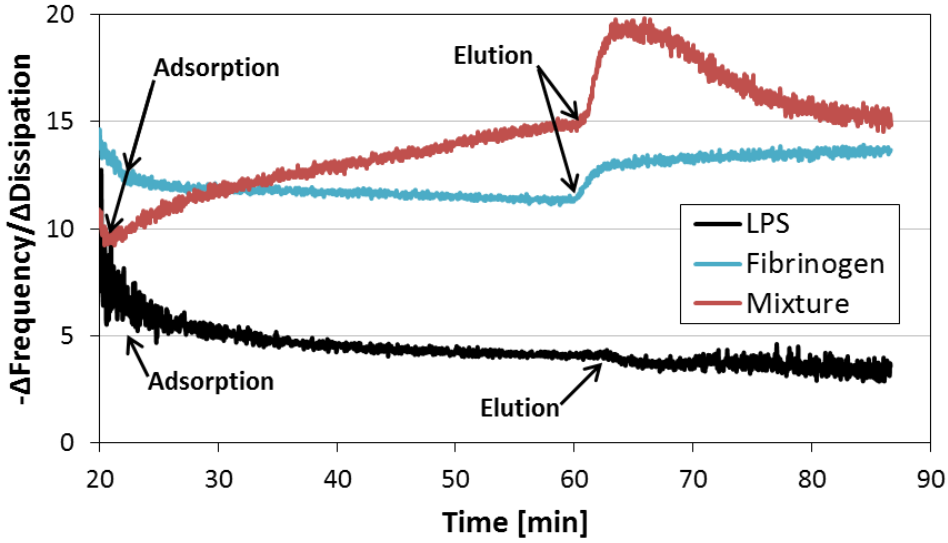

Figure 52: -ΔFrequency/ΔDissipation of LPS (black), Fibrinogen (blue), and a Fibrinogen/LPS mixture (red) on surfaces with tethered WLBU2. Data shown contains only adsorption and elution ratios. Mass loading was seen to decrease upon elution in all cases.

In both Figure 51 and Figure 52, the overall shape of the curves is similar for each surface. For the surfaces challenged with LPS, the ratio, $-\Delta f/\Delta D$, does not appear to change much upon elution. This suggests that the overall structure of the LPS does not change upon elution, or

more specifically, that there is unlikely to be an under layer of spread LPS. The slight decrease, in fact, indicates that the layer becomes less rigid, as mass was seen to decrease (frequency increases) upon elution in all figures showing ΔF vs time. For fibrinogen, the situation is quite the opposite, because the ratio of -ΔFrequency/ΔDissipation increases upon elution, and the mass decreased, the layer must (i) become rigid upon elution, or (ii) loosely bound fibrinogen is removed, revealing a rigid underlayer of associated protein. Finally, for the fibrinogen/LPS mixture on the entrapped WLBU2 surface, ratio of frequency to dissipation is nearly identical to that for fibrinogen at the end of the adsorption cycle, but upon elution comes almost to the same point as that for LPS. This pattern is consistent with a system wherein a smaller molecule with slight affinity for the presented surface approaches that surface more quickly than its larger counterpart that has a higher affinity. Over time the larger, higher affinity molecule would replace the smaller one, resulting in a surface that initially behaves like one containing only the smaller molecule, but ends similarly to a system containing only the larger. As this pattern is seen in Figure 51 and the pattern is similar, albeit not to the same extent in Figure 52, it may be hypothesized that even in a complex milieu containing physiological quantities of fibrinogen, LPS capture is possible with both entrapped and tethered WLBU2.

Conclusions

Analysis of the interaction between surface immobilized, PEG chain entrapped, and PEG chain tethered WLBU2 with LPS using QCM-D, and CD, as well as the effects of γ-irradiation on PEGylated WLBU2 using UV/Vis spectroscopy and NMR, all reveal that WLBU2 can interact with LPS in a manner keeping with its purpose whether irradiated, PEGylated, or tethered. In this way, we have shown that WLBU2 holds promise for use in a hemoperfusive device for the capture of sepsis causing LPS. QCM-D data suggest that LPS capture by tethered WLBU2 likely retains its overall structure, meaning the LPS membranes do not rupture, which would pass LPS fragments back into the body after treatment. Introduction of a more complex milieu, i.e. fibrinogen and fibrinogen/LPS mixtures, reveals that fibrinogen interacts with WLBU2, very likely by electrostatic association as WLBU2 carries a net positive charge, while fibrinogen carries a net negative charge. Furthermore, QCM-D reveals a possible complex between fibrinogen and LPS, rendering this system of less interest when considering the potential capture of LPS from whole blood. We are currently evaluating more relevant concentrations of LPS from solutions

containing blood plasma, while also working toward an optimized surface concentration of presented WLBU2. Results from that work will contribute to the subject of a future report.

Acknowledgments

The authors thank Dr. Kerry McPhail for the use of her CD instrument. The authors also thank Greg McKelvey, and Dan Cheung for their contributions to this work by data collection in NMR and effects of γ-irradiation, as well as Jennifer Neff and Allvivo Vascular Inc. for providing EGAP-PDS. This work was supported in part by the National Institute of Biomedical Imaging and Bioengineering (NIBIB, grant no. R01EB011567). The content is solely the responsibility of the authors and does not necessarily represent the official views of NIBIB or the National Institutes of Health.

CONCLUSIONS

Successful hemoperfusion for sepsis treatment requires surface modification that will ensure highly selective capture of bacteria and endotoxin that enter the interface, without evoking a host cell response, without nonspecific adsorption of protein, and without platelet activation and blood cell damage owing to surface interaction. *Our central hypothesis was that stable location of the antibacterial peptide WLBU2 at an otherwise nonfouling polyethylene oxide (PEO) brush-coated interface, in a fashion allowing peptide mobility and solvent accessibility to be largely preserved, will enable these requirements to be met.* In short, the overall goal of this project was to build a surface, from the bottom up, including how to prepare and modify surfaces for covalent attachment of PEO tethers that will provide a non-fouling interfaces for clinical use, while adding additional therapeutic benefit of antimicrobial peptides for the prevention and treatment of bacterial infection, which commonly results in SIRS, sepsis, or septic shock.

In chapter 3, we showed that PEO-PPO-PEO triblock coatings adsorbed on silica surfaces modified with TCVS and γ-irradiated in the presence of triblock solution were resistant to elution by SDS and showed good fibrinogen repulsion. Nisin adsorption to these PEO layers was detected by zeta potential measurements. Nisin appeared substantially more resistant to elution in the presence of fibrinogen when entrapped in PEO than when adsorbed at an uncoated surface. These tests were conducted in a microsphere motif; while suggestive of the potential efficacy of these coatings, the next important step was to move to a surface more closely related to that in a clinical device, and to directly investigate changes in adsorbed mass in real-time.

In chapter 4, we took the first important steps toward preparing surfaces for the direct investigation of changes in adsorbed mass, specifically using OWLS. When preparing this, or any, surface for chemical modification, it is important to understand the requirements of surface cleaning to ensure reproducible, analyzable results. Chapter 4 showed that the SDS/SC-2 method is effective at cleaning OWLS waveguides off-the-shelf, and showed excellent protein adsorption reproducibility after *ex situ* and *in situ* cleaning of the waveguide. This cleaning method is safer than the other methods that were tested and might also be effective for

cleaning surfaces used in other optical techniques. The SDS/SC-2 method was also tested on Au coated quartz QCM-D sensors carrying thin, patterned gold electrode overlayers (Q-Sense, Sweden) and it was found that the Au electrodes overlayer was almost completely removed by the SC2 portion of the cleaning procedure, rendering the sensors useless. The SDS/SC-2 method presented therein is therefore not recommended for use on those sensors which rely on thin coatings of noble or other metals (e.g. QCM, SPR). For Au coated sensors, it was later found that replacing the SC-2 portion with the SC-1 (replace the acid with a base), and including a UV/O_3 clean resulted in good reproducibility for use in QCM-D.

In chapter 5, analysis of the interfacial behavior of mixtures of LPS and peptide using interfacial tensiometry as well as OWLS, evaluation of peptide structure in such mixtures using CD, and determination of the particle size distributions in such mixtures using DLS, strongly suggest peptide insertion and stabilization of intact LPS vesicles in the case of WLBU2, and peptide-induced destabilization of LPS vesicles in the case of PmB. The research shown in chapter 5 layed the foundation for the potential of tethered peptide to capture LPS from solution. One of the primary outcomes from that work was that we learned what to expect when LPS and WLBU2 interact, and are able to better predict what may occur when LPS is captured in a tethered motif.

Finally, in chapter 6 analysis of the interaction between surface immobilized, PEG chain entrapped, and PEG chain tethered WLBU2 with LPS using QCM-D, and CD, as well as the effects of γ-irradiation on PEGylated WLBU2 using UV/Vis spectroscopy and NMR, all reveal that WLBU2 can interact with LPS in a manner keeping with its purpose whether irradiated, PEGylated, or tethered. In this way, we have shown that WLBU2 holds promise for use in a hemoperfusive device for the capture of sepsis causing LPS. QCM-D data suggest that LPS capture by tethered WLBU2 likely retains its overall structure, meaning the LPS membranes do not rupture, which would pass LPS fragments back into the body after treatment. Introduction of a more complex milieu, i.e. fibrinogen and fibrinogen/LPS mixtures, reveals that fibrinogen interacts with WLBU2, very likely by electrostatic association as WLBU2 carries a net positive charge, while fibrinogen carries a net negative charge. Furthermore, QCM-D reveals a possible complex between fibrinogen and LPS, rendering this system of less interest when considering the

potential capture of LPS from whole blood. This is the keystone work of the project, and provides direct evidence supporting the potential efficacy of using peptides in a tethered motif to capture LPS from a solution containing a complex milieu of proteins and human blood cells.

FUTURE WORK

In a single sentence, this work has shown that tethered WLBU2 can capture LPS from solution. The aim of the larger work which this project supports is to build a hemoperfusive device for the capture of bacteria and bacterial fragments from whole human blood in a clinical relevant setting and time frame. Possibly, the greatest value of the work presented here, is that it opens very many avenues for investigating the design and production of a real device, revealing very many important questions to be addressed. The most immediate opportunities to be addressed in the Biomaterials and Biointerfaces lab include (i) testing the peptide's bioactivity upon tethering, (ii) optimize the surface coating for capture of clinically relevant concentrations of LPS, (iii) capture live bacteria, (iv) capture LPS and/or bacteria from more relevant solution conditions, i.e. blood plasma, (v) monitor the fate of LPS vesicles, and (vi) measure capture when tethered to a biocompatible device material, such as polycarbonate or polyurethane.

Activity of tethered WLBU2

Although the primary cause of sepsis is bacterial cell fragments from Gram(-) bacteria, being the actual progenitors of the fragments, it is important to investigate the interaction between tethered WLBU2 and relevant bacteria. As this project progresses closer and closer toward a clinical device, it will become increasingly important to investigate the interaction between the tethered peptide and bacteria such as *S. epidermidis*. Currently the project has been using *E. coli* as a relevant Gram(-) analogue. The first next step is to more fully investigate the activity of WLBU2 with various PEO tether lengths against *E. coli*. Figure 53 shows preliminary data along these lines. The data shown represents comparisons in the growth profile of WLBU2, EGAP-WLBU2 free in solution, and *E. coli* alone, all normalized to the absorption of the growth medium. In the data, WLBU2, EGAP-WLBU2, and H_2O, respectively, were introduced soon after the lag phase was completed, judged by the OD_{600}.

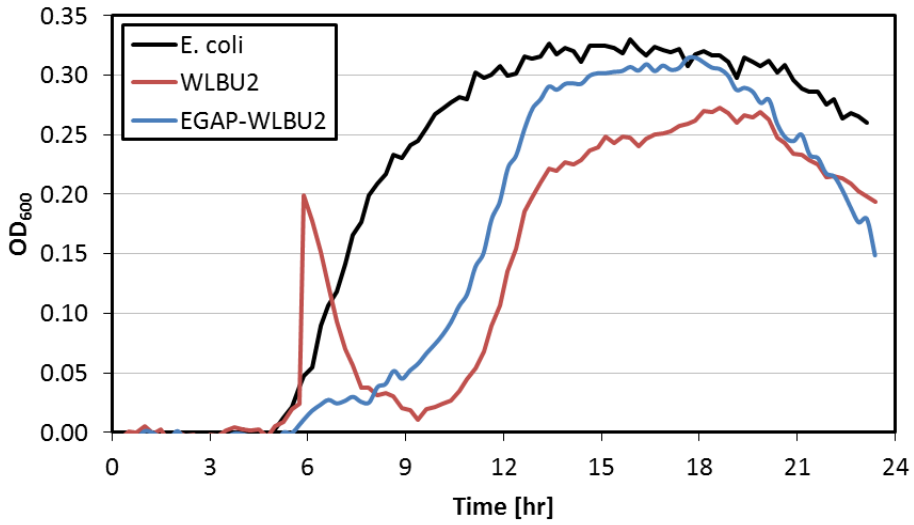

Figure 53: Growth profile of *E. coli* (black), WLBU2 (red), and EGAP-WLBU2 (blue), normalized to the growth medium.

Of interest in the data in Figure 53 is the initial spike in absorption upon introduction of WLBU2, which is not seen in the other two sets of data. Initially thought to be an anomaly, reproduction of this event suggests WLBU2 causes an initial aggregation of cells in the beam path of the system that eventually die and lyse. A similar aggregation phenomenon was suggested anecdotally in chapter 5. Because this event is not present for the EGAP-WLBU2, we can hypothesize that the aggregation may be caused by the creation of WLBU2 "bridges" between cells, and more broadly in LPS vesicles.

The next phase of this research is to repeat this experiment to verify the results seen, and continue testing activity as the length and type of tether is optimized. Eventually these tests need to be performed using *S. epidermidis*.

Coating optimization

Although we successfully demonstrated the ability of WLBU2 to capture LPS from solution, the actual value was remarkably low. The next step in addressing capture of LPS is to optimize the coating conditions and density of WLBU2. One way to accomplish this would be to primarily rely on QCM-D and Au nanoparticles to measure capture and structure of WLBU2 when challenged by LPS. Because traditional QCM relies on the use of Au coated sensors, we can take advantage

of thiol chemistry to approximate covalent attachment. Optimizing the tether strategy will require two simultaneous approaches. First, the tether length should be adjusted to maximize WLBU2 activity, and access to LPS in solution. One important factor to consider when adjusting the tether length, is that very likely the ability of WLBU2 to interact with LPS vesicles will increase as the tether length decreases, to the point where the tether is gone. The tether for WLBU2, when attached to a surface should be longer than the chain length required for non-fouling surface characteristics, but short enough so as not to interrupt blood flow in a disruptive manner while still capturing LPS. Second, the total amount of WLBU2 in a given area should be optimized to reduce peptide waste, maximize non-fouling, but capture appropriate quantities of LPS over relevant timespans and blood volumes. To accomplish this, it is recommended to use heterobifunctional tethers that include a thiol on one end, and an NHS group on the other. In this way, the thiol will interact directly with an Au surface, and the NHS will react covalently with the amine group on WLBU2. The best way to approach modulation of chain density in a laboratory setting is with a backfill study. In brief, PEGylated WLBU2 with a free thiol would be adsorbed to the gold surface, whether QCM sensor, nanoparticle, or other surface. Next, a PEG-thiol to include non-fouling characteristic should be exposed to the surfaces for varied times. Shorter chain lengths will preferentially replace the longer tethers interacting with the surface. In effect, longer contact times will reduce the amount of WLBU2 at the surface, thereby reducing WLBU2 density. These surfaces should then be measured using CD to look at WLBU2 structural change, QCM-D to measure capture quantity, and XPS to calculate the actual density of WLBU2 at the surface. Since these surfaces will contain Au, PEG, and WLBU2, the signal from nitrogen can be tracked to directly quantify the amount of WLBU2, just be sure the buffer system does not contain nitrogen!

Live bacteria

Although it is strongly suggested in chapter 5, we have not directly investigated whether WLBU2 will capture live bacteria, and not lyse these cells over clinically relevant time periods. Although it seems simple, investigating this capture in an appropriate manner provides unique challenges that must be overcome. First, measuring adsorbed mass, while necessary, does not provide information regarding whether the bacterial cell is alive or dead. If the cells are captured, immediately killed, and lyse, this information may be lost in QCM-D, showing up in the data as

slowed kinetic capture. If kill does not happen, the adsorbed mass data should look similarly to data shown in chapter 6. If kill is slow, the data may reveal a slow loss of mass after an initial spike in adsorbed mass. Regardless of these curve shapes, the actual ratio of dead/alive cells will be difficult to discern. One method to investigate this would be to collect the waste during a QCM-D, or OWLS run, and measure the CFUs (on an agar plate), and compare to the original CFUs prior to surface adsorption. If cell concentrations are sufficiently high, a live/dead stain could be conducted to even more directly investigate this ratio.

As an aside, if it is desired to perform experiments of this nature in OWLS, it will be important to ensure the waveguides can sense deep enough into solution to capture the relatively huge size of the bacterial cells.

Blood plasma

In chapter 6, we attempted to take the first steps in investigating capture of LPS in a complex milieu, by adding a relevant blood protein to the solution, fibrinogen. This investigation revealed a complex interaction between LPS and fibrinogen, as well as a substantial interaction between fibrinogen and WLBU2. There are two key problems with this particular investigation. First, because of the complexity of the interactions, this system is not a sufficient clinical analogue. Secondly, the amount of LPS in solution is well beyond what can be expected to be seen in a clinical situation. The next step, therefore, becomes obvious: test using blood plasma and clinically relevant amounts of LPS. If this occurs after the optimization of peptide density, then the amount of LPS can likely be appropriately reduced and still measure capture, if not, the concentration should remain high so capture can be evaluated. Moving toward a blood plasma system should start with reduced plasma concentrations, likely around 10%, and evaluating before moving forward.

Monitor the fate of LPS vesicles

Much of the work related to this is already underway. It is important to locate LPS vesicles and to monitor whether they are being disrupted, both *in situ* and in a prototype device. As previously discussed, one of the major goals of this project is to capture LPS in a way that leaves the vesicle largely intact. Two ways, which can be used separately or simultaneously, to monitor

the fate of these vesicles is to load the vesicles with a fluorescent dye, and to procure or create a fluorescently tagged version of LPS. With the former, we will be able to check to see if vesicles are breaking open upon interaction with WLBU2, or any other peptide of choice. In use in the Biomaterials and Biointerfaces lab currently is loading vesicles with calcein dye. At sufficiently high concentrations of calcein, the natural fluorescence of the molecule is quenched. Therefore, if the vesicle containing the dye, which has been dialyzed to remove excess and external dye, breaks open, the solution fluorescence will increase, indicating the vesicles have been disrupted. This work was begun with an Honors Thesis by Anthony Amsberry. The second method, fluorescent tagging of individual LPS monomers, will help us to fluorescently locate LPS, regardless of vesicle rupture. This will provide another method for evaluating the ability of modified surfaces to capture LPS, and will allow the evaluation of materials and prototypes unsuitable for sensing techniques such as OWLS or QCM-D.

Biomedical Polymers

Finally, while Au, TCVS, and SiO_2 reduce the complexity of the system, and allow easier laboratory research, they are not surfaces that can be expected to be used in a clinical device. These surfaces are more likely to be polycarbonate or polyurethane. For these surfaces, changes to conjugation strategies will need to take place. Polycarbonate may be easier to work with, but it is less chemically resistant than polyurethane. If polyurethane is desired, a clinical device will require a thermoplastic, rather than a thermoset polyurethane so the device can be molded to include the desired structures of the microfluidics. Analyzing mass adsorption on this type of surface may be as simple as spin coating QCM-D sensors with the desired polymer prior to moving forward.

Final Remarks

This project represents an extremely exciting foray into medical device design for the purpose of treatment of sepsis. We have been able to demonstrate capture of LPS using a tethered peptide. It is important, however to remember, that while we have shown the promise of WLBU2, some other peptide may be more appropriate for this effort. Regardless, it seems a hemoperfusive device that reduces reliance on antibiotics and can treat a variety of bacterial infections in whole human blood may indeed be on the horizon.

REFERENCES

1. Czura CJ. "Merinoff Symposium 2010: Sepsis"—Speaking with One Voice. Molecular Medicine 2011;17(1-2):2.
2. Dombrovskiy VY, Martin AA, Sunderram J, Paz HL. Rapid increase in hospitalization and mortality rates for severe sepsis in the United States: A trend analysis from 1993 to 2003*. Critical care medicine 2007;35(5):1244-1250.
3. Wood KA, Angus DC. Pharmacoeconomic implications of new therapies in sepsis. Pharmacoeconomics 2004;22(14):895-906.
4. Matsuno N, Ikeda T, Ikeda K, Hama K, Iwamoto H, Uchiyama M, Kozaki K, Narumi Y, Kikuchi K, Degawa H. Changes of cytokines in direct endotoxin adsorption treatment on postoperative multiple organ failure. Therapeutic Apheresis 2001;5(1):36-39.
5. Angus DC, Wax RS. Epidemiology of sepsis: An update. Critical Care Medicine 2001;29(7):S109-S116.
6. Angus DC, Linde-Zwirble WT, Lidicker J, Clermont G, Carcillo J, Pinsky MR. Epidemiology of severe sepsis in the United States: analysis of incidence, outcome, and associated costs of care. Critical care medicine 2001;29(7):1303-1310.
7. Cohen J. The immunopathogenesis of sepsis. Nature 2002;420(6917):885-891.
8. Davies B, Cohen J. Endotoxin removal devices for the treatment of sepsis and septic shock. The Lancet Infectious Diseases 2011;11(1):65-71.
9. Shoji H. Extracorporeal endotoxin removal for the treatment of sepsis: endotoxin adsorption cartridge (Toraymyxin). Therapeutic Apheresis and Dialysis 2003;7(1):108-114.
10. Vincent J-L, Laterre P-F, Cohen J, Burchardi H, Bruining H, Lerma FA, Wittebole X, De Backer D, Brett S, Marzo D. A pilot-controlled study of a polymyxin B-immobilized hemoperfusion cartridge in patients with severe sepsis secondary to intra-abdominal infection. Shock 2005;23(5):400-405.
11. Ikeda T. Hemoadsorption in critical care. Therapeutic Apheresis 2002;6(3):189-192.
12. Ueno T, Sugino M, Nemoto H, Shoji H, Kakita A, Watanabe M. Effect Over Time of Endotoxin Adsorption Therapy in Sepsis. Therapeutic Apheresis and Dialysis 2005;9(2):128-136.
13. Anspach FB, Hilbeck O. Removal of endotoxins by affinity sorbents. Journal of Chromatography A 1995;711(1):81-92.
14. Buttenschoen K, Radermacher P, Bracht H. Endotoxin elimination in sepsis: physiology and therapeutic application. Langenbeck's Archives of Surgery 2010;395(6):597-605.
15. Li J, Nation RL, Turnidge JD, Milne RW, Coulthard K, Rayner CR, Paterson DL. Colistin: the re-emerging antibiotic for multidrug-resistant Gram-negative bacterial infections. Lancet Infectious Diseases 2006;6(9):589-601.
16. Hogardt M, Schmoldt S, Götzfried M, Adler K, Heesemann J. Pitfalls of polymyxin antimicrobial susceptibility testing of *Pseudomonas aeruginosa* isolated from cystic fibrosis patients. Journal of Antimicrobial Chemotherapy 2004;54(6):1057-1061.
17. Scott MG, Yan H, Hancock REW. Biological properties of structurally related α-helical cationic antimicrobial peptides. Infection and immunity 1999;67(4):2005-2009.
18. Gough M, Hancock RE, Kelly NM. Antiendotoxin activity of cationic peptide antimicrobial agents. Infection and immunity 1996;64(12):4922-4927.

19. Cirioni O, Giacometti A, Ghiselli R, Bergnach C, Orlando F, Silvestri C, Mocchegiani F, Licci A, Skerlavaj B, Rocchi M. LL-37 protects rats against lethal sepsis caused by gram-negative bacteria. Antimicrobial agents and chemotherapy 2006;50(5):1672-1679.
20. Deslouches B, Islam K, Craigo JK, Paranjape SM, Montelaro RC, Mietzner TA. Activity of the de novo engineered antimicrobial peptide WLBU2 against Pseudomonas aeruginosa in human serum and whole blood: implications for systemic applications. Antimicrobial agents and chemotherapy 2005;49(8):3208-3216.
21. Deslouches B, Phadke SM, Lazarevic V, Cascio M, Islam K, Montelaro RC, Mietzner TA. De novo generation of cationic antimicrobial peptides: influence of length and tryptophan substitution on antimicrobial activity. Antimicrobial agents and chemotherapy 2005;49(1):316-322.
22. Deslouches B, Gonzalez IA, DeAlmeida D, Islam K, Steele C, Montelaro RC, Mietzner TA. De novo-derived cationic antimicrobial peptide activity in a murine model of Pseudomonas aeruginosa bacteraemia. Journal of antimicrobial chemotherapy 2007;60(3):669-672.
23. Montelaro RC, Mietzner TA. Virus derived antimicrobial peptides. U.S. Patent 6,887,847; 2005.
24. Gonzalez I, Wong X, De Almeida D, Yurko R, Watkins S, Islam K, Montelaro R, El-Ghannam A, Mietzner T. Peptides as potent antimicrobials tethered to a solid surface: Implications for medical devices. Nature Precedings; 2008.
25. Skinner MC, Kiselev AO, Isaacs CE, Mietzner TA, Montelaro RC, Lampe MF. Evaluation of WLBU2 peptide and 3-O-octyl-sn-glycerol lipid as active ingredients for a topical microbicide formulation targeting Chlamydia trachomatis. Antimicrobial agents and chemotherapy 2010;54(2):627-636.
26. Costa F, Carvalho IF, Montelaro RC, Gomes P, Martins MCL. Covalent immobilization of antimicrobial peptides (AMPs) onto biomaterial surfaces. Acta Biomaterialia 2011;7(4):1431-1440.
27. Onaizi SA, Leong SSJ. Tethering antimicrobial peptides: Current status and potential challenges. Biotechnology Advances 2011;29(1):67-74.
28. Wheeler AP, Bernard GR. Treating patients with severe sepsis. New England Journal of Medicine 1999;340(3):207-214.
29. The Ohio State University Medical Center: Sepsis. SepsisAlliance.org2011.
30. Silva E, Pedro Mde A, Sogayar AC, Mohovic T, Silva CL, Janiszewski M, Cal RG, de Sousa EF, Abe TP, de Andrade J. Brazilian sepsis epidemiological study (BASES study). Crit Care 2004;8(4):R251-60.
31. Burchardi H, Schneider H. Economic aspects of severe sepsis. Pharmacoeconomics 2004;22(12):793-813.
32. Dellinger RP, Levy MM, Carlet JM, Bion J, Parker MM, Jaeschke R, Reinhart K, Angus DC, Brun-Buisson C, Beale R. Surviving Sepsis Campaign: international guidelines for management of severe sepsis and septic shock: 2008. Intensive care medicine 2008;34(1):17-60.
33. Petsch D, Anspach FB. Endotoxin removal from protein solutions. Journal of biotechnology 2000;76(2):97-119.
34. Gross E, Morell JL. Structure of nisin. Journal of the American Chemical Society 1971;93(18):4634-4635.
35. Hurst A. Nisin. Advances in applied microbiology 1981;27:85-123.

36. van Heusden HE, de Kruijff B, Breukink E. Lipid II induces a transmembrane orientation of the pore-forming peptide lantibiotic nisin. Biochemistry 2002;41(40):12171-12178.
37. Hasper HE, de Kruijff B, Breukink E. Assembly and stability of nisin-lipid II pores. Biochemistry 2004;43(36):11567-11575.
38. Delves-Broughton J, Blackburn P, Evans RJ, Hugenholtz J. Applications of the bacteriocin, nisin. Antonie van Leeuwenhoek 1996;69(2):193-202.
39. Mattick ATR, Hirsch A. A powerful inhibitory substance produced by group N streptococci. Nature 1944;154(3913):551.
40. Whitehead HR, Riddet W. Slow development of acidity in cheese manufacture. Government Printer; 1933.
41. Hirsch A. Growth and nisin production of a strain of Streptococcus lactis. Journal of General Microbiology 1951;5(1):208-221.
42. Berridge NJ, Newton GGF, Abraham EP. Purification and nature of the antibiotic nisin. Biochemical Journal 1952;52(4):529.
43. Wiedemann I, Breukink E, van Kraaij C, Kuipers OP, Bierbaum G, de Kruijff B, Sahl H-G. Specific binding of nisin to the peptidoglycan precursor lipid II combines pore formation and inhibition of cell wall biosynthesis for potent antibiotic activity. Journal of Biological Chemistry 2001;276(3):1772-1779.
44. Twomey D, Ross RP, Ryan M, Meaney B, Hill C. Lantibiotics produced by lactic acid bacteria: structure, function and applications. Antonie Van Leeuwenhoek 2002;82(1-4):165-185.
45. Willey JM, van der Donk WA. Lantibiotics: peptides of diverse structure and function. Annu. Rev. Microbiol. 2007;61:477-501.
46. Schnell N, Entian K-D, Schneider U, Götz F, Zähner H, Kellner R, Jung G. Prepeptide sequence of epidermin, a ribosomally synthesized antibiotic with four sulphide-rings. 1988.
47. Piper C, Draper LA, Cotter PD, Ross RP, Hill C. A comparison of the activities of lacticin 3147 and nisin against drug-resistant Staphylococcus aureus and Enterococcus species. Journal of Antimicrobial Chemotherapy 2009;64(3):546-551.
48. Breukink E, Wiedemann I, Van Kraaij C, Kuipers OP, Sahl HG, De Kruijff B. Use of the cell wall precursor lipid II by a pore-forming peptide antibiotic. Science 1999;286(5448):2361-2364.
49. Hsu S-TD, Breukink E, Tischenko E, Lutters MAG, de Kruijff B, Kaptein R, Bonvin AMJJ, van Nuland NAJ. The nisin–lipid II complex reveals a pyrophosphate cage that provides a blueprint for novel antibiotics. Nature structural & molecular biology 2004;11(10):963-967.
50. Breukink E, de Kruijff B. Lipid II as a target for antibiotics. Nature Reviews Drug Discovery 2006;5(4):321-323.
51. Hasper HE, Kramer NE, Smith JL, Hillman JD, Zachariah C, Kuipers OP, De Kruijff B, Breukink E. An alternative bactericidal mechanism of action for lantibiotic peptides that target lipid II. Science 2006;313(5793):1636-1637.
52. Guiotto A, Pozzobon M, Canevari M, Manganelli R, Scarin M, Veronese FM. PEGylation of the antimicrobial peptide nisin A: problems and perspectives. Il Farmaco 2003;58(1):45-50.
53. Ainsworth GC, Brown AM, Brownlee G. Aerosporin, an antibiotic produced by Bacillus aerosporus Greer. Nature 1947;160(263):878.

54. Lopes J, Inniss WE. Electron microscopy of effect of polymyxin on Escherichia coli lipopolysaccharide. Journal of bacteriology 1969;100(2):1128.
55. Evans ME, Feola DJ, Rapp RP. Polymyxin B sulfate and colistin: old antibiotics for emerging multiresistant gram-negative bacteria. The Annals of pharmacotherapy 1999;33(9):960-967.
56. Pulaski EJ, Baker HJ, Rosenberg ML, Connell Jr JF. Laboratory and clinical studies of polymyxin B and E. Journal of Clinical Investigation 1949;28(5 Pt 1):1028.
57. Kunin CM, Bugg A. Binding of polymyxin antibiotics to tissues: the major determinant of distribution and persistence in the body. Journal of Infectious Diseases 1971;124(4):394-400.
58. Pedersen MF, Pedersen JF, Adsen PO. A clinical and experimental comparative study of sodium colistimethate and polymyxin B sulfate. Investigative urology 1971;9(3):234.
59. Vinnicombe J, Stamey TA. The relative nephrotoxicities of polymyxin B sulfate, sodium sulfomethyl-polymyxin B, sodium sulfomethyl-colistin (colymycin), and neomycin sulfate. Investigative urology 1969;6(5):505.
60. Thomas CJ, Surolia A. Kinetics of the interaction of endotoxin with polymyxin B and its analogs: a surface plasmon resonance analysis. FEBS letters 1999;445(2):420-424.
61. Neosporin. 2013 April 10, 2013. Neosporin: First Aid Products FAQ. <http://www.neosporin.com/first-aid/first-aid-faq>. Accessed 2013 April 10, 2013.
62. Cooperstock MS. Inactivation of endotoxin by polymyxin B. Antimicrobial agents and chemotherapy 1974;6(4):422-425.
63. Morrison DC, Jacobs DM. Binding of polymyxin B to the lipid A portion of bacterial lipopolysaccharides. Immunochemistry 1976;13(10):813-818.
64. Thomas CJ, Gangadhar BP, Surolia N, Surolia A. Kinetics and mechanism of the recognition of endotoxin by polymyxin B. Journal of the American Chemical Society 1998;120(48):12428-12434.
65. Kwa A, Kasiakou SK, Tam VH, Falagas ME. Polymyxin B: similarities to and differences from colistin (polymyxin E). Expert review of anti-infective therapy 2007;5(5):811-821.
66. Zavascki AP, Goldani LZ, Li J, Nation RL. Polymyxin B for the treatment of multidrug-resistant pathogens: a critical review. Journal of antimicrobial chemotherapy 2007;60(6):1206-1215.
67. Cardoso L, Araujo M, Góes A, Pacífico L, Oliveira R, Oliveira S. Polymyxin B as inhibitor of LPS contamination of Schistosoma mansoni recombinant proteins in human cytokine analysis. Microbial cell factories 2007;6(1):1.
68. Hancock REW. Peptide antibiotics. The Lancet 1997;349(9049):418-422.
69. Hancock REW, Lehrer R. Cationic peptides: a new source of antibiotics. Trends in biotechnology 1998;16(2):82-88.
70. Hancock REW. Cationic peptides: effectors in innate immunity and novel antimicrobials. The Lancet Infectious Diseases 2001;1(3):156-164.
71. Friedrich CL, Moyles D, Beveridge TJ, Hancock REW. Antibacterial action of structurally diverse cationic peptides on gram-positive bacteria. Antimicrobial agents and chemotherapy 2000;44(8):2086-2092.
72. Hancock REW, Chapple DS. Peptide antibiotics. Antimicrobial Agents and Chemotherapy 1999;43(6):1317-1323.
73. Hancock REW, Rozek A. Role of membranes in the activities of antimicrobial cationic peptides. FEMS Microbiology Letters 2002;206(2):143-149.

74. Marr AK, Gooderham WJ, Hancock REW. Antibacterial peptides for therapeutic use: obstacles and realistic outlook. Current opinion in pharmacology 2006;6(5):468-472.
75. Piers KL, Brown MH, Hancock RE. Improvement of outer membrane-permeabilizing and lipopolysaccharide-binding activities of an antimicrobial cationic peptide by C-terminal modification. Antimicrobial agents and chemotherapy 1994;38(10):2311-2316.
76. Wilcox S. Cationic Peptides: A New Hope. The Science Creative Quarterly2004.
77. Turner J, Cho Y, Dinh N-N, Waring AJ, Lehrer RI. Activities of LL-37, a cathelin-associated antimicrobial peptide of human neutrophils. Antimicrobial agents and chemotherapy 1998;42(9):2206-2214.
78. Schaller-Bals S, Schulze A, Bals R. Increased levels of antimicrobial peptides in tracheal aspirates of newborn infants during infection. American journal of respiratory and critical care medicine 2002;165(7):992-995.
79. Bucki R, Namiot DB, Namiot Z, Savage PB, Janmey PA. Salivary mucins inhibit antibacterial activity of the cathelicidin-derived LL-37 peptide but not the cationic steroid CSA-13. Journal of antimicrobial chemotherapy 2008;62(2):329-335.
80. Chen C, Brock R, Luh F, Chou P-J, Larrick JW, Huang R-F, Huang T-h. The solution structure of the active domain of CAP18—a lipopolysaccharide binding protein from rabbit leukocytes. FEBS letters 1995;370(1):46-52.
81. Tencza SB, Douglass JP, Creighton DJ, Montelaro RC, Mietzner TA. Novel antimicrobial peptides derived from human immunodeficiency virus type 1 and other lentivirus transmembrane proteins. Antimicrobial agents and chemotherapy 1997;41(11):2394-2398.
82. Zidovetzki R, Rost B, Armstrong DL, Pecht I. Transmembrane domains in the functions of Fc receptors. Biophysical chemistry 2003;100(1):555-575.
83. Novak KF, Diamond WJ, Kirakodu S, Peyyala R, Anderson KW, Montelaro RC, Mietzner TA. Efficacy of the de novo-derived antimicrobial peptide WLBU2 against oral bacteria. Antimicrobial agents and chemotherapy 2007;51(5):1837-1839.
84. McClanahan JR, Peyyala R, Mahajan R, Montelaro RC, Novak KF, Puleo DA. Bioactivity of WLBU2 peptide antibiotic in combination with bioerodible polymer. International Journal of Antimicrobial Agents 2011;38(6):530-533.
85. Dakss M, Kuhn L, Heidrich P, Scott B. Grating coupler for efficient excitation of optical guided waves in thin films. Applied physics letters 1970;16(12):523-525.
86. Tiefenthaler K, Lukosz W. Integrated optical switches and gas sensors. Optics Letters 1984;9(4):137-139.
87. Spohn P, Prenosil J, Tiefenthaler K. A novel instrumental set-up for in-situ detection of protein adsorption with grating coupler sensors (GCS). Analytical Letters 1990;23(3):411-424.
88. Spohn P, Seifert M. Interaction of aqueous solutions with grating couplers used as integrated optical sensors and their pH behaviour. Sensors and Actuators 1988;15(4):309-324.
89. Horvath R, Fricsovszky G, Papp E. Application of the optical waveguide lightmode spectroscopy to monitor lipid bilayer phase transition. Biosensors and bioelectronics 2003;18(4):415-428.
90. Horváth R, Pedersen HC, Skivesen N, Selmeczi D, Larsen NB. Optical waveguide sensor for on-line monitoring of bacteria. Optics letters 2003;28(14):1233-1235.

91. Székács A, Adányi N, Székács I, Majer-Baranyi K, Szendrő I. Optical waveguide light-mode spectroscopy immunosensors for environmental monitoring. Applied optics 2009;48(4):B151-B158.
92. Hild E. 2000 April 6, 2013. Planar wave guides as chemical and biological sensors. MicroVaccum Ltd. <http://www.owls-sensors.com/pdf/theory.pdf>. Accessed 2013 April 6, 2013.
93. De Feijter JA, Benjamins dJ, Veer FA. Ellipsometry as a tool to study the adsorption behavior of synthetic and biopolymers at the air–water interface. Biopolymers 1978;17(7):1759-1772.
94. Ramsden JJ. Concentration scaling of protein deposition kinetics. Physical Review Letters 1993;71(2):295-298.
95. Sauerbrey G. Use of quartz vibration for weighing thin films on a microbalance. J. Physik 1959;155:206-212.
96. Martins MCL, Sousa SR, Antunes JC, Barbosa MA. Protein adsorption characterization. Nanotechnology in Regenerative Medicine: Springer; 2012. p 141-161.
97. Johannsmann D. Studies of Contact Mechanics with the QCM. Piezoelectric sensors: Springer; 2007. p 151-170.
98. Johannsmann D. Studies of Viscoelasticity with the QCM. Piezoelectric Sensors: Springer; 2007. p 49-109.
99. qsense. December 30. The QCM-D Principle. <http://www.q-sense.com/support-education/faq-qcm-d/the-qcm-d-principle>. Accessed 2013 December 30.
100. Keller C, Kasemo B. Surface specific kinetics of lipid vesicle adsorption measured with a quartz crystal microbalance. Biophysical Journal 1998;75(3):1397-1402.
101. Dugdale DC, Ramsey PG. *Staphylococcus aureus* bacteremia in patients with Hickman catheters. The American journal of medicine 1990;89(2):137-141.
102. Raad II, Bodey GP. Infectious complications of indwelling vascular catheters. Clinical infectious diseases 1992:197-208.
103. Raad I, Narro J, Khan A, Tarrand J, Vartivarian S, Bodey G. Serious complications of vascular catheter-relatedStaphylococcus aureus bacteremia in cancer patients. European Journal of Clinical Microbiology and Infectious Diseases 1992;11(8):675-682.
104. Bower C, Bothwell M, McGuire J. Lantibiotics as surface active agents for biomedical applications. Colloids and Surfaces B: Biointerfaces 2001;22(4):259-265.
105. Bower C, Parker J, Higgins A, Oest M, Wilson J, Valentine B, Bothwell M, McGuire J. Protein antimicrobial barriers to bacterial adhesion: in vitro and in vivo evaluation of nisin-treated implantable materials. Colloids and Surfaces B: Biointerfaces 2002;25(1):81-90.
106. Tai Y-C, Joshi P, McGuire J, Neff JA. Nisin adsorption to hydrophobic surfaces coated with the PEO–PPO–PEO triblock surfactant Pluronic< sup>®</sup> F108. Journal of colloid and interface science 2008;322(1):112-118.
107. Tai Y-C, McGuire J, Neff JA. Nisin antimicrobial activity and structural characteristics at hydrophobic surfaces coated with the PEO–PPO–PEO triblock surfactant Pluronic< sup>®</sup> F108. Journal of colloid and interface science 2008;322(1):104-111.
108. Malmsten M, Emoto K, Van Alstine JM. Effect of chain density on inhibition of protein adsorption by poly (ethylene glycol) based coatings. Journal of colloid and interface science 1998;202(2):507-517.

109. Rovira-Bru M, Giralt F, Cohen Y. Protein adsorption onto zirconia modified with terminally grafted polyvinylpyrrolidone. Journal of colloid and interface science 2001;235(1):70-79.
110. Archambault JG, Brash JL. Protein resistant polyurethane surfaces by chemical grafting of PEO: amino-terminated PEO as grafting reagent. Colloids and Surfaces B: Biointerfaces 2004;39(1):9-16.
111. Halperin A. Polymer brushes that resist adsorption of model proteins: Design parameters. Langmuir 1999;15(7):2525-2533.
112. Sheth S, Leckband D. Measurements of attractive forces between proteins and end-grafted poly (ethylene glycol) chains. Proceedings of the National Academy of Sciences 1997;94(16):8399-8404.
113. Fang F, Satulovsky J, Szleifer I. Kinetics of protein adsorption and desorption on surfaces with grafted polymers. Biophysical journal 2005;89(3):1516-1533.
114. Unsworth LD, Sheardown H, Brash JL. Protein-resistant poly (ethylene oxide)-grafted surfaces: Chain density-dependent multiple mechanisms of action. Langmuir 2008;24(5):1924-1929.
115. Katira P, Agarwal A, Hess H. A random sequential adsorption model for protein adsorption to surfaces functionalized with poly (ethylene oxide). Advanced Materials 2009;21(16):1599-1604.
116. McPherson TB, Shim HS, Park K. Grafting of PEO to glass, nitinol, and pyrolytic carbon surfaces by γ irradiation. Journal of biomedical materials research 1997;38(4):289-302.
117. Popat KC, Johnson RW, Desai TA. Characterization of vapor deposited thin silane films on silicon substrates for biomedical microdevices. Surface and Coatings Technology 2002;154(2):253-261.
118. Park K, Shim HS, Dewanjee MK, Eigler NL. In vitro and in vivo studies of PEO-grafted blood-contacting cardiovascular prostheses. Journal of Biomaterials Science, Polymer Edition 2000;11(11):1121-1134.
119. Rajam S, Ho C-C. Graft coupling of PEO to mixed cellulose esters microfiltration membranes by UV irradiation. Journal of membrane science 2006;281(1):211-218.
120. Hild E. 2000 May 5, 2013. Planar wave guides as chemical and biological sensors. <http://www.owls-sensors.com/pdf/theory.pdf>. May 5, 2013.
121. Lukosz W. Integrated optical chemical and direct biochemical sensors. Sensors and Actuators B: Chemical 1995;29(1–3):37-50.
122. Nellen PM, Tiefenthaler K, Lukosz W. Integrated optical input grating couplers as biochemical sensors. Sensors and Actuators 1988;15(3):285-295.
123. Ramsden JJ. Optical biosensors. Journal of Molecular Recognition 1997;10(3):109-120.
124. Brandt GB, Supertzi EP, Henningsen T. Substrate cleaning for integrated optical waveguides. Applied Optics 1973;12(12):2898-2900.
125. Cras JJ, Rowe-Taitt CA, Nivens DA, Ligler FS. Comparison of chemical cleaning methods of glass in preparation for silanization. Biosensors and Bioelectronics 1999;14(8):683-688.
126. Gould G, Irene EA. The Influence of Silicon Surface Cleaning Procedures on Silicon Oxidation. Journal of the Electrochemical Society 1986;134(4):1031-1033.
127. Henke L, Nagy N, Krull UJ. An AFM determination of the effects on surface roughness caused by cleaning of fused silica and glass substrates in the process of optical biosensor preparation. Biosensors and Bioelectronics 2002;17(6):547-555.

128. Kern W. The evolution of silicon wafer cleaning technology. Journal of the Electrochemical Society 1990;137(6):1887-1892.
129. Svensson O, Arnebrant T. Adsorption of serum albumin on silica–The influence of surface cleaning procedures. Journal of Colloid and Interface Science 2010;344(1):44-47.
130. Höök F, Vörös J, Rodahl M, Kurrat R, Böni P, Ramsden JJ, Textor M, Spencer ND, Tengvall P, Gold J. A comparative study of protein adsorption on titanium oxide surfaces using in situ ellipsometry, optical waveguide lightmode spectroscopy, and quartz crystal microbalance/dissipation. Colloids and Surfaces B: Biointerfaces 2002;24(2):155-170.
131. Bhalla V, Carrara S, Stagni C, Samorì B. Chip cleaning and regeneration for electrochemical sensor arrays. Thin Solid Films 2010;518(12):3360-3366.
132. Svendsen IE, Santos O, Sotres J, Wennerberg A, Breding K, Arnebrant T, Lindh L. Adsorption of HSA, IgG and laminin-1 on model hydroxyapatite surfaces–effects of surface characteristics. Biofouling 2012;28(1):87-97.
133. Halthur TJ, Arnebrant T, Macakova L, Feiler A. Sequential adsorption of bovine mucin and lactoperoxidase to various substrates studied with quartz crystal microbalance with dissipation. Langmuir 2010;26(7):4901-4908.
134. Olsen C, Van Tassel PR. Polyelectrolyte adsorption kinetics under an applied electric potential: Strongly versus weakly charged polymers. Journal of colloid and interface science 2009;329(2):222-227.
135. Aslan S, Deneufchatel M, Hashmi S, Li N, Pfefferle LD, Elimelech M, Pauthe E, Van Tassel PR. Carbon nanotube-based antimicrobial biomaterials formed via layer-by-layer assembly with polypeptides. Journal of colloid and interface science 2012.
136. Calonder C, Tie Y, Van Tassel PR. History dependence of protein adsorption kinetics. Proceedings of the National Academy of Sciences of the United States of America 2001;98(19):10664-10669.
137. Schilke KF, Snider JL, Jansen LE, McGuire J. Direct imaging of the surface distribution of immobilized cleavable polyethylene oxide-polybutadiene-polyethylene oxide triblock surfactants by atomic force microscopy. Surface and Interface Analysis 2012.
138. Ramsden JJ. Biomimetic protein immobilization using lipid bilayers. Biosensors and Bioelectronics 1998;13(6):593-598.
139. Kern W, Puotinen DA. Cleaning solutions based on hydrogen peroxide for use in silicon semiconductor technology. RCA Reviews 1970;31:187-206.
140. Almazán-Almazán MC, Paredes J, Pérez-Mendoza M, Domingo-García M, López-Garzón F, Martínez-Alonso A, Tascón J. Surface characterisation of plasma-modified poly (ethylene terephthalate). Journal of colloid and interface science 2006;293(2):353-363.
141. Grace JM, Gerenser LJ. Plasma treatment of polymers. Journal of dispersion science and technology 2003;24(3-4):305-341.
142. Dowling DP, Miller IS, Ardhaoui M, Gallagher WM. Effect of surface wettability and topography on the adhesion of osteosarcoma cells on plasma-modified polystyrene. Journal of biomaterials applications 2011;26(3):327-347.
143. Kleinhans C, Barz J, Wurster S, Willig M, Oehr C, Müller M, Walles H, Hirth T, Kluger PJ. Ammonia plasma treatment of polystyrene surfaces enhances proliferation of primary human mesenchymal stem cells and human endothelial cells. Biotechnology journal 2012.
144. Wood K, Angus D. Pharmacoeconomic Implications of New Therapies in Sepsis. Pharmacoeconomics 2004;22(14):895-906.

145. Matsuno N, Ikeda T, Ikeda K, Hama K, Iwamoto H, Uchiyama M, Kozaki K, Narumi Y, Kikuchi K, Degawa H and others. Changes of Cytokines in Direct Endotoxin Adsorption Treatment on Postoperative Multiple Organ Failure. Therapeutic Apheresis 2001;5(1):36-39.
146. Anspach FB. Endotoxin removal by affinity sorbents. Journal of Biochemical and Biophysical Methods 2001;49(1–3):665-681.
147. Shoji H. Extracorporeal Endotoxin Removal For The Treatment of Sepsis:Endotoxin Adsorption Cartridge (Toraymyxin). Therapeutic Apheresis and Dialysis 2003;7(1):108-114.
148. Vincent J-L, Laterre P-F, Cohen J, Burchardi H, Bruining H, Lerma FA, Wittebole X, De Backer D, Brett S, Marzo D and others. A Pilot-Controlled Study of a Polymyxin B-Immobilized Hemoperfusion Cartridge in Patients With Severe Sepsis Secondary To Intra-Abdominal Infection. Shock 2005;23(5):400-405.
149. Ikeda T. Hemoadsorption in Critical Care. Therapeutic Apheresis 2002;6(3):189-192.
150. Hlady V, Buijs J. Protein adsorption on solid surfaces. Current Opinion in Biotechnology 1996;7(1):72-77.
151. Neff JA, Tresco PA, Caldwell KD. Surface modification for controlled studies of cell–ligand interactions. Biomaterials 1999;20(23-24):2377-2393.
152. Li J, Nation RL, Turnidge JD, Milne RW, Coulthard K, Rayner CR, Paterson DL. Colistin: the re-emerging antibiotic for multidrug-resistant Gram-negative bacterial infections. The Lancet Infectious Diseases 2006;6(9):589-601.
153. Gough M, Hancock R, Kelly N. Antiendotoxin activity of cationic peptide antimicrobial agents. Infection and Immunity 1996;64(12):4922-4927.
154. Scott MG, Yan H, Hancock REW. Biological Properties of Structurally Related *a*-Helical Cationic Antimicrobial Peptides. Infection and Immunity 1999;67(4):2005-2009.
155. Cirioni O, Giacometti A, Ghiselli R, Bergnach C, Orlando F, Silvestri C, Mocchegiani F, Licci A, Skerlavaj B, Rocchi M and others. LL-37 protects rats against lethal sepsis caused by Gram-negative bacteria. Antimicrobial Agents & Chemotherapy 2006;50(5):1672-1679.
156. Deslouches B, Islam K, Craigo JK, Paranjape SM, Montelaro RC, Mietzner TA. Activity of the *de novo* engineered antimicrobial peptide WLBU2 against *Pseudomonas aeruginosa* in human serum and whole blood: Implications for systemic applications. Antimicrobial Agents & Chemotherapy 2005;49(8):3208-3216.
157. Deslouches B, Phadke SM, Lazarevic V, Cascio M, Islam K, Montelaro RC, Mietzner TA. *De novo* generation of cationic antimicrobial peptides: Influence of length and tryptophan substitution on antimicrobial activity. Antimicrobial Agents & Chemotherapy 2005;49(1):316-322.
158. Gonzalez IA, Wong XX, De Almeida D, Yurko R, Watkins S, Islam K, Montelaro RC, El-Ghannam A, Mietzner TA. Peptides as potent antimicrobials tethered to a solid surface: Implications for medical devices. Nature Precedings 2008.
159. Skinner MC, Kiselev AO, Isaacs CE, Mietzner TA, Montelaro RC, Lampe MF. Evaluation of WLBU2 peptide and 3-*O*-octyl-*sn*-glycerol lipid as active ingredients for a topical microbicide formulation targeting *Chlamydia trachomatis*. Antimicrobial Agents & Chemotherapy 2010;54(2):627-636.
160. Pace CN, Vajdos F, Fee L, Grimsley G, Gray T. How to measure and predict the molar absorption coefficient of a protein. Protein Science 1995;4(11):2411-2423.

161. Ryder MP, McGuire J, Schilke KF. Cleaning requirements for silica-coated sensors used in optical waveguide lightmode spectroscopy. Surface and Interface Analysis 2013;45(11-12):1805-1809.
162. Popat KC, Johnson RW, Desai TA. Characterization of vapor deposited thin silane films on silicon substrates for biomedical microdevices. Surface and Coatings Technology 2002;154(2-3):253-261.
163. Dill JK, Auxier JA, Schilke KF, McGuire J. Quantifying nisin adsorption behavior at pendant PEO layers. Journal of Colloid and Interface Science 2013;395(0):300-305.
164. Lampi MC, Wu X, Schilke KF, McGuire J. Structural attributes affecting peptide entrapment in PEO brush layers. Colloids and Surfaces B: Biointerfaces 2013;106(0):79-85.
165. Ramsden JJ. Porosity of pyrolysed sol-gel waveguides. Journal of Materials Chemistry 1994;4(8):1263-1265.
166. Whitmore L, Wallace BA. DICHROWEB, an online server for protein secondary structure analyses from circular dichroism spectroscopic data. Nucleic Acids Research 2004;32(suppl 2):W668-W673.
167. Whitmore L, Wallace BA. Protein secondary structure analyses from circular dichroism spectroscopy: Methods and reference databases. Biopolymers 2008;89(5):392-400.
168. Herráez A. Biomolecules in the computer: Jmol to the rescue. Biochemistry and Molecular Biology Education 2006;34(4):255-261.
169. Maupetit J, Derreumaux P, Tuffery P. PEP-FOLD: an online resource for de novo peptide structure prediction. Nucleic Acids Research 2009;37(suppl 2):W498-W503.
170. Thévenet P, Shen Y, Maupetit J, Guyon F, Derreumaux P, Tufféry P. PEP-FOLD: an updated *de novo* structure prediction server for both linear and disulfide bonded cyclic peptides. Nucleic Acids Research 2012;40(W1):W288-W293.
171. Wu X, Ryder MP, McGuire J, Schilke KF. Adsorption, structural alteration and elution of peptides at pendant PEO layers. Colloids and Surfaces B: Biointerfaces 2013;112(0):23-29.
172. Bohner M, Ring T, Rapoport N, Caldwell K. Fibrinogen adsorption by PS latex particles coated with various amounts of a PEO/PPO/PEO triblock copolymer. Journal of Biomaterials Science, Polymer Edition 2002;13(6):732-745.
173. Hermanson G. Bioconjugate techniques 2nd ed. Academic Press; 2008.
174. Ferry JD. Viscoelastic properties of polymers. Wiley New York; 1980.
175. Philippoff W. Relaxations in polymer solutions, liquids and gels. Physical acoustics: principles and methods 1965;2(part B):1-90.
176. Pace C. [24] Evaluating contribution of hydrogen bonding and hydrophobic bonding to protein folding. Methods in enzymology 1995;259:538-554.
177. Emsley J. Very strong hydrogen bonding. Chemical Society Reviews 1980;9(1):91-124.
178. Larson J, McMahon T. Gas-phase bihalide and pseudobihalide ions. An ion cyclotron resonance determination of hydrogen bond energies in XHY-species (X, Y= F, Cl, Br, CN). Inorganic Chemistry 1984;23(14):2029-2033.
179. Sanderson R. Chemical Bonds and Bonds Energy. Access Online via Elsevier; 1976.
180. Grönbeck H, Curioni A, Andreoni W. Thiols and disulfides on the Au (111) surface: The headgroup-gold interaction. Journal of the American Chemical Society 2000;122(16):3839-3842.

181. Nuzzo RG, Zegarski BR, Dubois LH. Fundamental studies of the chemisorption of organosulfur compounds on gold (111). Implications for molecular self-assembly on gold surfaces. Journal of the American Chemical Society 1987;109(3):733-740.
182. Bernabeu P, Caprani A. Influence of surface charge on adsorption of fibrinogen and/or albumin on a rotating disc electrode of platinum and carbon. Biomaterials 1990;11(4):258-264.

APPENDIX A:

ADSORPTION, STRUCTURAL ALTERATION AND ELUTION OF PEPTIDES AT PENDANT PEO LAYERS

Xiangming Wu, Matthew P. Ryder, Joseph McGuire, Karl F. Schilke*

Colloids and Surfaces B: Biointerfaces

http://www.sciencedirect.com/science/journal/09277765

Volume 112, Pages 23-29

Abstract

An experimentally based, quantitative understanding of the entrapment and function of small peptides within PEO brush layers does not currently exist. Earlier work provided a rationale for expecting that an ordered, compact peptide will enter the PEO phase more readily than a peptide of similar size that adopts a less ordered, less compact form, and that amphiphilicity will promote peptide retention within the hydrophobic region of the PEO brush. Here we more deliberately describe criteria for peptide integration and structural change within the PEO brush, and discuss the reversibility of peptide entrapment with changing solvent conditions. For this purpose, circular dichroism (CD) was used to record the adsorption and conformational changes of (amphiphilic) WLBU2 and (non-amphiphilic) polyarginine peptides at uncoated (hydrophobic) and PEO-coated silica nanoparticles. Peptide conformation was controlled between disordered and α-helical forms by varying the concentration of perchlorate ion. We show an initially more ordered (α-helical) structure promotes peptide adsorption into the PEO layer. Further, a partially helical peptide undergoes an increase in helicity after entry, likely due to concomitant loss of capacity for peptide-solvent hydrogen bonding. Peptide interaction with the PEO chains resulted in entrapment and conformational change that was irreversible to elution with changing solution conditions in the case of the amphiphilic peptide. In contrast, the adsorption and conformational change of the non-amphiphilic peptide was reversible. These results indicate that responsive drug delivery systems based on peptide-loaded PEO layers can be controlled by modulation of solution conditions and peptide amphiphilicity.

Introduction

In an earlier paper, we suggested the potential for surface coatings based on entrapment of bioactive agents into PEO brush layers for short-term medical device applications [1]. In particular, strategies featuring drug-loaded but otherwise nonfouling coatings for blood contact hold promise for enhancing the performance of medical devices, ranging from anti-infective catheters to hemoperfusion modules with microscale flow features. Lampi et al. [1] used optical waveguide lightmode spectroscopy (OWLS) to describe the adsorption of poly-*L*-glutamic acid and the cationic amphiphilic peptide WLBU2 at polyethylene oxide (PEO) brush layers. Circular dichroism (CD) was also used to describe the structures of poly-*L*-lysine and WLBU2 at solid, hydrophobic surfaces, and in the PEO brush. The solution structure of each peptide was controlled between disordered and more ordered (α-helical) forms by varying the salt concentration in the peptide solutions. Although protein adsorption at sparse PEO brush layers is predicted and observed in practice [2-4], an experimentally based, quantitative understanding of the adsorption and function of small peptides at PEO brush layers does not currently exist. The results of our previous work [1] provide a rationale for expecting that a more ordered and compact (e.g. α-helical) peptide will enter the PEO phase more readily than a peptide of similar size that adopts a less ordered, less compact form. Furthermore, because a hydrophobic inner core is predicted to exist in PEO brushes [5], it is expected that amphiphilicity will promote the retention of peptides within this region of the PEO brush.

WLBU2 (RRWVRRVRRWVRRVVRVVRRWVRR) is an engineered, 24-residue cationic amphiphilic peptide (CAP), with 13 positively charged arginine residues, and 11 nonpolar valine or tryptophan residues. It shows substantial promise for clinical applications, due to its wide spectrum antimicrobial activity against both Gram-negative and Gram-positive bacteria under physiological conditions. Segregation of the positively-charged Arg and hydrophobic Val/Trp groups onto opposing faces of an α-helix confers the ability to disrupt bacterial cell membranes, even when immobilized [6-12]. While the hydrophobic residues in WLBU2 make it a highly amphiphilic peptide, poly-*L*-arginine (PLR) is chemically homogeneous and not amphiphilic, and thus serves as an excellent control for the effects of amphiphilicity on peptide adsorption and entrapment in PEO brush layers. When dissolved in water under neutral pH, polyarginine adopts a combination of random and extended (e.g. polyproline-II and 2.5_1 helix) structures, while

WLBU2 shows little appreciable stable structure [1,6-9,13-17]. However, in the presence of perchlorate ion (ClO_4^-), both peptides will adopt a rigid α-helical structure [16].

In this paper, we more deliberately describe criteria for integration and structural changes of peptides within the PEO brush, and discuss the reversibility of peptide entrapment with changing solvent conditions for amphiphilic and non-amphiphilic motifs. For this purpose, circular dichroism (CD) was used to record the adsorption and conformational changes of PLR and WLBU2 at bare (hydrophobic) and PEO-coated silica nanoparticles. In order to elucidate the effect of structure on peptide interaction with the PEO brushes, the solution conformation of polyarginine and WLBU2 peptides was controlled between the disordered and α-helical forms by varying the concentration of perchlorate ion.

Materials and Methods

Peptides and materials

Lyophilized 30-residue average (4.7 kDa, PDI < 1.20) synthetic poly-*L*-arginine hydrochloride (PLR) was purchased from Alamanda Polymers (Huntsville, AL). PLR was dissolved at 5.0 mg/mL in HPLC water, and separated into 1.0 mL aliquots that were frozen and thawed prior to each experiment. The 5.0 mg/mL PLR stock was diluted to 0.2 mg/mL in HPLC water, or with 0.05 M or 0.5 M perchloric acid ($HClO_4$), to invoke either disordered or helical conformations, respectively. Similarly, lyophilized WLBU2 (3.4 kDa) was purchased from GenScript (Piscataway, NJ), and dissolved at 5 mg/mL in HPLC water and frozen in 1 mL aliquots. The WLBU2 stock solution was thawed prior to use, and diluted to 0.2 mg/mL in HPLC water, or with 0.2 M or 0.5 M $HClO_4$. All peptides were used as supplied, without further purification. Diluted peptide solutions were degassed for 40 min under vacuum immediately before use.

Self-assembled PEO brush layers were formed by suspension of hydrophobic silica nanoparticles (R816, Degussa, 190 m^2/g, 10-12 nm) in Pluronic® F108 (BASF) in HPLC water for 10 h on a rotator. About 3.3 mg/m^2 of F108 are required for complete surface coverage [18]; a 5x excess of F108 over this amount was used to ensure good coverage of the silica nanoparticles. Uncoated and F108-coated nanoparticles were then incubated with PLR or WLBU2 at 0.2 mg/mL under different solvent conditions, for a desired period of time (2h to 7 d) at 20 °C. Nanoparticle

concentrations (2 mg/mL and 10mg/mL) were selected based on previous OWLS results [1], and provided either sufficient surface area for complete adsorption of the peptide, or a 5x excess surface area for adsorption (to minimize peptide-peptide interactions).

Evaluation of peptide secondary structure

Peptide secondary structure in the presence or absence of nanoparticles was evaluated in triplicate by circular dichroism (CD) using a Jasco J-815 spectropolarimeter (Easton, MD) at 25 °C. The instrument was calibrated using 0.6 mg/mL *D*(+)–camphorsulfonic acid. Spectra were recorded in a cylindrical cuvette (0.1 cm pathlength) from 185 to 260 nm in 0.5 nm increments, and10 scans were averaged in order to increase the signal-to-noise ratio. The 0.2 mg/mL peptide samples prepared as outlined above were filtered (0.20 μm) prior to contact with nanoparticles and recording of CD spectra. Nanoparticles were rinsed by centrifugation (10,000 rpm, 20 min) and removal of the supernatant, after which the pellet was resuspended in water or $HClO_4$ of desired concentrations, and the process repeated a total of three times. All CD spectra were blanked against peptide-free solutions or NP suspensions.

Stabilization of F108 coatings on OWLS waveguides

SiO_2-coated OW2400c OWLS sensors were purchased from MicroVacuum (Budapest, Hungary). Sensors were cleaned using 3% aqueous SDS (30 min) followed by 10 min wash in 5:1:1 mixture of H_2O:HCl:H_2O_2 solution at 80 °C for 10 min. After cleaning, surfaces were rinsed with water, and dried under a stream of nitrogen. The sensor surfaces were then modified by vapor deposition of trichlorovinylsilane (TCVS, TCI America, Portland, OR). 200 μL of TCVS was evaporated at 20°C into a stream of dry nitrogen carrier gas, which was directed over the waveguide surfaces for 4 hrs. The silanized waveguides were then immersed in a solution of 5% w/v Pluronic® F108 in water, and were rotated in solution overnight. After incubation, samples were γ-irradiated with a ^{60}Co source to a total dose of 3 kGy to covalently the F108 to the surface [19,20]. The irradiated waveguides were rinsed with water, dried with N_2, and stored desiccated under N_2 in the dark until used.

Measurement of the rate and extent of peptide adsorption

Peptide adsorption was measured with an OWLS 210 instrument (MicroVacuum, Budapest, Hungary). A Rheodyne manual sample injector was used to inject sample solutions through a flow loop (~4.0 mL) into the OWLS flow cell. Flow rates were maintained at 50 µL/min for 40 minutes of sample adsorption time, and solution temperature was kept at 20 °C by the internal TC heater/cooler unit. Incident angle scans were performed from -5° to 5° at a step size of 0.01°. Both peaks of each of the transverse electric and magnetic modes were measured to determine the relative refractive index of the surface adlayer. OWLS experiments began with a baseline of peptide-free water or perchloric acid, followed by injection of 0.1 mg/mL peptide in water or perchloric acid, and a subsequent rinse with either perchloric acid or water.

Results and Discussion

Effect of perchlorate ions on structure of PLR

Polyarginine (PLR) exhibits a "disordered" (polyproline-II) structure in water under pH < 12, and an α-helical structure under pH > 12 [14]. However, pH could not be used in this study to influence peptide structure, as the silica nanoparticles used for CD would be hydrolyzed at basic pH [21]. Instead, perchlorate ions (ClO_4^-) were used to induce the α-helical conformation of PLR [16]. Circular dichroism spectra of PLR show it to be disordered in water, but the peptide becomes more helical with increased concentration of perchloric acid (Figure A. 1, left). This structural change is indicated by the change in the spectrum from a characteristic "random coil" to "*α*-helix" form, as well as an increase in ellipticity at 222 nm [22-24]. All CD experiments were performed in triplicate and errors were below 4%. Deconvolution of representative CD spectra with Dichroweb [25,26] indicate that the helicity of PLR increases from approximately 2% in water to 31% in 0.05 M $HClO_4$, and reaches 61% *α*-helix in 0.5 M $HClO_4$.

Effect of perchlorate ions on structure of WLBU2

While WLBU2 is almost completely disordered in water [9], it exhibits a high α-helix content in $HClO_4$, increasing from 3% in water to 15% in 0.2 M or 30% in 0.5 M $HClO_4$, respectively (Figure A. 1, right). The lower *α*-helix content observed for WLBU2, when compared to PLR at equivalent $HClO_4$ concentrations, may be due to the lower arginine content (13 of 24 amino

acids) of WLBU2. However, computed "absolute" helicity values are dependent upon the model implemented in the software, and should only be used for comparative purposes [22,26].

$HClO_4$ concentrations above 0.5 M did not further increase the calculated helicity of either PLR or WLBU2 in an aqueous milieu (data not shown), although WLBU2 is reported to reach 81% α-helix in a membrane-mimetic solvent (20% trifluoroethanol) [9]. No conformational change was observed for either PLR or WLBU2 in aqueous solutions of PEO (data not shown), indicating that peptide conformation is largely unaffected by the presence of free PEO chains. This implies that any structural change observed in the presence of a PEO brush is due to the unusual environment of the brush layer, and cannot be attributed to individual PEO-peptide interactions.

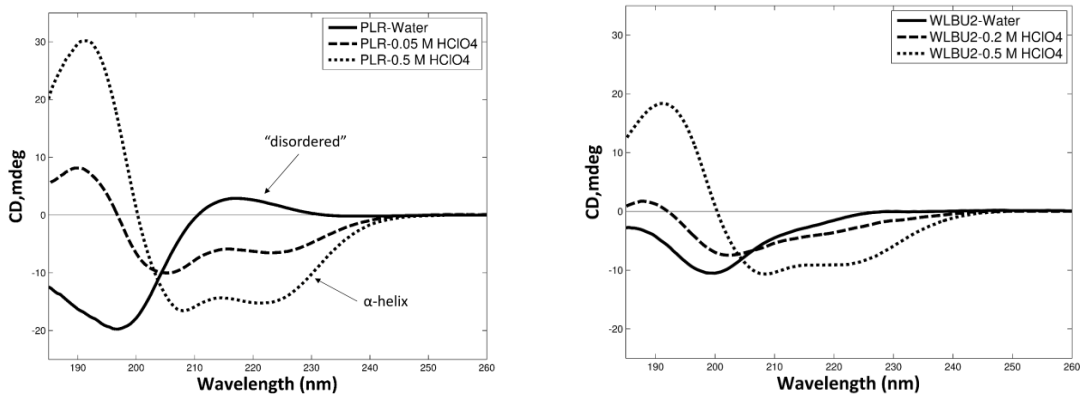

Figure A. 1 CD spectra of PLR (left) in water, 0.05 M $HClO_4$, 0.5 M $HClO_4$ and WLBU2 (right) in water, 0.2 M $HClO_4$, 0.5 M $HClO_4$. Characteristic spectra for peptides in "disordered" (random coil) and α-helix conformations are labeled.

Adsorption of disordered PLR and WLBU2

Both WLBU2 and PLR show substantially disordered structure when dissolved in water (Figure A. 1). Our previous OWLS and CD experiments showed that disordered poly-*L*-lysine (PLL) and WLBU2 have little affinity for F108-coated surfaces [1]. Here, we applied CD to the evaluation of PLR and WLBU2 structure in the presence and absence of uncoated (hydrophobic) and F108-coated nanoparticles. Spectra recorded for disordered PLR in the presence of uncoated and F108-coated nanoparticles are quite similar (Figure A. 2). The CD signal is greatly decreased after washing the bare or coated nanoparticles one time with water. This result indicates that the disordered peptides do not interact strongly with the nanoparticles, and are easily eluted

from bare or F108-coated surfaces. Similar behavior has been observed for disordered PLL at hydrophobic and F108-coated OWLS sensors [1]. Presumably, the large solution volume of the swollen, "disordered" peptide prevents penetration and integration into the PEO brush. Slightly more PLR was retained on the bare nanoparticles, presumably through electrostatic interactions between the positively charged guanidinium groups and negatively charged uncoated nanoparticle surface. However, this interaction with the bare surface is apparently too weak to cause any substantial conformational changes in the PLR [27].

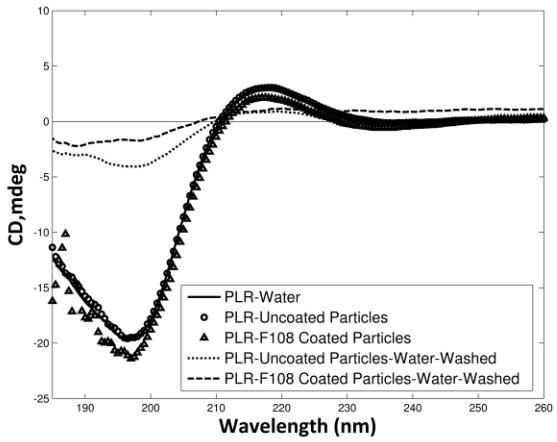

Figure A. 2 CD spectra of PLR in water, and in suspension with uncoated and F108-coated nanoparticles before and after washing.

As with PLR, the "disordered" conformation of WLBU2 in water is similar and independent of the presence or absence of F108-coated nanoparticles. The loss of CD signal indicates that the peptide was almost completely removed after washing with water (Figure A. 3).

However, a substantial conformational difference was observed for WLBU2 in water and in suspension with bare, hydrophobic nanoparticles. Unlike PLR, WLBU2 is amphiphilic and its hydrophobic groups have great affinity for the uncoated hydrophobic surface. We speculate that initial adsorption of the hydrophobic side-chains causes a conformational change which induces and stabilizes a partially α-helical structure. The CD signal is only partially reduced by washing with water, indicating that a large population of adsorbed and non-elutable peptides remains on the nanoparticles. Figure A. 3 also suggests that the wash preferentially removes loosely-bound "disordered" peptides, as the remaining adsorbed peptides produce a weak yet characteristic α-helical spectrum.

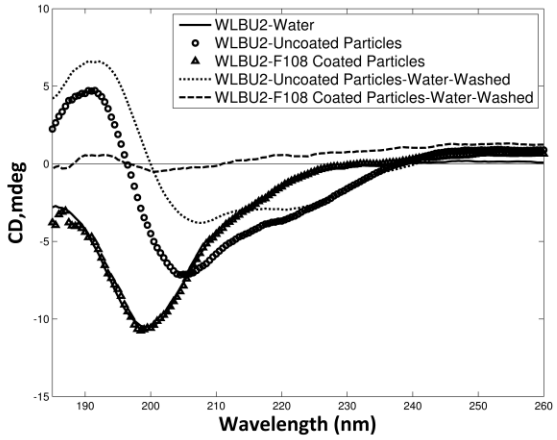

Figure A. 3 CD spectra of WLBU2 in water, and in suspension with uncoated and F108-coated nanoparticles before and after washing.

Adsorption of α-helical PLR and WLBU2

As discussed above, both PLR and WLBU2 are substantially α-helical (61% and 30%) in 0.5M $HClO_4$. The α-helix conformation of PLR in 0.5M $HClO_4$ was mostly independent of the presence of uncoated hydrophobic nanoparticles (Figure A. 4, left). However, the helicity of PLR increased slightly, from 61% to 82%, in the presence of F108-coated nanoparticles. This phenomena is more obvious in Figure A. 4 (right), in which PLR of a lower helicity (31% in 0.05 M $HClO_4$) was added to suspensions of uncoated and F108-coated nanoparticles. Again, no conformational change occurred in the presence of the uncoated nanoparticles, but an increase in helicity (from 31% to 49%) was observed in the presence of the F108-coated nanoparticles. These results suggest an interaction between the peptide and PEO brush, in which a peptide with a small amount of initial α-helix conformation becomes more helical as a result of contact with the brush, while a completely disordered peptide is completely excluded from the brush and undergoes no conformational change.

Perchlorate ions stabilize a peptide's α-helical structure by competing with water molecules which would normally solvate the peptide, causing a loss of hydration and promoting the intra-peptide hydrogen-binding characteristic of the α-helix conformation [28]. Theoretical and experimental evidence suggests that a hydrophobic region that is favorable for protein adsorption exists in the interior of a PEO brush [4,5,29]. A similar effect is expected when a partially dehydrated, helical peptide penetrates into the hydrophobic inner region of the PEO brush,

promoting the peptide's further dehydration and increasing its helicity. Similar conformational changes in response to the hydrophobic cell membrane are thought to be responsible for PLR's cell-penetrating and cytotoxic properties [30].

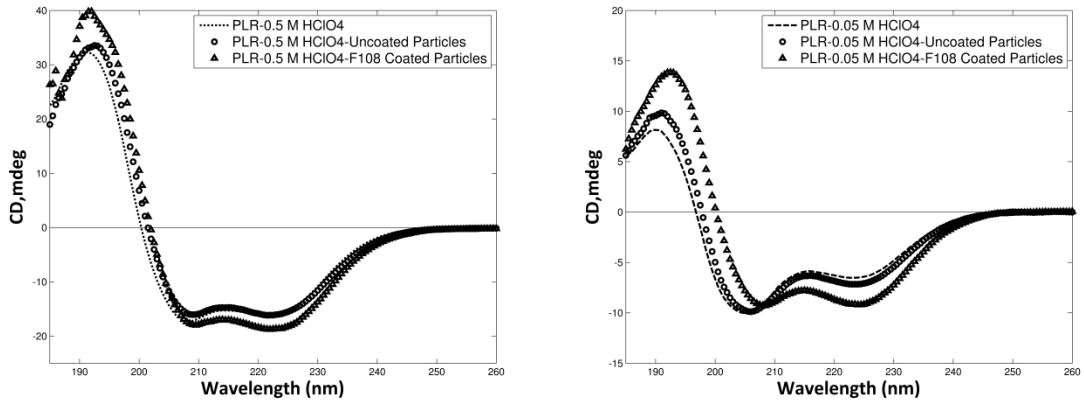

Figure A. 4 CD spectra of: (left) PLR in 0.5 M $HClO_4$, and in suspension with uncoated and F108-coated nanoparticles, (right) PLR in 0.05 M $HClO_4$, and in suspension with uncoated and F108-coated nanoparticles.

Stability of peptides at nanoparticle surfaces

The data presented thus far suggest that an increase in α-helix conformation is associated with integration of the peptides into F108 brushes. If so, these peptides should be more resistant to elution than would peptides which were conformationally changed but merely loosely-bound or unassociated with the brush. Uncoated and F108-coated nanoparticles were incubated with α-helical PLR in 0.5 M $HClO_4$ solution, and then washed twice with 0.5 M $HClO_4$ (maintaining conditions which promote α-helix structure). The partial decrease in CD signal after each wash with 0.5 M $HClO_4$ (Figure A. 5) is consistent with some loss of peptide with each rinse. However, the residual CD signal after washing indicates that considerable α-helical peptide remained on both surfaces after rinsing them with $HClO_4$. Importantly, the spectra are nearly identical in the presence or absence of F108, suggesting that the interactions of the helical peptide with the hydrophobic surface are closely mimicked by the apolar conditions which are expected to exist within the F108 brush [4,5].

In contrast, however, when the nanoparticle suspensions were contacted with α-helical PLR in $HClO_4$ and then washed with water, the peptide was nearly completely eluted from both F108-

coated and uncoated surfaces (Figure A. 5), although a small residual signal suggests some ordered helical form for the remaining peptides. Remarkably similar behavior was observed for nanoparticles contacted with "disordered" peptides in water (**Error! Reference source not found.**). The bulk concentration of perchlorate ion would be greatly reduced during washing, thus eliminating the helix-stabilizing microenvironment and allowing the peptide to resume a "disordered" conformation. Taken together, these results suggest that elution of peptides from the F108 brush is at once governed and controllable by bulk solution conditions.

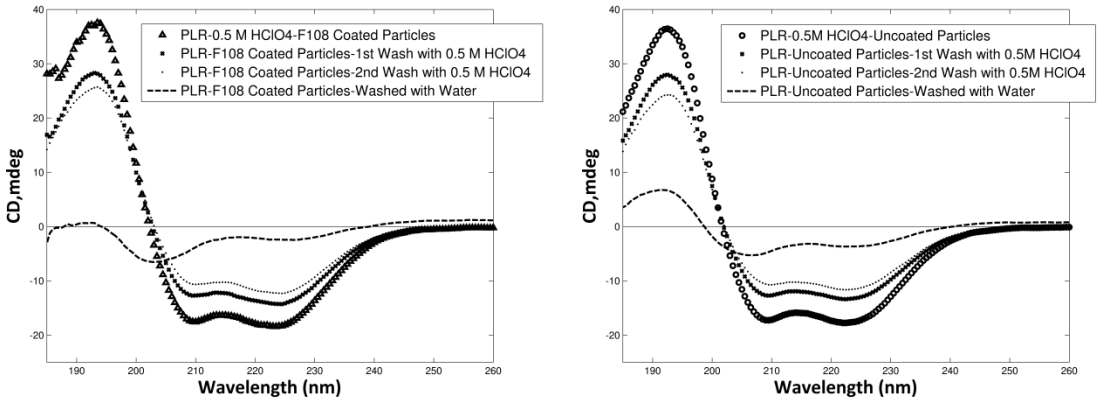

Figure A. 5 CD spectra of: PLR in $HClO_4$, and in suspension with F108-coated (left) and uncoated (right) nanoparticles before and after washing with $HClO_4$ or water.

Optical waveguide lightmode spectroscopy (OWLS)

OWLS experiments were carried out to verify that α-helical peptides are stably adsorbed on F108-coated surfaces, and their rate of elution is primarily determined by solution conditions (Figure A. 6). One obvious criticism of the CD experiments is that the F108 is not covalently linked to the nanoparticle surface, and thus some results might be interpreted as competitive displacement of the triblocks by the peptides (especially the inherently amphiphilic WLBU2). Although no obvious desorption of triblocks by nisin (a CAP of similar size to WLBU2) was observed in previous work [18,31], we investigated peptide adsorption at immobilized F108 brushes using TCVS-modified OWLS waveguides on which we covalently immobilized F108 using γ-irradiation [18,19]. Results with polyarginine in water (Figure A. 6) are entirely consistent with those in this work: contact of the F108-coated waveguide with disordered PLR resulted in negligible adsorption, while ordered peptide adsorbed strongly. As suggested above, the adsorbed α-helical peptide was relatively resistant to elution under helix-promoting solution

conditions, but was quickly and completely desorbed when eluted with water (which favors the "disordered" form of the peptide, Figure A. 5). OWLS experiments were performed in two replicates and errors were less than 5%.

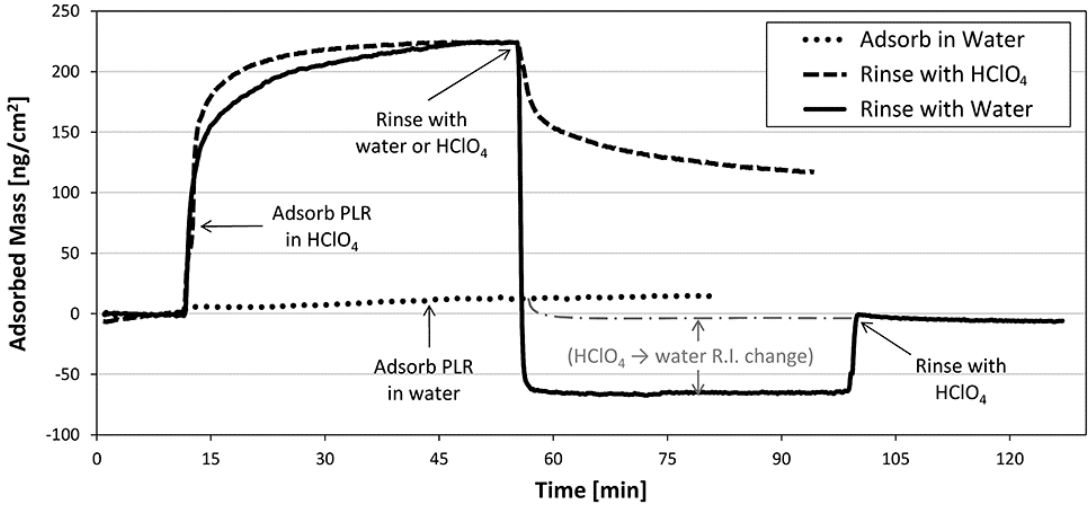

Figure A. 6 Adsorption and elution profiles of PLR on an OWLS waveguide coated with immobilized F108. Baseline was achieved using HPLC H_2O or 0.5M perchloric acid, followed by adsorption of 0.1 mg/mL PLR in H_2O or $HClO_4$, and then elution with H_2O or $HClO_4$. Little PLR adsorption was observed in water (···), suggesting that aqueous (disordered) PLR does not integrate into the F108 brush layer. α-Helical PLR adsorbed substantially from $HClO_4$, but was nearly completely removed from the brush by rinsing with water (–). In contrast, PLR adsorbed from and rinsed with $HClO_4$ (– –) was only partially eluted, suggesting stable integration of the peptide in the brush.

Changes in peptide structure in F108 brushes

WLBU2 in 0.5 M $HClO_4$ (initially 30% helical) achieves considerable α-helix content (39%) after adsorption onto a bare hydrophobic surface (Figure A. 7, left) and into a PEO layer (43% helical). The increase in helicity is more obvious in Figure A. 7 (right), when WLBU2 is in 0.2 M $HClO_4$ (initially 15% α-helical), its helicity increases to 43% after entrapment into the PEO layer. Importantly, regardless of the initial helicity, the final α-helix content of the adsorbed WLBU2 is the same (43%) after adsorption into a PEO layer. This is different from the behavior of PLR (Figure A. 4), suggesting a conformational change due to the strong interaction between hydrophobic groups on the peptide and the hydrophobic inner region of PEO layer. Figure A. 7 also suggests that the interaction between WLBU2 and the PEO brush, while strong, allows for

good molecular flexibility, since the final helicity of partially-ordered WLBU2 in the PEO brush is greater than on the bare surface (Figure A. 7, right).

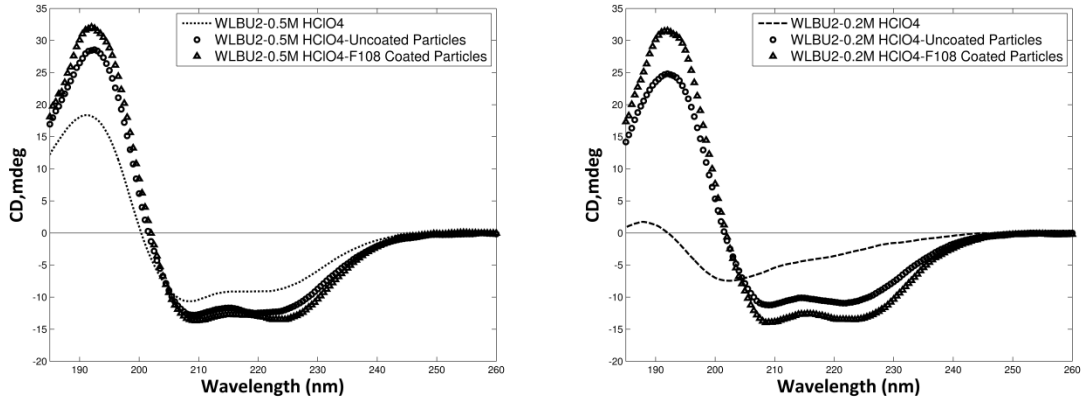

Figure A. 7 CD spectra of: (left) WLBU2 in 0.5 M $HClO_4$, and in suspension with uncoated and F108-coated nanoparticles, (right) WLBU2 in 0.2 M $HClO_4$, and in suspension with uncoated and F108-coated nanoparticles.

As previously described with PLR, uncoated and F108-coated nanoparticles were incubated with α-helical WLBU2 in $HClO_4$ solution, and then washed with $HClO_4$ or water. In all cases, a small fraction of peptide was removed by washing (Figure A. 8). However, while changing the solvent from the helix-promoting $HClO_4$ to water (which favors a "disordered" conformation) resulted in nearly complete loss of PLR (see Figure A. 5Figure A. 6), solution changes had little effect on the intensity or shape of CD spectra of adsorbed WLBU2 (Figure A. 8). It is reasonable to expect that amphiphilicy is the cause of this retention of WLBU2 (but not PLR) at F108-coated surfaces following a solvent change. While WLBU2 present in the hydrophilic outer region of PEO layer might be removed by rinsing with peptide-free buffer, an amphiphilic peptide WLBU2 which is entrapped in the hydrophobic inner region should show greater resistance to elution than would a non-amphiphilic peptide PLR. Moreover, the WLBU2 entrapped in the brush maintains its α-helical structure, even when the surrounding solvent has been changed from $HClO_4$ to water (Figure A. 8), while entrapped PLR undergoes a helix-coil transition in response to changes in solution conditions (Figure A. 5). For both PLR and WLBU2, results on F108-coated and uncoated nanoparticles are similar, which indicates the similarity between bare hydrophobic surfaces and the inner region of PEO layers. Previous study shows that nisin entrapped PEO brush layers are able to maintain their non-fouling (protein-repellent) characteristics, while the presence of nisin

on uncoated hydrophobic surface does not hinder protein adsorption. Competitive adsorption might happen on an uncoated hydrophobic surface, causing those pre-adsorbed peptide being displaced by surrounding proteins. Therefore, the presence of PEO layer can stabilize peptide storage, as well as giving non-fouling characteristics to the surface of blood contacting medical devices.

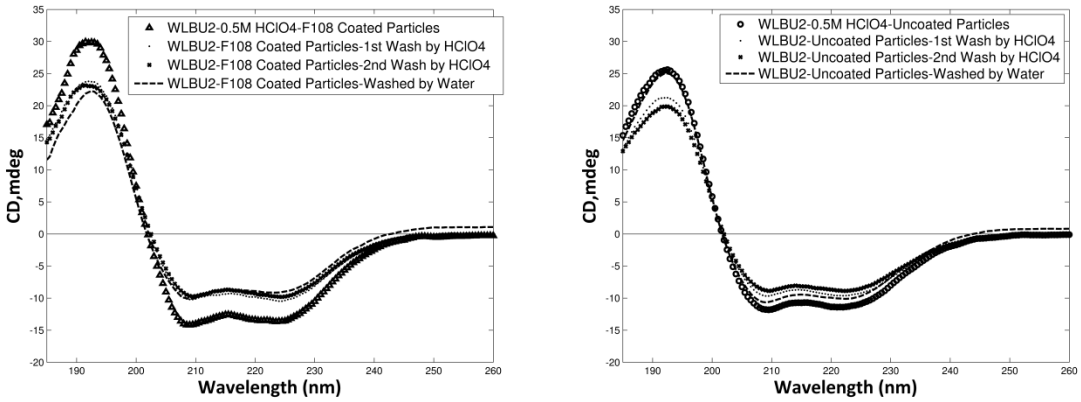

Figure A. 8 CD spectra of: WLBU2 in $HClO_4$, and in suspension with F108-coated (left) and uncoated (right) nanoparticles before and after washing with $HClO_4$ or water.

In summary, an initially more ordered (α-helical) structure promotes the adsorption of a peptide into the PEO layer. A partially helical peptide undergoes an increase in helicity, probably due to the loss of peptide-solvent H-bonding in the apolar region within the brush [16,30]. An amphiphilic peptide (e.g. WLBU2) is expected to have a much stronger interaction with the hydrophobic inner region of the PEO layer than a non-amphiphilic one (e.g. PLR). This interaction results in entrapment and conformational change of the amphiphilic peptide that is irreversible with respect to elution. In contrast, the adsorption and conformational change of non-amphiphilic peptides are reversible, making such peptides highly elutable because of their weak interaction with the brush.

Conclusions

The results reported here direct us to expect that some minimal degree of structural order (α-helix) is necessary for peptide entry into the PEO layer, and that peptide location within the hydrophobic inner region of the PEO brush may result in an increase in α-helix content. Once the non-amphiphilic peptide polyarginine (PLR) was entrapped among the PEO chains of the

F108 brush, we found it to be partially elutable as long as the same helix-stabilizing solvent used during the adsorption step was used for elution. However, in contact with water (which favors its disordered, non-adsorbable conformation), the adsorbed PLR was entirely elutable.

In contrast, the amphiphilic peptide WLBU2 was highly resistant to elution in all cases, even upon contact with a solvent which promotes its disordered form. Previously, we suggested that the well-known helix-coil transition of homopolyamino acids (e.g. PLL or PLR) might be used to reversibly anchor peptides or their conjugates within a PEO brush as a novel drug-delivery strategy. It appears, however, that the property of amphiphilicity (such as exhibited by WLBU2) is required to control peptide desorption from a PEO brush when the bulk solution conditions are changed. This work provides direction for development of responsive drug delivery systems based on modulation of solvent conditions and bioactive peptide structure within PEO brush layers. Moreover, entrapment of therapeutic peptides may also support novel drug delivery strategies (e.g., PEO-coated nanoparticle carriers) that can potentially overcome barriers to oral delivery of peptide drugs [32]. Current work underway in our laboratory toward these ends features the sequential and competitive adsorption behavior of peptide mixtures at pendant PEO brush layers, and will contribute to the subject of future reports.

Acknowledgments

The authors thank Dr. Kerry McPhail of the OSU College of Pharmacy for use of her CD instrument, and Dr. Victor Hsu and Dr. Elisar Babar for valuable discussion on interpretation of the CD spectra. This work was supported in part by the National Institute of Biomedical Imaging and Bioengineering (NIBIB, grant no. R01EB011567). The content is solely the responsibility of the authors and does not necessarily represent the official views of NIBIB or the National Institutes of Health.

References

1. Lampi MC, Wu X, Schilke KF, McGuire J. Structural attributes affecting peptide entrapment in PEO brush layers. Colloids and Surfaces B: Biointerfaces 2013;106(0):79-85.
2. Bosker WTE, Iakovlev PA, Norde W, Cohen Stuart MA. BSA adsorption on bimodal PEO brushes. Journal of Colloid and Interface Science 2005;286(2):496-503.
3. Fang F, Satulovsky J, Szleifer I. Kinetics of Protein Adsorption and Desorption on Surfaces with Grafted Polymers. Biophysical Journal 2005;89(3):1516-1533.
4. Sheth SR, Leckband D. Measurements of attractive forces between proteins and end-grafted poly(ethylene glycol) chains. Proceedings of the National Academy of Sciences of the United States of America 1997;94(16):8399-8404.
5. Lee H, Kim DH, Witte KN, Ohn K, Choi J, Akgun B, Satija S, Won Y-Y. Water Is a Poor Solvent for Densely Grafted Poly(ethylene oxide) Chains: A Conclusion Drawn from a Self-Consistent Field Theory-Based Analysis of Neutron Reflectivity and Surface Pressure–Area Isotherm Data. Journal of Physical Chemistry B 2012;116(24):7367-7378.
6. Costa F, Carvalho IF, Montelaro RC, Gomes P, Martins MCL. Covalent immobilization of antimicrobial peptides (AMPs) onto biomaterial surfaces. Acta Biomaterialia 2011;7(4):1431-1440.
7. Deslouches B, Gonzalez IA, DeAlmeida D, Islam K, Steele C, Montelaro RC, Mietzner TA. *De novo*-derived cationic antimicrobial peptide activity in a murine model of *Pseudomonas aeruginosa* bacteraemia. Journal of Antimicrobial Chemotherapy 2007;60(3):669-672.
8. Deslouches B, Islam K, Craigo JK, Paranjape SM, Montelaro RC, Mietzner TA. Activity of the *de novo* engineered antimicrobial peptide WLBU2 against *Pseudomonas aeruginosa* in human serum and whole blood: Implications for systemic applications. Antimicrobial Agents and Chemotherapy 2005;49(8):3208-3216.
9. Deslouches B, Phadke SM, Lazarevic V, Cascio M, Islam K, Montelaro RC, Mietzner TA. *De novo* generation of cationic antimicrobial peptides: Influence of length and tryptophan substitution on antimicrobial activity. Antimicrobial Agents and Chemotherapy 2005;49(1):316-322.
10. Gonzalez IA, Wong XX, De Almeida D, Yurko R, Watkins S, Islam K, Montelaro RC, El-Ghannam A, Mietzner TA. Peptides as potent antimicrobials tethered to a solid surface: Implications for medical devices. Nature Precedings 2008.
11. Onaizi SA, Leong SSJ. Tethering antimicrobial peptides: Current status and potential challenges. Biotechnology Advances 2011;29(1):67-74.
12. Skinner MC, Kiselev AO, Isaacs CE, Mietzner TA, Montelaro RC, Lampe MF. Evaluation of WLBU2 peptide and 3-*O*-octyl-*sn*-glycerol lipid as active ingredients for a topical microbicide formulation targeting *Chlamydia trachomatis*. Antimicrobial Agents and Chemotherapy 2010;54(2):627-636.

13. Adzhubei AA, Sternberg MJE, Makarov AA. Polyproline-II Helix in Proteins: Structure and Function. Journal of Molecular Biology in press(0).
14. Bochicchio B, Tamburro AM. Polyproline II structure in proteins: Identification by chiroptical spectroscopies, stability, and functions. Chirality 2002;14(10):782-792.
15. Mikhonin AV, Myshakina NS, Bykov SV, Asher SA. UV Resonance Raman Determination of Polyproline II, Extended 2.5_1-Helix, and *β*-Sheet Ψ Angle Energy Landscape in Poly-*L*-Lysine and Poly-*L*-Glutamic Acid. Journal of the American Chemical Society 2005;127(21):7712-7720.
16. Rifkind JM. Helix–coil transition of poly-L-arginine: A comparison with other basic polypeptides. Biopolymers 1969;8(5):685-688.
17. Tiffany ML, Krimm S. Circular dichroism of the "random" polypeptide chain. Biopolymers 1969;8(3):347-359.
18. Tai Y-C, McGuire J, Neff JA. Nisin antimicrobial activity and structural characteristics at hydrophobic surfaces coated with the PEO–PPO–PEO triblock surfactant Pluronic® F108. Journal of Colloid and Interface Science 2008;322(1):104-111.
19. McPherson TB, Shim HS, Park K. Grafting of PEO to glass, nitinol, and pyrolytic carbon surfaces by γ irradiation. Journal of Biomedical Materials Research 1997;38(4):289-302.
20. Tseng Y-C, McPherson T, Yuan CS, Park K. Grafting of ethylene glycol-butadiene block copolymers onto dimethyl-dichlorosilane-coated glass by γ-irradiation. Biomaterials 1995;16(13):963-972.
21. Salmio H, Brühwiler D. Distribution of Amino Groups on a Mesoporous Silica Surface after Submonolayer Deposition of Aminopropylsilanes from an Anhydrous Liquid Phase. The Journal of Physical Chemistry C 2006;111(2):923-929.
22. Greenfield NJ. Methods to estimate the conformation of proteins and polypeptides from circular dichroism data. Analytical Biochemistry 1996;235(1):1-10.
23. Greenfield NJ, Fasman GD. Computed circular dichroism spectra for the evaluation of protein conformation. Biochemistry 1969;8(10):4108-4116.
24. Woody RW. Theory of circular dichroism of proteins. In: Fasman GD, editor. Circular dichroism and the conformational analysis of biomolecules. New York: Plenum Press; 1996. p 25-30.
25. Whitmore L, Wallace BA. DICHROWEB, an online server for protein secondary structure analyses from circular dichroism spectroscopic data. Nucleic Acids Research 2004;32(suppl 2):W668-W673.
26. Whitmore L, Wallace BA. Protein secondary structure analyses from circular dichroism spectroscopy: Methods and reference databases. Biopolymers 2008;89(5):392-400.
27. Puddu V, Perry CC. Peptide Adsorption on Silica Nanoparticles: Evidence of Hydrophobic Interactions. ACS Nano 2012;6(7):6356-6363.

28. Asciutto EK, General IJ, Xiong K, Asher SA, Madura JD. Sodium Perchlorate Effects on the Helical Stability of a Mainly Alanine Peptide. Biophysical Journal 2010;98(2):186-196.
29. Halperin A. Polymer brushes that resist adsorption of model proteins: Design parameters. Langmuir 1999;15(7):2525-2533.
30. Takechi Y, Mizuguchi C, Tanaka M, Kawakami T, Aimoto S, Okamura E, Saito H. Physicochemical Mechanism for the Lipid Membrane Binding of Polyarginine: The Favorable Enthalpy Change with Structural Transition from Random Coil to *α*-Helix. Chemistry Letters 2012;41(10):1374-1376.
31. Tai Y-C, Joshi P, McGuire J, Neff JA. Nisin adsorption to hydrophobic surfaces coated with the PEO–PPO–PEO triblock surfactant Pluronic® F108. Journal of Colloid and Interface Science 2008;322(1):112-118.
32. De Jong WH, Borm PJ. Drug delivery and nanoparticles: applications and hazards. International Journal of Nanomedicine 2008;3(2):133.

APPENDIX B:

CONCENTRATION EFFECTS ON PEPTIDE ELUTION FROM PENDANT PEO LAYERS

Xiangming Wu, Matthew P. Ryder, Joseph McGuire, Karl F. Schilke*

Submitted to Colloids and Surfaces B: Biointerfaces

www.elsevier.com/locate/colsurfb

Abstract

In earlier work, we have provided direction for development of responsive drug delivery systems based on modulation of structure and amphiphilicity of bioactive peptides entrapped within pendant polyethylene oxide (PEO) brush layers. Amphiphilicity promotes retention of the peptides within the hydrophobic inner region of the PEO brush layer. In this work, we describe the effects of peptide surface density on the conformational changes caused by peptide-peptide interactions, and show that this phenomenon substantially affects the rate and extent of peptide elution from PEO brush layers. Three cationic peptides were used in this study: the arginine-rich amphiphilic peptide WLBU2, the chemically identical but scrambled peptide S-WLBU2, and the non-amphiphilic homopolymer poly-*L*-arginine (PLR). Circular dichroism (CD) was used to evaluate surface density effects on the structure of these peptides at uncoated (hydrophobic) and PEO-coated silica nanoparticles. UV spectroscopy and a quartz crystal microbalance with dissipation monitoring (QCM-D) were used to quantify changes in the extent of peptide elution caused by those conformational changes. For amphiphilic peptides at sufficiently high surface density, peptide-peptide interactions result in conformational changes which compromise their resistance to elution. In contrast, elution of a non-amphiphilic peptide is substantially independent of its surface density, presumably due to the absence of peptide-peptide interactions. The results presented here provide a strategy to control the rate and extent of release of bioactive peptides from PEO layers, based on modulation of their amphiphilicity and surface density.

Keywords

peptide elution; PEO brush; WLBU2; cationic amphiphilic peptides; polyarginine; circular dichroism (CD); α-helix; coiled-coils

Introduction

In an earlier paper [1], we used circular dichroism (CD) to evaluate the structures of poly-*L*-arginine (PLR) and the cationic, amphiphilic peptide (CAP) WLBU2 in pendant PEO layers, as well as the reversibility of peptide location in such layers with changing solvent conditions. Those results indicated that some minimal degree of structural order (α-helix) is necessary for peptide entry into the PEO layer, and that peptide location within the hydrophobic inner region of the PEO brush may result in a cooperative increase in α-helix content. In addition, while peptide interaction with the PEO chains resulted in entrapment and conformational change that was irreversible to elution with changing solution conditions in the case of WLBU2, the adsorption and conformational change of the non-amphiphilic PLR was reversible.

Current work underway in our laboratory features the sequential and competitive adsorption behavior of peptides, including WLBU2 and PLR, at pendant PEO brush layers. In sequential adsorption experiments it is necessary to vary surface density of the first peptide introduced to the layer in order to properly interpret its replacement by the second peptide introduced. We determined during the course of these experiments that our previous conclusion of entrapment and conformational change being irreversible to elution for the amphiphilic WLBU2 was contextual, being valid only when its surface density is sufficiently low. Our objectives with this paper are to establish an improved understanding of surface density effects on peptide elution from PEO layers, and to provide evidence of concentration-dependent, peptide-peptide interactions likely contributing to those effects. The adsorption behavior of three peptides was evaluated for this purpose, including, in addition to WLBU2 and PLR, a peptide chemically identical to WLBU2 but of scrambled sequence (S-WLBU2).

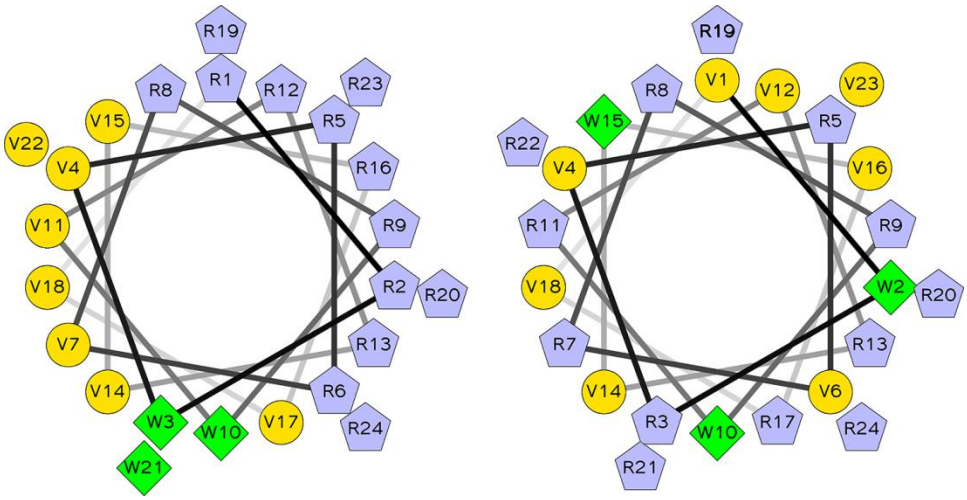

Figure B. 1 Helix wheel representations of WLBU2 (left), with face-segregation of positively-charged Arg residues on the α-helix, and S-WLBU2 (right) which has uniformly distributed charge.

WLBU2 is a synthetic, 24-residue CAP with 13 positively charged arginine residues, and 11 non-polar valine or tryptophan residues. It shows substantial promise for clinical applications, due to its wide spectrum antimicrobial activity against both Gram-negative and Gram-positive bacteria under physiological conditions [2-8]. The structure of WLBU2 in water is substantially disordered, but the peptide gains considerable secondary structure, involving segregation of its positively-charged and hydrophobic groups onto opposing faces of an α-helix, in the presence of counterions, membrane-mimetic solvents, or bacterial membranes. Moreover, WLBU2 retains its antimicrobial activity when immobilized at solid surfaces by a number of methods [2,6-8]. While chemically identical to WLBU2, the scrambled sequence of S-WLBU2 eliminates the ordered segregation of positively-charged and hydrophobic residues of WLBU2 during helix formation (Figure B. 1), and is associated with a very low hydrophobic moment in comparison to WLBU2 (0.1 vs. 10.7, respectively). PLR is chemically homogeneous and not amphiphilic. When dissolved in water under neutral pH, PLR adopts a combination of random coil and extended structures (e.g. polyprolone-II and 2.5_1 helix), while both WLBU2 and S-WLBU2 show a random coil structure [1,3-5,9-13]. An α-helical conformation can be achieved in all three peptides by addition of perchlorate ions (ClO_4^-) [12].

Materials and Methods

Peptides and materials.

Synthetic poly-*L*-arginine hydrochloride (PLR, n ≈ 30, M_n = 5.8 kDa, PDI < 1.20) was purchased from Alamanda Polymers (Huntsville, AL). The 24-residue peptides WLBU2 (RRWVRRVRRWVRRVVRVVRRWVRR, 3.4 kDa) and the scrambled sequence S-WLBU2 (VWRVRVRRRWRVRVWVRVRRRRVR) were purchased from Genscript (Piscataway, NJ). All peptides were used without further purification. Stock solutions of each peptide at 5 mg/mL in HPLC water were frozen in 1 mL aliquots, which were thawed and then diluted immediately before use to 0.2 mg/mL in 0.2 M $HClO_4$ (to induce α-helical conformation). Diluted peptide solutions were degassed under vacuum immediately before use.

Self-assembled PEO brush layers were formed by suspension of hydrophobic silica nanoparticles (R816, Degussa, 190 m^2/g, 10-12 nm) in Pluronic® F108 (BASF) in HPLC water for 10 h on a rotator. The expected surface coverage of F108 is about 3.3 mg/m^2 [14,15]; a 5× excess of F108 over this amount was used to ensure good coverage of the nanoparticles (NPs). Uncoated and F108-coated NPs were then incubated with PLR, WLBU2 or S-WLBU2 (0.2 mg/mL in 0.2 M $HClO_4$) for 2 h at 20 °C. The concentration of NPs was varied from 1 to 10 mg/mL to provide different available surface areas for peptide adsorption.

Evaluation of peptide structure and elutability.

Peptide secondary structure, in the presence or absence of nanoparticles, was evaluated by circular dichroism (CD) using a Jasco J-815 spectropolarimeter (Easton, MD) at 25 °C. The spectra from each of three replicates for each sample exhibited only slight (~5%) differences in signal intensity; representative spectra are thus shown throughout. The instrument was calibrated with 0.6 mg/mL *D*(+)-camphorsulfonic acid. Spectra were recorded from 185 to 260 nm in 0.5 nm increments (0.1 cm path length), with 5 scans recorded and averaged in order to increase the signal-to-noise ratio. All peptide solutions were filtered (0.20 μm) prior to contact with NPs and recording of CD spectra. All spectra were blanked against peptide-free solutions.

After the CD measurements, the peptide-NP suspensions were rinsed by centrifugation (10,000 rpm, 20 min) and resuspension in water; this process was repeated twice to remove excess peptide. The amount of peptide removed in each of the supernatants from the NPs was then quantified by UV spectrophotometry against the original peptide solutions at 230 nm (for PLR) or 280 nm (for WLBU2 and S-WLBU2), and the total eluted peptide calculated from this data.

Preparation of QCM-D sensors.

QSX303 silicon dioxide QCM-D sensors (Q-Sense, Linthicum, MD) were cleaned according to manufacturer's protocol: 10 min UV/ozone treatment followed by immersion in 2% sodium dodecyl sulfate (SDS) for 30 min, and a 10 min rinse with HPLC water. After cleaning, sensors were dried under a stream of nitrogen and placed in the UV/ozone chamber again for 10 min.

The sensor surfaces were then modified by vapor deposition of trichlorovinylsilane (TCVS, TCI America, Portland, OR). 200 µL of TCVS was evaporated at 20 °C into a stream of dry nitrogen carrier gas, which was directed over the sensor surfaces for 4 h. The silanized, hydrophobic sensors were then incubated overnight with 5% Pluronic® F108 in water, and then γ-irradiated to 0.3 Mrad to covalently attach the F108 to the surface [14,16]. The irradiated sensors were rinsed with water, dried with nitrogen, and stored in the dark to avoid oxidation of the vinyl moieties.

Measurement of the rate and extent of peptide adsorption and elution.

The adsorption and elution of peptides were measured with a Q-Sense E4 QCM-D (Q-sense, Linthicum, MD). QCM-D allows simultaneously measuring changes in resonance frequency (ΔF) and energy dissipation (ΔD) of QCM-D sensors. Sample solutions were pumped across F108-coated silica sensors at 100 µL/min, and the sample stage was held at 25 °C. QCM-D experiments began with a baseline of peptide-free 0.2M $HClO_4$, followed by introduction of 0.1 mg/mL or 0.005 mg/mL peptide in 0.2M $HClO_4$, and a subsequent rinse with water. Adsorption and elution steps were each allowed to proceed for 40 min.

Results and Discussion

Relationship between peptide surface density and peptide elution from PEO layers.

Peptide concentration at PEO-coated nanoparticle surfaces was varied by altering nanoparticle concentration (from 1 to 10 mg/mL) in peptide-nanoparticle suspensions with constant peptide concentration (0.2 mg/mL). More than 95% of the dissolved peptide was entrapped in every suspension tested, corresponding to peptide surface densities ranging from about 0.02 to 0.2 molecules/nm^2. The elutability of each peptide recorded after contact with peptide-free water is plotted against peptide surface density in Figure B. 2.

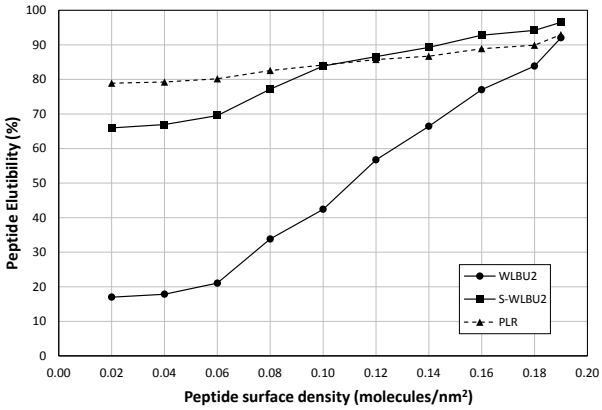

Figure B. 2 Effect of surface peptide density on elutability of WLBU2, S-WLBU2 and PLR from F108-coated nanoparticles.

As shown in Figure B. 2, entrapped WLBU2 showed a substantially greater concentration dependence on elution than shown by entrapped S-WLBU2 or PLR. The high resistance to elution at low peptide surface density is consistent with our earlier report and attributed to association of the amphiphilic WLBU2 with PEO chain segments in the hydrophobic inner region of the brush [1,14,17]. The elutability of S-WLBU2 and PLR was less strongly affected by the peptide surface density, and both were more elutable than WLBU2 at all but the highest surface density tested.

S-WLBU2, while comprised of the same amino acids and carrying the same +13 charge as WLBU2, features arginine residues alternating with valine or tryptophan to distribute the positive charge uniformly around the α-helix (**Error! Reference source not found.**). The

tryptophan residues are also distributed along the full length of the peptide. S-WLBU2 was designed to have a very low hydrophobic moment, and these attributes are consistent with its elution from the PEO layer being greater than that recorded for WLBU2 at low peptide surface densities. The non-amphiphilic PLR is highly elutable from PEO layers (Figure B. 2), which is consistent with our earlier work using CD and optical waveguide lightmode spectroscopy [1]. The total absence of hydrophobic residues and the abundant positive charges on all sides of PLR lead to electrostatic repulsion among peptides within the brush, as well as making PLR highly soluble in water. In fact, the elutability of PLR is only slightly dependent on its surface density (Figure B. 2).

WLBU2 and S-WLBU2 both exhibit substantially increased elutability at high peptide surface densities (i.e. low nanoparticle concentrations). It is fair to expect that this high elutability is due to intermolecular interactions, which interfere with the stable hydrophobic association of the individual peptides within the brush, or otherwise promote their enhanced solubility in water.

WLBU2 is highly α-helical in $HClO_4$, and its entrapment in PEO is accompanied by a further increase in its helicity [1]. Upon sufficiently close approach, peptides like WLBU2 which possess an amphiphilic-segregated α-helical conformation are able to form *α*-helical, "coiled-coil" conformations. These structures, which are comprised of two or more intertwined α-helical chains, are stabilized through multiple interchain hydrophobic interactions [18]. For example, Zhou *et al*. produced a two-stranded *α*-helical coiled-coil consisting of two identical 35-residue polypeptides. The peptides were designed with polar (lysine and glutamic acid) and non-polar (leucine and alanine) residues distributed on average 3.5 residues apart, in order to form face-segregated amphiphilic *α*-helices. These synthetic peptides spontaneously self-assembled into coiled-coil structures in physiological conditions [19,20]. WLBU2 has a very similar distribution of polar and nonpolar residues, and is thus also expected to form *α*-helical coiled-coil structures at sufficiently high concentration. Such coiled-coils may consist of two or more peptides [18,21], and in the case of WLBU2 would likely feature a hydrophobic interior, with an exterior dominated by positively-charged arginine groups. Such a coiled-coil structure would be expected to behave very similarly to the highly cationic but non-amphiphilic PLR, in terms of its interaction with the

PEO brush (Figure B. 3). With respect to S-WLBU2, it has been shown [22,23] that peptides with alternating hydrophobic and polar residues are able to self-assemble into stable β-sheet conformations. It is reasonable to expect that, as favorable peptide-PEO interactions which hold entrapped peptides in place give way at high surface densities to peptide-peptide associations, the peptides become more elutable as the population of coiled-coils increases.

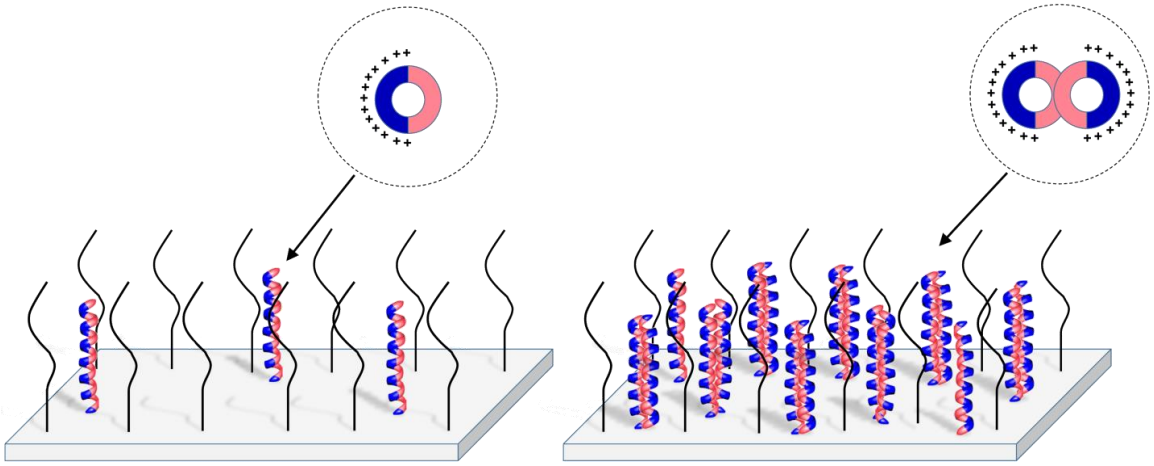

Figure B. 3 Schematic representation of WLBU2 as single-stranded amphiphilic α-helices at low peptide surface density (left), and formation of less-amphiphilic α-helical coiled-coil structures at high peptide surface density (right). Figure not to scale.

Surface density effects on peptide structure in PEO layers.

Formation of coiled-coil or other structures associated with increasing peptide surface density and elutability should be detectable by specific changes in the CD signal. The surface density of peptides at uncoated (hydrophobic) and PEO-coated nanoparticle surfaces was varied as above, by altering the nanoparticle concentration (from 1 to 10 mg/mL) in peptide-nanoparticle suspensions with constant peptide concentration (0.2 mg/mL). CD spectra were acquired for WLBU2 in contact with uncoated or PEO-coated nanoparticles at different peptide surface densities (Figure B. 4).

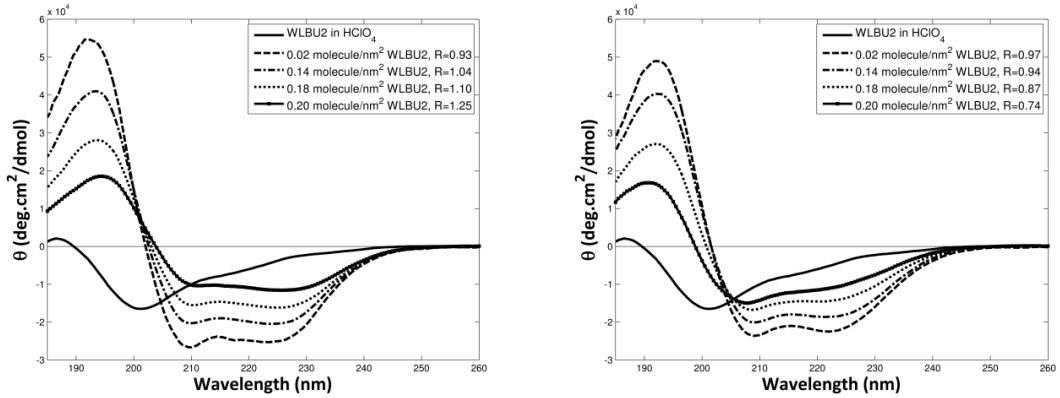

Figure B. 4 CD spectra of WLBU2 in 0.2M $HClO_4$ at different peptide surface densities on F108-coated (left) and uncoated (right) NPs.

The CD spectrum of an α-helix typically exhibits a maximum at 193 nm, and two minima at 208 and 222 nm. An increase in the magnitude of ellipticity at 222 nm for a given sample is associated with an increase in α-helix content [24,25]. Deconvolution of these CD spectra with DichroWeb [26,27] indicate that WLBU2 in 0.2 M $HClO_4$ exhibits 17% α-helicity. In the presence of F108-coated nanoparticles at 1, 2, 4 and 10 mg/mL (corresponding to decreasing peptide surface densities of 0.20, 0.18, 0.14 and 0.02 molecules/nm^2), the helicity of WLBU2 was increased to 50, 65, 84 and 95%, respectively. The increase in helicity is due to promotion of hydrogen-bonding along the peptide backbone, which accompanies the change in microenvironment caused by location within the hydrophobic interior of the PEO layer [1,5,17]. Interference with this intra-chain hydrogen-bonding by neighboring peptides is presumably responsible for the reduction in α-helix content observed at increased peptide surface densities (Figure B. 4, left panel).

While the ellipticity at 222 nm is primarily responsive to the α-helix content, the minimum at 208 nm is itself sensitive to helix-helix interactions [20,28]. In fact, CD has been applied extensively to the study of the formation of α-helical, coiled-coil structures [28-32]. In particular, the ratio, R, of the ellipticities at 222 nm and 208 nm can be used to distinguish coiled-coils from single-stranded α-helices. Typically, a value of $R > 1$ (i.e. $\vartheta_{222\ nm} > \vartheta_{208\ nm}$) is associated with coiled-coil structures, while a value of $R \leq 1$ is indicative of single-stranded α-helices [28-32]. WLBU2 exhibits a large amount of predominantly single-stranded α-helix structure (R = 0.93) on F108-coated

nanoparticles at a surface density of 0.02 peptides/nm^2 (dashed line in Figure B. 4, left panel). This suggests that at sufficiently low peptide surface density, peptides exist mainly as single α-helical molecules (Figure B. 3, left). As the surface density of peptides increases, the ratio R increases to values greater than unity, indicating the formation of a substantial number of α-helical coiled-coil structures (**Error! Reference source not found.**, right) [29-32].

While the CD spectra of WLBU2 adsorbed at uncoated, hydrophobic nanoparticles (Figure 4, right panel) indicate an increase in α-helicity, especially at low peptide surface density, there is no evidence of α-helical coiled-coils, as $R < 1$ at all of the surface densities tested. The increase in peptide helicity is likely due to the preferential association of the non-polar Val/Trp residues with the hydrophobic surface, which promotes the segregation of polar and non-polar residues onto opposing sides of the peptide and stabilizes the α-helix [14]. Electrostatic repulsion by the positively-charged Arg residues on the solvent-exposed helix face would make formation of coiled-coil structures unfavorable, even if the peptide surface density were high. However, peptides which are entrapped within a PEO brush apparently do not directly interact with the underlying surface [16]. Thus, WLBU2 peptides entrapped in a PEO brush still form highly-charged coiled-coil structures, with low resistance to elution, at sufficiently high surface density.

Similarly to WLBU2, the CD spectra of S-WLBU2 in suspension with PEO-coated nanoparticles (Figure B. 5, left panel) indicate a substantial gain (from 17 to 89%) in α-helix content after entering the brush, when the surface density is low (0.02 peptides/nm^2). However, with increasing peptide surface density, the structure adopted by the peptide becomes β-sheet rather than α-helical coiled-coils. The CD spectra of peptides with β-sheet conformation usually have a single minimum between 210 and 220 nm, and a single maximum between 195 and 200 nm, and overall intensities much lower than the minima consistent with α-helices [24,25]. Deconvolution of the spectra with DichroWeb indicate that S-WLBU2 exhibits 31% β-sheet and 53% α-helix structure at a surface density of 0.14 peptides/nm^2, has 54% β-sheet and 16% α-helix at 0.18 peptides/nm^2, and reaches 67% β-sheet with only negligible α-helix (3%) at 0.20 peptides/nm^2. The amino acid sequence of S-WLBU2 is not conducive to formation of face-segregated amphiphilic α-helices (Figure B. 1); instead, the peptide likely extends into β-strands, isolating the alternating non-polar residues onto one side of the sheet [23]. At sufficiently high

peptide surface densities, these *β*-strands may self-assemble into stable *β*-sheet structures stabilized by inter-chain hydrogen-bonding and hydrophobic interactions [33].

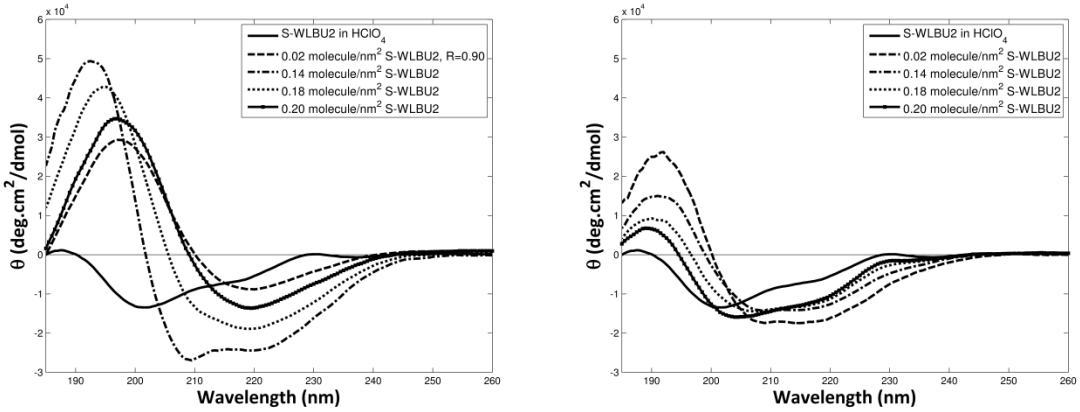

Figure B. 5 CD spectra of S-WLBU2 in 0.2M $HClO_4$ at different peptide surface densities on F108-coated (left) and uncoated (right) NPs.

The effects of peptide concentration on the conformation of adsorbed S-WLBU2 are less obvious at uncoated, hydrophobic surfaces than at PEO-coated surfaces (Figure B. 5, right panel). While S-WLBU2 in a PEO brush was almost completely α-helical (89%) at the lowest peptide surface density (0.02 peptides/nm^2), the same peptide adopts a substantial *β*-sheet structure (30%) on the uncoated, hydrophobic surface. Interactions between the hydrophobic surface and the alternating, non-polar residues of S-WLBU2 likely result in extension of the peptide chain, thus favoring *β*-sheet formation on the surface. Increasing the surface density of S-WLBU2 appears only to increase the number of layers of β-sheet, as no major conformational change is associated with increasing peptide density (Figure B. 5, right panel).

Unlike WLBU2 and S-WLBU2, PLR is a non-amphiphilic homopolymer with positive charges which uniformly surround the *α*-helix. Accordingly, electrostatic repulsions are expected to prevent peptide-peptide interactions, even at high surface density. CD spectra show that the helicity of PLR in 0.2 M $HClO_4$ solution is 55%, and is increased to 65% after contact with a PEO layer (Figure B. 6, left). Changes in surface density have little or no further effect on the conformation of PLR, whether on PEO-coated or uncoated hydrophobic surfaces (Figure B. 6).

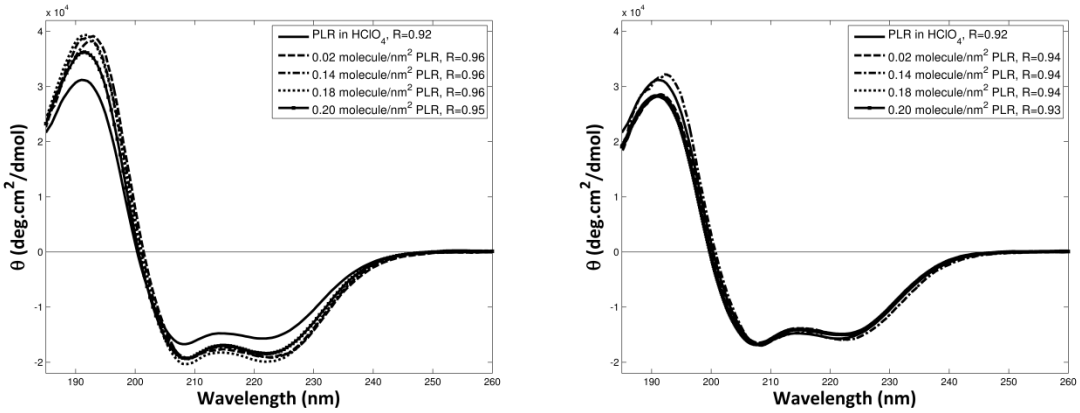

Figure B. 6 CD spectra of PLR in 0.2M $HClO_4$ at different peptide surface densities on F108-coated (left) and uncoated (right) NPs.

In summary, interactions between peptide molecules within the PEO brush layer are highly dependent on the properties of the peptide, specifically amphiphilicity, distribution of polar and non-polar residues, and charge. Elution of an amphiphilic peptide from the PEO brush layer is significantly affected by its surface density, while elution of a non-amphiphilic peptide is substantially independent of surface density. This difference in elution behavior is attributed to peptide-peptide interactions in the former case and the absence of such interactions in the latter.

Direct detection of peptide adsorption and elution at covalently immobilized PEO layers.

We used QCM-D to measure the effect of surface concentration on the rate and extent of peptide elution. Figure B. 7 shows the representative changes in resonant frequency (Δ*F*) and viscous dissipation (Δ*D*) upon adsorption and elution of peptides from F108-coated silica sensors [34,35]. The decrease in frequency (indicative of an increase in adsorbed mass) upon introduction of WLBU2 to F108-coated sensors at a peptide concentration of 0.1 mg/mL was about three times greater than that recorded for WLBU2 at 0.005 mg/mL (Figure B. 7, top panels). Upon elution, the frequency change indicated rapid and substantially complete removal of WLBU2 from the PEO brush that had been introduced at 0.1 mg/mL. However, a much slower, and only partial, removal of WLBU2 was observed when the peptide had been introduced at 0.005

mg/mL. These results are consistent with the greater resistance to elution by peptides at low surface density within the brush observed on nanoparticles (Figure B. 2).

Modeling of the frequency and dissipation data of Figure B. 7, in order to determine the adsorbed mass and effective layer viscosity, could not be performed with good certainty, as neither the Sauerbrey equation nor the Voigt model are appropriately applied in this context. The Sauerbrey equation should only be used with relatively uniform, rigid, thin films that show negligible dissipation change, while the Voigt model did not successfully calculate adsorbed mass from a simultaneous decrease in frequency and dissipation [36,37]. Qualitatively, however, the frequency and dissipation patterns in Figure B. 7 (top panel) likely represent the incorporation of WLBU2 into an initially "soft" dissipative surface (i.e. a pendant PEO layer, as opposed to a solid surface), and a concomitant increase in the layer stiffness. In comparison, a decrease in layer stiffness (i.e. increased viscoelasticity) is associated with protein adsorption on a rigid surface, suggesting that the observed frequency change was not due to adsorption of WLBU2 at "bare spots" in the brush. In contrast, the changes in resonant frequency (ΔF) for S-WLBU2 indicate a rapid and nearly complete removal of the peptide, whether originally introduced at high or low concentrations (Figure B. 7, bottom panels). This suggests that elution of the scrambled peptide is much less affected by its concentration at the surface than the face-segregated α-helix formed by WLBU2. Using optical waveguide lightmode spectroscopy (OWLS), we have observed that, like S-WLBU2, the non-amphiphilic PLR remains completely elutable from a PEO brush, even at very low surface peptide density [1].

Interestingly, the dissipation recorded during the adsorption of S-WLBU2 at high concentration decreased rapidly at first, then slowly increased (Figure B. 7, bottom left). An increase in the dissipation is associated with decreases in the stiffness of the adsorbed layer. Such a change would be consistent with a slow conformational change undergone by S-WLBU2 at the interface. Presumably, S-WLBU2 retains the α-helix structure induced by perchlorate ion during the initial adsorption, but rearranges to a β-sheet conformation as the peptide concentration in the PEO layer becomes sufficiently high. This is also consistent with recent reports that α-helical peptide layers adsorbed on gold QCM-D sensors are more rigid than peptide layers adsorbed as β-sheets [36]. No such increase in dissipation was recorded during adsorption of S-WLBU2 at low

concentration (Figure B. 7, bottom right), suggesting that there is no significant α-helix → β-sheet transition of S-WLBU2 within the PEO layer. The QCM-D results of Figure B. 7 are entirely consistent with the other results discussed above, and are also in agreement with the hypothesis that highly-elutable coiled-coil structures are formed at high peptide densities in the PEO brush.

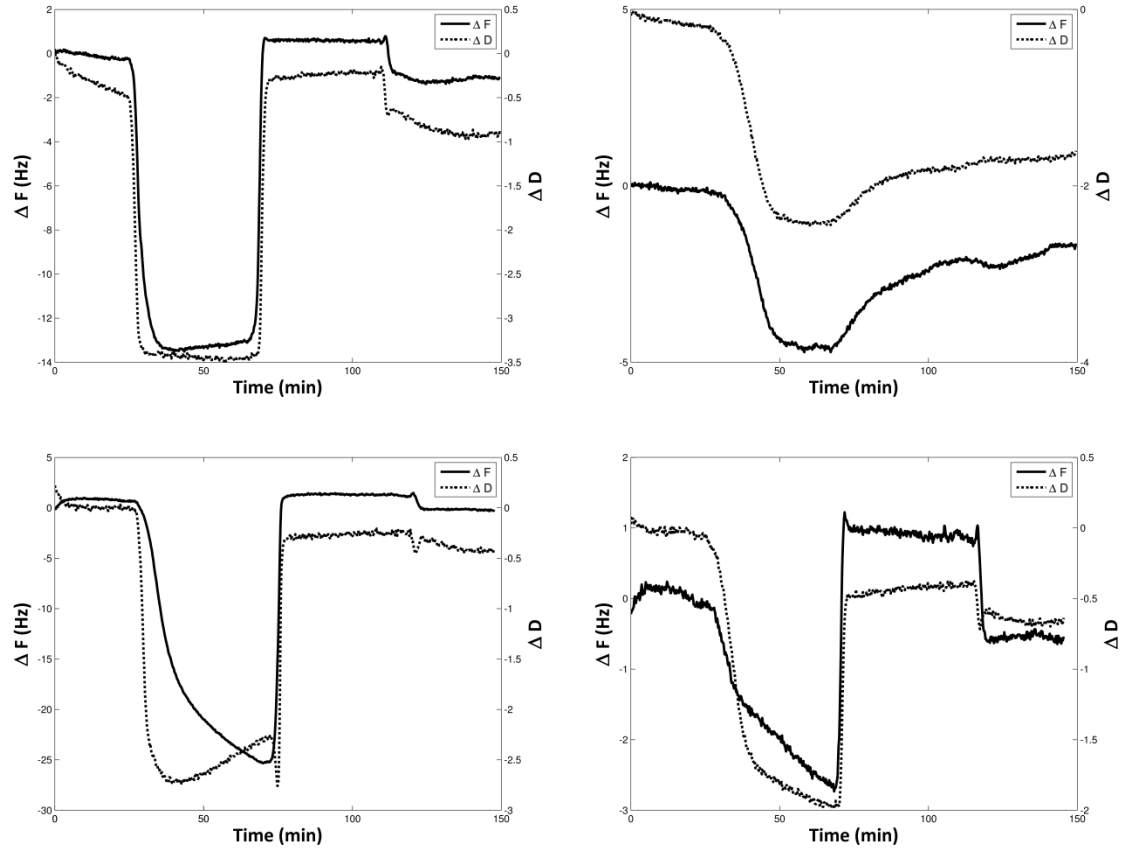

Figure B. 7 Representative Δ*F* and Δ*D* vs. time for WLBU2 (top panels) and S-WLBU2 (bottom panels) adsorption and elution on F108-coated SiO_2 QCM-D sensors. Baselines were achieved using 0.2 M $HClO_4$, followed by introduction of peptide in $HClO_4$, then elution with H_2O, and finally switch back to $HClO_4$. Peptide concentrations used for QCM-D experiments were 0.1 mg/mL (left panels) and 0.005 mg/mL (right panels). Note change of scale between peptide concentrations (left and right panels).

Conclusions

Elution of peptides from PEO brush layers is governed by their amphiphilicity and surface density. Peptides of high amphiphilicity can be expected to interact strongly with PEO chains after location within the layer, thus promoting their resistance to elution. However, at sufficiently high surface density, peptide-peptide interactions may result in conformational

changes (e.g. formation of coiled-coils) which can compromise this resistance to elution. In this work, WLBU2, a peptide with a face-segregated amphiphilic α-helical structure, was observed to form α-helices and coiled-coils, while the amphiphilic peptide (S-WLBU2) with a more uniform charge distribution formed β-sheets. These conformational changes (from α-helix to coiled-coil and β-sheet) increased the elutability of WLBU2 and S-WLBU2, presumably by reducing the amphiphilic character of the resulting complex. In contrast, the non-amphiphilic peptide (PLR) showed no substantial change in structure or elutability with increasing peptide surface density.

Entrapment of bioactive peptides within otherwise non-fouling PEO brush layers holds promise for contributing to development of responsive drug delivery systems. These results will inform research efforts focused on the sequential and competitive adsorption and release of such peptides at PEO layers. They will also be valuable for development of systems to control the rate and extent of therapeutic peptide release from PEO layers, based on modulation of their amphiphilicity and surface density.

Acknowledgments

The authors thank Dr. Kerry McPhail of the OSU College of Pharmacy for use of her CD instrument. This work was supported in part by the National Institute of Biomedical Imaging and Bioengineering (NIBIB, Grant No. R01EB011567). The content is solely the responsibility of the authors and does not necessarily represent the official views of NIBIB or the National Institute of Health.

References

1. Wu X, Ryder MP, McGuire J, Schilke KF. Adsorption, structural alteration and elution of peptides at pendant PEO layers. Colloids and Surfaces B: Biointerfaces 2013;112(0):23-29.
2. Costa F, Carvalho IF, Montelaro RC, Gomes P, Martins MCL. Covalent immobilization of antimicrobial peptides (AMPs) onto biomaterial surfaces. Acta Biomaterialia 2011;7(4):1431-1440.
3. Deslouches B, Gonzalez IA, DeAlmeida D, Islam K, Steele C, Montelaro RC, Mietzner TA. *De novo*-derived cationic antimicrobial peptide activity in a murine model of Pseudomonas aeruginosa bacteraemia. Journal of Antimicrobial Chemotherapy 2007;60(3):669-672.
4. Deslouches B, Islam K, Craigo JK, Paranjape SM, Montelaro RC, Mietzner TA. Activity of the *de novo* engineered antimicrobial peptide WLBU2 against *Pseudomonas aeruginosa* in human serum and whole blood: Implications for systemic applications. Antimicrobial Agents & Chemotherapy 2005;49(8):3208-3216.
5. Deslouches B, Phadke SM, Lazarevic V, Cascio M, Islam K, Montelaro RC, Mietzner TA. *De novo* generation of cationic antimicrobial peptides: Influence of length and tryptophan substitution on antimicrobial activity. Antimicrobial Agents & Chemotherapy 2005;49(1):316-322.
6. Gonzalez IA, Wong XX, De Almeida D, Yurko R, Watkins S, Islam K, Montelaro RC, El-Ghannam A, Mietzner TA. Peptides as potent antimicrobials tethered to a solid surface: Implications for medical devices. Nature Precedings 2008.
7. Onaizi SA, Leong SSJ. Tethering antimicrobial peptides: Current status and potential challenges. Biotechnology Advances 2011;29(1):67-74.
8. Skinner MC, Kiselev AO, Isaacs CE, Mietzner TA, Montelaro RC, Lampe MF. Evaluation of WLBU2 peptide and 3-*O*-octyl-*sn*-glycerol lipid as active ingredients for a topical microbicide formulation targeting *Chlamydia trachomatis*. Antimicrobial Agents & Chemotherapy 2010;54(2):627-636.
9. Adzhubei AA, Sternberg MJE, Makarov AA. Polyproline-II Helix in Proteins: Structure and Function. Journal of Molecular Biology 2013;425(12):2100-2132.
10. Bochicchio B, Tamburro AM. Polyproline II structure in proteins: Identification by chiroptical spectroscopies, stability, and functions. Chirality 2002;14(10):782-792.
11. Mikhonin AV, Myshakina NS, Bykov SV, Asher SA. UV Resonance Raman Determination of Polyproline II, Extended 2.5_1-Helix, and *β*-Sheet Ψ Angle Energy Landscape in Poly-*L*-Lysine and Poly-*L*-Glutamic Acid. Journal of the American Chemical Society 2005;127(21):7712-7720.
12. Rifkind JM. Helix–coil transition of poly-L-arginine: A comparison with other basic polypeptides. Biopolymers 1969;8(5):685-688.
13. Tiffany ML, Krimm S. Circular dichroism of the “random” polypeptide chain. Biopolymers 1969;8(3):347-359.

14. Lampi MC, Wu X, Schilke KF, McGuire J. Structural attributes affecting peptide entrapment in PEO brush layers. Colloids and Surfaces B: Biointerfaces 2013;106(0):79-85.
15. Tai Y-C, McGuire J, Neff JA. Nisin antimicrobial activity and structural characteristics at hydrophobic surfaces coated with the PEO–PPO–PEO triblock surfactant Pluronic® F108. Journal of Colloid and Interface Science 2008;322(1):104-111.
16. Dill JK, Auxier JA, Schilke KF, McGuire J. Quantifying nisin adsorption behavior at pendant PEO layers. Journal of Colloid and Interface Science 2013;395(0):300-305.
17. Lee H, Kim DH, Witte KN, Ohn K, Choi J, Akgun B, Satija S, Won Y-Y. Water Is a Poor Solvent for Densely Grafted Poly(ethylene oxide) Chains: A Conclusion Drawn from a Self-Consistent Field Theory-Based Analysis of Neutron Reflectivity and Surface Pressure–Area Isotherm Data. Journal of Physical Chemistry B 2012;116(24):7367-7378.
18. Parry DAD, Fraser RDB, Squire JM. Fifty years of coiled-coils and α-helical bundles: A close relationship between sequence and structure. Journal of Structural Biology 2008;163(3):258-269.
19. Zhou NE, Kay CM, Hodges RS. Synthetic model proteins. Positional effects of interchain hydrophobic interactions on stability of two-stranded *α*-helical coiled-coils. Journal of Biological Chemistry 1992;267(4):2664-2670.
20. Zhou NE, Kay CM, Hodges RS. Synthetic model proteins: the relative contribution of leucine residues at the nonequivalent positions of the 3-4 hydrophobic repeat to the stability of the two-stranded *α*-helical coiled-coil. Biochemistry 1992;31(25):5739-5746.
21. Grigoryan G, Keating AE. Structural specificity in coiled-coil interactions. Current Opinion in Structural Biology 2008;18(4):477-483.
22. Rubinov B, Wagner N, Rapaport H, Ashkenasy G. Self-replicating amphiphilic beta-sheet peptides. Angewandte Chemie. International Ed. In English 2009;48(36):6683-6.
23. Wang K, Keasling JD, Muller SJ. Effects of the sequence and size of non-polar residues on self-assembly of amphiphilic peptides. International Journal of Biological Macromolecules 2005;36(4):232-240.
24. Greenfield NJ. Methods to estimate the conformation of proteins and polypeptides from circular dichroism data. Analytical Biochemistry 1996;235(1):1-10.
25. Greenfield NJ, Fasman GD. Computed circular dichroism spectra for the evaluation of protein conformation. Biochemistry 1969;8(10):4108-4116.
26. Whitmore L, Wallace BA. DICHROWEB, an online server for protein secondary structure analyses from circular dichroism spectroscopic data. Nucleic Acids Research 2004;32(suppl 2):W668-W673.

27. Whitmore L, Wallace BA. Protein secondary structure analyses from circular dichroism spectroscopy: Methods and reference databases. Biopolymers 2008;89(5):392-400.
28. Cooper TM, Woody RW. The effect of conformation on the CD of interacting helices: a theoretical study of tropomyosin. Biopolymers 1990;30(7-8):657-76.
29. Cukalevski R, Lundqvist M, Oslakovic C, Dahlback B, Linse S, Cedervall T. Structural changes in apolipoproteins bound to nanoparticles. Langmuir 2011;27(23):14360-9.
30. Fiumara F, Fioriti L, Kandel ER, Hendrickson WA. Essential role of coiled coils for aggregation and activity of Q/N-rich prions and polyQ proteins. Cell 2010;143(7):1121-35.
31. Lazo ND, Downing DT. Circular Dichroism of Model Peptides Emulating the Amphipathic α-Helical Regions of Intermediate Filaments. Biochemistry 1997;36(9):2559-2565.
32. Potekhin SA, Melnik TN, Popov V, Lanina NF, Vazina AA, Rigler P, Verdini AS, Corradin G, Kajava AV. De novo design of fibrils made of short α-helical coiled coil peptides. Chemistry & Biology 2001;8(11):1025-1032.
33. Schneider JP, Kelly JW. Templates that induce *a*-helical, *b*-sheet, and loop conformations. Chemical Reviews 1995;95(6):2169-2187.
34. Höök F, Kasemo B, Nylander T, Fant C, Sott K, Elwing H. Variations in Coupled Water, Viscoelastic Properties, and Film Thickness of a Mefp-1 Protein Film during Adsorption and Cross-Linking: A Quartz Crystal Microbalance with Dissipation Monitoring, Ellipsometry, and Surface Plasmon Resonance Study. Analytical Chemistry 2001;73(24):5796-5804.
35. Höök F, Vörös J, Rodahl M, Kurrat R, Böni P, Ramsden JJ, Textor M, Spencer ND, Tengvall P, Gold J and others. A comparative study of protein adsorption on titanium oxide surfaces using in situ ellipsometry, optical waveguide lightmode spectroscopy, and quartz crystal microbalance/dissipation. Colloids and Surfaces B: Biointerfaces 2002;24(2):155-170.
36. Binazadeh M, Zeng H, Unsworth LD. Effect of peptide secondary structure on adsorption and adsorbed film properties on end-grafted polyethylene oxide layers. Acta Biomaterialia 2014;10(1):56-66.
37. Voinova MV, Jonson M, Kasemo B. 'Missing mass' effect in biosensor's QCM applications. Biosensors and Bioelectronics 2002;17(10):835-841.

APPENDIX C:

SEQUENTIAL AND COMPETITIVE ADSORPTION OF PEPTIDES AT PENDANT PEO LAYERS

Xiangming Wu, Matthew P. Ryder, Joseph McGuire, Karl F. Schilke*

For submission to Biomaterials Literature

Abstract

Our earlier work provided direction for development of responsive drug delivery systems based on modulation of structure, amphiphilicity and surface density of bioactive peptides entrapped within pendant polyethylene oxide (PEO) brush layers. At low peptide surface density, amphiphilicity promotes retention of the peptides within the hydrophobic inner region of the PEO layer, thereby increases their adsorption affinity. Peptide-peptide interactions which take place when peptide surface density is sufficiently high can substantially affect the rate and extent of peptide elution from the PEO brush layer. In this work, we describe the sequential and competitive adsorption behavior of peptides at pendant PEO brush layers, and show that adsorption and desorption of each peptide is governed by peptide amphiphilicity. Three cationic peptides were used in this study: the arginine-rich amphiphilic peptide WLBU2, the chemically identical but scrambled peptide S-WLBU2, and the non-amphiphilic peptide poly-*L*-arginine (PLR). Optical waveguide lightmode spectroscopy (OWLS) was used to quantify the rate and extent of peptide adsorption and elution at surfaces coated with PEO. UV spectroscopy and time-of-flight secondary ion mass spectrometry (TOF-SIMS) were used to quantify the extent of peptide exchange during the course of sequential and competitive adsorption. Circular dichroism (CD) was used to evaluate conformational changes of peptide mixture at PEO-coated silica nanoparticles. Results show that amphiphilic peptides are able to displace adsorbed non-amphiphilic peptides in PEO layers, while non-amphiphilic peptides cannot displace amphiphilic peptides. Peptides of high amphiphilicity are expected to dominate the competitive adsorption with less amphiphilic or non-amphiphilic peptides in PEO layers.

Introduction

In earlier papers [1, 2], we used circular dichroism (CD), optical waveguide lightmode spectroscopy (OWLS), and quartz crystal microbalance with dissipation monitoring (QCM-D) to study the adsorption and desorption behavior of poly-*L*-arginine (PLR) and the cationic amphiphilic peptide (CAP) WLBU2 in pendant PEO layers. Those results indicated that the adsorption of small peptides is governed by their secondary structure, while the entrapment and elution at the PEO layer is determined by peptide amphiphilicity and surface density. Specifically, some degree of structural order (α-helix) is necessary for peptide entry into PEO layers [1]. At low peptide surface density, interactions between non-polar groups of WLBU2 and the hydrophobic inner region of the PEO brush result in irreversible entrapment and resistance to elution. However, at high peptide surface density, intermolecular interactions of WLBU2 resulted in conformational changes which can compromise this resistance to elution. The non-amphiphilic peptide PLR does not show strong peptide-PEO chain interactions and its entrapment is always reversible [2].

WLBU2 is a synthetic, 24-residue CAP with 13 positively charged arginine residues, and 11 non-polar valine or tryptophan residues. It shows substantial promise for clinical applications, due to its wide spectrum antimicrobial activity against both Gram-negative and Gram-positive bacteria under physiological conditions [3-9]. The structure of WLBU2 in water is substantially disordered, but the peptide gains considerable secondary structure, involving segregation of its positively-charged and hydrophobic groups onto opposing faces of an α-helix, in the presence of counterions, membrane-mimetic solvents, or bacterial membranes. Moreover, WLBU2 retains its antimicrobial activity when immobilized at solid surfaces by a number of methods [3, 7-9]. While chemically identical to WLBU2, the scrambled sequence of S-WLBU2 eliminates the ordered segregation of positively-charged and hydrophobic residues of WLBU2 during helix formation [2], and is associated with a very low hydrophobic moment in comparison to WLBU2 (0.1 vs. 10.7, respectively) [10]. PLR is chemically homogeneous and not amphiphilic. When dissolved in water under neutral pH, PLR adopts a combination of random coil and extended structures (e.g. polyprolone-II and 2.5_1 helix), while both WLBU2 and S-WLBU2 show a random coil structure [1, 4-6, 11-14]. An α-helical conformation can be achieved in all three peptides by addition of perchlorate ions (ClO_4^-) [1, 13].

In this paper, we describe the sequential and competitive adsorption behavior of peptides, including PLR, WLBU2 and S-WLBU2, at pendant PEO brush layers. Solution depletion method and CD were used to evaluate competitive peptide exchange and peptide conformational change at PEO-coated silica nanoparticles. OWLS and time-of-flight secondary ion mass spectrometry (TOF-SIMS) were used to directly detect peptide sequential and competitive adsorption on covalently-immobilized PEO brush layers.

Materials and Methods

Peptides and materials.

Synthetic poly-*L*-arginine hydrochloride (PLR, n ≈ 30, M_n = 5.8 kDa, PDI < 1.20) was purchased from Alamanda Polymers (Huntsville, AL). The 24-residue peptides WLBU2 (RRWVRRVRRWVRRVVRVVRRWVRR, 3.4 kDa) and the scrambled sequence S-WLBU2 (VWRVRVRRRWRVRVWVRVRRRRVR) were purchased from Genscript (Piscataway, NJ). All peptides were used without further purification. Stock solutions of each peptide at 5 mg/mL in HPLC water were frozen in 1 mL aliquots, which were thawed and then diluted immediately before use to 0.2 mg/mL in 0.2 M $HClO_4$ (to induce α-helical conformation). Diluted peptide solutions were degassed under vacuum immediately before use.

Self-assembled PEO brush layers were formed by suspension of hydrophobic silica nanoparticles (R816, Degussa, 190 m^2/g, 10-12 nm) in Pluronic® F108 (BASF) in HPLC water for 10 h on a rotator [1, 16]. The complete surface coverage of F108 is about 3.3 mg/m^2 [16, 17]. A 5× excess of F108 over this amount was used to ensure good coverage of the nanoparticles. In the peptide sequential adsorption experiments, F108-coated nanoparticles were incubated with the first peptide (PLR, WLBU2 or S-WLBU2) under 0.2 M $HClO_4$ for 40 min at 20 °C. In the peptide competitive adsorption experiments, a mixture of PLR and WLBU2, or PLR and S-WLBU2 were incubated with F108-coated nanoparticles under the same conditions. The concentration of nanoparticles was varied between 1 mg/mL to 4 mg/mL, in order to provide different available surface area (0.2 – 0.05 peptides/nm^2) for peptide adsorption and exchange.

Quantify peptide exchange on PEO-coated nanoparticles.

In the peptide sequential adsorption experiments, the peptide-nanoparticle suspensions were rinsed by centrifugation (10,000 rpm, 20 min) and resuspension in 0.2 M $HClO_4$; this process was repeated twice to remove excess peptide. The amount of peptide removed in each of the supernatants from the nanoparticles was then quantified by UV spectrophotometry at 230 nm (for PLR) or 280 nm (for WLBU2 and S-WLBU2), in order to calculate the initial amount of first peptide in the PEO layer. The second peptide was then introduced to the resuspended nanoparticles, followed by 40 min incubation and rinsing with $HClO_4$. The amount of each peptide in the supernatants was again quantified by UV spectrophotometry at 230 nm and 280 nm. In the competitive adsorption experiment, F108-coated nanoparticles were incubated with peptide mixture for 40 min. The peptide-nanoparticle suspensions were centrifuged, and the change in supernatant absorbance at 230 and 280 nm was used to calculate the amount of each peptide entrapped the PEO layer. Experiments were conducted in three replicates and only slight (< 5%) differences in absorbance were observed.

Evaluation of time-dependent peptide secondary structure.

The secondary structure change of WLBU2 and S-WLBU2 with respect to time after introduction to F108-coated nanoparticles was evaluated by circular dichroism (CD) using a Jasco J-815 spectropolarimeter (Eaton, MD) at 25 °C. The instrument was calibrated using 0.6 mg/mL *D*(+)–camphorsulfonic acid. Spectra were recorded in a cylindrical cuvette (0.1 cm pathlength) from 185 to 260 nm in 0.5 nm increments, and five scans were averaged to increase the signal-to-noise ratio. All peptide solutions were filtered (0.2 μm) prior to contact with nanoparticles and recording of CD spectra. All spectra were blanked against peptide-free nanoparticles suspensions. The spectra from each of three replicates for each sample exhibited only slight (~5%) differences in signal intensity; representative spectra are thus shown throughout.

Stabilization of F108 coatings on OWLS waveguides and silicon wafers.

SiO_2-coated OW2400c OWLS sensors (MicroVacuum, Budapest, Hungary) and silicon wafers with 300 nm thermal SiO_2 were cleaned by submersion in 5% w/v sodium dodecyl sulfate (SDS) for 30 min, followed by 10 min wash at 80 °C in 5:1:1 mixture of H_2O:HCl:H_2O_2, then rinsed with HPLC

H_2O and dried under a stream of nitrogen [18]. The surfaces of OWLS sensors and silicon wafers were then modified by vapor deposition of trichlorovinylsilane (TCVS, TCI America, Portland, OR). 200 µL of TCVS was evaporated at 20°C into a stream of dry nitrogen carrier gas, which was directed over the waveguide and silicon wafers surfaces for 4 h. The silanized waveguides and silicon wafers were then immersed in a solution of 5% w/v Pluronic® F108 in water, and were rotated in solution overnight. After incubation, samples were γ-irradiated to 0.3 kGy to covalently attach the F108 to the surface [16, 19]. The irradiated sensors were rinsed with HPLC water, dried with nitrogen, and stored in the dark to avoid oxidation of the vinyl moieties.

Measurement of the rate and extent of peptide adsorption.

Peptide sequential and competitive adsorption were measured with an OWLS 210 instrument (MicroVacuum, Budapest, Hungary). A Rheodyne manual sample injector was used to inject sample solutions through a flow loop (~4.0 mL) into the OWLS flow cell. Flow rates were maintained at 50 µL/min and solution temperature was kept at 20 °C by the internal TC heater/cooler unit. Incident angle scans were performed from -5° to 5° at a step size of 0.01°. Both peaks of each of the transverse electric and magnetic modes were measured to determine the relative refractive index of the surface adlayer. OWLS experiments began with a baseline of peptide-free perchloric acid ($HClO_4$), followed by injection of 0.2 mg/mL peptide $HClO_4$, and a subsequent rinse with $HClO_4$. Adsorption and elution steps were each allowed to proceed for 40 min.

Peptide adsorption on F108-coated silicon wafers.

For sequential adsorption of peptides to the PEO brush layer, F108-coated silicon wafers were incubated with freshly made peptide solutions (PLR, WLBU2 or S-WLBU2) at 20 °C for 40 min, then rinsed with peptide-free $HClO_4$ to remove loosely-bound peptides. The rinsed wafers were then incubated with the second peptide for 40 min and the above rinse step was repeated. In competitive adsorption experiments, F108-coated silicon wafers were incubated with either a binary mixture of PLR and WLBU2, or PLR and S-WLBU2, followed by a rinse step with peptide-free $HClO_4$. After rinse, all peptide-loaded wafers, and peptide-free F108-coated and uncoated

TCVS silicon wafers were dried under vacuum at ambient temperature overnight prior to analysis with TOF-SIMS.

Time-of-flight secondary ion mass spectrometry (TOF-SIMS).

Positive secondary ion spectra were acquired for each sample on a TOF-SIMS IV instrument (Ion-TOF GmbH, Germany) using a pulsed 25 keV bismuth primary ion beam. The dose density of the primary beam was kept below 10^{12} ions/cm^2 to ensure that the static limit was not exceeded. Spectra were collected from three randomly chosen 100 × 100 μm areas on each sample. Secondary ions were collected over a range of 0 – 400 *m/z*. The mass resolution of each spectra was between 4000 and 8000, and the spectra were calibrated to less than 20 ppm using three or more C_nH_{2n-1} peaks (*n* from 2 to 5). Peak intensities were normalized against the total ion intensity of each spectrum.

Results and discussion

Peptide sequential and competitive adsorption on PEO-coated nanoparticles.

Our earlier report [1] demonstrated that peptides of high amphiphilicity such as WLBU2 (hydrophobic moment 10.7) are able to interact strongly with the hydrophobic inner region of the PEO brush layer, and resulted in peptide entrapment and conformational change that is irreversible to elution [1, 16, 20]. In contrast, the adsorption and conformational change is reversible with changing solution conditions for a chemically identical but less amphiphilic peptide (S-WLBU2, hydrophobic moment 0.1) or a non-amphiphilic peptide (PLR). When the surface density of WLBU2 is sufficiently high, the peptide-PEO interaction would be compromised and result in an increase in the elutability [2]. It is still fair to expect that the adsorption affinity of a peptide at a PEO layer is increased with its amphiphilicity.

In all peptide sequential and competitive adsorption experiments, the concentration of each peptide was held at a concentration (0.2 mg/mL), which theoretically fully covers the surface of 1 mg/mL F108-coated nanoparticles in monolayers [16, 17]. Figure C. 1 shows the percentage of first peptide displaced by the second (e.g., %PLR displaced by WLBU2 in the case of PLR → WLBU2) during the whole course of sequential adsorption of two peptides. Generally, an

amphiphilic peptide (WLBU2 or S-WLBU2) is able to displace most of the non-amphiphilic peptide PLR (98% and 76%, respectively) in a PEO layer when there is limited space for peptide adsorption (e.g. 1 mg/mL F108-coated NPs, peptide surface density 0.2 molecules/nm^2). While only small amount of adsorbed WLBU2 or S-WLBU2 (8% and 6%, respectively) in the PEO brush layer can be displaced by the sequentially introduced PLR. This is consistent with the well-known displacement of adsorbed fibrinogen or other biopolymers by introduction of proteins of higher adsorption affinity for the surface [21-23]. As the peptide surface density decreased to 0.1, 0.07 and 0.05 molecules/nm^2, while the concentration of peptides being held at 0.2 mg/mL, the amount of PLR displaced by WLBU2 or S-WLBU2 substantially decreased (Figure C. 1). This is due to the increase in the amount of nanoparticles provides more available surface area for peptide adsorption, therefore more WLBU2 or S-WLBU2 can be incorporate into the PEO layer without significantly displacing pre-adsorbed PLR.

It is important to note that the amount of PLR displaced by S-WLBU2 is always less than that by WLBU2 (Figure C. 1). We have previously shown that the interaction between S-WLBU2 and the hydrophobic inner region of the PEO layer is weaker than for WLBU2, due to the low amphiphilicity of S-WLBU2 [2]. Taken together, it is reasonable to expect that the ability of one peptide to displace the other at a PEO brush layer is directly related to their amphiphilicity and free surface area.

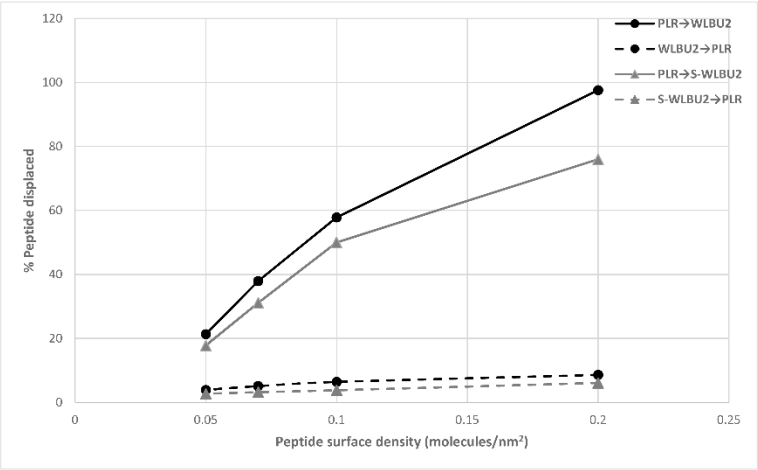

Figure C. 1: Percentage of first peptide being displaced by the second during the sequential adsorption of PLR, WLBU2 and S-WLBU2.

When peptides are introduced to F108-coated nanoparticles in a binary mixture, the amphiphilic peptide (WLBU2 or S-WLBU2) usually dominates the adsorption (Table 1). When the mixture of PLR and WLBU2 is introduced to 1 mg/mL F108-coated nanoparticles, 95% of WLBU2 adsorb into the PEO brush layer from the solution, while only 8.5% PLR is able to enter the brush. The percentage of adsorbed PLR increases with the concentration of nanoparticles, due to the presence of space in the PEO layer that is not occupied by WLBU2. Similarly, when the mixture of PLR and S-WLBU2 was introduced to 1 mg/mL F108-coated nanoparticles, 94% S-WLBU2 and 9% PLR adsorbs. As the concentration of nanoparticles increases, surface area increases and PLR is again able to adsorb to a greater extent. The change in the amount of adsorbed WLBU2 and S-WLBU2 with respect to nanoparticle concentration is negligible. These results strongly suggest that an amphiphilic peptide, which has greater adsorption affinity, will dominate the PEO layer when competing with a non-amphiphilic peptide for the fixed surface capacity. This is entirely consistent with many previous findings on competitive protein adsorption: proteins of greater affinity for the solid surfaces normally dominate the adsorption from binary or ternary mixtures [23-25].

Table 1. Competitive adsorption of PLR and WLBU2, and PLR and S-WLBU2 binary mixture

	PLR+WLBU2 mixture		PLR+S-WLBU2 mixture	
	%PLR adsorbed	%WLBU2 adsorbed	%PLR adsorbed	%S-WLBU2 adsorbed
1 mg/mL NPs (0.2 peptide/nm^2)	8%	95%	9%	94%
2 mg/mL NPs (0.1 peptide/nm^2)	19%	97%	23%	96%
3 mg/mL NPs (0.07 peptide/nm^2)	25%	98%	32%	98%
4 mg/mL NPs (0.05 peptide/nm^2)	47%	99%	63%	98%

Real-time peptide sequential and competitive adsorption at covalently immobilized PEO layers.

Figure C. 2 shows the adsorption and elution kinetics of sequential and competitive adsorption of PLR, WLBU2 and S-WLBU2 on covalently attached PEO layers. Both PLR and WLBU2 have very similar and fast adsorption kinetics, while the adsorbed mass of WLBU2 is significantly higher than PLR (Figure C. 2a). PLR is resistant to elution with $HClO_4$, a helix-stabilizing solvent [1], while a large portion of the adsorbed WLBU2 is elutable. This is due to the high peptide surface

density ~550 ng/cm^2 (i.e., 1.1 molecules/nm^2) which promotes hydrophobic interactions between WLBU2 molecules. At high surface density, WLBU2 forms intertwined α-helical coiled-coils, which compromise its resistance to elution [2]. Unlike WLBU2, PLR is non-amphiphilic and has positive charges which uniformly surround the α-helix. The electrostatic repulsions are expected to prevent interactions and increase the average distance between PLR molecules, therefore the adsorbed mass of PLR in the PEO layer is substantially less than WLBU2 [2].

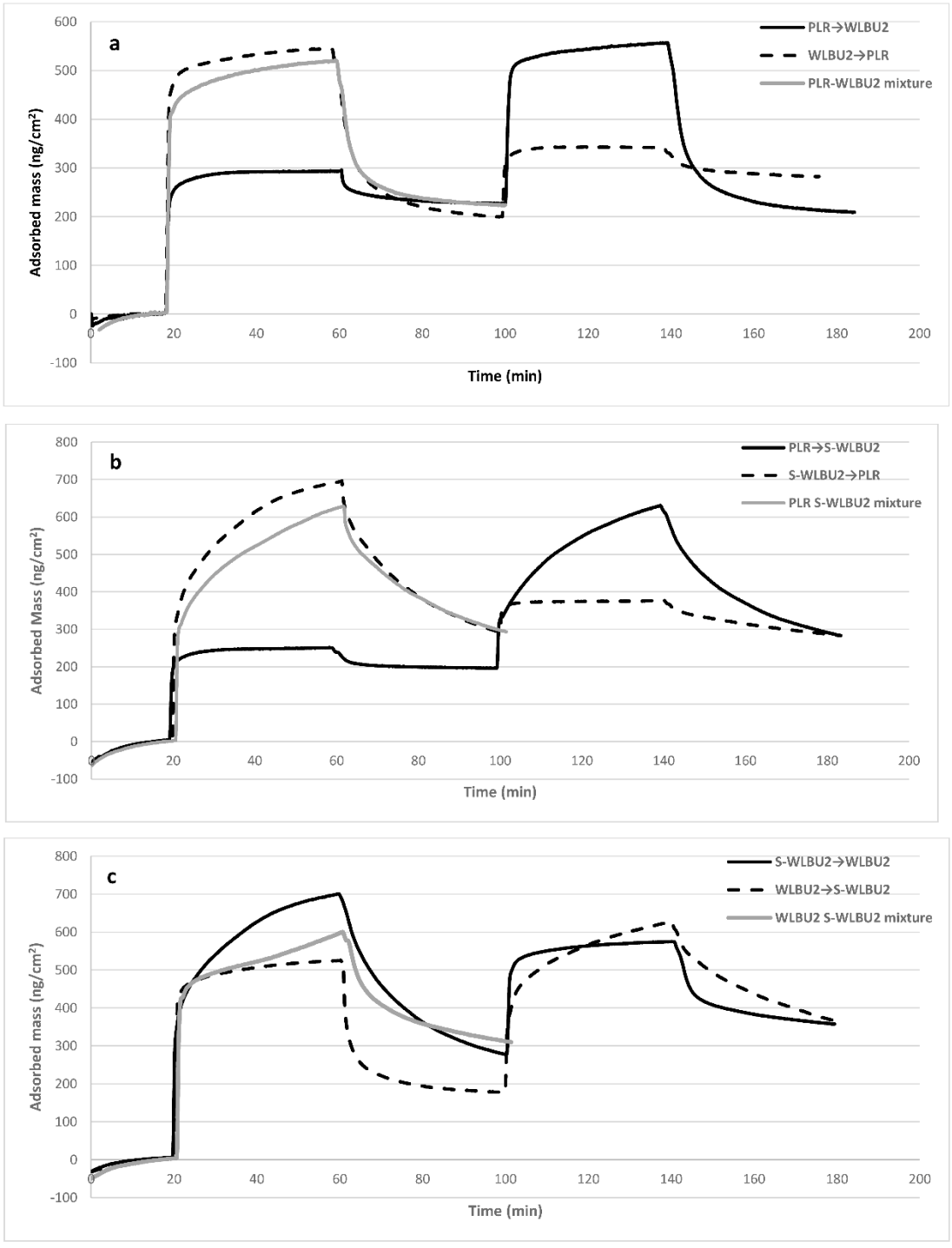

Figure C. 2: Sequential and competitive adsorption of (a) PLR and WLBU2, (b) PLR and S-WLBU2, (c) WLBU2 and S-WLBU2. Baseline was achieved using 0.2 M $HClO_4$, followed by adsorption of peptide 1 (sequential adsorption) or peptide 1 & 2 mixture (competitive adsorption), and then elution with 0.2 M $HClO_4$. Adsorption of peptide 2 started immediately after elution for sequential adsorption experiments, followed by elution with 0.2 M $HClO_4$.

The difference in adsorption patterns of PLR and WLBU2 are used to evaluate their adsorption when introduced to the PEO layer sequentially or simultaneously. As shown in Figure C. 2a, the sequential adsorption and elution of WLBU2 is not affected by the presence of pre-adsorbed PLR in the PEO layer. The adsorbed mass of WLBU2 at the peptide-free PEO layer reaches 550 ng/cm^2, and decreases to 200 ng/cm^2 after elution with $HClO_4$. Similarly, at the PLR-occupied PEO layer, the adsorbed mass also reaches 550 ng/cm^2 upon introduction of WLBU2, and decreased to 200 ng/cm^2 after elution. At the WLBU2-adsorbed PEO layer, however, the adsorbed mass increased from 200 to 340 ng/cm^2 and decreased to 294 ng/cm^2 upon elution. Both of these values are higher than observed for PLR adsorption and elution in a peptide-free PEO layer (300 and 230 ng/cm^2, respectively). This indicates the co-existence of the two peptides after sequential introduction of WLBU2 and PLR to a PEO layer. Based on these results and those from F108-coated nanoparticles that have been presented above (Figure C. 1), it is fair to expect that PLR does not displace pre-adsorbed WLBU2 to a large extent, while WLBU2 can displace most of the pre-adsorbed PLR. The competitive adsorption of the binary mixture of PLR and WLBU2 is much more similar to the adsorption of WLBU2 than of PLR. This suggests that WLBU2 dominates the competitive adsorption with PLR at a PEO layer. The slight difference between adsorption and elution kinetics is likely due to the presence of small amounts of PLR.

In contrast, when S-WLBU2 is introduced to the PEO-coated surface, however, it adsorbs to a higher extent than does WLBU2 (Figure C. 2b). Previously, we have shown that WLBU2 adopts an α-helical coiled-coil conformation, while S-WLBU2 adopts a β-sheet structure at high peptide surface density in the PEO layer [2]. It has been shown that polylysine in a β-sheet conformation adsorbs more slowly, but to a significantly higher extent than α-helical polylysine on bare gold surfaces, presumably due to stronger intermolecular hydrogen binding among β-sheet polylysine [26-28]. More specifically, the early-stage fast adsorption is likely due to strong interactions between S-WLBU2 and the surface. The large surface area of β-sheet S-WLBU2 promotes intermolecular hydrogen binding and hydrophobic interactions to form dense aggregates, and consequently drive further peptide adsorption with a slower rate [28, 29].

As shown in Figure C. 2b, the adsorption of S-WLBU2 is somewhat affected by the existence of PLR in the PEO layer. The adsorbed mass of S-WLBU2 at a peptide-free PEO layer reaches 700

ng/cm^2 after 40 min, and was decreased to 620 mg/cm^2 in the presence of pre-adsorbed PLR. This can be either S-WLBU2 can only partially displace PLR, or the displacement by S-WLBU2 is slower than WLBU2 displacing PLR. Introduction of PLR after S-WLBU2 (Figure C. 2a) again indicates the co-existence of PLR and S-WLBU2 at the PEO layer. The adsorption of PLR and S-WLBU2 mixtures is very similar to S-WLBU2 → PLR, suggesting that adsorption is dominated by S-WLBU2 (Figure C. 2b).

In addition, we investigated the effect of structure on sequential and competitive adsorption using WLBU2 and S-WLBU2 (Figure C. 2c). WLBU2 adsorbed to a slightly higher extent (60 ng/cm^2 more) on a S-WLBU2-loaded PEO layer than on a peptide-free PEO layer, while the peptide remaining on the surface after 40 min elution is significantly higher (180 ng/cm^2 more). However, S-WLBU2 adsorbed to a lower extent (80 ng/cm^2 less) in the presence of WLBU2 in the PEO layer, and the elution shows slower kinetics than at a PEO layer which contains only S-WLBU2. This suggests the co-existence of the two peptides after being sequentially introduced to the PEO layer, and presumably peptide-peptide interactions promote their resistance to elution. When WLBU2 and S-WLBU2 are introduced to the PEO-coated surface simultaneously (Figure C. 2c, gray curve), the adsorption appears to occur by a two-step process. The early step (first 10 min) appears identical to WLBU2-only adsorption, followed by a slow adsorption which is similar to S-WLBU2 adsorption kinetics. It is reasonable to expect that the highly amphiphilic peptide WLBU2 dominates the early adsorption, while the adsorption of S-WLBU2 is hindered by WLBU2 until WLBU2 approaching its maximum adsorbed mass (550 ng/cm^2). Further increase in the adsorbed mass is likely due to the slow adsorption of S-WLBU2 driven by intermolecular interactions of peptides [29]. The increase in the resistance to elution with $HClO_4$ again suggests the existence of interactions between WLBU2 and S-WLBU2 in the PEO layer.

Circular dichroism was applied to evaluate time-dependent conformational changes of WLBU2 and S-WLBU2 mixture after being introduced to F108-coated nanoparticles in $HClO_4$. We have shown that both WLBU2 and S-WLBU2 show a low α-helicity (15%) in 0.2 M $HClO_4$ solution [1], and once adsorbed into the PEO layer to a large extent, WLBU2 forms α-helical coiled-coils while S-WLBU2 forms β-sheets [2]. In the first two minutes of the experiment (Figure C. 3), CD shows an α-helical coiled-coil conformation, which exhibits two minima around 208 and 222 nm with

ellipticity ratio $\theta_{222nm} > \theta_{208\ nm}$ (indicating coiled-coil conformation) [30-33]. Note that after 5 min, spectrum is substantially β-sheet. This confirms that WLBU2 dominates the early adsorption. After 60 min, the peptides have largely undergone a transition from α-helical coiled-coil to β-sheet [34-35], and no further change in spectra was observed. Moreover, the supernatant had negligible absorbance at 280 nm, which indicates the complete adsorption of both WLBU2 and S-WLBU2. These results suggest that WLBU2 adsorbs at a much higher rate than S-WLBU2. As S-WLBU2 adsorbed to some large extent, interactions between WLBU2 and S-WLBU2 will result in the conformational change of WLBU2 (from α-helical coiled-coils to β-sheet), which possibly drives further S-WLBU2 adsorption.

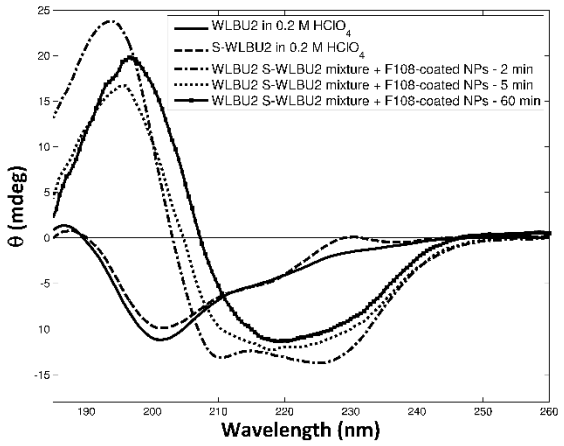

Figure C. 3: CD of the secondary structure of WLBU2 and S-WLBU2 mixture after incubation with F108-coated nanoparticles suspension for 2, 5 and 60 min.

In order to obtain more quantitative results of the peptide exchange in the PEO layer, TOF-SIMS was applied to analyze the PEO-coated surface after sequential and competitive adsorption of peptides at PEO layers.

TOF-SIMS analysis on covalently immobilized PEO layers.

Peptide sequential and competitive adsorption of PLR, WLBU2 and S-WLBU2 on OWLS waveguides was repeated on F108-coated silicon wafers.

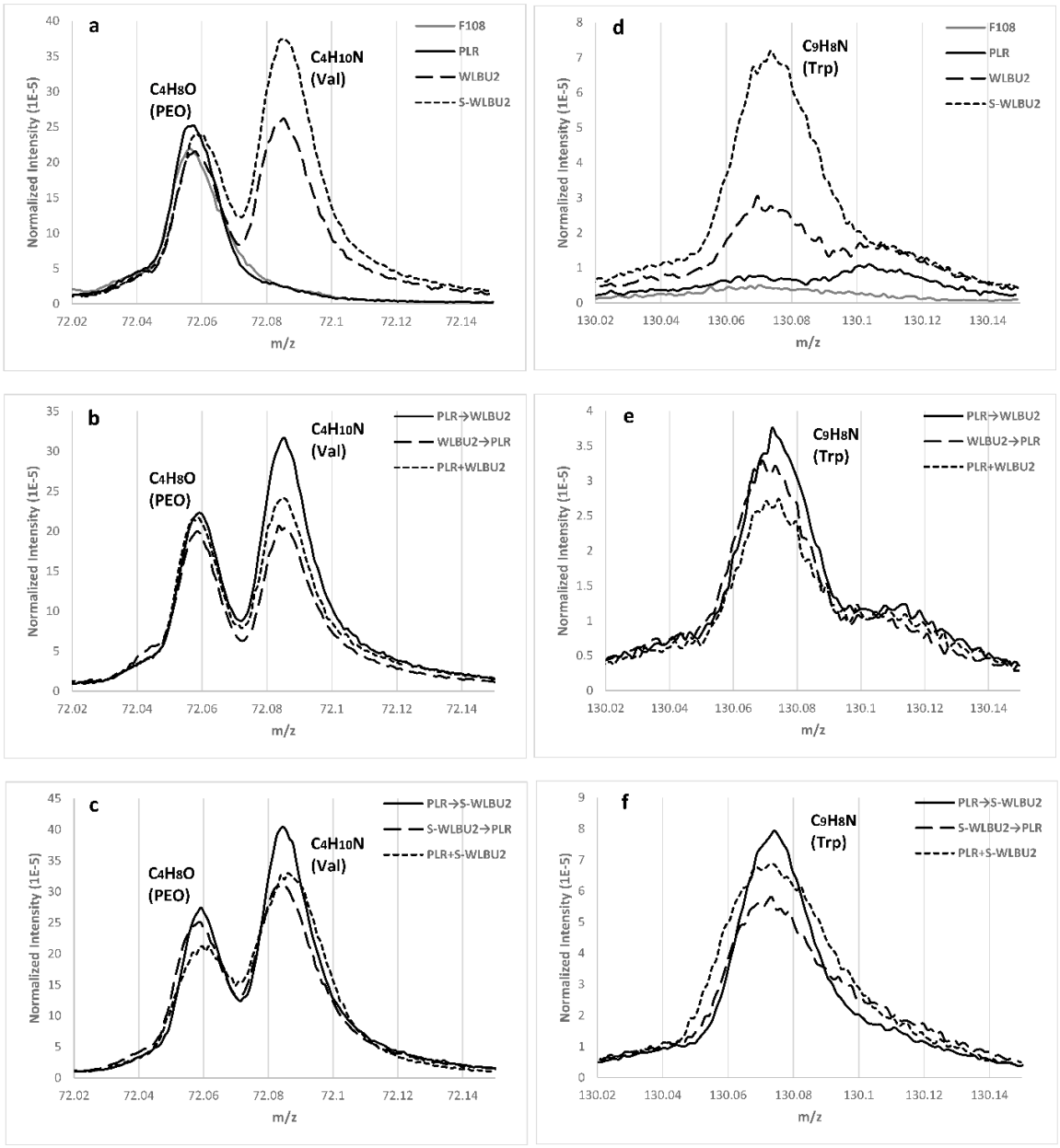

Figure C. 4: Representative scondary ion intensity of PEO, valine and tryptophan from peptide-adsorbed PEO layers on silicon wafers. All intensitites were normalized to total ion yield.

Peptide-free F108-immobilzed silicon wafer substrates show increased hydrocarbon and strong polyether signals (e.g., C_2H_5O, C_4H_8O) with respect to bare TCVS-silanized silicon wafers (data not shown). This confirms the presence of the PEO layer on the surface. Individual peaks corresponding to valine and tryptophan in WLBU2 and S-WLBU2 can be used to distinguish them

from PLR on the surface. Interferences on the amino acid peaks from the underlying substrate can be neglected in these tests since the spectra of bare TCVS and peptide-free F108-immobilized wafers both show negligible intensities at the characteristic peaks of arginine (*m/z* 59.05, 70.07, 100.08 and 127.1), valine (*m/z* 72.08 and 83.09) and tryptophan (*m/z* 130.07 and 159.09) [36-38]. Figure C. 4 shows the characteristic peaks of valine ($C_4H_{10}N$, *m/z* 72.08) and tryptophan (C_9H_8N, *m/z* 130.07) on surfaces before and after challenge with peptides. Surfaces contacted with WLBU2 or S-WLBU2 exhibit strong peaks at both 72.08 (Val) and 130.07 (Trp), while these peaks are absent on PLR-only and peptide-free PEO-coated surfaces (Figure C. 4, a and d). After sequential or simultaneous introduction of PLR and WLBU2, all the surfaces show strong peaks at both 72.08 and 130.07, and the normalized intensities of those peaks are similar to the surface contacted with WLBU2 only (Figure C. 4, b and e). This suggests that the presence of PLR in the PEO layer or solution does not interfere with the adsorption of WLBU2. Similarly, the presence of PLR does not have significant impact on S-WLBU2 (Figure C. 4, c and f). Both findings are consistent with OWLS results presented above.

The secondary ion intensity ratio (*R*) can provide more quantitative insight into the surface composition. *R* was calculated as the sum of intensities of valine (*m/z* 72.08 and 83.09) and tryptophan (*m/z* 130.07 and 159.09) divided by the sum of intensities of arginine (*m/z* 70.07, 100.08 and 127.1) [39, 40].

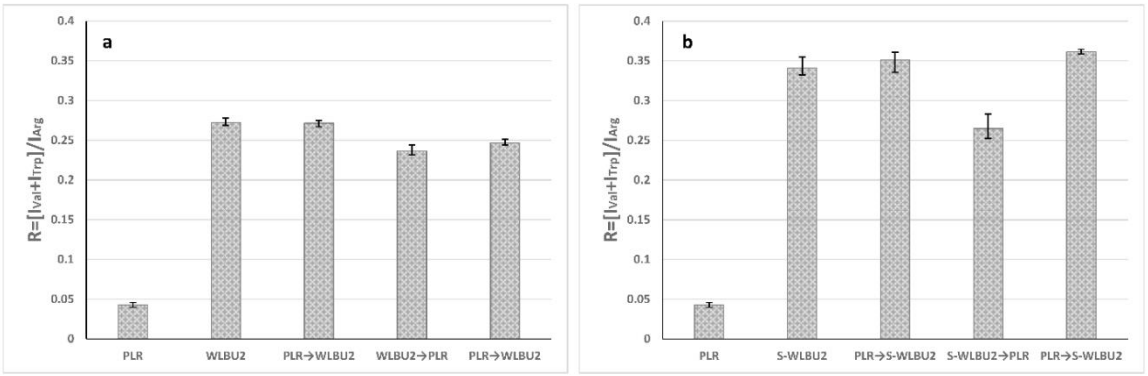

Figure C. 5: TOF-SIMS secondary ion peak intensity ratios (*R*) of: (a) PLR and WLBU2, and (b) PLR and S-WLBU2 sequential and competitive adsorption on PEO-coated silicon wafers. Peak ratios were calculated as the sum of intensities of valine and tryptophan peaks divided by the sum of intensities of arginine peaks. Error bars represent the standard deviation across three analysis areas.

Since PLR does not have valine and tryptophan residues, the *R* value of PLR-occupied surface is very low (0.0425). For WLBU2 and S-WLBU2 contacted surfaces, the ratios increased to 0.272 and 0.341, respectively (Figure C. 5). Thus, if a surface contains both PLR and WLBU2 or S-WLBU2, its *R* value should lie between 0.0425 and 0.272 or 0.341, depending on the relative amount of each peptide. As shown in Figure C. 5a, the *R* of WLBU2 adsorption on a PLR-adsorbed PEO layer (0.271) indicates the peptide on the surface is nearly 100% of WLBU2, which further suggests the complete displacement of PLR by WLBU2. The *R* values for sequential adsorption PLR on a WLBU2-adsorbed surface and the competitive adsorption of PLR and WLBU2 mixture are both slightly less than 0.271 (0.236 and 0.247, respectively). This confirms the co-existence of two peptides (Figure C. 2), and PLR only presences in a very small amount in the PEO layer. Similarly, S-WLBU2 displaces most adsorbed PLR in the PEO layer, and hinders PLR adsorption (Figure C. 5b).

In summary, the results from two distinct surface analytical techniques (OWLS and TOF-SIMS) are both consistent with results from the solution depletion method using PEO-coated nanoparticles. They also further suggest that amphiphilic peptides (WLBU2 and S-WLBU2) can displace adsorbed non-amphiphilic peptides (e.g. PLR) at PEO brush layers, while PLR can displace neither WLBU2 nor S-WLBU2. When peptides are introduced simultaneously and compete for a limited surface capacity, the amphiphilic peptides are expected to dominate the adsorption.

Conclusions

The results reported here direct us to expect that the sequential and competitive adsorption behaviors of peptides at pendant PEO brush layers are governed by primarily peptide amphiphilicity. When the surface capacity is limited, amphiphilic peptides, which have strong interactions with PEO chains, are able to displace adsorbed non-amphiphilic peptides in a PEO layer, while non-amphiphilic peptides cannot displace amphiphilic peptides. Peptides of high amphiphilicity are expected to dominate the competitive adsorption over less amphiphilic or non-amphiphilic peptides. Moreover, in this work, the interactions between adsorbed WLBU2 and S-WLBU2 in the PEO brush layer resulted in peptide conformational changes which promote their resistance to elution. Entrapment of bioactive peptides within otherwise non-fouling PEO

brush layers holds promise for development of responsive drug delivery systems. These results will provide information for further research on issues surrounding peptide loading and releasing at PEO layers. Current work is underway in our laboratory toward characterizing the time-dependent adsorption/desorption behavior of amphiphilic peptide mixtures at pendant PEO brush layers, and will contribute to the subject of future reports.

Acknowledgements

The authors thank Dr. Kerry McPhail of the OSU College of Pharmacy for use of her CD instrument, and Dr. Joseph Baio for valuable discussion on interpretation of the TOF-SIMS data. This work was supported in part by the National Institute of Biomedical Imaging and Bioengineering (NIBIB, Grant No. R01EB011567). The content is solely the responsibility of the authors and does not necessary represent the official views of NIBIB or the National Institute of Health.

References

[1] X. Wu, M.P. Ryder, J. McGuire, K.F. Schilke, *Adsorption, structural alteration and elution of peptides from pendant PEO layers*, Colloids Surf. B. Biointerfaces 112 (2013) 23-29.
[2] X. Wu, M.P. Ryder, J. McGuire, K.F. Schilke, *Concentration effects on peptide elution from pendant PEO layers*, submitted to Colloids Surf. B. Biointerfaces.
[3] F. Costa, I.F. Carvalho, R.C. Montelaro, P. Gomes, M.C.L. Martins, *Covalent immobilization of antimicrobial peptides (AMPs) onto biomaterial surfaces*, Acta Biomater. 7 (2011) 1431-1440.
[4] B. Deslouches, I.A. Gonzalez, D. DeAlmeida, K. Islam, C. Steele, R.C. Montelaro T.A. Mietzner, *De novo-derived cationic antimicrobial peptide activity in a murine model of Pseudomonas aeruginosa bacteraemia*, J. Antimicrob. Chemother. 60 (2007) 669-672.
[5] B. Deslouches, K. Islam, J.K. Craigo, S.M. Paranjape, R.C. Montelaro T.A. Mietzner, *Activity of the de novo engineered antimicrobial peptide WLBU2 against Pseudomonas aeruginosa in human serum and whole blood: Implications for systemic applications*, Antimicrob. Agents Chemother. 49 (2005) 3208-3216.
[6] B. Deslouches, S.M. Phadke, V. Lazarevic, M. Cascio, K. Islam, R.C. Montelaro, T.A. Mietzner, *De novo generation of cationic antimicrobial peptides: Influence of length and tryptophan substitution on antimicrobial activity*, Antimicrob. Agents Chemother. 49 (2005) 316-322.
[7] I.A. Gonzalez, X.X. Wong, D. De Almeida, R. Yurko, S. Watkins, K. Islam, R.C. Montelaro, A. El-Ghannam T.A. Mietzner, *Peptides as potent antimicrobials tethered to a solid surface: Implications for medical devices*, Nat. Precedings (2008).
[8] S.A. Onaizi, S.S.J. Leong, *Tethering antimicrobial peptides: Current status and potential challenges*, Biotechnol. Adv. 29 (2011) 67-74.
[9] M.C. Skinner, A.O. Kiselev, C.E. Isaacs, T.A. Mietzner, R.C. Montelaro, M.F. Lampe, *Evaluation of WLBU2 peptide and 3-O-octyl-sn-glycerol lipid as active ingredients for a topical microbicide formulation targeting Chlamydia trachomatis*, Antimicrob. Agents Chemother. 54 (2010) 627-636.
[10] T. C. Terwilliger, *The helical hydrophobic moment: a measure of the amphiphilicity of a helix*. Nature, 299 (1982), 371-374.
[11] A.A. Adzhubei, M.J.E. Sternberg, A.A. Makarov, *Polyproline-II helix in proteins: Structure and function*, J. Mol. Biol. 425 (2013) 2100-2132.
[12] A.V. Mikhonin, N.S. Myshakina, S.V. Bykov, S.A. Asher, *UV resonance raman determination of polyproline II, extended 2.51-helix, and β-sheet ψ angle energy landscape in poly-L-lysine and poly-L-glutamic acid*, J. Am. Chem. Soc. 127 (2005) 7712-7720.
[13] J.M. Rifkind, *Helix–coil transition of poly-L-arginine: A comparison with other basic polypeptides*, Biopolymers 8 (1969) 685-688.
[14] M.L. Tiffany, S. Krimm, *Circular dichroism of the "random" polypeptide chain*, Biopolymers 8 (1969) 347-359.
[16] M.C. Lampi, X. Wu, K.F. Schilke, J. McGuire, *Structural attributes affecting peptide entrapment in PEO brush layers*, Colloids Surf. B. Biointerfaces 106 (2013) 79-85.
[17] Y.-C. Tai, J. McGuire, J.A. Neff, *Nisin antimicrobial activity and structural characteristics at hydrophobic surfaces coated with the PEO–PPO–PEO triblock surfactant Pluronic® F108*, J. Colloid Interface Sci. 322 (2008) 104-111.
[18] M.P. Ryder, J. McGuire K.F. Schilke, *Cleaning requirements for silica-coated sensors used in optical waveguide lightmode spectroscopy*, Surf. Interface Anal. 45 (2013) 1805-1809.

[19] J.K. Dill, J.A. Auxier, K.F. Schilke, J. McGuire, *Quantifying nisin adsorption behavior at pendant PEO layers*, J. Colloid Interface Sci., 395 (2013) 300-305.
[20] H. Lee, D.H. Kim, K.N. Witte, K. Ohn, J. Choi, B. Akgun, S. Satija Y.-Y. Won, *Water is a poor solvent for densely grafted poly (ethylene oxide) chains: A conclusion drawn from a self-consistent field theory-based analysis of neutron reflectivity and surface pressure–area isotherm data*, J. Phys. Chem. B 116 (2012) 7367-7378.
[21] S.Y. Jung, S.M. Lim, F. Albertorio, G. Kim, M.C. Gurau, R.D. Yang, M.A. Holden, P.S Cremer, *The Vroman effect: A molecular level description of fibrinogen displacement*, J. Am. Chem. Soc. 125 (2003), 12782-12786.
[22] E. Dickinson, *Mixed biopolymers at interfaces: Competitive adsorption and multilayer structures,* Food Hydrocolloid. 25 (2011), 1966-1983.
[23] M. Rabe, D. Verdes, S. Seeger, *Understanding protein adsorption phenomena at solid surfaces*, Adv. Colloid. Interfac. 162 (2011), 87-106.
[24] S.L. Hirsh, D.R. McKenzie, N.J. Nosworthy, J.A. Denman, O.U. Sezerman, M.M.M. Bilek, *The Vorman effect: Competitive protein exchange with dynamic multilayer protein aggregates*, Colloids Surf. B. Biointerfaces 103 (2013) 395-404.
[25] H. Noh, E.A. Vogler, *Volumetric interpretation of protein adsorption: competition from mixtures and the Vroman effect*, Biomaterials 28 (2007) 405-422.
[26] K. Wang, J.D. Keasling, S.J. Muller, *Effects of the sequence and size of non-polar residues on self-assembly of amphiphilic peptides,* Int. J. Biol. Macromol. 36 (2005) 232-240.
[27] J.P. Schneider, J.W. Kelly, *Templates that induce α-helical, β-sheet, and loop conformations,* Chem. Rev. 95 (1995) 2169-2187.
[28] M. Binazadeh, H. Zeng, L.D. Unsworth, *Effect of peptide secondary structure on adsorption and adsorbed film properties,* Acta Biomater. 9 (2013) 6403-6413.
[29] J.J Grigsby, H.W. Blanch, J.M. Prausnitz, *Effect of secondary structure on the potential of mean force for poly-lysine in the α-helix and β-sheet conformations*, Biophys. Chem. 99 (2002) 107-116.
[30] T.M. Cooper, R.W. Woody, *The effect of conformation on the CD of interacting helices: a theoretical study of tropomyosin*, Biopolymers 30 (1990) 657-676.
[31] N.D. Lazo, D.T. Downing, *Circular dichroism of model peptides emulating the amphipathic α-helical regions of intermediate filaments,* Biochemistry 36 (1997) 2559-2565.
[32] F. Fiumara, L. Fioriti, E.R. Kandel, W.A. Hendrickson, *Essential role of coiled coils for aggregation and activity of Q/N-rich prions and polyQ proteins,* Cell 143 (2010) 1121-1135.
[33] R. Cukalevski, M. Lundqvist, C. Oslakovic, B. Dahlback, S. Linse, T. Cedervall, *Structural changes in apolipoproteins bound to nanoparticles,* Langmuir, 27 (2011) 14360-14369.
[34] N.J. Greenfield, *Methods to estimate the conformation of proteins and polypeptides from circular dichroism data*, Anal. Biochem. 235 (1996) 1-10.
[35] N.J. Greenfield, G.D. Fasman, *Computed circular dichroism spectra for the evaluation of protein conformation*, Biochemistry (Mosc). 8 (1969) 4108-4116.
[36] N.T. Samuel, M.S. Wagner, K.D. Dornfeld, D.G. Castner, *Analysis of poly (amino acids) by static time-of-flight secondary ion mass spectrometry (TOF-SIMS),* Surf. Sci. Spectra 8 (2001) 163-184.
[37] D.S. Mantus, B.D. Ratner, B.A. Carlson, J.F. Moulder, *Static secondary ion mass spectrometry of adsorbed proteins*. Anal. Chem. 65 (1993) 1431-1438.
[38] K.F. Schilke, J. McGuire, *Detection of nisin and fibrinogen adsorption on poly (ethylene oxide) coated polyurethane surfaces by time-of-flight secondary ion mass spectrometry (TOF-SIMS)*, J. Colloid Interface Sci., 358 (2011) 14-24.

[39] J.E. Baio, T. Weidner, G. Interlandi, C. Mendoza-Barrera, H.E. Canavan, R. Michel, D.G. Castner, *Probing albumin adsorption onto calcium phosphates by x-ray photoelectron spectroscopy and time-of-flight secondary ion mass spectrometry*, J. Vac. Sci. Technol. B 29 (2011), 04D113 1-6.
[40] L. Baugh, T. Weidner, J.E. Baio, P.C.T. Nguyen, L.J. Gamble, P.S. Stayton, D.G. Castner, *Probing the orientation of surface-immobilized protein G B1 using ToF-SIMS, sum frequency generation, and NEXAFS spectroscopy*. Langmuir, 26 (2010), 16434-16441.

APPENDIX D:

STEREOSCOPIC 3D VIEW OF MOST RELEVANT PEPTIDES USED IN THIS WORK:

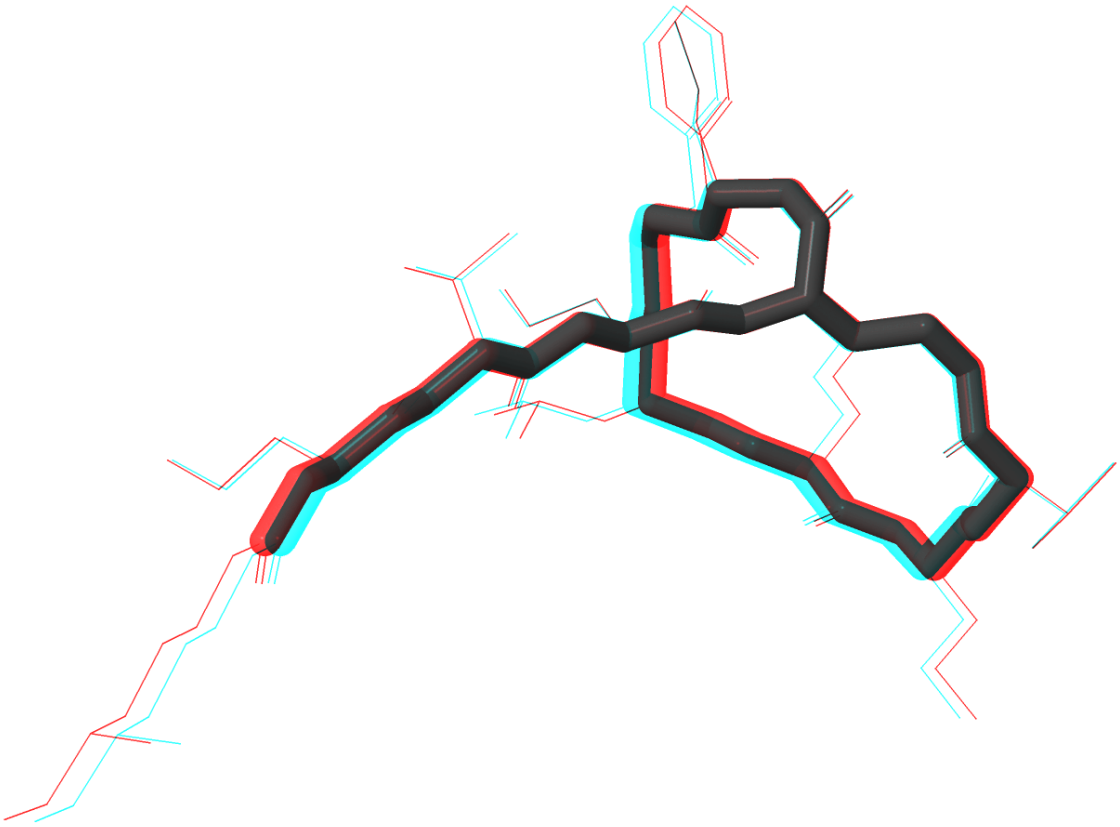

Figure D. 1: Polymyxin B, amino acid "backbone" is represented by sticks, side chains and hydrocarbons are shown in wireframe.

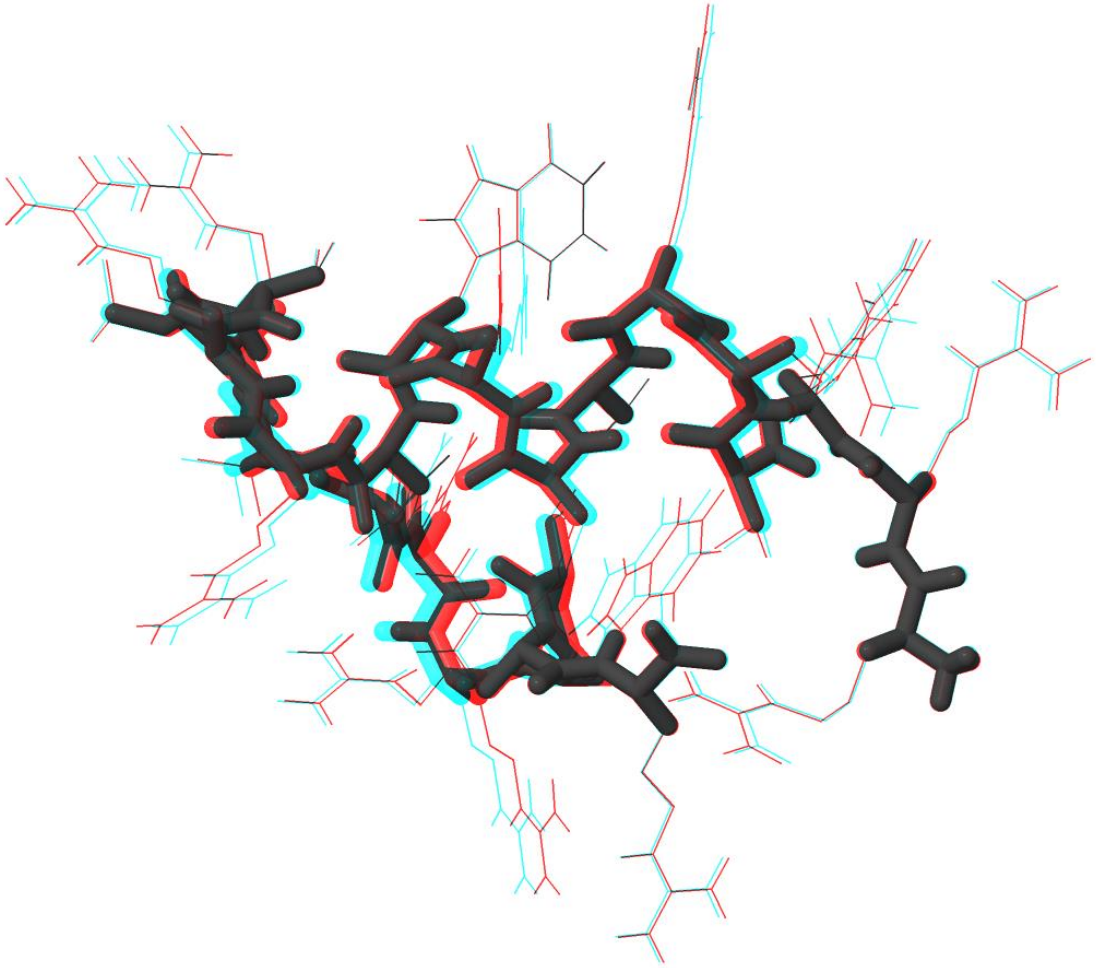

Figure D. 2: WLBU2 in random coil configuration. Peptide backbone is shown as sticks, side chains are shown in wire frame.

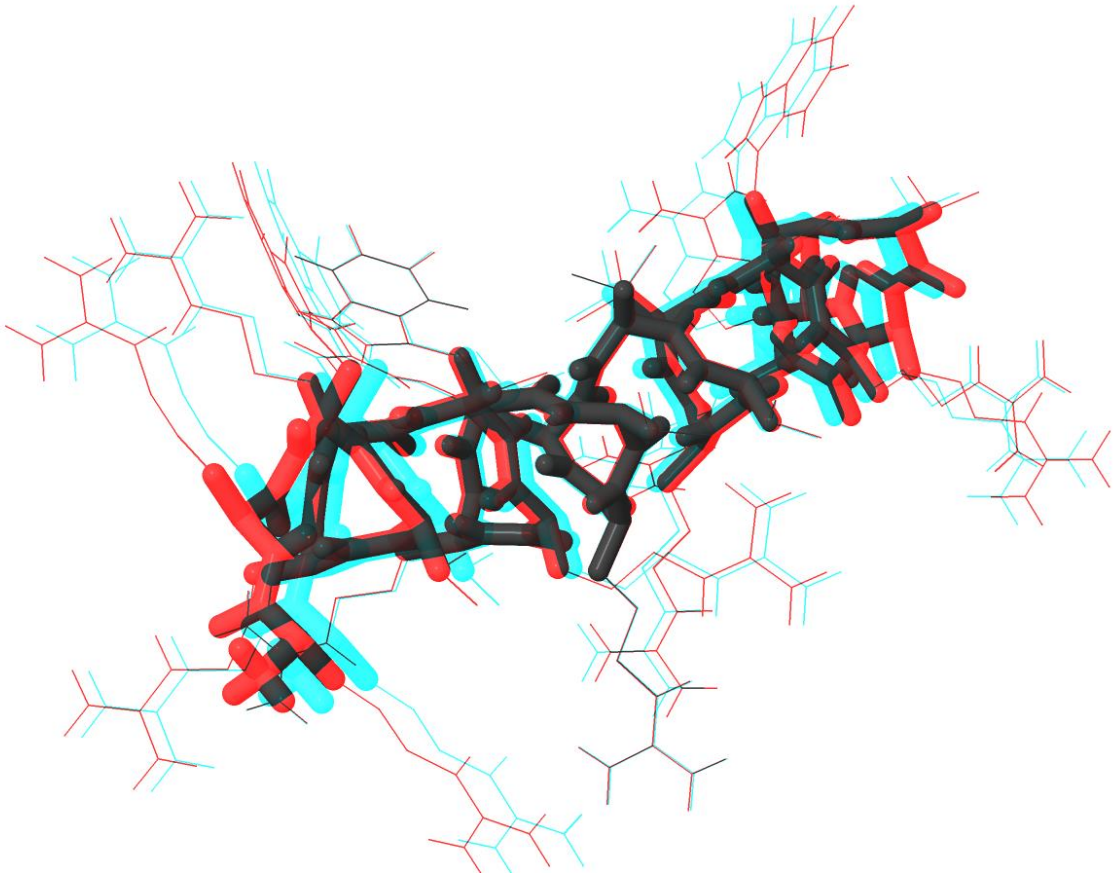

Figure D. 3: WLBU2 in α-helix configuration. Peptide backbone is shown as sticks, side chains are shown in wire frame.

Figure D. 4: Crystal structure of human fibrinogen in cartoon structure. From the protein data bank (3GHG)

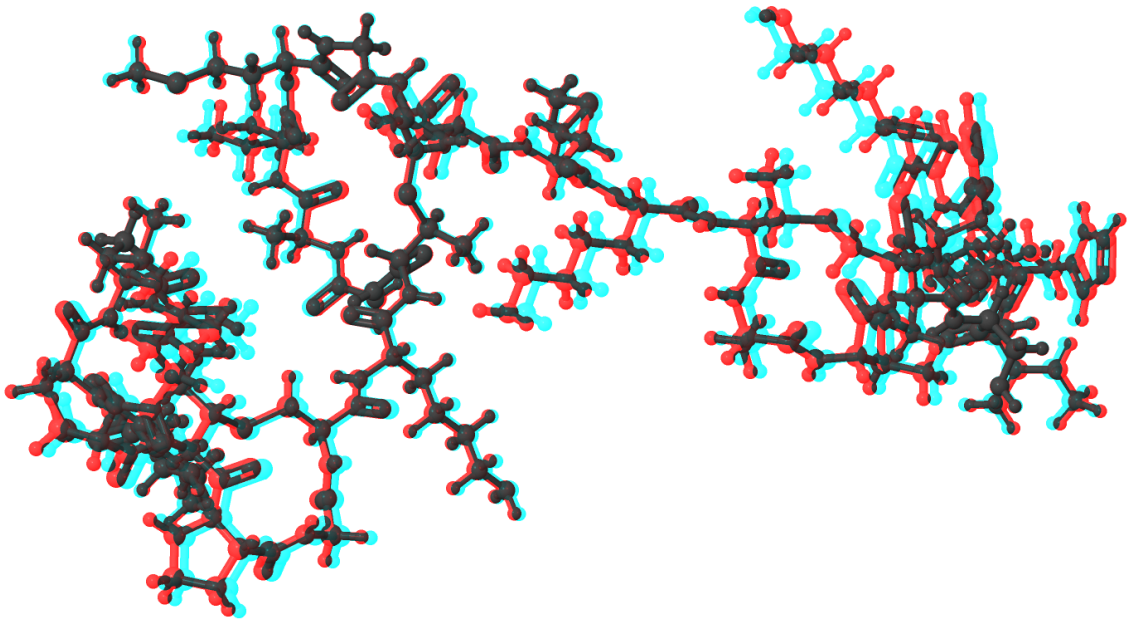

Figure D. 5: Ball and stick model of nisin from pubchem. InChi = NVNLLIYOARQCIX-GSJOZIGCSA-N

APPENDIX E:

MATLAB CODE FOR BASELINE CORRECTION

```
%Matthew P Ryder
%December 13, 2013
%for doing baseline correction of QCM-D data,
%based on typical adsorption kinetics
function baseline = QCM
%% Administrative
clc; close all; clear all; format compact;
global Time F5 maxval K Gmax res wres err Gest Kest t

%% Initiation
display('Before proceding, please be sure your file')
display('has a sheet with the baseline data labeled base.1')
display('and a sheet with all the data to be corrected labeled correct.2')
display('Enjoy!')
display(' ')
filename=input( 'Input filename   ', 's');
sheet='base.';
sheet2='correct.';

%% Data Input

data=xlsread(filename,[sheet num2str(1)]);
[m y]=size(data);
Time=data(:,1);
F5=data(:,2);
maxval=max(data(:,2));



%% Model the baseline
Gest= maxval;
Kest= -0.05;
t=Time;
guesses = [Gest, Kest];
estimates = fminsearch(@gamma, guesses);
Gmax = estimates(1);
K = estimates(2);
G=Gmax.*(1-exp(K.*t));
res=F5-G;
wres = res./err;
J = sum(sum(wres.^2));

disp 'estimates of Gmax and K';
Gmax
K
```

```
%% Plot residual, etc.
figure(1)
subplot(1,2,1)
plot(Time, F5, 'k-', Time, G, 'b--'); hold on
xlabel('Time [min]'); ylabel('\Delta Frequency(5th)'); legend('data','model',0);
title([filename num2str(' baseline')]);
subplot(1,2,2); plot(Time,res,'o');
xlabel('Time [min]'); ylabel('residual');
title([filename num2str(' residual')]);

%% View and continue
pause

%% Apply correction - read in
data2=xlsread(filename,[sheet2 num2str(2)]);
[n y]=size(data2);
Time2=data2(:,1);
F52=data2(:,2);

%% Apply correction - delete baseline
F=Gmax.*(1-exp(K.*Time2));
New = F52-F;

figure(2)
plot(Time2, F52,'-k',Time2,F,'-b',Time2, New,'-r');
xlabel('Time [min]'); ylabel('\Delta Frequency(5th)');
legend('Original','Baseline','Corrected',0);
title([filename]);

%% Export new data to *.txt file
output(:,1)=Time2;
output(:,2)=New;
save([filename num2str('.txt')],'output', '-ASCII');
print(2,'-dtiff','-r600',[filename num2str('.tiff')]);


function J = gamma(estimates)
global Time F5 maxval K Gmax res wres err Gest Kest t
err = 0.5*ones(size(F5));
Gmax = estimates(1);
K = estimates(2);
t = Time;
G=Gmax.*(1-exp(K.*t));
res=F5-G;
wres = res./err;
J = sum(sum(wres.^2));
```